Combustion of biomass and solid recovered fuels on the grate

Von der Fakultät Energie-, Verfahrens- und Biotechnik
der Universität Stuttgart zur Erlangung der Würde eines Doktors
der Ingenieurwissenschaften (Dr.-Ing.) genehmigte Abhandlung

Vorgelegt von

Piotr Nowak

aus Kraków (Polen)

Hauptberichter:	Prof. Dr.-Ing. Helmut Seifert
Mitberichter:	Apl. Prof. Dr.-Ing. habil. Günter Baumbach
Tag der mündlichen Prüfung:	01.10.2019

Institut für Feuerungs- und Kraftwerkstechnik (IFK) der Universität Stuttgart

2019

Content

Abstract

Development of an environmentally friendly use of biomass and solid recovered fuels (SRF) for energy production is an important task of the Institute of Technical Chemistry at KIT. This task is being realized with help of a so called 3-step characterization concept for a detailed description of these fuels. In the first step a chemical composition of a biomass or an SRF is determined. The second step is focused on the combustion specific characterization of a fuel in the laboratory scale fixed batch reactor "KLEAA", in which the combustion behaviour is described with local temperatures in the fuel bed, air ratios, gas composition above the bed and characteristic numbers: ignition time, reaction front velocity, mass conversion rate and specific heat release. In the third step a transfer of the results form a fixed bed onto a moving bed is performed. This step is possible when the mixing in the moving bed is limited, i.e. on a travel or a forward acting grate and for fuels with a low ash content. Furthermore, local primary air flows have to be equal for both beds. The resulting combustion behaviour on the moving grate can be validated in the pilot scale facility "TAMARA" equipped with a forward acting grate.

Experimental estimation of the combustion behaviour can be additionally reinforced with a numerical model "KLEAA Code", which was initially developed for woody biomass. The model is based on a one dimensional cascade of ideally stirred batch reactors. The fuel is considered as a porous bulk, through which the gas passes through, therefore the mass, element and energy balance is formulated for both phases. The heat transfer occurs between the phases through convection and radiation, and between solid particles through conduction and radiation. Mass transfer is allowed to occur in the model in one direction – from the solid phase into the gas. The solid fuel is considered in the pyrolysis model to consist of cellulose, hemicellulose and lignin, for which heterogeneous, thermal decomposition reactions are formulated. Additionally, the cellulose decomposes partially into tar, which decomposes further into gas. The pyrolysis model consists therefore of five heterogeneous reactions.

The "KLEAA Code" was initially developed, to allow a simulation of the combustion of wood spheres (model fuel) in the KLEAA reactor, but it can be extended to also allow conducting simulations for the combustion of technical fuels such as wood chip and SRFs on a moving grate. Extending the model has to include a mathematical description of the differences between the physical, chemical and geometrical features of said fuels.

Defining these differences makes up the core part of this dissertation and was realized by characterization of three fuels according to the 3-step characterization concept – wood chips and

two solid recovered fuels “BIOBS” and “SBS®1”, both produced by REMONDIS Rheinland GmbH. The physio-chemical analysis in the first step was complemented by a detailed sorting analysis and a near-infrared detection of the main components in the SRFs. Both analyses have proven that the SRFs can be summarized as a mixture of a woody biomass, inert matter (glass, stones, sand) and a number of various plastics. On the basis of these results the “SBS®1” was chosen as a representative solid recovered fuel and a thermogravimetric analysis was performed. It allowed to summarize an SRF as a mixture of wood, polyethylene and ash. In the results, the development of the pyrolysis model included an additional reaction for the thermal decomposition of polyethylene. A necessary characterization of the physical and geometrical properties of the chosen fuels was realized using two parameters important in the models of heat exchange, pyrolysis and char burnout in the “KLEAA Code”: density of the fuel and the specific surface area of its particles. A new measurement methodology for the determination of both parameters was developed. The density was measured with a pycnometer built especially with SRFs in mind. In contrast to other pycnometers in which a liquid or a gas is used, a very fine powder with liquid-like kinematic properties was applied. This allowed to avoid a measurement inaccuracy resulting from a liquid penetrating the pores of the fuel particles. The method was validated for materials with a known geometry and density, and showed a high reproducibility and plausibility of the results. Next the density of the investigated fuels was measured. As expected the wood chips are characterized by a density close to the density of the hard wood, whereas the density of the solid recovered fuel is noticeably higher, regardless of a considerable content of light, spongy particles.

Determination of the specific surface area of the fuel particles was carried out indirectly, by measuring the pressure drop in a cold, unreacted fuel bulk. The surface area was then calculated with three different formulas describing the relation between the pressure drop and the surface area of the particles. In order to validate this method several measurements were performed on bulks consisting of particles with a known geometry, such as spheres, cubes and plates, whereas the best results were obtained for spheres. Furthermore a formula showing the lowest sensibility towards the gas velocity through the fuel bulk was chosen. The measured specific surface areas for the wood chips and the SRF were considerably higher than the surface areas calculated directly from the Sauter mean diameter of their particles.

Characterization of the combustion behaviour of both solid recovered fuels and of the wood chips was realized in the fixed bed reactor „KLEAA” (second step) and in the pilot scale grate firing “TAMARA”. It was described with temporal or local temperatures in the fuel bed, air ratios, gas composition above the bed and with characteristic numbers: ignition time, reaction front velocity, mass conversion rate and specific heat release. The combustion behaviour of the wood chips and of

the “BIOBS” can be described as representative. The quasi-stationary main combustion zone and the following char burnout were observed for the wood chips as expected. “BIOBS” combusted on the other hand without a distinct char burnout, which is a typical combustion behaviour for very wet, biogenic fuels. The results obtained for both fuels in the fixed bed were then transferred onto a moving bed and were validated in the pilot scale plant “TAMARA”. The second solid recovered fuel, the “SBS®1” combusted in the fixed bed differently from typical, biogenic fuels – combustion of volatiles coming from plastic particles laying on the bottom of the reactor was observed also during the char burnout.

The last part of the dissertation discusses the combustion behaviour of the wood chips and the „SBS®1“ simulated with the extended “KLEAA Code”. The measured fuel densities, the specific surface areas and the composition of the solid recovered fuel (assumed as a mixture of wood and polyethylene) were applied as input in the model. The simulated combustion behaviour for the wood chips was accurate in the main combustion zone, but the char burnout was too short comparing to the measurement. The simulated concentration of carbon monoxide and hydrogen above the fuel bed in the main combustion zone were at the same time higher than measured, which indicates that the carbon gasification with water occurs too fast in the model. The combustion behaviour of the “SBS®1” was simulated with a limited accuracy at the beginning of the main combustion zone. Neither the distinct char burnout, nor the combustion of plastics at its end were observed, which may be explained by the missing mass transport of the solid phase between the fuel layers (ideally stirred reactors) in the model. Furthermore the description of a solid recovered fuel with only average surface areas of its particles and with a simplified composition is most probably not sufficient.

The validation of the “KLEAA Code” for the combustion on the moving grate was performed for the wood chips and in a very limited extent for the „SBS®1“. The moving grate of “TAMARA” consists of four separate primary air zones, but the combustion of all three fuels occurred only in the first one due to a high, unavoidable false air input. The mass conversion was simulated correctly for the wood chips and with a moderate accuracy for the solid recovered fuel. Measuring the gas composition in the first primary air zone was however possible only at one location. The gas components measured at these positions were compared with the simulated ones and showed a similar accuracy as for the fixed bed.

Future work should include further development of the measuring methodology for the fuel density and for the specific surface area. An extensive database of the measured values would help to determine the plausibility of the measurements. The development of the “KLEAA Code” should

include incorporating the heat losses and refining the pyrolysis model. Furthermore a more complex description of solid recovered fuels can be recommended.

Kurzfassung

Ein wesentlicher Schwerpunkt der Arbeiten des Instituts für Technische Chemie (ITC) am KIT liegt in der Entwicklung umweltfreundlicher, thermischer Verfahren zur Anwendung von Biomassen, Ersatzbrennstoffen und alternativen Brennstoffen in Hochtemperaturprozessen. Dies wird im ITC mit Hilfe eines im Institut entwickelten 3-Schritt-Charakterisierungskonzeptes realisiert. Eine Biomasse bzw. ein Ersatzbrennstoff wird im ersten Schritt hinsichtlich der chemischen Zusammensetzung untersucht. Im zweiten Schritt erfolgt eine verbrennungstechnische Charakterisierung des Brennstoffs in einem Festbett-Laborreaktor namens „KLEAA“, wobei das ermittelte Abbrandverhalten mit zeitlich lokalen Betttemperaturen, Luftzahlen, Gaszusammensetzung und Kennzahlen wie Zündzeit, Reaktionsfrontgeschwindigkeit, Massenumsatzrate und spezifische Wärmefreisetzung beschrieben wird. Der dritte Schritt umfasst die Übertragung der Ergebnisse vom Festbett auf eine Vorschubrostfeuerung. Dies ist möglich, wenn die Vermischung des Brennstoffs auf dem Rost begrenzt ist, nämlich bei niedrigem Aschegehalt, für einen Wander- oder Vorschubrost, wenn die effektive Brennstoffbettgeschwindigkeit auf dem Rost bekannt ist und wenn die lokale, spezifische Primärluftmenge gleich ist. Das Ergebnis kann in der Pilotanlage des ITC „TAMARA“, die mit einer solchen Feuerung ausgerüstet ist, validiert werden.

Zur Unterstützung und Ergänzung der experimentellen Abschätzung des Verbrennungsverhaltens im Festbett wurde am ITC das numerische Modell „KLEAA Code“ für holzartige Biomasse entwickelt. Dieses auf einer eindimensionalen Kaskade perfekt gemischter Rührkessel basierendes Konzept betrachtet den Brennstoff als eine poröse Schüttung, die vom Gas durchströmt wird. Die Massen-, Element- und Energiebilanz wird daher für beide Phasen formuliert. Die Wärmeübertragung wird sowohl zwischen Feststoff und Gas, als auch zwischen Feststoffpartikeln in benachbarten Rührkesseln berücksichtigt. Sie erfolgt durch Konvektion und Strahlung zwischen den Phasen, und durch Leitung und Strahlung zwischen den Feststoffpartikeln. Stoffübergang ist nur in Richtung vom Feststoff in die Gasphase möglich. Das Pyrolysemodell betrachtet den festen Brennstoff als Zellulose, Hemizellulose und Lignin, für deren heterogene Zersetzung eigene Reaktionen formuliert werden. Die Zellulose zersetzt sich zum Teil in als Levoglucosan angenommenen Teer, der sich weiter in die Gasphase zersetzt. Das Pyrolysemodell besteht daher aus fünf heterogenen Reaktionen.

Der zunächst für kugelförmige Holzpartikel (Modelbrennstoff) im Festbett validierte „KLEAA Code“ kann so erweitert werden, dass es eine Simulation des Verbrennungsprozesses von technischen biogenen Brennstoffen wie Holzhackschnitzel (HHS) und abfallbasierten Ersatzbrennstoffen auch auf einem Vorschubrost ermöglicht. Die Erweiterung des Modells muss dementsprechend chemische, physikalische und geometrische Unterschiede sowohl zwischen einer holzartigen Biomasse und

einem Ersatzbrennstoff, als auch zwischen kugelförmigen und realen Brennstoffpartikeln berücksichtigen.

Die Charakterisierung dieser Unterschiede bildet einen wesentlichen Teil der vorliegenden Dissertation. Um dieses Ziel zu erreichen wurden Holzhackschnitzel (HHS) und zwei durch REMONDIS Rheinland GmbH hergestellte Ersatzbrennstoffe „BIOBS“ und „SBS®1“ gewählt und gemäß dem 3-Schritt-Charakterisierungskonzept untersucht. Die physikalisch-chemische Charakterisierung der Brennstoffe im ersten Schritt wurde um eine detaillierte Sortieranalyse und eine Nahinfraroterkennung der Hauptkomponenten erweitert. Beide Analysen bewiesen, dass die Ersatzbrennstoffe hauptsächlich aus holzartiger Biomasse, Inertstoffen (Glas, Steine, Sand) und einer Mischung von zahlreichen Kunststoffen bestehen. Basierend auf diesen Analysen wurde der repräsentative Ersatzbrennstoff „SBS®1“ gewählt und thermogravimetrisch untersucht, womit dieser Brennstoff sich modellhaft als Mischung von Holz, Polyethylen und Asche mit einem bestimmten Verhältnis zueinander definieren lässt. Die Erweiterung des Pyrolysemodells im „KLEAA Code“ zur Unterscheidung eines Ersatzbrennstoffs von Holz umfasst daher eine zusätzliche Reaktion für die thermische Zersetzung von Polyethylen.

Eine notwendige physikalische und geometrische Charakterisierung der gewählten Brennstoffe erfolgte durch zwei Parameter, die in den Modellen der Wärmeübertragung, Pyrolyse und Feststoffabbrands im „KLEAA Code“ wesentlich sind: die Dichte der Brennstoffpartikel und ihre spezifische Oberfläche. Zur Bestimmung beider Eigenschaften wurde eine neue Grundlage für ein systematisches Messverfahren erstellt. Die Partikeldichte wurde mit einem neuen, speziell für Ersatzbrennstoffe konzipierten Pyknometer gemessen. Im Unterschied zu bekannten Pyknometern, in denen eine Flüssigkeit oder Gas Einsatz finden, wurde ein pulverförmiger Feststoff mit kinematischen Eigenschaften einer Flüssigkeit verwendet. Eine Verfälschung der Messergebnisse durch die in die Poren der Brennstoffpartikel eindringende Flüssigkeit wurde dadurch eliminiert. Das Messprinzip wurde zuerst für Stoffe mit einer bekannten Geometrie und Dichte validiert, und zeigte eine hohe Reproduzierbarkeit der Ergebnisse. Anschließend wurde die Dichte von untersuchten Brennstoffen gemessen. Die Dichte von Holzhackschnitzeln (HHS) war, wie erwartet, sehr ähnlich wie für Hartholz. Der gewählte Ersatzbrennstoff besitzt, trotz einem sichtbaren Anteil von schaumförmigen, leichten Partikeln, eine merklich höhere Dichte als Holz.

Die Bestimmung der spezifischen Oberfläche wurde indirekt durch die Messung des Druckverlustes über ein Brennstoffbett im kalten Zustand realisiert. Zur Validierung der Methode wurden Messungen mit Schüttungen mit einer klar definierbaren Geometrie, wie Kugeln, Quader und Würfel durchgeführt. Die beste Übereinstimmung der tatsächlichen und gemessenen Partikeloberfläche lässt sich für Kugeln erkennen. Drei bekannte Formeln, die einen Zusammenhang zwischen dem

Druckverlust und der Partikeloberfläche herstellen, wurden betrachtet. Gewählt wurde die, die die niedrigste Sensitivität bezüglich der Gasgeschwindigkeit durch das Bett nachweist. Damit wurden die Partikeloberflächen für HHS und einen Ersatzbrennstoff bestimmt, die deutlich höher waren, als die aus der mittleren, mittels einer Siebanalyse ermittelten Partikelgröße (über Sauter-Durchmesser) berechneten.

Die verbrennungstechnische Charakterisierung beider Ersatzbrennstoffe und der HHS wurde in dem Laborreaktor „KLEAA“ (zweiter Schritt) und in der halbtechnischen Vorschubrostfeuerung „TAMARA“ (dritter Schritt) bei definierten Prozessbedingungen durchgeführt. Basierend auf den globalen und lokalen Massen-, Elementar- und Energiebilanzen wurde das Abbrandverhalten mit den zeitlichen bzw. lokalen Betttemperaturen, Luftzahlen, Gaszusammensetzungen und modellhaft mit den Kennzahlen Zündzeit, Reaktionsfrontgeschwindigkeit, Massenumsatzrate und der spezifischen Wärmefreisetzung beschrieben. Das Abbrandverhalten im Laborreaktor kann für HHS und dem Ersatzbrennstoff „BIOBS“ mit sehr hohem biogenen Anteil als repräsentativ bezeichnet werden. Für HHS wurden eine quasi-stationäre Hauptverbrennungsphase und ein nachfolgender Koksausbrand beobachtet. Der feuchte Ersatzbrennstoff verbrannte sehr homogen, ohne eine klare Unterscheidung zwischen beiden Phasen, was ein typisches Verbrennungsverhalten für nasse, biogene Brennstoffe ist. Das im Laborreaktor ermittelte und auf den Vorschubrost „TAMARA“ übertragene Abbrandverhalten wurde durch Testläufe für beide Brennstoffe bestätigt. Der zweite, für Ersatzbrennstoffe repräsentative Brennstoff „SBS®1“ verbrannte jedoch anders – eine Freisetzung von flüchtigen Bestandteilen wurde auch in der Koksausbrandphase beobachtet, was auf die Verbrennung von auf dem Reaktorboden liegenden Kunststoffteilchen zurückzuführen ist. Für diesen Brennstoff erfolgte keine Übertragung der Ergebnisse vom Festbett auf den Vorschubrost.

Im letzten Teil der Arbeit wurde die Verbrennung von HHS und des gewählten Ersatzbrennstoffs „SBS®1“ mit dem erweiterten Modell des „KLEAA Code“ für das Festbett berechnet. Die gemessenen Brennstoffdichten, Partikeloberflächen und die chemische Zusammensetzung des Ersatzbrennstoffs (als Holz- und Polyethylen-Gemisch angenommen) wurden dabei verwendet. Die durchgeführte Simulation fürs Hackgut lieferte ein sehr gutes Ergebnis bezüglich des Massenumsatzes in der Hauptverbrennungszone. Der Koksausbrand konnte aber nicht korrekt simuliert werden und war zu kurz im Vergleich zu dem gemessenen. Die simulierten Konzentrationen von Kohlenstoffmonoxid und Wasserstoff waren in der Hauptverbrennungszone höher als die gemessenen, was auf einen zu hohen Kohlenstoffumsatz im Modell hinweist. Das Verbrennungsverhalten des Ersatzbrennstoffs wurde nur mit einer begrenzten Genauigkeit am Anfang der Hauptverbrennungszone simuliert. Weder ein klar sichtbarer Koksausbrand, noch die in der Praxis beobachtete Verbrennung von Kunststoffen im Koksausbrand konnte im Modell wiedergegeben werden, was wahrscheinlich durch

eine fehlende Berücksichtigung des Feststofftransports zwischen den Schichten (Rührkesseln) zu erklären ist. Des Weiteren ist die Beschreibung eines sehr komplexen Ersatzbrennstoffs mit nur mittleren Partikeloberflächen und einer vereinfachten Zusammensetzung höchstwahrscheinlich nicht ausreichend.

Die Validierung des „KLEAA Codes“ wurde für die Vorschubrostfeuerung für HHS und in einem sehr begrenzten Umfang für den Ersatzbrennstoff „SBS®1“ durchgeführt. Der Rost „TAMARA“ besteht aus vier gleich langen Primärluftzonen, wobei die Verbrennung für alle Brennstoffe auf Grund hoher Falschluftmengen schon in den ersten beiden Zonen vollständig abgeschlossen war. Der Massenumsatz wurde in diesem Bereich für HHS korrekt und auch für „SBS®1“ einigermaßen befriedigend simuliert. Die Messung der Gaszusammensetzung über dem Rost war in der ersten Primärluftzone jedoch nur an einer Messstelle möglich. Die Messwerte für die Gaskomponenten an dieser Messposition wurden mit ihren simulierten Verläufen verglichen und zeigten eine ähnliche Genauigkeit wie für das Festbett.

Die zukünftige Arbeit sollte eine weitere Entwicklung der Messmethode zur Bestimmung der Brennstoffdichte und der Partikeloberfläche umfassen. Eine umfangreiche Datenbasis der Ergebnisse kann eine Plausibilitätsprüfung der gemessenen Werte deutlich erleichtern. Die Weiterentwicklung des Modells sollte die Wärmeverluste und eine Verfeinerung des Pyrolysemodells berücksichtigen. Des Weiteren ist eine genauere, modellhafte Beschreibung eines Ersatzbrennstoffs hinsichtlich der Zusammensetzung und der physikalischen Parameter wünschenswert.

List of symbols

Symbol	Description	Unit
a	cube's edge length	m
A	surface area	m^2
c	gas concentration	$\%$
c_p	specific heat capacity (constant pressure)	$J/kg \cdot K$
D	diffusion coefficient	$-$
d_p	particle diameter	m
e	distance between two consecutive thermocouples in the KLEAA fixed bed reactor	mm
Gr	Grashof number	$-$
h	specific enthalpy	J/kg
H	enthalpy	J
$\dot{H}$	enthalpy flow	W
HR_{Grate}	specific heat release	W/m^2
IR	ignition rate	$kg/m^2 \cdot s$
k	reaction rate coefficient	$1/s$
k_0	Arrhenius factor	$1/s$
ΔL	height of the material bulk in the pressure drop measuring instrument	m
l	mean free path length of gas particles flowing through a packing	m
l_{zone}	length of a grate zone	m

M	molar mass	$kg/kmol$
m	mass	kg
$\dot{m}$	mass flow	kg/s
MCR	mass conversion rate	$kg/m^2 \cdot s$
NCV	net calorific value	kJ/kg
n	relative heat loss	$\%$
Nu	Nusselt number	$-$
P	pressure	Pa
p	plate's edge length	m
Δp	pressure drop	Pa
Pr	Prandtl number	$-$
q	plate's edge width	m
$\dot{Q}$	heat flow	W
r	reaction rate	kg/s
R	gas constant	$kJ/kmol \cdot K$
Ra	Rayleigh number	$-$
Re	Reynolds number	$-$
s	plate's edge height	m
S_V	Specific volumetric surface area of the fuel	m^2/m^3
t	time	s

t_{IG}	ignition time	s
t_{res}	total actual residence time of a fuel particle on the grate	s
$t_{res,i}$	theoretical residence time of a fuel particle in the grate zone i	s
$t_{res,theor}$	total theoretical residence time of a fuel particle on the grate	s
T	temperature	K
u	velocity	m/s
u_{bed}	effective velocity of the fuel bed on the moving grate	m/s
u_{RF}	reaction front velocity	m/s
u_{GB}	velocity of a single grate bar	m/s
u_{Grate}	component of the grate bars velocity perpendicular to the grate surface	m/s
V	volume	m^3
v_g	velocity of the gas	m/s
$\dot{V}$	volumetric flow	m^3/s
w	amplitude	mm
x	mass fraction	kg/kg_{gas}
y	volume fraction	m^3/m^3_{gas}

α	absorptivity coefficient	$-$
α	heat transfer coefficient	$W/m^2 \cdot K$
η	dynamic viscosity of the gas	$kg/m \cdot s$
ε	emissivity coefficient	$-$
φ	level of coverage	$-$
γ	accommodation coefficient	$-$
$\xi_{Ash,F}$	ash content in the fuel	kg_{ash}/kg_{fuel}
ξ_{FA}	fraction of the leaked air incoming into the primary air zone	$-$
λ	thermal conductivity	$W/m \cdot K$
ν	kinematic viscosity	m^2/s
ψ	porosity of the material bulk in the pressure drop measuring instrument	$-$
Ψ	heat loss factor	$-$
ρ_{bulk}	bulk density of the solid	kg/m^3
ρ_{solid}	density of solid measured with the pycnometer	kg/m^3
ρ_{fluid}	density of the fluid used during the pycnometry	kg/m^3
ρ_{air}	air density	kg/m^3
σ	Stefan-Boltzmann constant	$W/m^2 \cdot K^4$
ϑ	temperature	$°C$
ω	angle between the grate bar surface and the overall grate surface	°

Indices and abbreviations:

Ash	ash
$Burn$	burnout
BW	water supplied to the boiler
Dry	drying
f	furnace gas
LA	leaked air
fb	fuel bed
FG	flue gas
fs	between furnace (gas) and solid
$fuel$	of the fuel
gas	of the gas
GCS	Gas cleaning system
het	heterogeneous
i	variable
in	incoming
j	fuel layer (control volume)
k	gas species
ll	between consecutive fuel layers (control volumes)
lam	laminar
out	outgoing
PA	primary air
PLS	Process control system
pp	between solid particles
pyr	pyrolysis
RG	raw gas

re	of the reaction
rad	radiative
res	residence
s	solid
sp	solid particle
SA	secondary air
sg	between solid and gas
th	theoretical
tur	turbulent
w	furnace wall
wf	between furnace wall and furnace (gas)
ws	between wall and solid
wv	water vapour

1. Introduction

1.1. Motivation

Co-firing biomass material and bio-waste with coal in power and CHP plants is a widely recognized method and an important way to achieve internationally agreed targets for the reduction of greenhouse gas emissions. Because of limited resources of fresh, forest biomass the power plant operators face the challenge of finding other sources of cheap and sustainable biofuels. Agricultural waste, by-products of the forest management and solid recovered fuels (SRF) from municipal and commercial solid waste with a high biogenic fraction can be in this case an attractive alternative, provided that the utilisation of such secondary fuels is economical, environment-friendly and does not cause reduction of the plant availability. Generally higher inhomogeneity of these fuels than of regular fuels leads in power plants with forward acting grate firing to non-homogenous local combustion conditions in the fuel bed and in the combustion chamber, what makes optimisation of the combustion process and fulfilling above-mentioned conditions difficult. Such fuels contain also more harmful substances, including chlorine, which can damage firing installations especially through a high-temperature corrosion of the boiler tubes. Even relatively clean biomass waste can change the combustion behaviour in the furnace and alter the melting temperature of solid combustion products what can lead to slagging of the furnace and boiler walls. Last but not least, these alternative fuels present different combustion behaviour than regular fuels and they need to be described with regard to the combustion process. Investigation and solving of the above-mentioned problems is scheduled in the German strategy for the development of sustainable, renewable energy sources in the upcoming years constituted by the German Federal Ministry for Environment Protection, Nature Conservation and Nuclear Safety (1). In response to this plan, an experimental research of physicochemical processes in a fuel bed during combustion of various SRFs, biomass types and their mixtures have been performed at the Institute of Technical Chemistry, at KIT inter alia in the framework of EU project “RECOMBIO” (2).

The project was concerned with the development and demonstration of innovative approaches to the highly efficient co-utilisation of biomass and Solid Recovered Fuels (SRF) produced, among others, from municipal solid waste (MSW) and commercial waste (CIW) for electricity production and combined heat and power (CHP) usage, at competitive costs, high plant availability and advanced energy efficiency.

The production of a quality controlled biomass, bio-residues, SRF and also an intelligent fuel management at the manufacturer and user side was essential to the project success, and was investigated and demonstrated in the frame of the project. The findings are substantial for the future

biomass power generation or CHP projects, as different technologies meeting the best available techniques (BAT) standards were incorporated to demonstrate the highly efficient utilisation chain for the intelligent co-utilisation of biomass and SRFs. Institute for Technical Chemistry at KIT investigated physiochemical properties of two solid recovered fuels, SBS®1 and BIOBS delivered by REMONDIS GmbH and characterised their combustion behaviour in a fixed bed reactor and in a pilot-scale waste incinerator, which geometry and main components correspond to large-scale waste incinerators and power plants equipped with forward acting grates.

It was suggested in the project RECOMBIO to perform a number of demonstrations of relevant SRF production and utilisation technologies with new developments, substantial investments, long-term monitoring, assessment of the key technical aspects, Life Cycle Analyses (LCA) and enhanced material recycling. The achievement of the goals, transfer of knowledge and technology gained in the project occurred through the normal business activities of the utilities, producers, and manufactures. Along with providing valuable information to support future decisions by key utilities, manufacturers, authorities, etc., the results assist the European Commission regarding re-examining targets set in the European Union's Directives and the recovery option in the waste hierarchy of the Waste Directive.

The overall objective was to enhance the future use of biomass and SRFs, facilitate the creation of a sustainable energy market across Europe and demonstrating the use of short-term available technologies that can reduce CO_2 emissions significantly and cost-efficiently (2).

1.2. The scope of the thesis

Tasks discussed in this thesis can be divided into two categories – experimental and theoretical. Experimental part includes the work realised for the project RECOMBIO. Different mixtures of chosen SRFs with biomass were investigated regarding their combustion behaviour in the fixed bed reactor KLEAA at the Institute for Technical Chemistry at KIT. Combustion in this reactor can be described using several key parameters; reaction front velocity, ignition rate, mass conversion rate and specific heat release. These characteristic numbers build up a model which is easily applicable to describe the combustion on a forward acting grate and which has proven itself to be a convenient tool for a preliminary estimation of basic parameters of the grate (e.g., length, width). Results obtained from the combustion tests at KLEAA were transferred using this model to describe the combustion process of the investigated fuels in a forward acting grate furnace. In order to validate obtained combustion characteristics, a measurement campaign in the pilot scale grate furnace TAMARA (also at KIT) has been conducted.

A better understanding of the combustion process of woody biomass and solid recovered fuels in grate furnaces demands more detailed model calculations. Such mathematical model of a combustion process in a fixed bed reactor which can be later on transferred to a grate furnace is being developed at ITC under the name "KLEAA Code" (3). Although its boundary conditions have been defined with the particular reference to the KLEAA reactor it can be easily modified and applied for different batch reactors (3). A version of the model available at the beginning of the project RECOMBIO allowed simulation of the combustion of wood spheres.

Certain modifications discussed in chapter 6 made simulating the combustion of SRFs in a grate furnace using the "KLEAA Code" model possible. Defining these assumptions, appropriate laboratory experiments needed for improvement of the model and its validation are the theoretical objectives of this thesis. Within this part of the work a usefulness of the model as a tool to simulate the SRF combustion in forward acting grate firings has to be determined through comparison of the results generated by the model with actual experimental data obtained at KLEAA and TAMARA research facilities. Schematic overview of the objectives can be found below (Figure 1.1). Dashed lines symbolise the tasks to be carried out.

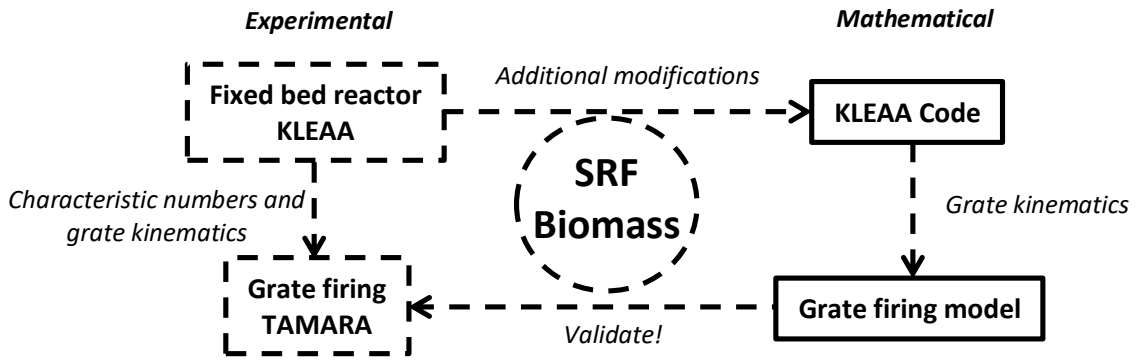

Figure 1.1 – Schematic overview of the scope of the thesis

Objectives of the thesis can be summarised as follows:

- Investigation of the combustion behaviour of SRF/biomass mixtures in the KLEAA fixed bed reactor,
- Transfer of these results to a forward acting grate using characteristic numbers,
- Validation of the results during measurement campaign in the grate furnace TAMARA,
- Defining improvements which are needed to simulate the SRF combustion with the KLEAA Code,
- Experiments to determine physical properties of chosen SRFs and biomass needed for the simulation,

- Simulation of the combustion of the experimentally investigated fuels,
- Comparison of the results, validation and evaluation of the KLEAA Code.

2. Theory and literature overview

General information about solid recovered fuels will be provided in this chapter. Further on the current state of knowledge in the field of experimental research of the combustion behaviour in different combustion systems will be discussed. The final part of this chapter consists of the current state of mathematical modelling of the combustion in fixed and moving solid fuel beds.

2.1. Solid Recovered Fuels

2.1.1. Definition and standardisation

There was no legal or universally accepted definition of solid recovered fuels in the EU before the beginning of RECOMBIO which was a major obstacle before achieving the project objectives. Generally the term "waste-derived fuels" refers to a combustible, high calorific fraction of the municipal, commercial or industrial waste i.e., paper, wood, plastics and cardboards subjected to the biological (composting), physical (drying) and mechanical (shredding) treatment. The term "solid recovered fuel" stands for a waste-derived fuel with a quality specified according to certain properties of the fuel. A unification of the existing definitions of refuse-derived fuels (RDF) and their standardisation under the name SRF is a task of the European Committee for Standardisation (CEN; CEN/TC 343). CEN/TC 343 defines SRF as *solid fuel prepared from non-hazardous waste* (hazardous waste as defined in directive 91/689/EEC (4)) *to be utilised for energy recovery in incineration or co-incineration plants, and meeting the classification and specification laid down in CEN/TS*. CEN/TC Work Group 2 (Fuel Specifications and Classes) decided to classify SRF using a system based on a limited number of properties. Currently, the classification is defined by the standard EN 15359 (5) and distinguishes three aspects, each characterised by a single property:

Table 2.1. Significant aspects and properties of SRFs

Aspect	Property
Economics	Net calorific value (NCV)
Technology	Chlorine content (Cl)
Emissions	Hg in flue gas

Net calorific value has a significant importance for economic aspects, as it defines the fuel price, transportation costs and potential profit for the power plant operator. Minimum NCV of 3 MJ/kg (as received) has been determined on the basis of experience in SRF combustion in cement kilns and on the calculated calorific gain according to EN 13531 (6). In order to be recoverable in form of energy (heat), the waste shall give a calorific gain in the recovery process. This is assumed to be fulfilled when the NCV exceeds the amount of energy needed to adiabatically heat up the gaseous products

of combustion from the ambient temperature (25°C) to a specified final temperature. In case of the waste, this final temperature is determined by the Waste Incineration Directive (7) and equals 850°C for the gaseous products of combustion containing 6 vol. % of oxygen. Combustion temperatures calculated in (6) for common packaging materials (and an usual input material for the production of SRFs) indicate, that 2.5MJ/kg is the lowest possible NCV by which these temperatures exceed 850°C and satisfy requirements of (7). NCV of 3MJ/kg specified as the minimum by (5) might still be considered a very low value by power plant standards (Table 2.2), but SRFs with such low NCVs are mostly fired in cement kilns, where the ash produced from these fuels is meant to enrich raw cement mix and the heat production is of secondary importance.

Chlorine present in SRFs and other fuels contributes to the forming of salts which in a molten state are responsible for the high-temperature corrosion of the heat exchanging surfaces in boilers (superheaters). Other halogens have similar effects, but their concentration in fuels is usually very low in comparison to chlorine. Fuels with less than 0.3 [wt. % dry] of chlorine content can be used in boilers with no major problems. In practice up to 3 [wt. % dry] of chlorine can be found in currently produced solid recovered fuels. This value represents also the highest allowed content of chlorine in a waste-derived fuel, below which this fuel can be recognised as an SRF (5) (Table 2.2).

Fossil fuels, waste and refuse derived fuels contain traces of toxic heavy metals such as mercury, thallium, cadmium, lead or arsenic which are released during the combustion according to (8) and (9). Although mercury is found in fuels in relatively low concentrations in comparison to other heavy metals (9) it has the lowest vaporisation temperature (10) (Figure 2.1). Vapours of other heavy metals condense mostly on the surface of fly ash particles and are efficiently removed from the gas phase in cyclones and ESP filters (11) while mercury tends to be discharged with the flue gas into the atmosphere. Due to its high volatility, toxicity and tendency to accumulate in organisms, mercury is one of the most dangerous gaseous pollutants and has been chosen as a key property determining the aspect of emissions in the future CEN standard for SRFs (Table 2.2).

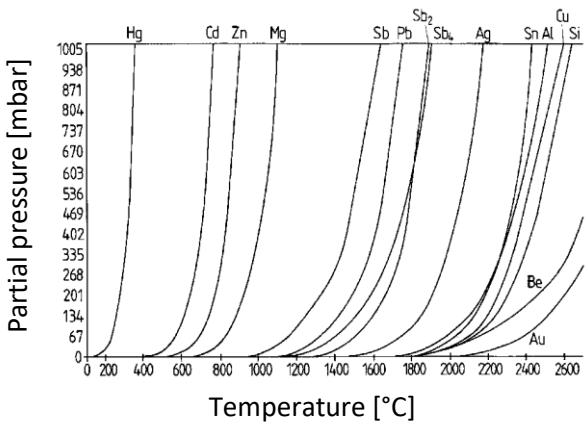

Figure 2.1. Partial pressure of heavy metals vapours in raw gas (10)

Classification system relies on 5 classes defined by ranges of each property and can be applied for trading, permitting procedures and other activities.

Table 2.2. Classification of SRFs according to EN 15359 (5), *as received

Classification property	Designation	Unit	Classes				
			1	2	3	4	5
Net cal. val.	NCV, net	MJ/kg (ar*)	≥25	≥20	≥15	≥10	≥3
Chlorine	Cl	% (dry, median)	≤0.2	≤0.6	≤1.0	≤1.5	≤3.0
Mercury	Hg	mg/MJ (median)	≤0.02	≤0.03	≤0.08	≤0.15	≤0.50
		mg/MJ (80^{th} percentile)	≤0.04	≤0.06	≤0.16	≤0.30	≤1.00

Solid recovered fuel can be characterised also by the content of the biogenic carbon. Ways for its determination are recommended in the EN 15440 (88) and comprise of three methods:

- Selective Dissolution Method (SDM) – based on the reaction of biomass in a mixture of sulfuric acid and hydrogen peroxide. The method is not appropriate if the SRF sample has biomass components that are insoluble in sulfuric acid or fossil-based components that are soluble in the acid. According to EN 15440, SDM must not be applied if the following materials are contained at levels above 5%: solid fuels (e.g. hard coal, coke, brown coal, lignite and peat), charcoal, biodegradable plastics of fossil origin, non-biodegradable plastics of biogenic origin, oil or fat present as a constituent of biomass, natural and/or synthetic rubber residues, wool, viscose, silicon rubber, or nylon, polyurethane or other polymers containing molecular amino groups. For rubber residues, the threshold is 10%.
- Manual Sorting – This method entails visual inspection, thus it is ineffective when the SRF components are shredded finely or compressed. It is only applicable to materials with a particle size greater than 10 mm and where optically and physically distinguishable fractions can be separated and quantified.
- Carbon-14 Method – This method measures the radiocarbon content of the mixed wastes and is applicable to all materials. The biogenic content of SRF is linked to the age of the carbon released as carbon dioxide during combustion. It is based on the analysis of the radioactive isotope carbon-14 which allows a distinction of fossil carbon, in which the originally existing 14C is decayed, and modern (biogenic) carbon, which exhibits the current 14C/12C-Level. Thus the biogenic fraction is proportional to its 14C content and can easily be determined.

As mentioned before solid, refuse-derived fuels consist of the high calorific fraction of municipal, commercial or industrial wastes subjected to a biological and mechanical treatment, which is carried out at mechanical biological treatment plants specially configured for this purpose.

2.1.2. Production

The concept of mechanical biological treatment of waste (MBT) has been developed as an answer to the need for reduction of biodegradable waste quantities sent to landfill and for the potential recovery of resources during the process. Components (Table 2.3) of two main stages, mechanical and biological can be organized in different ways, depending on the objectives of a particular MBT plant i.e.:

- Maximising resource recovery,
- Produce compost,
- Produce soil fertiliser,
- Produce biologically stabilised waste for landfilling,
- Produce biogas for heat and/or power generation,
- Produce solid recovered fuel (12).

Table 2.3. Typical components of an MBT plant (12), *Near Infra-Red detectors for separation of certain materials (e.g., PVC)

Process stage	Process elements						
Mechanical	Drum	Screen (static/vibrating)	Magnet	Eddy current	Hand picking	Air classification	NIR*
Biological	Open window composting	In-Hall composting	Tunnel composting	In-Vessel composting	Anaerobic digestion	Percolation	Bio-drying

Mechanical processing including sorting and size classification is conducted before any biological treatment in most cases. MBT plant of REMONDIS-GmbH in Erftstadt which produces two fuels investigated in the project RECOMBIO is similar in this concept. It consists in general of:

- Waste admission area for municipal, commercial and bulky waste,
- Sorting and splitting plant,
- Facility for bio-drying of low calorific fractions for municipal solid waste incinerators,
- Fuel production plant where the individual shredded waste fractions are mixed together in accordance with the fuel recipe,
- Storage for produced fuels (13).

Production of both fuels, BIOBS (German: BIOBrennStoff) and SBS®1 (German: SubstitutBrennStoff, first quality) includes sorting of the input material with a near-infrared detector and splitting its stream with wind shifters. Heavy fraction – stones, glass, ferrous and non-ferrous metals, and alloys are separated in this procedure in several steps. A stream of the prepared material is then shredded in a two-step process. Physical and chemical properties of these fuels will be extensively discussed in Chapters 4 and 5.

2.2. Combustion process of solid fuels – stages of the process

In this section, the stages of combustion of solid fuel will be discussed. As stated before, the thesis concerns fuels mentioned for grate furnaces i.e., solid, combustible material with particle sizes varying between several millimetres up to several centimetres. Combustion behaviour of these fuels can be investigated in reactors where the combustion takes place in a fixed bed. Under "fixed bed" a fuel packing in an insulated, cylindrical vessel is meant, where the primary air is supplied from below and the ignition takes place due to absorption of the heat radiation coming into the top layer of the fuel. The process itself can be divided into a number of quasi-stationary stages: drying, pyrolysis (devolatilisation), gasification and char combustion (burnout) (Figure 2.2).

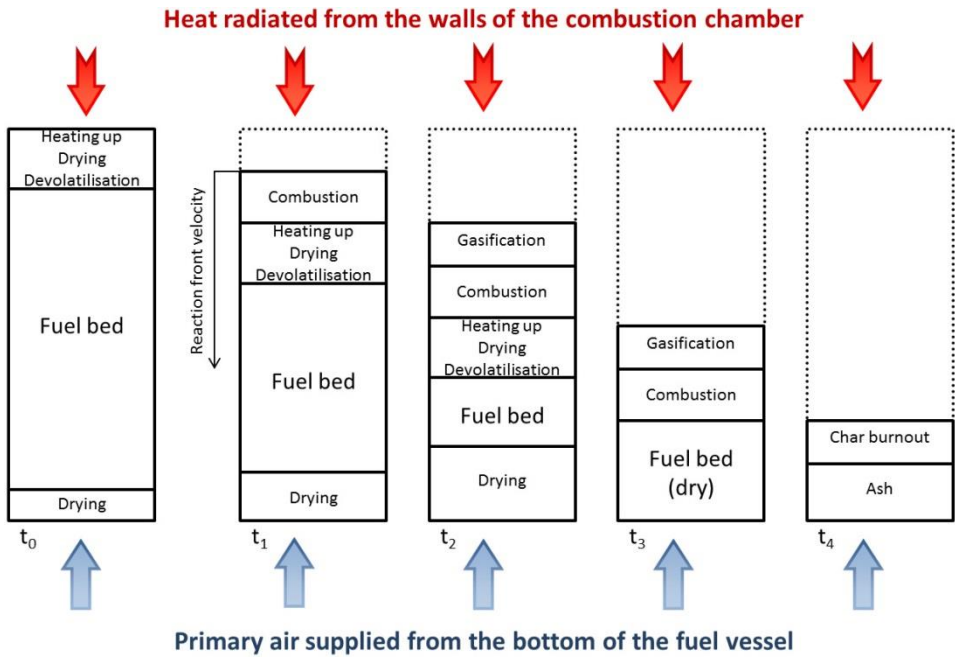

Figure 2.2 – Simplified presentation of the combustion stages in a fixed fuel bed

It is assumed that the air supplied into the porous fuel bed from below is not preheated. The top layer of the fuel is submitted to a radiative heating from the source above the fuel bed (i.e., walls of a combustion chamber). At first (t_0) two fronts are formed under influence of both factors – drying front from below and heating front from the top, which also leads to drying of the humid fuel. Increasing temperature leads in one moment to the release of volatiles through pyrolysis and then to

their further heating up, cracking and finally ignition (t_1). Further on the so-called main combustion phase starts and takes place (t_2). In the meantime, the fuel is dried from below by the incoming primary air and the remaining water is completely removed from the fuel some time (t_3) during the main combustion zone. When all the volatiles from the fuel are released (t_4) the remaining fixed carbon is ignited and burned out.

2.2.1. Drying

The first combustion stage of a humid, solid fuel – drying can be subdivided with regard to the temperature of the fuel into evaporation which takes place when the temperature of a humid fuel lies below boiling point and boiling which starts when the temperature of the fuel reaches the boiling point. The rate of drying or more precisely the rate of the vaporisation of water out of a fuel particle depends on three factors; the rate at which the water is transported out from the pores in a fuel particle, the rate of the water vapour transport from the surface of a particle and the heat transfer rate from the surroundings into the fuel particles. At first, the humidity being vaporized from the surface of the particle is being constantly replaced by the water from the capillaries (pores). The rate of this process is independent of the water content in the fuel and is largely governed by the transport kinetics from the surface of the particle to the surroundings. In the second stage, the drying front travels into the pores when the water on the surface of the particle cannot be replaced fast enough through the capillary action. This process proceeds at a lower rate than the first one, as it is slowed down by the diffusion. During the last, third stage the hygroscopic humidity from the particle insides is being vaporized. Because of the lack of water on the surface of a particle, it is much hotter on the surface than in the insides, therefore degassing, pyrolysis and drying can occur simultaneously in this phase.

2.2.2. Pyrolysis

Pyrolysis is a thermal decomposition of a solid fuel in the atmosphere without adding oxidizing agents. This simple definition does not express the whole complexity of pyrolysis which is a thermochemical chain of processes resulting in the production of a huge amount of chemical compounds. Description of this process can be simplified for most engineering applications and the pyrolysis products can be divided into three groups: permanent gases (CO_2, CO, CH_4, H_2 and hydrocarbons with a low boiling point), pyrolytic liquid (tars and water) and char. Yields and composition of these products are governed by several key parameters such as temperature, pressure, residence time and heating rate. Physicochemical parameters of the fuel; composition, ash content and composition, particle size and surface area, density and moisture also have a significant impact on the composition of the products. More detailed mathematical description and modelling of biomass pyrolysis along with the model used in the thesis will be described in Chapter 6.

2.2.3. Gasification and combustion

The gasification of a solid fuel can be divided into the heterogeneous conversion of the fixed carbon into gaseous products and the homogenous conversion of gaseous volatiles produced during pyrolysis. The most important reactions taking place during the gasification phase are listed below. Reaction enthalpies are calculated on the basis of the standard enthalpies of formation and Hess's law:

Heterogeneous:

- Boudouard reaction: $C_{fix} + CO_2 \leftrightarrow 2CO$ $\Delta_R H = 172.5\ \frac{kJ}{mol}$
- Water gas reaction: $C_{fix} + H_2O \leftrightarrow CO + H_2$ $\Delta_R H = 131.3\ \frac{kJ}{mol}$
- Forming of methane: $C_{fix} + 2H_2 \leftrightarrow CH_4$ $\Delta_R H = -74.9\ \frac{kJ}{mol}$

Homogeneous:

- Cracking of tars: $C_n H_m O_l \rightarrow iCO + jH_2 + kC_v H_w$ $\Delta_R H > 0.0\ \frac{kJ}{mol}$
- Water-gas shift reaction: $CO + H_2O \leftrightarrow CO_2 + H_2$ $\Delta_R H = -41.2\ \frac{kJ}{mol}$
- Forming of methane: $CO + 3H_2 \leftrightarrow CH_4 + H_2O$ $\Delta_R H = -206.2\ \frac{kJ}{mol}$

If the process takes place under abundance of oxygen (air ratio $\lambda \geq 1$) the combustion can occur additionally to the gasification. Two types of the combustion can be distinguished – homogenous burnout of the gasification and pyrolysis products and the heterogeneous burnout of fixed carbon:

Heterogeneous:

- Partial oxidation of fixed carbon: $C_{fix} + 0.5O_2 \rightarrow CO$ $\Delta_R H = -110.5\ \frac{kJ}{mol}$
- Oxidation of fixed carbon: $C_{fix} + O_2 \rightarrow CO_2$ $\Delta_R H = -393.5\ \frac{kJ}{mol}$

Homogeneous:

- Oxidation of carbon monoxide: $CO + 0.5O_2 \rightarrow CO_2$ $\Delta_R H = -283.0\ \frac{kJ}{mol}$
- Oxidation of hydrogen: $H_2 + 0.5O_2 \rightarrow H_2O$ $\Delta_R H = -285.9\ \frac{kJ}{mol}$
- Burnout of volatiles: $C_n H_m O_l + (n + 0.25m - 0.5l)O_2 \rightarrow nCO_2 + 0.5mH_2O$ $\Delta_R H < 0.0\ \frac{kJ}{mol}$

2.3. Experimental investigation of the combustion behaviour of solid fuels in different combustion technologies

There are many different technologies currently utilized for the combustion of solid fuels. Grate firings with a fixed fuel bed (Figure 2.3a) are the first combustion technology for solid fuels, which found broader use in the industry. Successive improvements of its construction over the 19th century (e.g., mechanical fuel feeding) led to the implementation of reciprocating grate bars at the beginning of the 20th century (Figure 2.3b). Widely used combustion systems are also boilers with a bubbling fluidized bed (Figure 2.3c), circulating fluidized bed (Figure 2.3d), boilers equipped with a burner designed for combustion of pulverized fuels (Figure 2.3e) and rotary kilns (Figure 2.3f). Systems c-f are not a subject of this thesis and will be mentioned only briefly in 2.3.3.

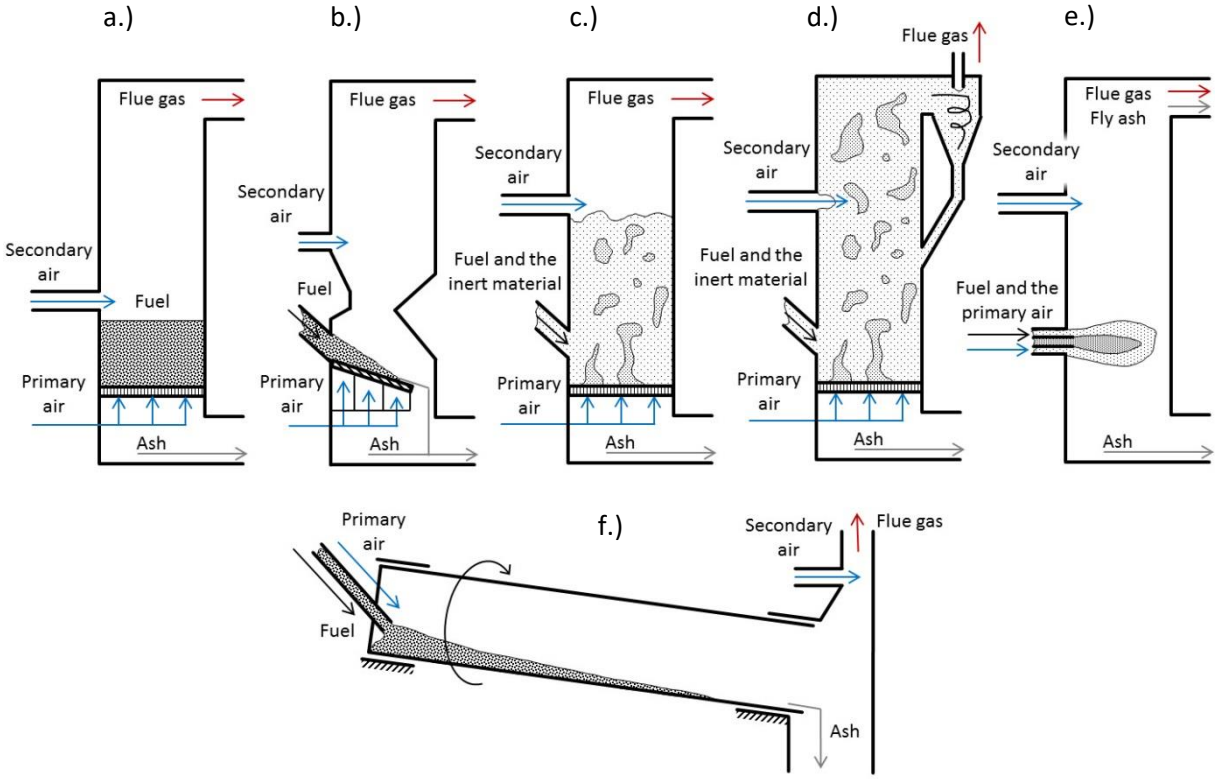

Figure 2.3 – Combustion technologies for solid fuels

2.3.1. Combustion in a fixed bed

Systems for the combustion of solid fuels in fixed beds for the electricity or steam production are nowadays obsolete and have been replaced by systems with moving grates, fluidized beds and burners for pulverized fuels. Combustion in fixed beds has, however, its well-established place in the steel industry in form of blast furnaces used for smelting of metals. Furthermore, small wood-burning stoves and boilers are commonly used for domestic heating. Relevant for this study is, however, the scientific use of laboratory scale facilities where the combustion takes place in a fixed fuel packing (e.g., KLEAA reactor). These small fixed bed reactors allow relatively simple and cheap investigation

of the combustion behaviour of a wide variety of solid fuels under fully controlled conditions. It can be assumed that all stages of combustion mentioned in 2.2 occur in a fixed bed chronologically one after another while locally in a moving bed (along the grate) which allows an easy transfer of the results from a small, laboratory scale fixed bed reactor onto large moving beds. Below in this section, a short overview of already carried out research in fixed beds is discussed. In section 2.3.2 an overview of the research of combustion in moving beds is presented.

In 1934 Nicholls (14) investigated the combustion behaviour of coal and coke in a packed bed and described a propagation of the reaction front in this bed. Nicholls connected the speed of fuel conversion and its ignition rate to the primary air flow, primary air temperature and the diameter of a fuel particle and derived a mathematical model describing these relationships. Nicholls noticed that the ignition rate is higher than the fuel conversion rate for small primary air flows and both values become higher when the primary air flow increases. Furthermore, it has been noticed that the ignition rate decreases with the increasing diameter of the fuel particles.

Increasing interest in waste incineration led Weintraub (15) to the research on the combustion of a model waste consisting of wood chips, paper, cardboard, and vegetables. The study was focused on the combustion behaviour of volatiles released from the bed in relation to the primary air flow and water content in the fuel. The conclusion was that the fuel conversion rate drops with increasing humidity of the fuel and rises with increasing primary air flow.

An important research on the combustion of waste was carried out by Rogers (16). Similar to the previous study a simplified (model) waste was combusted in a fixed bed, whereas primary air flow was varied. Rogers concluded that the combustion process of waste propagates analogous to the combustion of coal i.e., a reaction zone after ignition is formed, which moves in the opposite direction to the primary air flow and propagates faster when the primary air flow is increased. Additionally, it has been found out that the burnout behaviour changes as the reaction front reaches the bottom of the fuel bed. Two different kinds of the combustion behaviour were defined – underfeed burning which means that the combustion occurs in the opposite direction and overfeed burning (char burnout) taking place at the end of the grate with slower conversion rate and co-current to the primary air flow (similar as in 24).

Influence of the fuel particle size, fuel humidity and also primary air flow on the combustion behaviour of shredded municipal solid waste and wood was also researched by Gort in his doctoral dissertation (17). Gort determined three regimes of the investigated process: gasification regime, combustion regime, and complete combustion regime. At small amounts of supplied primary air the process is under-stoichiometric, released volatiles are not completely oxidised and partially

unburned solid is accumulated on top of the bed. Under this regime, the ignition front propagates faster than the conversion rate. With increasing primary air flow this regime passes to the combustion regime in which ignition and conversion rates are equal, unburned solid is not accumulated any more, but volatiles above the bed are still not completely combusted. The last regime – complete combustion regime takes place when the amount of supplied primary air is sufficient to guarantee also the complete burnout of volatiles above the bed. Gort also noticed that further increase of the primary air amount beyond the complete combustion regime leads to the reduction of ignition rate. Similar research was also conducted by Fatehi and Kaviany (18), Shin and Choi (19), Rönnbäck (20), Yang (21) (22) and van Kessel (23). All of these researchers performed combustion experiments of various wood particles and concluded, that the reaction front velocity increases with decreasing particle size. They also divided the combustion process into three regimes depending on the primary air amount.

A lot of research on the combustion behaviour of various biomasses, wastes and solid recovered fuels has been realized also at the Institute of Technical Chemistry at KIT (former ITC-TAB at Forschungszentrum Karlsruhe). Schumacher (24) used newly built fixed bed reactor KLEAA to investigate an influence of the water content, ash content, primary air amount and primary air temperature on the combustion behaviour of wooden cubes with a variable content of inert, ceramic rings. His conclusions were similar to those of the former researchers mentioned in this overview. Bleckwehl (25) developed and validated a mathematical model for the fuel characterization on the basis of several characteristic values (ignition time, ignition rate and mass conversion rate). He performed several combustion and co-combustion tests with wood chips, shredded municipal waste and pelletized fuel from waste (German BRAM – Brennstoff aus Müll) in order to do so. Afterwards Bleckwehl used the model to transfer obtained results onto the grate firing TAMARA. The model itself is a part of the so-called “three-step characterization concept” (see chapter 4) widely applied at ITC for the description of the combustion behaviour of low-quality fuels. Bleckwehl also found out that the fuel conversion rate strongly depends on the particle size (see also (17)) but not on the particle form. Three different forms (spheres, pellets and cuboids) with the same surface area of the particles were investigated and the rate of the fuel conversion was the same in each case.

Gehrmann et al. (26) investigated a co-firing behaviour of wood chips and an SRF mixed in different proportions and combusted under different primary air temperatures. The conclusion was that two phases of combustion can be identified when the primary air is preheated. These phases should not be confused with the quasi-stationary phase of volatiles release and the phase of char burnout. Phase I takes place in a humid fuel and proceeds as fast as with no air-preheating. When the ignition front travelling downwards reaches the drying front moving upwards (facilitated by the preheated

air) the phase II begins. It proceeds much faster than phase I and higher temperatures are obtained. Furthermore, Gehrmann found out that an increase of the SRF share in the fuel blend leads to an increased reactivity of the mixture i.e., speeds up the ignition front velocity.

2.3.2. Combustion in a moving bed

The combustion process occurs in this case on a moving (reciprocating) grate. The grate itself is usually divided into several primary air zones, which are separately controlled. This assures that every phase of the fuel conversion (drying, pyrolysis, degassing and char burnout) receives enough air to complete the process and that the temperature in the fuel bed is maintained at an optimal level. The geometry of the furnace should facilitate appropriate mixing of the raw gas with the secondary air and assure a long enough residence time for complete combustion (27). An exemplary grate firing system is presented below:

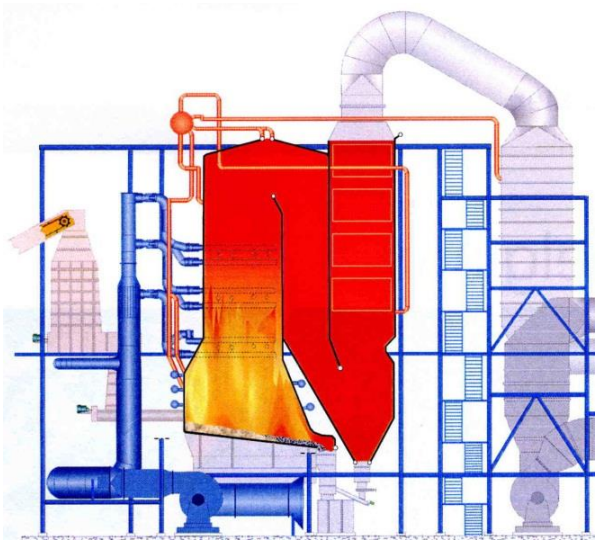

Figure 2.4 – Exemplary power plant with a moving grate firing (B&V Vølund, Wanze, Belgium)

Large-scale industrial grate firings were originally used for coal combustion but they were replaced by highly efficient burners for pulverized coal. Today they are still used for combustion of “difficult” fuels such as waste, biomass and SRFs. The reason for that is a much longer residence time and a good mixing of the combusting fuel in this system. Furthermore, fuels do not usually need special pre-treatment such as grinding or drying before combustion. As for power plants utilizing SRF, 15 out of 19 installations commissioned in Germany before 2008 were also equipped with grate firings (28).

Combustion on a grate has also several disadvantages. Because of the considerable amount of fuel on the grate and a long residence time a quick response to a changing output power demand is difficult to achieve. Possible poor mixing of the raw gas with air in the furnace can cause the occurrence of locally changing reducing and oxidizing conditions which can lead to a high-

temperature corrosion of boiler tubes (29). In order to prevent the corrosion, a combustion process is carried out with usually high air excess ratio (lambda 1.4-1.6) which reduces the efficiency of the process. Although combustion on a grate has been researched since decades and is well described, there is still need for a study aiming to find solutions to these problems and to improve flexibility, efficiency, and availability of firing systems equipped with moving grates.

This systematic research of combustion in large plants under defined conditions and with the possibility of testing non-standard fuels with different operating parameters is often difficult or impossible to carry out. The combustion behaviour, particle emissions and corrosion risk in such case can be different than for standard fuel for which a power plant was designed and can be unacceptable for the plant operator. For this reason, a lot of combustion tests are performed in laboratory fixed bed reactors and the results are transferred onto large grate firings with moving beds. Despite mentioned problems, there is a lot of research conducted also in pilot-scale grate firings and in large-scale power plants equipped with moving grates. Current state of knowledge in the field of combustion in fixed bed has already been discussed.

Similar to investigations in fixed bed reactors, first research in systems with moving grates were performed on regular fuels – coal and coke. In 1930s Löwenstein (30), Schulte (31), Werkmeister (32), Mayer and others carried out research with safe and economical utilization of coal in mind.

Beckmann (33) conducted in a pilot scale reverse-acting grate firing several combustion tests with lignite. The goal was to validate his model with measured oxygen concentrations and temperatures along the grate. Beckmann investigated also the influence of moving grate bars on mixing intensity of the fuel (34). He described this influence through residence time distribution on the grate for forward-acting and reverse-acting grates.

Combustion tests with wet (water content ca. 50 wt. %) forest waste were conducted by Thunman (35) in a reverse-acting grate (31 MW) in order to investigate ignition behaviour of the fuel. It was found out that the ignition takes place not only due to absorbed heat radiation from the furnace walls, but also from other sources. Thunman identified these sources to be back-mixing of the ignited material upwards the grate and heat conduction through the grate bars.

At ITC at the pilot scale waste incinerator TAMARA (500 kW) a number of research programs regarding the combustion behaviour were realized between 1989 and 2010. The most important measurements from the point of view of this study were these conducted by Bleckwehl (25) who characterised the combustion behaviour of wood chips, BRAM and shredded waste under varied operational conditions (primary air amount, primary air temperature) in order to validate a model he developed on the course of his doctoral studies. Bleckwehl compared mass conversion rates

calculated with the model and based on experiments at the KLEAA facility with those obtained at TAMARA plant to show that the mathematical description of the process and the transferring procedure produce satisfactory results. An extensive description of both research facilities is presented in chapter 3.

2.3.3. Other combustion technologies

Combustion on the grate, moving or fixed has its advantages and drawbacks mentioned in the previous chapter. When the drawbacks make the combustion of a certain fuel on the grate uneconomical or impossible, other combustion technologies are considered. One of several such combustion systems suited for the combustion and co-combustion of SRFs is a rotary kiln. It is a cylindrical vessel made from steel plate coated from the inside with firebrick, often sloped slightly to the horizontal. The tube slowly rotates on its axis. Cement industry has a broad experience in the use of waste derived fuels in rotary kilns. Hazardous and non-hazardous wastes are processed and used as secondary fuel because very high temperatures in cement kilns allow complete destruction of harmful substances in the waste. For that reason, rotary kilns are also used for utilization of waste classified as hazardous.

The material to be processed during cement production is fed into the upper end of the cylinder. As the kiln rotates, material (raw mix) gradually moves down towards the lower end, and may undergo a certain amount of stirring and mixing. Hot gases pass along the kiln, sometimes in the same direction as the processed material (co-current), but also in the opposite direction (counter-current). The fuel for this process may be gas, oil, pulverized coal or already mentioned solid recovered fuels.

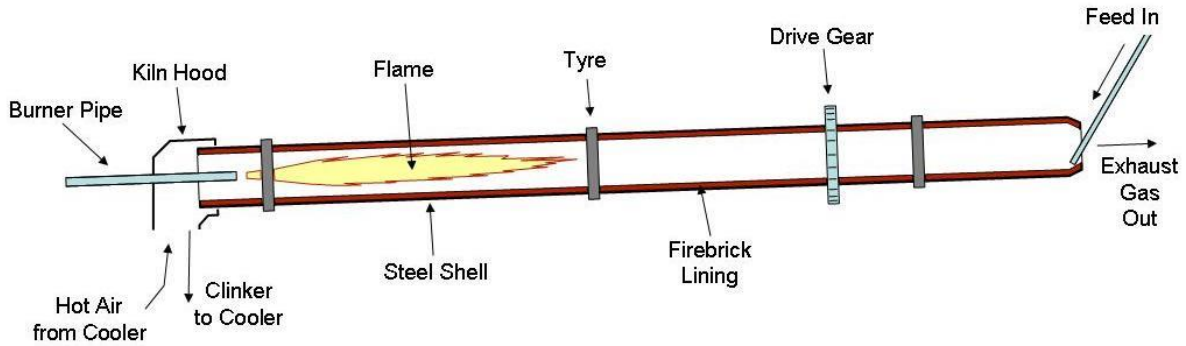

Figure 2.5 – Rotary cement kiln

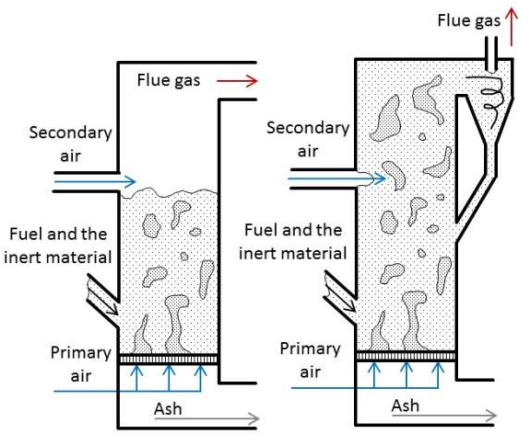

Figure 2.6 – Bubbling (left) and circulating (right) fluidised bed boiler

Another combustion technology – fluidized bed boiler (left) consists in general of a vessel with a perforated plate (grate) in the bottom. This container is filled with an inert, granular material (e.g., sand, dolomite) which is fluidized with the primary air supplied from the bottom. This means, that particles of this material are lifted and suspended by the flowing air (left). Ground fuel with the particle size up to several centimetres is added to this suspension, where both materials can mix and fuel particles can combust. A significant advantage of the fluidised bed combustion (FBC) is an excellent mixing of the fuel with the combustion air and with the inert phase which allows boiler operation with a low air excess ratio and with temperatures between 850-900°C. Operating in such low temperatures reduces thermal-NO_X emission from FBCs in comparison to the pulverised fuel combustion and also minimises the risk of sintering of the ash particles. Furthermore, the large heat capacity of the inert material allows seamless ignition and combustion of fuels with a low calorific value (36), such as very wet coal, sewage sludge and even coal sludge, which is combusted for example in an industrial power plant in Wachtberg operated by RWE Power AG. It is a waste coal dust from the production of coal briquettes mixed with water and should not be considered as a fuel per se, because of the negative calorific value. Co-combustion of sludge with coal is simply a way of safe and cheap disposal of this material and shows great fuel flexibility of fluidised bed boilers. CFBs are also an excellent combustion technology for combustion and co-combustion of solid recovered fuels, provided that the temperature in the firing exceeds 850°C and the residence time of the flue gas in this temperature is longer than 2 seconds, as regulated in (7). There are several power plants in Germany that fire solid recovered fuels as mono-fuel (28). Co-combustion of SRFs with coal and biomass is still a subject of research, also in the framework of the RECOMBIO project in power plants in Wachtberg (Germany) and in Anjalankoski (Finland).

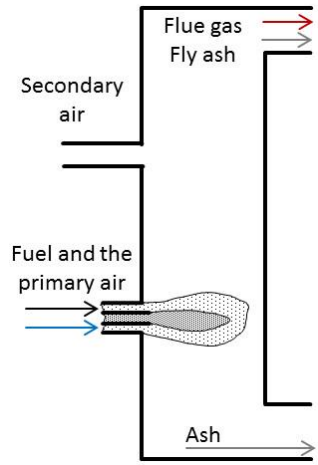

Figure 2.7 – Pulverised coal boiler

Another type of combustion technology is a pulverised-fuel burner (boiler). For this kind of the firing system, the fuel is finely ground (µm range) and then transported with the primary air through a burner into a combustion chamber (left). Small fuel particle size intensifies the combustion and burnout making a pulverized-fuel boiler very flexible and efficient comparing to a grate firing and a fluidized bed boiler. Typically PFBs are used for combustion of hard coal as it is relatively dry and easy to grind (36). Since the 1990's, a number of tests for co-firing biomass and waste with coal in PFBs have been performed in Europe.

Since then many power plants originally designed for coal were retrofitted to allow biomass co-firing in commercial use (37). Although co-firing of biomass and SRFs in a PFB is possible, it still presents significant technical problems. Several test programs at KIT at the half-industrial test station with multi-fuel burner BRENDA have been performed in order to address these issues. Tasks were to investigate flame stability under changing load (flexibility) and burnout behaviour during co-firing of SRFs with regular fuel i.e., pulverized hard coal and lignite (38). Co-combustion of solid recovered fuels were also demonstrated in power plant in Weisweiler in the framework of project RECOFUEL (39), but no further use of alternative fuels has been planned after the demonstration phase. Currently, several PFBs in Germany (Jänschwalde, Werne, Berrenrath, Flensburg and Schwarze Pumpe) co-fire solid recovered fuels with coal (40).

2.4. Modelling the combustion of solid fuels in fixed beds and in moving grate firings

Mathematical modelling is a simplified description of a system through mathematical means. A model may help explaining a system, studying the effects of different components and making predictions about its behaviour in reality. In the case of a fixed bed, the system is defined as a certain amount of combusting solid fuel contained in an insulated vessel with the air supplied from below. The fuel can be ignited through the absorption of radiation by the top layer of the fuel or through heating up of the fuel with the preheated primary air. A number of researchers have written models of combustion in such system using different approaches. Different model approaches are presented in the table below:

Table 2.4 – discussed model approaches

	Scale	Application	Advantages	Disadvantages	References
Zone models	1D	investigation of the conversion rate	simplicity	simplification	17, 18, 41
Reactor cascades	1D	simulation of the conversion rate, development of sub-models, supporting process control systems, input for CFD simulations	simplicity, modelling of phenomena at phase boundaries	no mixing	19, 33, 42, 43, 44, 48, 49, 50
Continuity models	2D	simulation of the of conversion rate, development of sub-models, supporting of process control systems, input for CFD simulations	modelling of the fuel mixing to some extent	relatively simple model of the diffusion, pyrolysis and solid burnout in favor of mixing	51, 52, 53, 54, 55, 56, 57
Descrete element method	2D, 3D	investigation of mixing phenomena, input for CFD simulations	excellent modelling of the fuel mixing	time and CPU power consuming simulations	58, 59, 60

The next section contains a short description of these models.

2.4.1. Modelling fixed beds

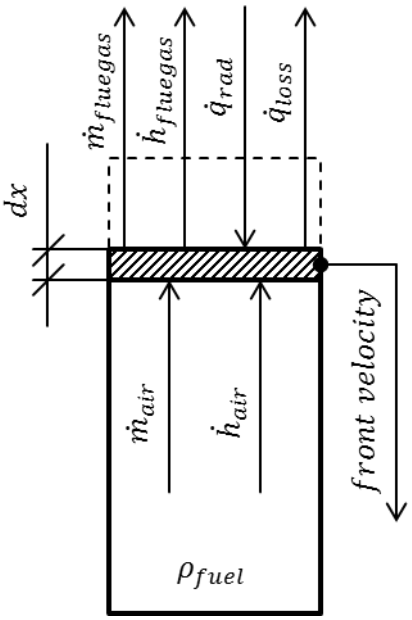

Figure 2.8 – Zone model

In one of the simpler methodologies all consecutive stages of the combustion – heating up, drying, degassing and burnout are modelled in a one-dimensional moving thin layer of the fuel bed (often called "reaction front") and the Lagrangian frame of reference is attached to this layer or a so-called zone. It is assumed in these models, known as "zone models" that there is no temperature gradient between the solid and gas phase i.e., there is only one phase for which energy balance is formulated. Reacting zone receives energy in form of the physical enthalpy of the supplied primary air, radiation from above and in form of the heat released during reactions. Outgoing heat fluxes are the enthalpy released with a certain amount of flue gas and also possible heat losses. Drying, pyrolysis (degassing), heterogeneous and homogeneous combustion are described as one-step reactions with their characteristic reaction rate constants and activation energies determined experimentally (thermogravimetry). Incoming mass flow into the reacting zone is, therefore, the primary air flow and outgoing flow is incremented by yields from drying, pyrolysis and char burnout. Furthermore, it is assumed that the fuel bed below reaction front is uninfluenced. Focus of these models is to describe the velocity of a reaction front in relation to the primary air flow and to several different fuel parameters such as particle size, shape, fuel density, humidity or ash content. Fatehi and Kaviany (18) wrote a model to investigate the influence of the air flow on the propagation of reaction front in a packing of wood particles. A similar model for coal, wood and

shredded waste was written by Gort (17), whereas both reaction and transport kinetics during heterogeneous reactions have been described. At ITC two analogous models have been formulated and validated for the KLEAA reactor. Schumacher (41) modelled the reaction front velocity, carbon conversion rate and combustion temperature in dependence on the particle size (wood cubes), fuel humidity, ash content, and the primary air flow. As mentioned in chapter 2.3.1 Bleckwehl developed and validated a model which describes fuels (specifically their conversion behaviour in a fixed bed) using the ignition time, reaction front velocity, ignition rate, mass conversion rate and the specific heat release. This model is used at ITC as the standard method of a quantitative fuel characterization and classification and is known as the "three-step characterization concept." A significant drawback of such models is that they consider fuel bed as a homogeneous phase. This includes several simplifications:

- Drying can occur only when humid fuel reaches 100°C. Due to the lack of gas and solid phase, there is no boundary layer at which evaporation below 100°C could take place,
- Heating up of the fuel over 100°C can occur first after complete drying,
- Released volatiles have the same temperature as the fuel and when the ignition temperature is reached, the volatiles are ignited. It is assumed that their concentration lies always within the flammability limits,
- Drying, degassing, ignition and combustion occur one after another which is a major simplification,
- Fuel below reacting zone is not affected by any physical and chemical processes.

More complex approach shown in (Figure 2.9) considers the fuel bed as two phases – solid and gaseous phase for which separate conservation equations are formulated. It is known from chapter 2.2 that both phases interact with each other during the stages of the combustion process which is reflected in mass and heat fluxes at the figure below.

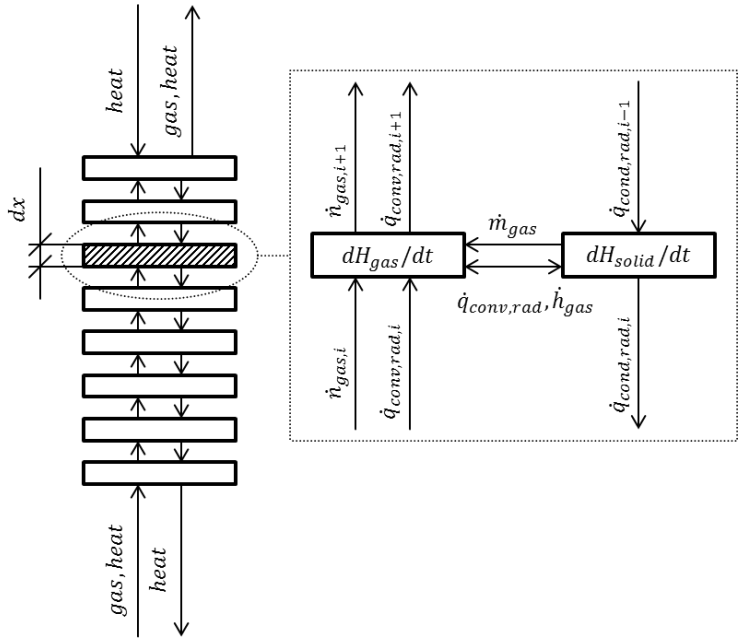

Figure 2.9 – Schematic presentation of cascade of ideally stirred batch reactors

The gas flows through a solid porous phase with a different temperature and composition, leading to a difference between partial pressures of the species around solid particles and in the incoming gas. These temperature and partial pressure gradients in both elements of the system effectively mean a heat flow between the solid and the gas phase and a mass flow from solid into gas. The heat is transported in the solid phase through the conduction and radiation. In the gas phase, on the other hand, the heat exchange occurs through the convection and radiation. Additionally, the heat transport between solid and gas through the convection is modelled. It is assumed that there is no mass flow from the gas into the solid. Fuel bed is divided into several discrete one-dimensional elements (finite volumes, layers) coupled together with the energy, mass and material conservation equations.

Because elements are one-dimensional there are no radial gradients within and each element can be described as an ideally stirred batch reactor, hence another name of this approach – “cascade of ideally stirred batch reactors.” These models are often used to investigate and develop sub-models for pyrolysis, diffusion or solid particles. A significant disadvantage of these models is that they do not consider mass flows from solid to solid (between layers), but only from the solid into gas phase

meaning that modelling of mixing of solid fuel particles in moving beds is impossible. Simulating fixed bed reactors with these models is however very accurate in comparison to zone models.

Raupenstrauch (42) developed a model which describes drying, degassing and combustion in a packed fuel (wood and coal) bed with consideration of the diffusion during heterogeneous reactions on the surface of solid particles. The purpose of the model is to predict self-heating up of the solid phase and describe the influence of fuel humidity and particle size on the propagation of the reaction front.

Lohf (43) developed a model of a fixed fuel bed which consists of a heat transfer model, gas phase model and a particle model. The rate of the solid conversion is described by the particle model in dependence on temperature in the solid and the current combustion stage. Boundary conditions are defined by the gas concentrations around the particles and the heat flux between the particle and gas phase which is governed by a global heat transfer coefficient. A similar model was written by Shin and Choi (19).

A model written by Mätzing – the "KLEAA Code" (44) considers the fixed fuel bed as a tight packing of wooden spheres divided into two separate phases (solid and gas) for which conservation equations are formulated, whereas heat transfer within the solid phase is described by an effective, conductive heat transfer coefficient. Further on Mätzing assumed that there are no temperature or gas concentration gradients within the control volumes and the system can be reduced to a one-dimensional cascade of ideally stirred batch reactors connected with each other via conservation equations. For a particle model, the shrinking-core model has been chosen. Observations with burning coal, wood briquettes, and tightly wrapped newspapers prove that this model approximates real combustion processes relatively well (45). Here it is assumed that the reaction occurs at the outer surface of the particle leaving behind completely converted material, an inert solid i.e., ash. Thus, at any time there exists an unreacted core of material which shrinks in size during the reaction. The density of this core remains the same over the course of the reaction. It is also assumed, that the outer skin of the particle where the reaction takes place is constant during the whole process. These factors are very important, as they describe fuels physically, determine the total amount of the fuel and influence the rate of heterogeneous reactions – char burnout and pyrolysis (degassing). One of the main focuses of the model is the development of a sub-model for pyrolysis. Mätzing used a one-step model for pyrolysis of biomass (46) (47) which describes the fuel as wood being decomposed in one reaction into gas (volatiles) and fixed carbon (char). Validation of the model for combustion of beech wood spheres has shown a fair correlation with the experimental results from the KLEAA fixed bed reactor. Compared values were: mass conversion rate, temperatures and gas concentrations (O_2, CO, CO_2, C_{org} and H_2O) above the fuel bed. Comparison of the results produced by the pyrolysis

model alone proved however that it does not correspond with the thermogravimetry of beech wood sample i.e., cellulose decomposes too fast. In order to address this problem, Mätzing developed a five-step pyrolysis model which is based on a three-step model but splits the decomposition of cellulose into two steps – decomposition of cellulose into gas (as other authors (47)) and into tars which is a novel approach. Tars are then decomposed into gas in one step. Ultimately the model is being designed to describe physical and chemical phenomena in a fuel (SRF and biomass) bed combusting on a moving grate and to serve as an input for CFD simulations. Implementation of the five-step pyrolysis model and of the novel method of physical characterisation of biomasses and SRFs described in 4.2.2. is expected to bring much better results of combustion simulations in comparison to other authors. The reader will find an extensive description of the "KLEAA Code" and its further development in Chapter 5.

2.4.2. Modelling of moving beds

Mathematical models also exist for the already mentioned moving fuel beds. One of several approaches is to visualize the combustion process on a moving grate divided into several horizontally connected ideally stirred batch reactors. This idea was firstly discussed by Gruber and Beckmann (48) (49) (33). Following this method, Beckmann developed a combustion model for model fuels – coal and a mixture of wood and plastics in grate firings. On the basis of the experimentally (in a fixed bed reactor) determined global reaction coefficient for these fuels and energy and mass conservation equations he describes the mass conversion for every element of the cascade, each representing a single grate (primary air) zone. The global reaction coefficient includes terms for drying, degassing, ignition, char burnout and considers transport kinetics and shrinking of the surface on which reactions take place. The number of elements is determined by the number of primary air zones in a grate firing. To validate the model Beckmann performed several test runs with coal in a pilot scale reverse-acting grate firing. Calculated oxygen concentrations and temperatures were compared with the experimental data and showed that the model predicts these values with acceptable accuracy. Gruber developed his own analogous model but he also divided vertically each element of the cascade. A similar two-dimensional matrix of ideally stirred reactors was modelled by Warnecke (50).

An interesting model is being developed since 1998 by the work group of Swithenbank. In this approach, the fuel on the moving grate is considered to be a two-dimensional porous continuum divided (discretised) into cells on which numerical calculations are carried out. Inside each cell, the concerned parameters (e.g., temperature, the percentage of moisture, carbon, etc.) are assumed to be uniform and, by reducing the cell size (hence increasing the cell number), the calculation can be made on a size-scale much smaller than the fuel particles. This means that the non-isothermal behaviour of a single particle can be accounted for to some extent (51) (52). The combustion process

is divided into drying, waste devolatilization, combustion of volatiles and char burnout for which reaction rates are calculated. These processes take place between layers in which fuel bed is divided – fresh fuel, dry fuel, devolatilised fuel and ash. Heat exchange between the layers occurs through conduction (with an effective heat conduction coefficient). Drying can take place under 100°C as evaporation and at 100°C through boiling out of water. Pyrolysis is modelled as a one-step process. For both, gas and solid phase transport equations are formulated according to the general governing equations summarised by Peters (53). Equations of particle movement in a packed bed take similar forms as those for a fluid but have an additional term accounting random particle movements caused by the mechanical disturbance of the moving grate and other random sources (51). This is a very important feature, as it allows simplified modelling of an influence of fuel mixing. Similar models were developed by Krüll (54) (55), Jaworski and Wandrasz (56) and Pättikangas (57).

Another recently developed model is discussed by Kurz in his dissertation (87). Here the fuel bed is described as a 2D continuum consisting of two phases – gas and biomass particles. The model is characterised by a detailed description of the pressure drop in the fuel bed and of the fuel mixing on the grate. The main advantage of the model is its ability to describe the thermal and hydrodynamic interaction between the fuel bed and the firebox. The pyrolysis is however described by a simple one-step model.

A model for description of solid conversion and solid motion in a three-dimensional fuel bed has been developed by Peters (53) (58). This approach is based on the discrete element method, meaning that processes during the fuel combustion are considered on the level of a single fuel particle and its pores. Conservation equations (mass, energy, material) and transport equations are formulated and solved for each fuel particle (Lagrange approach). This feature of the model makes it an excellent tool to investigate and describe fuel mixing in different types of grate firings, but is also characterised by a high calculation time. Peters validated the model with regard to mixing together with Hunsinger at TAMARA pilot plant (59). Similar but two-dimensional is being developed by Brosch (60).

3. Experimental setup

3.1. Description of the KLEAA fixed bed reactor

Combustion stages occurring locally on a moving grate (length and height of the fuel bed) – ignition, drying, pyrolysis, gasification, main combustion and the char burnout can be represented as processes taking place chronologically one after another in a fixed bed reactor (as explained in chapter 2.2). KLEAA was designed and built to investigate the behaviour of these processes during combustion of solid fuels. Furthermore experimental results obtained at KLEAA serve as a basis in the second stage of the three-step characterization concept described in chapter 4.

Main components of the KLEAA reactor are the combustion chamber, secondary combustion chamber, and the flue gas cleaning system. They are presented in the figure 3.1. The combustion chamber is divided into an insulated vessel, which can be detached from the upper, electrically heated part of the chamber and shifted away on rails in order to fill it with fuel. This operation is carried out while the vessel is at room temperature. Later on, the already filled vessel is shifted back into its position under the combustion chamber. This filling procedure guarantees that starting conditions of every experiment are the same. Furthermore, this procedure resembles feeding of the fuel into a firing equipped with a moving grate where cold fuel falls down onto the grate from a hopper and is rapidly submitted to the heat radiating from the firebox walls. Upper, fixed part of the combustion chamber, as well as the secondary combustion chamber, are electrically heated up to the maximum temperature of 1100°C. The fuel vessel has a volume of ca. 10 litres (diameter: 23cm, height: 25cm), which allows using solid fuels with a maximum particle size of 80mm. Primary air is supplied from below of the fuel bed through a metal latticed plate on which a thin layer of fine, inert gravel is placed before filling the vessel with the fuel. Air can be preheated up to 300°C. In the secondary combustion chamber, secondary air is supplied in order to assure a complete burnout of any combustible species present in the raw gas. At the entrance of the gas cleaning system, a heat exchanger is installed, which cools down the flue gas to the temperature of 180°C i.e., above the condensation temperature of acids. This measure is undertaken in order to avoid the corrosion of the piping and to protect the fabric filter located after the heat exchanger. The gas is cleaned from the solid particles in a fabric filter and passes to the last part of the system, the activated carbon filter where organic pollutants and volatile heavy metals are separated. Combustion tests are carried out under pressure of 0.5mbar below the atmospheric pressure which is kept constant by a centrifugal fan installed after the gas cleaning.

The experiment procedure starts with the filling of the fuel vessel with fuel, closing it with the combustion chamber and starting the primary air supply. The upper layer of the feedstock is ignited

by the heat radiating from the walls of the primary combustion chamber and the flame propagates downwards in the opposite direction to the primary air flow. Combustion gases can be sampled at two different locations – directly above the fuel bed surface and after the secondary combustion chamber where the combustion process is completed.

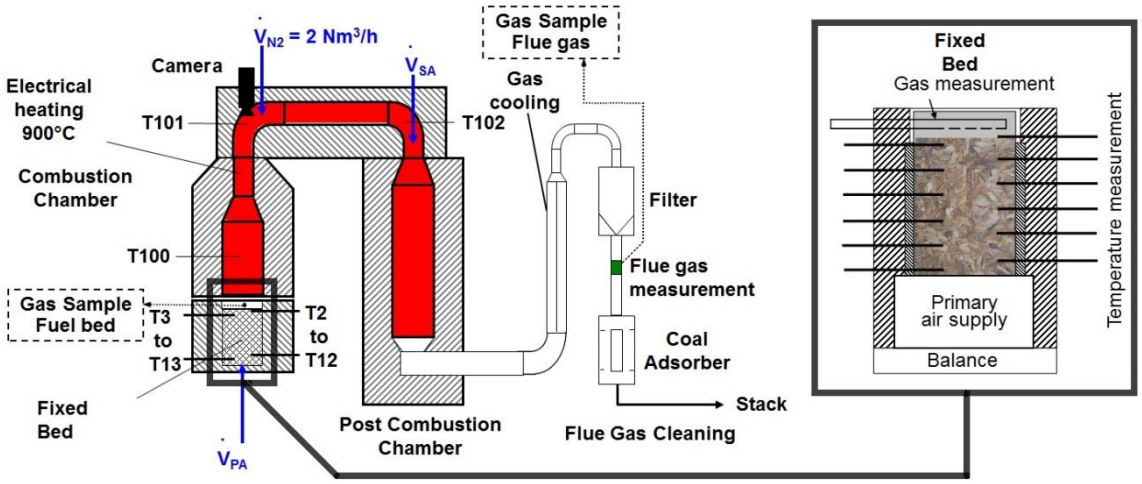

Figure 3.1 – KLEAA fixed bed reactor

Measuring the CO_2, CO, O_2, SO_2, C_{org} and H_2 above the bed was performed during all test runs. Additionally, the water concentration after the secondary combustion chamber was measured. The temperature in the fuel bed was measured by 12 “type K” NiCr-Ni-thermocouples (T2-T13) placed along the fuel vessel in 20mm distance between them. They allow gathering temperature distribution during the combustion process. The system is also equipped with a high-resolution scales under the fuel vessel used to measure the weight of the remaining feedstock in real time and in consequence calculating the mass conversion rate.

3.2. Description of the TAMARA pilot-scale pusher grate

TAMARA pilot-scale waste incinerator (Figure 3.2) was built at the Institute of Technical Chemistry in 1987. The name TAMARA is a German acronym standing for "Testanlage zur Müllverbrennung Abgasreinigung Rückstandsverwertung und Abwasserbehandlung", which means in English "Test Facility for Waste Incineration, Flue Gas Cleaning, Residue Treatment and Waste Water Treatment."

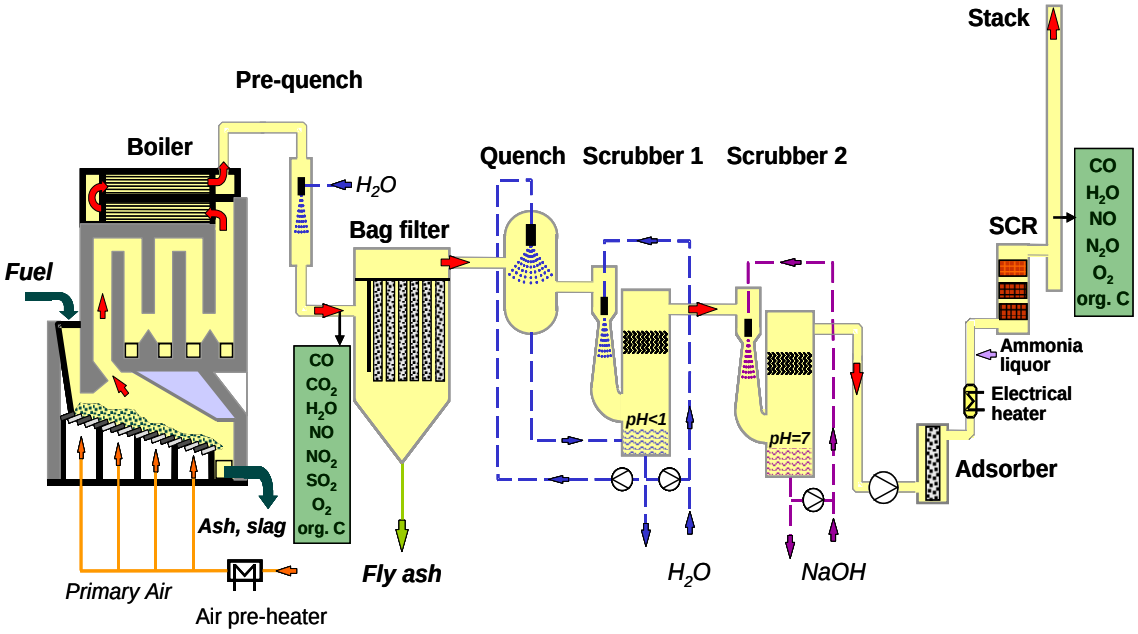

Figure 3.2 – schematic of TAMARA waste incinerator plant

The facility is equipped with a pusher, air-cooled grate (Figure 3.2) and allows firing a wide variety of fuels and wastes thanks to the gas cleaning line installed in accordance with the German Seventeenth Federal Emission Control Act (17. BImSchV). The 3.2m long and 0.8m wide grate is inclined to the horizontal by 8° and is divided into 4 separately controlled primary air zones. The velocity of the grate bars can be set for every primary air zone independently.

Flue gas is cooled down in a two-stage boiler and in a pre-quencher to ca. 180°C before entering the gas cleaning system in order to protect the fabric filter. The first wet scrubber where HCl is removed operates at pH=1. The second one where NaOH is injected for separation of SO_2 operates under pH=7. Next element of the line is an activated carbon filter in which organic pollutants (dioxins) and mercury are separated. At the end of the gas cleaning system, an SCR reactor for NO_X removal is installed.

Important parameters:

- Grate dimensions: 3200mm x 800mm
- Thermal power: up to 500 kW
- Maximum fuel load: 300 kg/h
- Maximum flue gas flow: 1500 Nm^3/h
- Maximum temperature in the post-combustion furnace: 1200 °C
- Residence time per primary air zone: 10-20 min

TAMARA is equipped with sensors allowing on-line measurement of process parameters such as temperature, pressure, flue gas flow and gas concentrations after the boiler and at the stack. Furthermore, it is possible to install a large variety of external measuring equipment, such as probes for gas analysis and temperature measurement or deposition probes. Such gas sampling probes were the key equipment for this study as they allowed mass, material and energy balance of the grate and in the effect calculating the mass conversion along the grate.

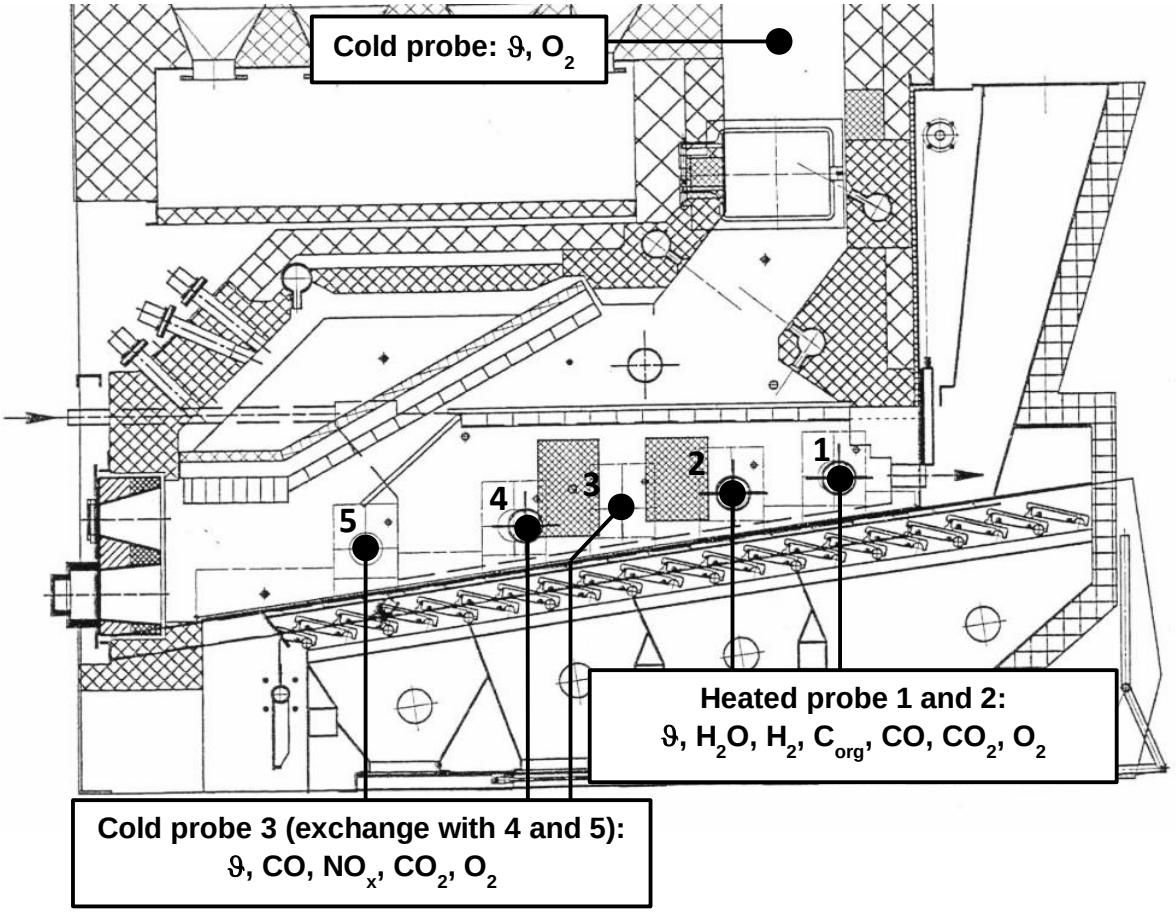

Figure 3.3 – Measurements above the grate

Probes 1 and 2 are equipped with an electric trace heating to prevent water and hydrocarbons condensation present in the drying and pyrolysis zone. At the point 3, between the second and third primary air zone, where in general the main combustion takes place and water vapour presence is not expected in high concentrations, an unheated gas sampling probe has been installed. It was also used at points 4 and 5. Secondary air was supplied via a nozzle in the first boiler pass and its volumetric flow was controlled in such a way that oxygen concentration measured with the probe in the first boiler pass was kept at 11 vol. % (dry) and the temperature did not exceed 1150°C.

Two different techniques were applied to evaluate the possibility of an accurate on-line chlorine content estimation in fired fuels. The first method utilized a laser sensor measuring hydrogen chloride concentration in the flue gas. Actual chlorine content in the fired fuel was calculated from the measured HCl concentration, flue gas volumetric flow, temperature, water vapour content and the fuel mass flow. The second method used a direct chlorine measurement with a near infrared detector. The device was placed above the conveyor belt supplying the fuel (Figure 3.4). The results delivered by both techniques were compared to the laboratory analysis of fuel samples taken in 2h long intervals.

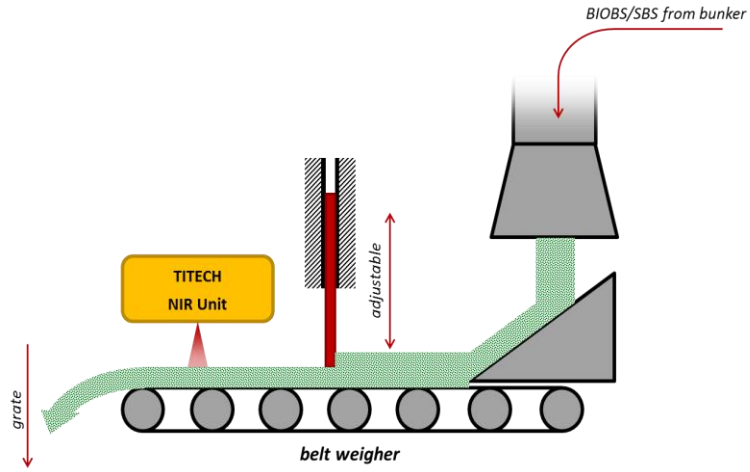

Figure 3.4 – Position of the NIR detector

4. Experimental method

The three-step characterisation concept mentioned in chapter 2.3.1 and its purpose will be explained in this chapter. Further on the procedure for the evaluation of the results will be discussed for each step. Finally, the method of measuring the solid density and the specific surface area of fuel particles will be presented.

4.1. Three-step combustion characterisation concept

The utilisation of solid bio-fuels and alternative, waste derived fuels for the production of heat and electricity has an established position in the power production industry and in smaller, domestic applications. In order to design new systems for such fuels, retrofit or optimise combustion processes in existing ones it is necessary to describe these fuels chemically and physically, but also to quantitatively describe their combustion in the system in which they are going to be utilised. Research of the combustion behaviour of coal has already been conducted at an extensive scale. Different coals can be classified by their volatiles content (61) (62) or their elementary composition (63). These and other methods of the coal characterisation are extensively described in the standard VGB-Richtlinie R210 (64). Up to date, there is no similar standard regarding combustion of Solid Recovered Fuels (25). European standard EN 15359 (5) treats of the classification of Solid Recovered Fuels, but their combustion behaviour is not discussed. Furthermore, the research of the combustion behaviour of biomass and various waste based fuels has been performed on prepared, homogenised samples as mentioned in chapter 2.3. Transferring the results onto large-scale plants where more complex fuels are fired on the grate is limited.

For this reason, Bleckwehl (25) suggested a characterisation concept based on characteristic numbers derived from the results of firing tests of real fuels (as fired in large-scale system) in a laboratory scale fixed bed reactor. The KLEAA reactor as described in chapter 3.1. allows conducting experiments on fuel samples up to 10 litres in volume which, given that the fuel is relatively homogeneous, is sufficient to reproduce combustion stages occurring in a moving grate firing while combusting this fuel. The process of the combustion characterisation consists of three steps (Figure 4.1) discussed below.

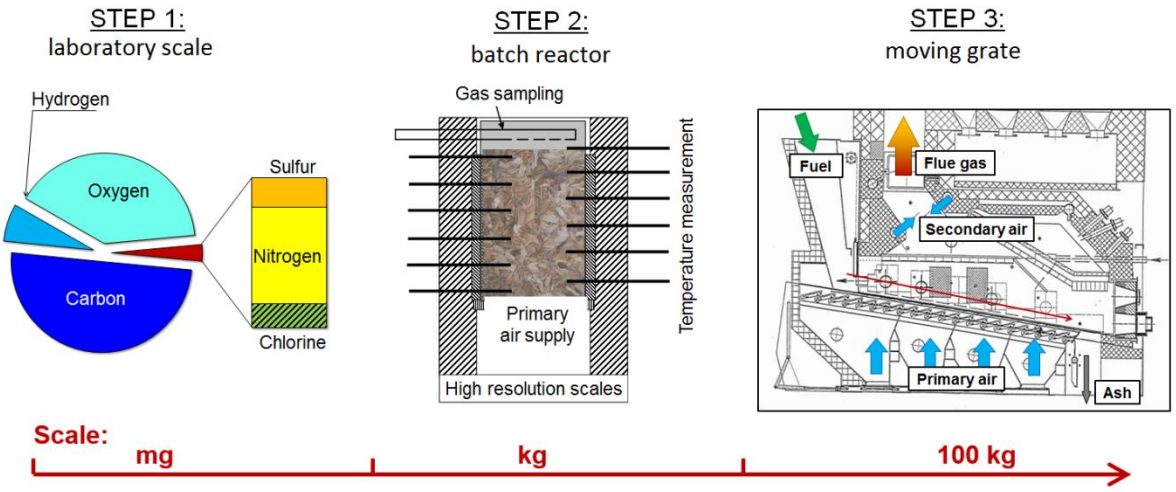

Figure 4.1 – Three step characterisation concept

- Step One – Chemical and physical properties of the fuels,
- Step Two – Characterisation of the combustion in a fixed bed (batch) reactor,
- Step Three – Characterisation of the combustion on a moving grate.

4.2. Step One – Chemical and physical properties of investigated fuels

4.2.1. Chemical properties

The first step in this concept of combustion characterization requires a complete analysis of chemical properties of the fuel. The proximate analysis, in this case, is carried out in accordance to several standards. First, a fuel sample is being dried as described in DIN 51718, at a temperature of 106°C (±2°C) over at least 24h and the water content is calculated from the difference between the weight of the original and dried sample. Procedure for finding ash content is described in standard DIN 51719. It is determined by the combustion of a sample in a muffle furnace at 815°C (±15°C) over 2h. Ash is then cooled down, weighted and the ash content is calculated. The content of volatiles is measured according to DIN 51720 in a similar manner as the ash content in a muffle furnace, but a sample is subjected to a pyrolysis under 900°C (±10°C) over 7 minutes. Char content is a mass of an original sample weight reduced by water and volatiles content. For the investigated solid recovered fuel also the content of the biogenic carbon was found according to (88) using selective dissolution method.

The elementary analysis is focused on the content of carbon, hydrogen, nitrogen, sulphur (CHNS) and oxygen in a fuel sample. CHNS-composition allows performing combustion calculations which are needed for the mass and energy balance. Analyses at ITC were carried out using LECO TruSpec unit. Fuel sample is completely combusted at a temperature of ca. 950°C in a pure oxygen atmosphere. Reaction products, CO_2, SO_2 and H_2O are detected by the infrared adsorption while N_2 is measured via heat conductivity detectors.

4.2.2. Physical properties

The three-step combustion characterisation concept can be reinforced by a simulation of the combustion performed with the KLEAA Code. As mentioned in Chapter 2.4., the KLEAA Code is a mathematical model for simulation of the combustion of a fuel charge consisting of spherical wood particles, packed in the KLEAA reactor. In order to simulate the combustion process, the fuels need to be characterized in the model by a set of values which define their physical properties and complement the chemical description of these fuels. These factors include the heat capacity of the fuel and its thermal conductivity which are assumed (see chapter 6). There are however two properties which need to be measured. The first one is the density of the solid ρ_s [kg/m³] which together with the initial size of a spherical particle define the initial mass of this particle. The second parameter is the specific surface area of a fuel particle S_V [m^2/m^3]. This factor greatly influences the fuel conversion rate as found by Bleckwehl (25). Bleckwehl combusted several bulks consisting of beech wood spheres with different diameters (3-50mm) in the KLEAA reactor. The operating parameters were identical to those chosen for this study (i.e., primary air was not preheated, the temperature of the combustion chamber was set to 900°C and the primary air flow to 10 Nm^3/h). According to the results obtained by Bleckwehl (25), the fuels with different particle forms burn with the equal mass conversion rate as long as the surface area of the fuel particles is the same for each of these fuels. Bulks consisting of particles identical in form (spheres) but with different size (diameter) combust however with different conversion rates; i.e., smaller particles with higher specific surface area burn faster as shown below in Figure 4.2:

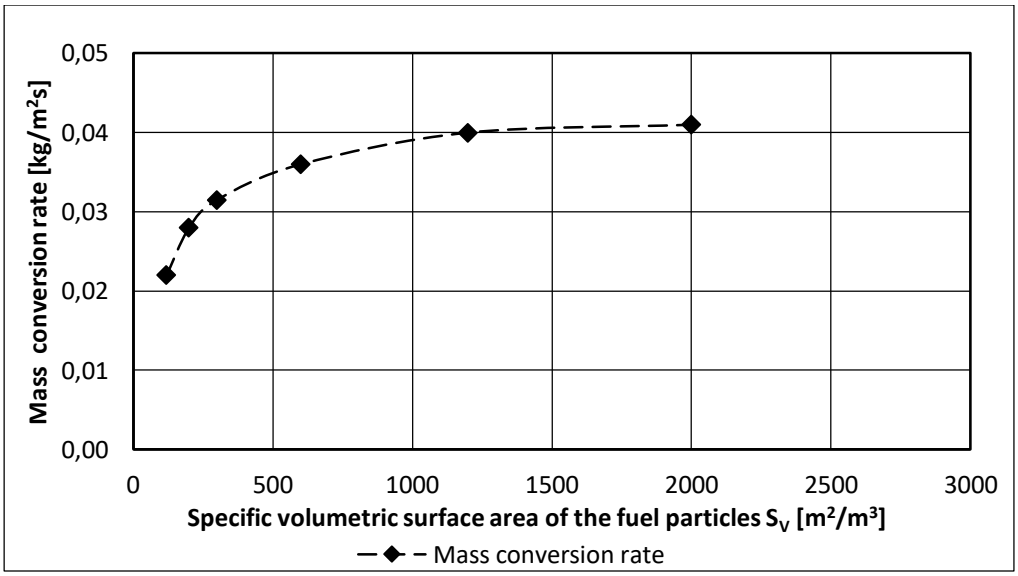

Figure 4.2 – Mass-conversion rate in function of the specific volumetric surface area, based on the research of Bleckwehl on beech wood spheres (25)

The most significant influence of the specific surface area on the mass conversion rate is visible in the range of 120 m^2/m^3 to 1200 m^2/m^3. The beech wood spheres used during the first validation of the

KLEAA Code (3) have the specific surface area of 600 m^2/m^3 i.e., in the middle of this range. Technical fuels like wood chips or solid recovered fuels investigated in this work are expected to have noticeably higher specific surface areas what explains the need for a model validation, especially for these fuels.

Based on the research of Bleckwehl it is assumed in this study that it is sufficient to measure only the specific surface of the particle and set it in the model in order to simulate the combustion process of a given woody fuel as the conversion rate of this fuel depends on this parameter (Figure 4.2) and a detailed description of the geometry of particles can be neglected while modelling the heat and mass transfer. The solid density, as well as the surface area of the fuel particles, can be directly found in the Equation 6.3 and Equation 6.29 in the KLEAA Code (see chapter 6).

Both properties are relatively easy to determine for homogenous materials with defined geometry and mass per particle, such as beech wood spheres. Wood chips and even more complex fuels like SRFs consist however of particles different in size, shape, and composition. In order to find these two properties and to allow simulation of complex technical fuels, several additional measurements are necessary. Finding the solid density and the specific surface area of the particles is carried out as a part of the Step One.

4.2.2.1. Measuring the solid density

The density of a substance is defined as its mass per unit volume it occupies. The mass is rather straightforward to determine and the measured value is unambiguous. The volume, however, can be understood differently, especially in case of granular or "fluffy" substances like solid recovered fuels. Should the volume of a container around such substance be considered, the density will be called the bulk density. This one is quite trivial to determine when the container has a simple geometry (box, cylinder, etc.). On the other hand, there is the raw (material or true) density. In this case, we need to exclude every volume which is not occupied by the material itself, e.g., we exclude all the voids within a fuel particle and on its surface. Between these two extremes, the volume we take into consideration while calculating the density can be defined in different ways. Various volumes are presented below in Figure 4.3. To answer the question which one we have to consider we have to take a closer look at the combustion process and how it is modelled in the KLEAA Code. All the reactions, in this case, are assumed to take place on the outer surface of the fuel particles, or more precise on the boundary layer, which can be identified as an "envelope" of the particles, hence the name "envelope density."

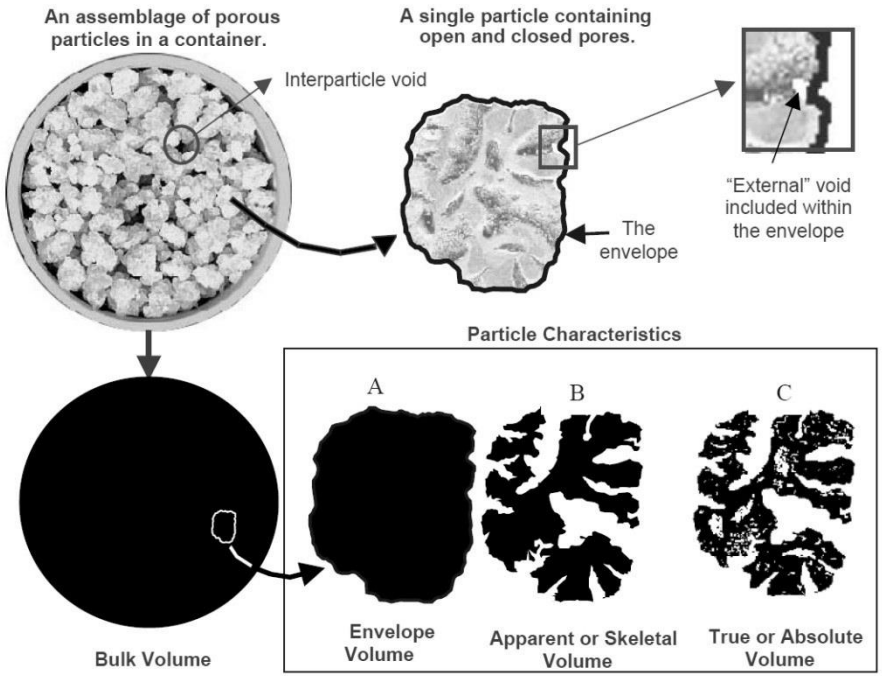

Figure 4.3 – different volume types (65), A – all pores are included, B – only the closed pores included, C – no pores included (true density)

Determining this density in case of the investigated fuels becomes problematic. When the geometry of a particle makes finding of its volume impossible one has to consider using a pycnometer to measure it. It is a vessel with a precisely known volume. Although a pycnometer is used to determine the density of a solid, it measures volume of the fluid displaced by the said solid; a balance is used to determine mass. A quantity of a dry, pre-weighed solid sample is placed in the pycnometer and the rest of the vessel is filled with a liquid with a known density (typically water, but also gases like helium when the absolute density is to be measured), the weight of the pycnometer filled only with the liquid having previously been established. The density of the sample can be determined from the known density of the fluid, the weight of the pycnometer filled only with the liquid, the weight of the pycnometer containing both sample and the liquid and the weight of the sample:

$$\rho_{solid} = \frac{(m_2 - m_1)}{(m_1 - m_0) - (m_3 - m_2)} \cdot \rho_{fluid} \qquad \text{Equation 4.1}$$

Where:

m_0 – mass of the empty pycnometer,

m_1 – mass of the pycnometer filled only with the fluid,

m_2 – mass of the pycnometer filled only with the solid,

m_3 – mass of the pycnometer filled with the solid and the fluid (voids between the solid particles filled with the fluid),

ρ_{fluid} – density of the fluid,

ρ_{solid} – density of the solid.

The measurement with the pycnometer was carried out three times for each solid (wood chip, SRFs) in order to assure the reproducibility of the results.

It has to be kept in mind however that a liquid such as water (standard method) will quickly penetrate the pores in particles of the investigated fuels during the measurement. This means that the density measured with a typical pycnometer will be higher than the envelope density since air containing pores in the fuel particles will be filled with water. If the structure of particles makes an accurate measurement with water impossible, another liquid is used. Mercury being a non-wetting liquid will not penetrate pores under ambient pressure and is a good choice while measuring density of relatively small samples i.e., when the sample material is very homogenous and consists of small particles like coal dust or finely ground minerals. Wood chips or solid recovered fuels are however much less homogeneous. It has been decided that the volume of the pycnometer should be comparable to the volume of the fuel vessel in the KLEAA reactor which is 10l. Amount of mercury needed for such pycnometer would be hard to obtain and certainly very hazardous to handle with. Alternatively to mercury, a measurement method by displacement of a dry medium has been suggested. The displacement technique applies also to a solid object immersed in a bed of much smaller solid particles. Solid particles do not penetrate pores (similar to mercury) and provide means by which envelope density can be determined in a safe manner. Unfortunately, there are no standards defining the procedure of such measurement and there is only one known-of commercial instrument for pycnometry based on the displacement of a dry medium – Micromeritics' GeoPyc Model 1360. Sample chambers of this instrument have volumes up to only 50cm³ which is not big enough to allow measurements on SRFs. The best results are obtained for particle sizes of around 2mm. Furthermore, the exact composition of the dry medium (Dry*Flo*®) with a high degree of flow-ability used in the instrument is the company's know-how. Further on such dry mediums will be called as quasi-fluids.

Because of the lack of an appropriate, commercially available equipment, a custom made pycnometer has been built. It is presented in Figure 4.4 below.

A. B. C. D.

Figure 4.4 – Built pycnometer filled with wood spheres (A), filled partially with wood spheres and the filling quasi-fluid (B, C) and completely filled with both substances (D)

At first quartz pearls with a particle size of 50-100µm have been suggested for measurements, but the first experiment showed that this material does not have enough flow-ability, tends to build agglomerates and adheres to more humid fuels (e.g. BIOBS). These inconveniences forced to search for an alternative and it has been found, that Lycopodium spores have all the needed features. They have an excellent flow-ability, are hydrophobic and practically all particles are of the same size of about 30µm. Furthermore, this material is relatively cheap, available in large amounts and is biologically harmless, although a use of a dust mask (class P1) is recommended while handling. A method of using Lycopodium in a laboratory scale pycnometer is under development and is being improved. Measurements with materials with a known density such as steel and wood spheres have shown a very good reproducibility of the results. Envelope densities of wood chips (as delivered, water content 15 wt.%) and of SBS®1 (as delivered, water content 20 wt.%) are presented in chapter 5. Envelope density determined in this way can be applied directly in the KLEAA Code.

4.2.2.2. Measuring the specific surface area of the fuel particles

The second important physical parameter of the fuel is the surface area of its particles. As mentioned before, the envelope or "outer" surface is required by the KLEAA Code model which excludes BET-measurement for its determination. Two methods of the surface area determination were considered. At first, it was assumed that it will be sufficient to calculate the specific surface area of a particle $S_v\ [1/m]$ based on its Sauter mean diameter $d_p\ [m]$ defined mathematically as:

$$d_p = \frac{6}{S_v}$$ Equation 4.2

Here it was assumed that the particles are spherical. To apply this method it is needed to determine the mean diameter. In order to do that a sieving analysis of all three fuels (wood chips, SBS®1 and BIOBS) has been performed.

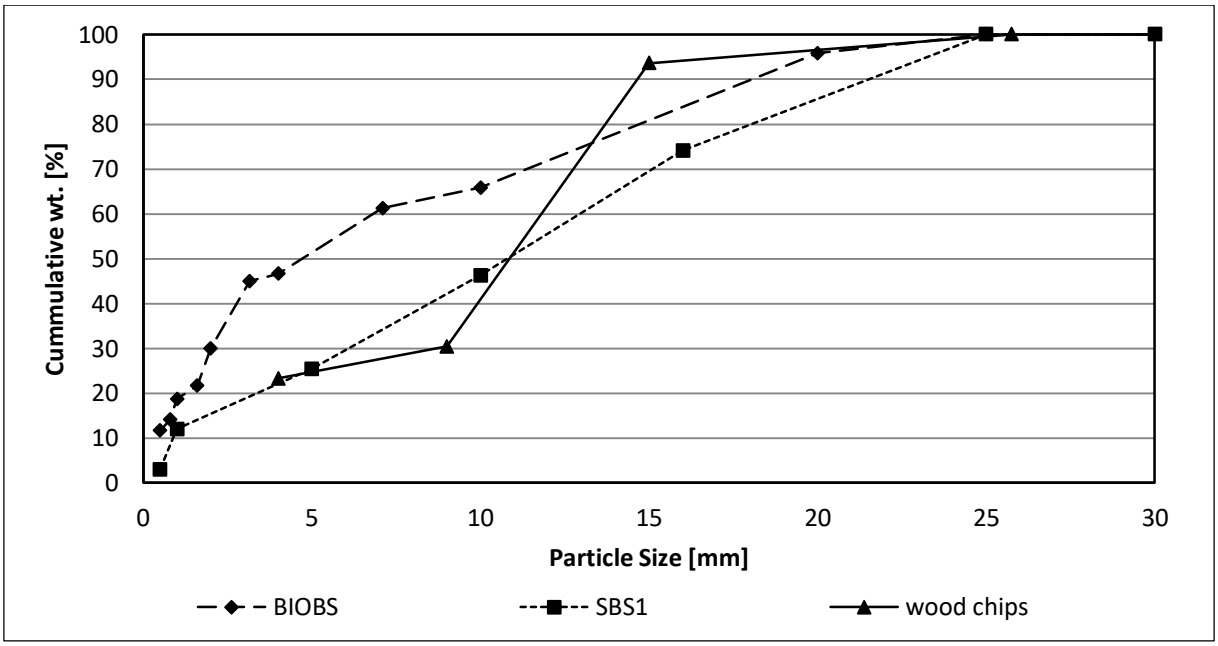

Figure 4.5 – Cumulative particle mass distribution for wood chips, SBS®1 and BIOBS

Based on this result the mean diameter has been calculated:

$$d_{p,mean} = \frac{1}{\sum \frac{m_{dp,i}}{d_{p,i}}} \qquad \text{Equation 4.3}$$

Where the $m_{dp,i}$ is the mass fraction of the particles with the diameter $d_{p,i}$. The calculated mean diameter $d_{p,mean}$ was assumed to be the Sauter mean diameter and the specific surface areas were calculated with the Equation 4.2. The results are presented below:

Table 4.1 – Sauter diameters and calculated specific surface areas for the investigated fuels

Fuel	Sauter mean diameter [mm]	Specific surface area [m^2/m^3]
Wood chips	9.0	665
SBS®1	6.7	900
BIOBS	3.8	1600

The simplification assumed in this method i.e. that all fuel particles are spheres is however far from true. For this reason, it was decided to look for an another method, which would take into account the low sphericity of the fuel particles. It has been found out that a pressure drop in a gas flow through a porous media is directly dependent of the outer specific surface area of the particles,

which is a known and well-investigated fact (66). Several equations presented below describe this phenomenon and allow to calculate the specific surface area provided that the pressure drop over a fuel bed height L, bulk density ρ_{bulk}, solid density ρ_{solid}, gas temperature T_g, its velocity v_g and the dynamic viscosity η of the gas are known:

Carman-Kozeny equation (66):

$$\frac{\Delta p}{\Delta L} = 4 \cdot \frac{(1-\psi)^2}{\psi^3} \cdot S_v^2 \cdot \eta \cdot v_g \qquad \text{Equation 4.4}$$

Ergun equation (66):

$$\frac{\Delta p}{\Delta L} = 150 \cdot \frac{(1-\psi)^2}{\psi^3} \cdot \frac{\eta \cdot v_g}{d_p^2} + 1.75 \cdot \frac{(1-\psi)^2}{\psi^3} \cdot \frac{p \cdot v_g^2}{d_p^2} \qquad \text{Equation 4.5}$$

Eisfeld & Schnitzlein (67):

$$\frac{\Delta p}{\Delta L} = 15.4 \cdot \left[\frac{p \cdot v_g \cdot d_p}{\eta} \cdot (1-\psi)\right]^{-0.332} \cdot \frac{(1-\psi)^2}{\psi^3} \cdot \frac{p \cdot v_g^2}{d_p} \qquad \text{Equation 4.6}$$

Porosity ψ is calculated with the equation:

$$\psi = 1 - \frac{\rho_{bulk}}{\rho_{solid}} \qquad \text{Equation 4.7}$$

Where the ρ_{solid} is the solid density calculated with the Equation 4.1 and the ρ_{bulk} is the bulk density of the solid calculated as follows:

$$\rho_{bulk} = \frac{m_{Fuel}}{V_{KLEAA}} \qquad \text{Equation 4.8}$$

m_{Fuel} is the total mass of the fuel in the fuel vessel of the KLEAA reactor and the V_{KLEAA} is the volume of this vessel.

In the equations by Ergun and Eisfeld-Schnitzlein (67) the packing is assumed to consist of monodisperse spheres with the equivalent particle diameter d_p. The specific surface area S_v can be therefore calculated from Equation 4.2. It is important that the d_p is smaller than the d_{tube} (67):

$$\frac{d_p}{d_{tube}} \leq 1{:}\,50 \qquad \text{Equation 4.9}$$

An instrument for the pressure drop measurement in granular solids has been built. It consists of a long tube made from Plexiglas with openings along it, which allow measuring the pressure drops. On the bottom of the tube, a fine grate is located, through which the air is supplied. For this purpose, the primary air supply of the KLEAA reactor is used. This assures, that the volumetric flow (and the velocity) of the incoming air is well controlled. The instrument is presented below:

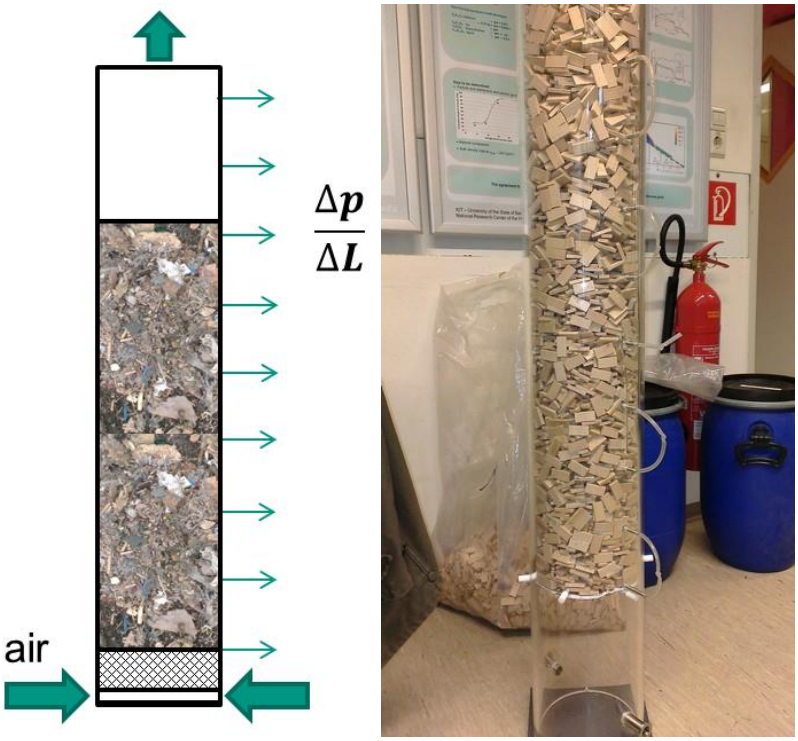

Figure 4.6 – Pressure drop measuring instrument

Preliminary measurements have shown a good reproducibility for granular solids consisting of spheres, cubes and plates with a known geometry:

Table 4.2 – Particle sizes

	Size	
Spheres	Diameter *d*	10 mm
Cubes	Edge *a*	10 mm
Plates	Edges *p, q, s*	5 mm, 10 mm, 15 mm

The tube has been filled with the particles, the gas flow was set to 10 Nm^3/h (laminar in the empty tube), the pressure drop was measured and the particles were removed from the tube. This procedure was repeated three times for each material; spheres, cubes, and plates. The deviation of the measured pressure drop for all forms did not exceed 2%. Since the sizes of all three particle forms were known (Table 4.2) it was possible to calculate the actual specific surface area of the particles:

$$S_v = \frac{A_p}{V_p}$$ Equation 4.10

Where the A_p is the surface of the particle and the V_p is its volume. This calculated, real specific surface was then compared with the one estimated with help of the pressure drop measurement and the Carman-Kozeny equation (Equation 4.4):

Table 4.3 – Calculated and measured specific surface area of the wood spheres, cubes and plates

	ρ_{solid}	ρ_{bulk}	porosity	dP/dL	Calculated S_v (Equation 4.10)	Measured S_v (Equation 4.4)	deviation
Unit	kg/m³	kg/m³	-	Pa/m	m²/m³		%
Spheres	690	450	0.35	41.5	600	728	21.3
Cubes	510	350	0.31	72.9	600	763	27.2
Plates	650	365	0.44	28.9	733	898	22.4

The foregoing results prove that the specific surface area measured with the proposed method has to be considered as a rather tentative value. The measured specific surface area for the investigated particles is over 20% higher than the calculated one. This inconsistency can be a result of the simplification in the Carman-Kozeny equation i.e., the assumption that the flow around the particles is laminar. Although the set gas flow guaranteed the laminar flow in the empty tube, the same flow through the packing might have been locally turbulent, which would have caused a higher pressure drop. The most probable reason for this was the turbulent flow through the packing caused by the sharp edges of the particles. For further investigation of this issue, the pressure drop for several other substances has been measured with a variable air flow, i.e., with different gas velocities. The limestone and dolomite were chosen for this experiment due to their availability, ease of handling and the diversity of the particles' sizes and shapes. EBS (German Ersatzbrennstoff), as well as the dried sewage sludge, are both recovered fuels what corresponds with the properties of the investigated SBS®1 and BIOBS. After the measurement, the specific surface areas of these materials have been calculated with each presented equation (4.4, 4.5, 4.6). The results are shown in the table 4.4:

Table 4.4 – Specific surface area of various materials with regard to different air volumetric flows

Material	$\dot{V}_{air}$	Carman-Kozeny			Ergun			Eisfeld-Schnitzlein		
		S_v [m²/m³]	S_v [%]	St. deviation [%]	S_v [m²/m³]	S_v [%]	St. deviation [%]	S_v [m²/m³]	S_v [%]	St. deviation [%]
Limestone 10-20mm	10	1133	100	15.5	703	100	3.0	533	100	3.0
	15	1320	116		726	103		547	103	
	20	1489	131		748	106		567	106	
Limestone 20-31mm	10	728	100	20.7	387	100	2.0	268	100	9.9
	15	920	126		403	104		311	116	
	20	1026	141		397	102		317	118	
Limestone >31mm	10	676	100	8.7	394	100	3.8	214	100	6.7
	15	768	114		370	94		211	99	
	20	785	116		366	93		189	88	
EBS	10	7639	100	11.6	6691	100	7.6	5840	100	1.5
	15	8708	114		7363	110		5802	99	
	20	9419	123		7699	115		5650	97	
Dolomite	10	1261	100	31.0	775	100	9.0	545	100	9.0
	15	1521	121		842	109		589	108	
	20	1687	161		844	118		596	118	
Sewage sludge	5	3298	86	10.0	3042	90	6.5	5030	113	9.5
	6	3372	88		3078	91		4746	107	
	10	3824	100		3375	100		4436	100	
	15	4101	107		3473	103		4021	91	
Wood chips	10	3410	-	-	4250	-	-	2000	-	-
SBS®1	10	11700	-	-	10700	-	-	10800	-	-
SBS®1 (porosity 0.4)	10	3150	-	-	2700	-	-	3000	-	-

A significant disadvantage of the formula proposed by Carman and Kozeny is that it is valid only for ideally smooth particles (67). In theory, the chosen air volumetric flows resulted with Reynolds numbers well below 2300, i.e., the flow was laminar. In practice, the rough particles or sharp edges (cubes, plates) can, however, disturb the laminar flow and introduce turbulences which are impossible to determine within the packing of a granular substance. Formula newly developed by Schnitzlein and Eisfeld (67) shows in such case a better convergence (low deviation) of the calculated specific surface areas while measuring pressure drop with different volumetric flows (ergo different Re numbers). The most prominent example of it is the measurement for EBS (German: Ersatzbrennstoff, English: Solid Recovered Fuel, see Table 4.4) i.e., for a solid recovered fuel. For this reason, the Eisfeld-Schnitzlein equation has been chosen for the estimation of the specific surface area of the SBS®1 and wood chips. There are two sets of results for the SBS®1 presented in Table 4.4. The first one i.e., specific surface areas 11700 m^2/m^3, 10700 m^2/m^3 and 10800 m^2/m^3 was obtained from the pressure drop measurement performed on the SBS®1 bulk “as poured” into the tube (Figure

4.6), what resulted in a very high porosity of the bulk. The discussed equations 4.3 to 4.5 provide the best results for the porosities around 0.4 (67). For this reason, the pressure drop in the SBS®1 bulk was performed again but the material was slightly compressed manually in order to obtain the desirable porosity.

It has to be kept in mind that the described measurement procedure is not a standardised one. There is no reference to which the obtained results can be compared and therefore validated. For this reason, they need to be treated as roughly estimated values.

4.3. Step Two – Characterisation of the combustion behaviour in the KLEAA reactor

The second step of the fuel characterization includes a combustion test of the fuel to be described and an evaluation of the results according to the model proposed by Bleckwehl (25). Combustion in the KLEAA reactor can be described with several fuel-specific characteristic numbers. They also allow describing the combustion behaviour in a grate firing. Although the model is simplified it can give an indication about the process and on how to adjust the combustion parameters in a grate firing.

The model is based on several characteristic numbers:

4.3.1. Ignition time t_Z

The ignition time, also known as ignition delay is defined as the time needed for the ignition of the upper layer of the feedstock, from the moment, when the fuel vessel with the fuel is moved under the heated furnace. The ignition time may be determined from the temperature T2 (see Figure 4.7), as well as from the concentration of oxygen in the flue gas. The video taken by the camera located above the combustion chamber may be used for control purposes. When the velocity of the feedstock on an exemplary moving grate is known, the ignition time allows estimating the location, where the fuel ignites.

4.3.2. Reaction front velocity u_{RF}

The reaction front velocity describes the velocity of the ignition front of the fuel bed. It is determined by the inflection points on temperature signals collected by each thermocouple:

$$\mathrm{u_{RF}} = \frac{l}{t}\left[\frac{mm}{min}\right] \qquad \text{Equation 4.11}$$

Where l is the distance between two consecutive thermocouples (e.g., T2 and T3) and equals 20mm. t is the time between the moments when the inflection points on the consecutive temperature signal were registered (see figure below):

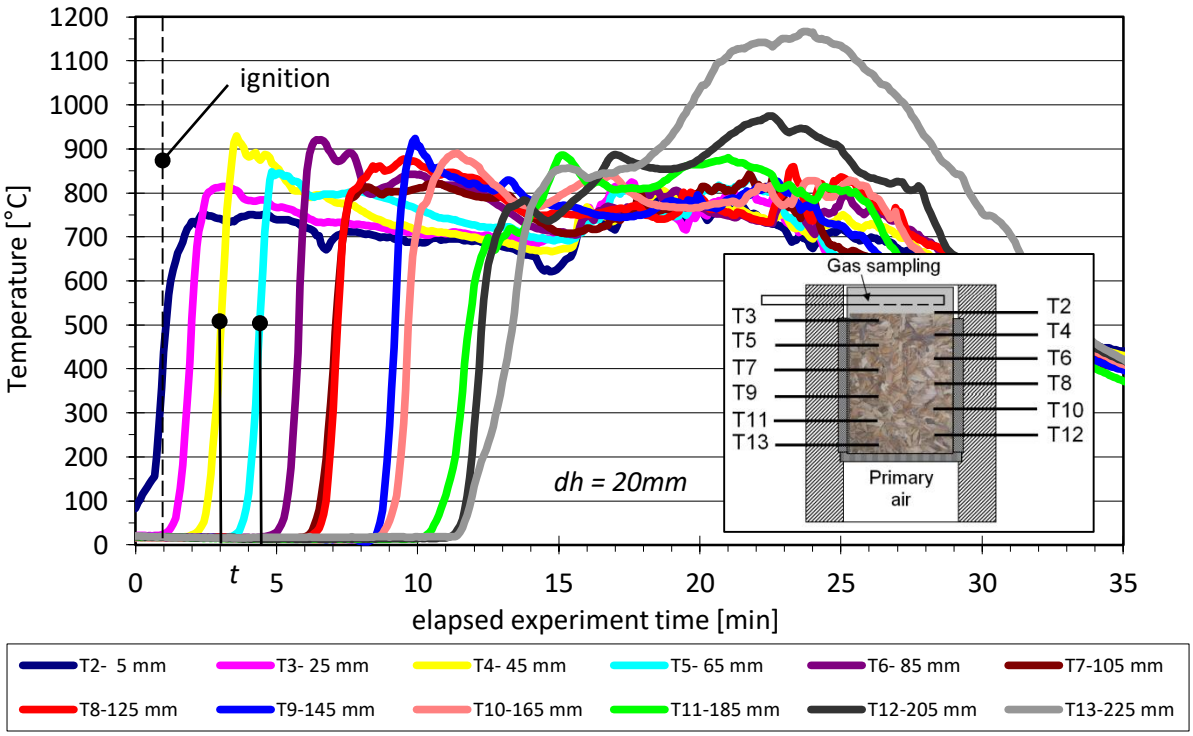

Figure 4.7 – Exemplary temperature signal from thermocouples installed in the fuel vessel. Wood chips combustion in the KLEAA reactor.

The distance l between two consecutive thermocouples is 20mm. Top of the fuel bed is at 0mm and the bottom of the vessel is at 240mm.

4.3.3. *Ignition rate IR*

The ignition rate IR is defined as the product of the reaction front velocity and the bulk density of the feedstock.

$$\mathrm{IR} = \mathrm{u_{RF}} \cdot \rho_{\mathrm{bulk}} \left[\frac{kg}{m^2 s}\right] \qquad \text{Equation 4.12}$$

The ignition rate describes the amount of the fuel that is ignited per area and time due to the movement of the reaction front. When transferring the results to an industrial process (moving grate), the IR allows estimating that area of the grate, where the reaction front reaches the grate bars.

4.3.4. *Mass conversion rate MCR*

The mass conversion rate MCR describes the fuel mass loss per area and time. For a comparison of the ignition rate and mass conversion rate, the latter is corrected by the ash content of the fuel. The MCR is defined by the formula:

$$MCR = \frac{-dm_F}{A_{Grate} \cdot (1-\xi_{Ash,F}) \cdot dt} \left[\frac{kg}{m^2 s}\right] \qquad \text{Equation 4.13}$$

where:

$m_F\ [kg]$ - fuel mass,

$A_{Grate}\ [m^2]$ - grate area (here fuel bed area),

$\xi_{Ash,F}\ [\%]$ - ash content.

The mass conversion rate is determined from the balance signal dm_F/dt by linearization. Two different combustion stages can be distinguished during the combustion of biomass; The quasi-stationary main combustion zone and the char burnout. Both stages are characterised by different mass conversion rates, MCR1 and MCR2:

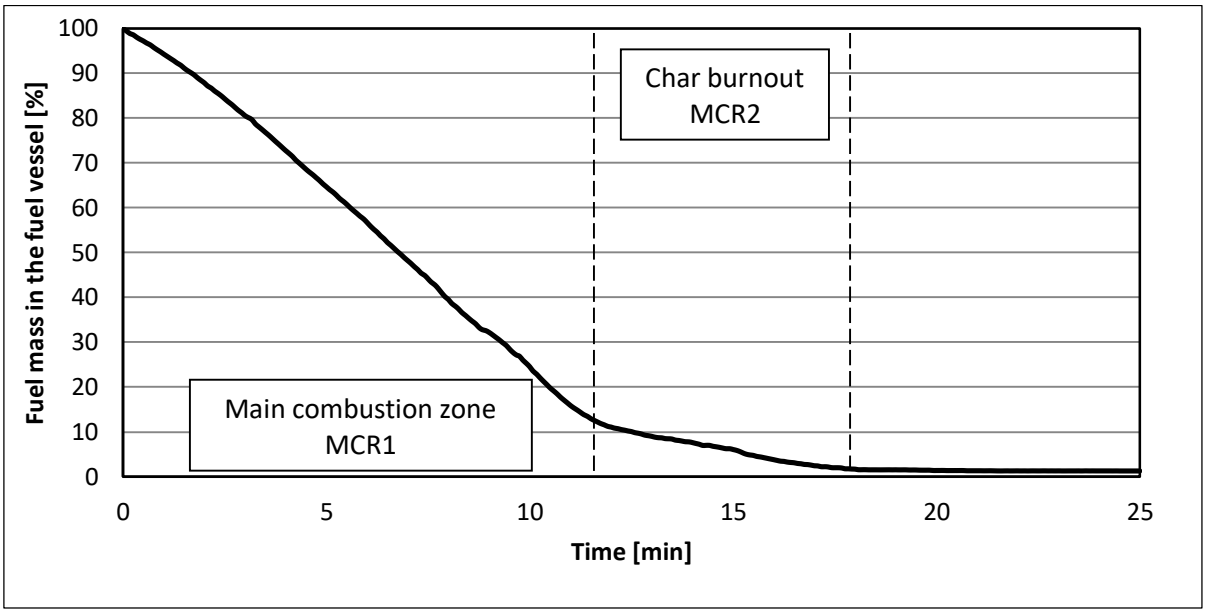

Figure 4.8 – Exemplary fuel conversion. Combustion of wood chips in the KLEAA reactor.

The mass conversion rate allows an estimation of the needed length of the grate.

4.3.5. Specific heat release HR_{Grate}

By multiplying the MCR by the lower heating value of the applied fuel NCV_F another characteristic – specific heat release HR_{Grate} can be determined:

$$HR_{Grate} = MCR \cdot NCV_F \left[\frac{W}{m^2}\right] \qquad \text{Equation 4.14}$$

It allows the calculation of a thermal output for a given fuel and the grate area. The specific heat release defines how wide the grate needs to be in order to reach a desired power output from the combustion of a given fuel. Secondly, it tells the power plant operator what is the thermal load of the grate bars and how they need to be cooled.

4.3.6. Local air ratio

The air ratio designated as λ describes the stoichiometry of the combustion process. If the air ratio is lower than 1, the combustion is under-stoichiometric (fuel-rich) and the fuel is not fully converted during the process i.e., there are unburned gaseous components present above the fuel bed – CO,

H_2, CH_4 and to some extent also higher hydrocarbons C_nH_m. At air ratios higher than 1 there is always an abundance of oxygen above the fuel bed and all the fuel can be completely converted to CO_2 and H_2O assuming an ideal mixing of the gases above the fuel bed. The local $\lambda(t)$ can be calculated from the equation:

$$\lambda(t) = \frac{\dot{n}_{O2,PL}}{\dot{n}_{O2,PL} - \dot{n}_{O2,RG} + \frac{1}{2}\dot{n}_{CO,RG} + 2\dot{n}_{Corg,RG} + \frac{1}{2}\dot{n}_{H2,RG}} \quad (25)$$ Equation 4.15

Where:

$\dot{n}_{O2,PL}$ – molar flow rate of the oxygen in the primary air,

$\dot{n}_{O2,RG}$ - molar flow rate of the oxygen in the flue gas,

$\dot{n}_{CO,RG}$ – molar flow rate of the carbon monoxide in the flue gas,

$\dot{n}_{Corg,RG}$ – molar flow rate of the methane in the flue gas,

$\dot{n}_{H2,RG}$ – molar flow rate of the hydrogen in the flue gas.

These local molar flow rates are calculated using the local gas concentrations measured above the fuel bed. The figure below shows exemplary profiles of the gas concentrations above the fuel bed in the KLEAA reactor:

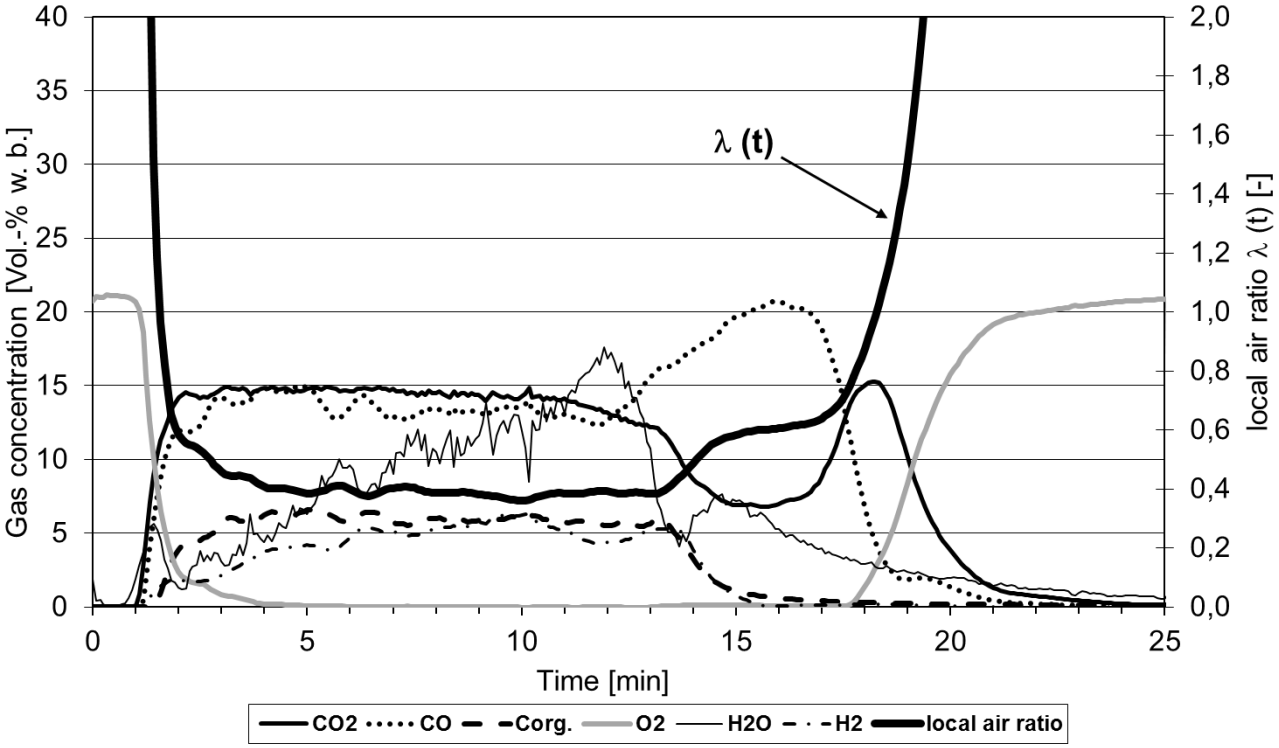

Figure 4.9 – Exemplary gas concentrations measured above the fuel bed. Combustion of wood chips (water content 15 wt.%) in the KLEAA reactor.

It is known from the studies mentioned in chapter 2.2 that the amount of the supplied primary air (i.e., also air ratio) has a significant impact on the fuel conversion rate and therefore also on the heat released during the process. Adjusting the primary air flow locally is, therefore, a convenient way to equally distribute the thermal load of the grate bars along the whole grate.

4.3.7. Transferring the results from a fixed bed on a moving bed

The transferring of the results onto a moving grate from the fixed bed is only possible when the specific primary air flows and temperatures in both experimental setups are the same. Blackwehl (25) also stated that the procedure can be applied only for fuels with a low ash content and only when the mixing of the fuel on the moving grate is limited.

It has already been mentioned that the stages of the combustion in a fixed bed occur chronologically, whereas the same stages take place on a moving bed locally over the length and height of the fuel bed. This means that if the velocity of the moving bed u_{bed} is known, one can translate time t related parameters like gas concentration $C(t)$ or temperature $\vartheta(t)$ to distance x related ones $C(x)$ and $\vartheta(x)$ with the following formula:

$$x = t \cdot u_{bed} \qquad \text{Equation 4.16}$$

Fuel mass in the fixed fuel vessel $m(t)$ expressed in % (as a part of the initial amount) is translated in the same manner but has to be expressed as mass flow $\dot{m}(x)$ in % for moving grates.

This technique allows finding the local combustion parameters in a grate firing in which fuel mixing processes are limited or do not take place at all. Examples are travelling grates and forward acting grates such as TAMARA. In reverse acting grates some fuel particles can be transported backwards from a grate zone where one combustion stage takes place to a different one (e.g., particles from the char burnout zone travel back into the main combustion zone), which changes the combustion parameters in both zones. The three-step characterisation concept has no means to model this behaviour.

Finding the effective fuel bed velocity on the grate is not an easy task. The relations between the grate bars geometry, their movement and the movement of fuel particles different in size are very difficult to describe. For this reason, a numerical and empirical approach to calculating an effective velocity of the fuel bed is preferred. Such approach has been undertaken by Džiugys and Hunsinger (68). A series of experiments at the TAMARA pilot plant has been conducted; a charge of wood chips with a number of particles marked with different colours has been placed on the grate and the drive of the grate bars has been turned on. The facility was cold at the time of the experiment and there was no combustion process occurring. During the experiment, the actual residence time of the fuel particles on the grate was measured. Theoretical residence time set in the process control system of

TAMARA is calculated on the other hand directly from the movement of the grate bars and the geometry presented in the table and in the figure below. A reciprocating grate bar moves forwards and backwards covering a distance (amplitude) *w* during a period of time *f*.

Table 4.5 – Kinematics of the grate

Zone	Amplitude *w* [mm]	Period *f* [s]
1	100	38
2		40
3		74
4		78

The velocity of an illustrative point attached to a grate bar can be easily calculated from the equation below:

$$u_{GB} = \frac{w}{f}$$ Equation 4.17

Grate bars are however inclined to the surface area of the grate by the angle ω=24°:

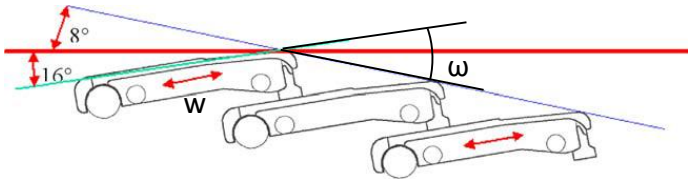

Figure 4.10 – Geometry of the grate bars (68)

For this reason, the velocity of a point pushed by a grate bar along the grate surface equals:

$$u_{Grate} = \frac{w}{f} \cdot cos\omega$$ Equation 4.18

Grate velocity defined in this way allows calculating the theoretical residence time which is set in the process control system for each primary air zone *i*:

$$t_{res,i,theor} = \frac{l_{Zone,i}}{u_{Grate,i}}$$ Equation 4.19

Total theoretical residence time is the sum of the residence times in each of the four primary air zones at the TAMARA plant:

$$t_{res,theor} = t_{res,1theor,} + t_{res,2,theor} + t_{res,3,theor} + t_{res,4,theor}$$ Equation 4.20

and based on the case investigated by Hunsinger (68) equals 33.6 minutes. The residence times experimentally determined in (68) differ however from the theoretical ones. It has been measured that smaller particles tend to stay longer on the grate, while the residence time is shorter for the bigger ones. The tendency is presented in the figure below:

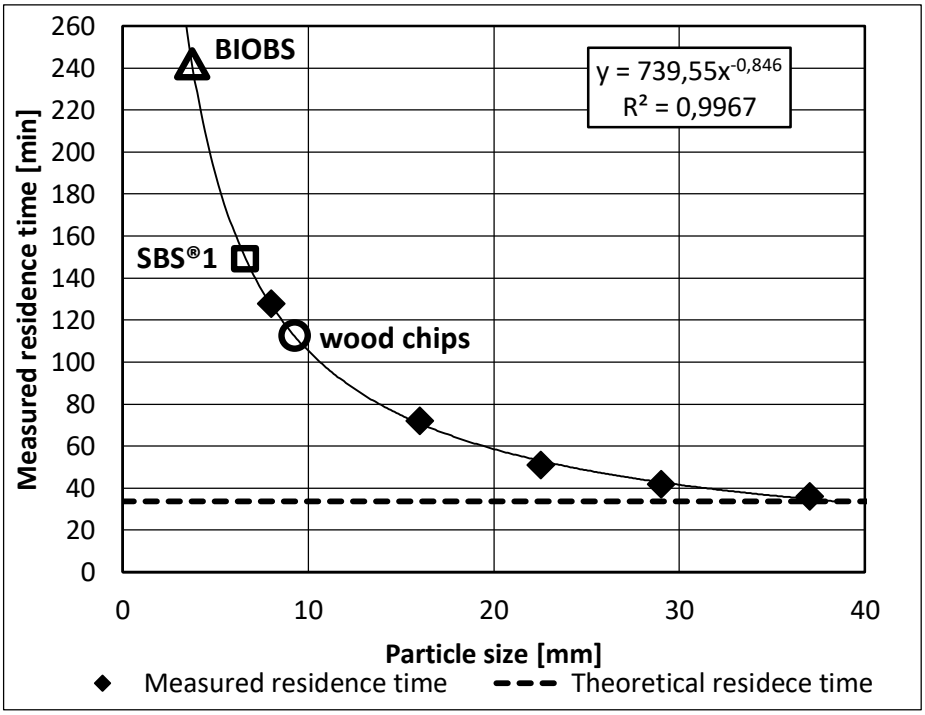

Figure 4.11 – Residence time of fuel particles on the grate (68)

When we consider for the sake of simplicity that all particles of the wood chips investigated in this thesis have the same particle size, we obtain a mean diameter of 9mm (sieving analysis). For this particle size the residence time measured in (68) is ca. 115 minutes (see Figure 4.11). Extrapolation of the measured residence times for the particle sizes of the SBS®1 and BIOBS gives the results presented in the table below:

Table 4.6 – Mean residence times for the fuel investigated in this thesis

Fuel	Mean diameter [mm]	Total residence time [min] t_{res}
Wood chips	9.0	115
SBS®1	6.7	148
BIOBS	3.8	239

The total residence time for the BIOBS i.e., 4h seems to be unrealistic considering the experience with the TAMARA facility. This residence time is most likely much shorter due to the tendency of the investigated fuels to agglomerate smaller single particles into bigger chunks (which means larger mean diameter and shorter residence time). It was furthermore observed that the finest fraction of the BIOBS and to some extent also of the SBS®1 consist in a small part of sand and small stones which do not combust and tend to fall down through the grate bars. The mean fuel bed velocity on the grate can be calculated:

$$u_{bed} = \frac{l_{Zone}}{t_{res}}$$ Equation 4.21

This equation can be applied to each primary air zone separately.

4.4. Step Three – Combustion in the TAMARA pilot plant

Once step one and step two have been carried out a description of the combustion behaviour in the large or pilot scale i.e., step three is conducted. It has been done at ITC by firing all three fuels, wood chips, SBS®1 and BIOBS in the TAMARA pilot plant. Data evaluation after the experiment starts with mass and energy balance of the whole plant in order to check the plausibility of the measurements. Then each primary air zone of the grate is balanced with the primary air and the fuel mass flow as input and the raw flue gas before the secondary air supply and ash or remaining fuel as output. The goal is to determine the mass conversion in each primary air zone, which is then normally compared with the one estimated in KLEAA reactor during step two. The procedure is discussed in chapter 4.4.2.

Combustion experiments planned for the TAMARA pilot plant as a part of the RECOMBIO project have had a demonstration character and a different goal than the validation of the fuel characteristics transferred from the step two. In total 10 experiments were carried out involving wood chips, SBS®1 and BIOBS including mixtures of wood chips and these solid recovered fuels. One of the most important aims of the measurement campaign was an evaluation of the high-temperature corrosion risk related to combustion of fuels with an elevated chlorine content i.e., SBS®1 and partially BIOBS. Another goal was to test and calibrate an on-line NIR-instrument measuring the chlorine content in the fuel and working under different conditions than standard ones. Normally an NIR-detector is located above a conveyor belt on which the fuel material is spread out so that every particle is visible for the detector. This assures a maximal accuracy of the chlorine measurement. In contrary to this procedure the detector was installed above a narrow conveyor on which a thick fuel layer was transported into the furnace and only the top layer of this fuel was visible. The accuracy of this measurement procedure has been assessed. Last but not least the particle size distribution of the fly ash has been measured.

4.4.1. Test program and combustion parameters

Since the combustion behaviour in the KLEAA changes in a rather linear manner with the changing content of the SRF in the fuel mixture only three mixing ratios have been chosen for analysis at TAMARA pilot plant; wood chips as reference fuel, a mixture of wood chips and 60% of an SRF and lastly 100% of an SRF (both BIOBS and SBS®1). Only the results of the experiments with pure wood chips and SBS®1 have been chosen for the validation of the simulations performed with the KLEAA Code.

The campaign started with warming the facility up to the operating temperature of around 1000°C in the first boiler duct. It has been controlled via the gas sampling probe installed in the first boiler pass (Figure 3.3). Oxygen concentration registered at this point was kept between 9-11%. To assure these conditions, the secondary air flow was adjusted. Fuel mass flow for all fuel mixtures was set to reach an equal thermal power output of about 450kW in all experiments. Combustion tests relevant for this thesis, as well as the main parameters are presented below in the table:

Table 4.7 – Main parameters set for the combustion tests in the TAMARA

Parameter	Unit	Fuel		
		Wood chips	SBS®1	BIOBS
Fuel mass flow	kg/h	120	105	150
Primary air Zone 1	m^3/h	50	45	35
Primary air Zone 2	m^3/h	100	90	70
Primary air Zone 3	m^3/h	200	210	140
Primary air Zone 4	m^3/h	50	55	35
Secondary air flow	m^3/h	160	120	100
Air temperature	°C	32	35	36
Theor. residence time Zone 1	min	6	6	6
Theor. residence time Zone 2	min	6	6	12
Theor. residence time Zone 3	min	12	12	12
Theor. residence time Zone 4	min	12	12	12

The fuel mass flows were initially calculated so the total thermal output equals roughly 450kW during the combustion of each fuel (see chapter 5 for the lower calorific values of the fuels.) It can be noticed that the residence time set in the second primary air zone for the BIOBS is two times longer than for the other fuels. This is caused by the fact that the BIOBS has a much higher water content (over 36 wt. % as opposed to 15 wt. % for wood chips and 20 wt. % for SBS®1) and the mass conversion rate in the main combustion zone measured in the KLEAA reactor is much slower for this fuel than for the wood chips and the SBS®1 (see chapter 5.2.2.). This means that this fuel needs to stay longer on the moving grate in order to assure complete combustion.

4.4.2. Data evaluation procedure

Mass, material and energy balance was used for the validation of the measurement results. Incoming and outgoing flows (Figure 4.12) were averaged over time ranges, when the gas sampling probes at

the fuel bed were in use and the combustion process was stable. Results of balancing will be presented in the next section.

4.4.2.1. Mass balance

The mass balance is presented in the figure below:

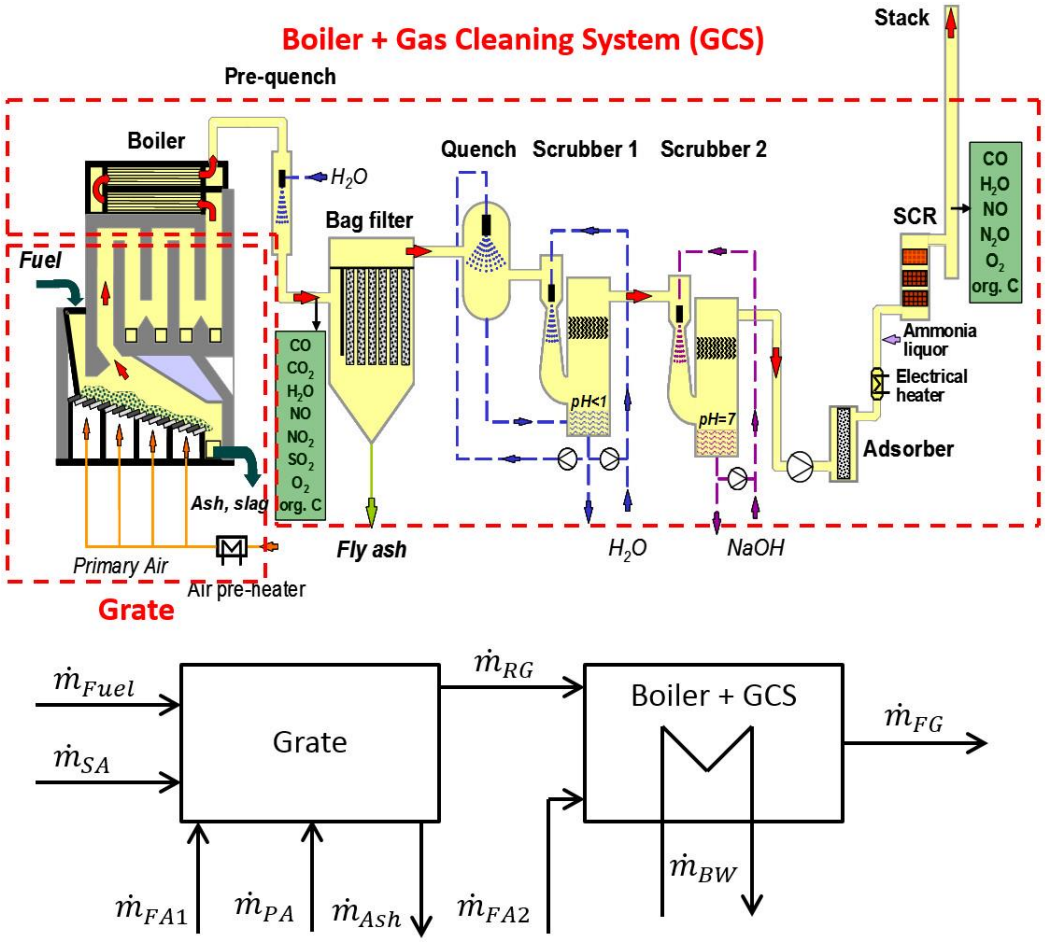

Figure 4.12 – Incoming and outgoing mass flows in TAMARA

Following mass flows presented in the figure above are known (measured):

$\dot{m}_{Fuel}$ – total amount of fuel supplied into the system (set in the Process Control System (PCS) in [kg/h]),

$\dot{m}_{Ash}$ - calculated from the proximate analysis,

$\dot{m}_{PA}$ – primary air mass flow (set in the PCS per grate zone),

$\dot{m}_{SA}$ – secondary air mass flow (set in the PCS),

$\dot{m}_{BW}$ – mass flow of the water supplied into the boiler (set in the PCS),

$\dot{m}_{FG}$ – mass flow of the flue gas (measured before the stack, wet).

Mass flows of the false air (also known as leaked air) $\dot{m}_{FA1}$ and $\dot{m}_{FA2}$ as well as the flow of the raw gas $\dot{m}_{RG}$ need to be calculated. The $\dot{m}_{FA2}$ is found from the mass balance of the block consisting of the boiler and the gas cleaning system:

$$\dot{m}_{FA2} = \dot{m}_{FG} - \dot{m}_{RG} \left[\frac{kg}{h}\right] \quad \text{Equation 4.22}$$

These mass flows are calculated from the volumetric flows $\dot{V}_{FA2}$ (calculated), $\dot{V}_{FG}$ (measured), $\dot{V}_{RG}$ (calculated) and the densities of the leaked air ρ_{FA2}, flue gas ρ_{FG} and the raw gas ρ_{RG}. The gases are considered to be ideal gases and their densities are calculated using their composition which is known (measured). The $\dot{V}_{RG}$ is not measured in TAMARA, therefore there are two unknowns in Equation 4.22 and an additional equation is needed in order to find all the variables. Here the oxygen mass balance is used:

$$\dot{m}_{RG} \cdot x_{O2,RG} + \dot{m}_{FA2} \cdot 0.23 = \dot{m}_{FG} \cdot x_{O2,FG} \quad \text{Equation 4.23}$$

After transforming the equations:

$$\dot{m}_{RG} = \dot{m}_{FG} \cdot \frac{0.23 - x_{O2,FG}}{0.23 - x_{O2,RG}} \quad \text{Equation 4.24}$$

Volumetric flow $\dot{V}_{FG}$ is measured at the stack and has to be transformed to obtain the mass flow $\dot{m}_{FG}$. It can be easily achieved as the gas concentrations in the flue gas are measured (see Annex A). The oxygen concentrations after the boiler $x_{O2,RG}$ and after the gas cleaning system $x_{O2,FG}$ are measured as dry volumetric concentrations and can be applied in Equation 4.24 after transforming.

After $\dot{m}_{RG}$ is found, the amount of the leaked air coming into the system in the grate area $\dot{m}_{FA1}$ can be calculated. This value is critical for the balancing of the grate itself and for the finding of the mass conversion values along the grate.

$$\dot{m}_{FA1} = \dot{m}_{Fuel} + \dot{m}_{PA} + \dot{m}_{SA} - \dot{m}_{RG} - \dot{m}_{Ash} \quad \text{Equation 4.25}$$

The only left unknowns in the equation above are the air mass flows. The volumetric flows $\dot{V}_{PA}$ and $\dot{V}_{SA}$ are set in the PCS in [m^3/h], therefore the air temperature (see Annex A) is needed to find the right air density and the mass flows $\dot{m}_{PA}$ and $\dot{m}_{SA}$:

$$\dot{m}_{PA} = \dot{V}_{PA} \cdot \rho_{air} \quad \text{Equation 4.26}$$

$$\dot{m}_{SA} = \dot{V}_{SA} \cdot \rho_{air} \quad \text{Equation 4.27}$$

All set and calculated volumetric and mass flows for wood chips and for SBS®1 are presented below in table 4.8. Primary air flow is split into each primary air (grate) zone:

Table 4.8 – Incoming and outgoing mass streams during wood chips and SBS®1 combustion in TAMARA

Flow	Unit	Wood chips				SBS®1				BIOBS			
$\dot{m}_{Fuel}$	[kg/h]	120				105				150			
$\dot{m}_{PA}$		57	114	230	57	50	102	236	62	41	81	161	40
$\dot{m}_{SA}$		178				136				115			
$\dot{m}_{FA1}$		523				540				520			
$\dot{m}_{FA2}$		250				168				165			
$\dot{m}_{BW}$		409				347				322			
$\dot{m}_{FG}$		1531				1394				1307			
$\dot{m}_{RG}$		1279				1226				1142			
$\dot{m}_{Ash}$		3				11				8			

The table above confirms the suspicion that there is a significant amount of the leaked air coming into the system in the grate area. The total amount of the leaked air $\dot{m}_{FA1}$ well exceeds the set amount of the primary air by 114 wt. % for wood chips and by 120 wt. % for the SBS®1. This means that the total amount of the primary air is for both experiments over the double the amount set in the PCS. Furthermore, the leaked air mass flows are not the same in each primary air zone. For this reason, an additional experiment was needed in order to find the leaked air distribution.

Before the measurements, when the plant was not heated up an attempt to find this distribution was undertaken. Primary air blowers were set to deliver the same amount of primary air into each zone and a known amount of carbon dioxide from high-pressure tanks was supplied to each zone below the grate. The CO_2 concentrations were then measured in each grate zone. The amount of the leaked air can be calculated from the mass and material balance:

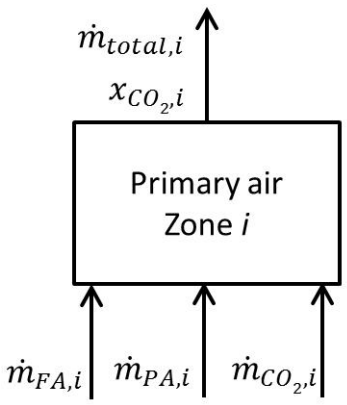

Figure 4.13 - CO_2 balance

$$\dot{m}_{total,i} = \dot{m}_{FA,i} + \dot{m}_{PA,i} + \dot{m}_{CO2,i}$$ Equation 4.28

$$\dot{m}_{total,i} \cdot x_{CO2,i} = \dot{m}_{FA,i} \cdot 0 + \dot{m}_{PA,i} \cdot 0 + \dot{m}_{CO2,i} \cdot 1$$ Equation 4.29

Therefore:

$$\dot{m}_{total,i} \cdot x_{CO2,i} = \dot{m}_{CO2,i}$$ Equation 4.30

And:

$$\dot{m}_{FA,i} = \frac{\dot{m}_{CO2,i}}{x_{CO2,i}} - \dot{m}_{CO2,i} - \dot{m}_{PA,i}$$ Equation 4.31

The amount of the primary air set for this experiment $\dot{m}_{PA,i}$ was however much lower than the primary air flows set during the measurements with wood chips and SBS®1. The reason for that was the convenience of the CO_2 concentration measurement. The smaller the primary air flow, the higher the CO_2 concentration detected over the grate and the higher the accuracy of the measurement. This means however that the estimated leaked air distribution has to be presented in a dimensionless form:

$$\xi_{FA,i} = \frac{\dot{m}_{FA,i}}{\dot{m}_{FA,total}}$$ Equation 4.32

The amount of the leaked air can be calculated with the equation above for any primary air flow. The leaked air ratio $\xi_{FA,i}$ for every primary air zone is shown below:

Table 4.9 – Leaked air distribution along the grate

	PA Zone 1	PA Zone 2	PA Zone 3	PA Zone 4
$\xi_{FA,i}$	0.607	0.105	0.184	0.105

With this leaked air factors, the actual, total amounts of the primary air supplied into each grate zone can be calculated and used in the grate balance. In this way, the mass conversion along the grate can be found. The mass balance takes the following form:

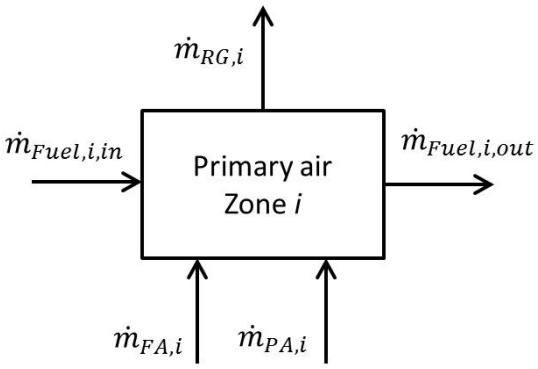

Figure 4.14 – Mass balance in the primary air zone *i*

$$\dot{m}_{Fuel,i,in} + \dot{m}_{FA,i} + \dot{m}_{PA,i} = \dot{m}_{RG,i} + \dot{m}_{Fuel,i,out} \quad \text{Equation 4.33}$$

There are two unknown values in the equation above; mass flow of the fuel leaving the primary air zone $\dot{m}_{Fuel,i,out}$ and the mass flow of the raw gas $\dot{m}_{RG,i}$. Primary air mass flow $\dot{m}_{PA,i}$ is set in the PCS. Starting from the first primary air zone, the $\dot{m}_{Fuel,1,in}$ is also set in the PCS. Furthermore:

$$\dot{m}_{Fuel,i,in} = \dot{m}_{Fuel,i-1,out} \quad \text{Equation 4.34}$$

It is possible to find these two unknowns with Equation 4.33 coupled with the nitrogen balance formulated for the primary air zone:

$$\dot{m}_{Fuel,i,in} \cdot x_{N2,Fuel} + \dot{m}_{FA,i} \cdot x_{N2,air} + \dot{m}_{PA,i} \cdot x_{N2,air} = \\ = \dot{m}_{RG,i} \cdot x_{N2,RG,i} + \dot{m}_{Fuel,i,out} \cdot x_{N2,Fuel} \quad \text{Equation 4.35}$$

Nitrogen flow related to the fuel N can be neglected based on the elementary analysis of the fuel. Nitrogen flows related to the primary and leaked air are easily calculated as the mass flows of the incoming air are known. Nitrogen concentration in the raw gas is found from the equation:

$$x_{N2,RG,i} = 1 - (x_{O2,RG,i} + x_{CO2,RG,i} + x_{H2O,RG,i} + x_{CO,RG,i} + x_{H2,RG,i} + x_{CH4,RG,i}) \quad \text{Equation 4.36}$$

All gas concentrations above the grate are measured in [Vol. %] and are presented in Annex B. In order to apply these values on the right side of Equation 4.36 it is necessary to express them in [wt. %]. It is possible to convert volumetric concentrations into weight fractions when the densities $[kg_j/Nm^3]$ of the flue gas and its species *j* are known. When we consider all the gases as ideal gases, the densities can be obtained from the ideal gas equation. Weight fractions of the gases measured above the grate in each primary air zone are presented in Annex C.

Equation 4.36 is put into Equation 4.35 and the raw gas mass flow from a grate zone *i* is obtained from the expression:

$$\dot{m}_{RG,i} = \frac{x_{N2,air} \cdot \left(\dot{m}_{FA,i} + \dot{m}_{PA,i}\right)}{x_{N2,RG,i}}$$ Equation 4.37

It is then put into Equation 4.33 and the fuel mass flow outgoing from the grate zone can be found:

$$\dot{m}_{Fuel,i,out} = \dot{m}_{Fuel,i,in} + \dot{m}_{FA,i} + \dot{m}_{PA,i} - \dot{m}_{RG,i}$$ Equation 4.38

Once this procedure is performed for every zone of the grate the fuel mass flow $\dot{m}_{Fuel}$ is expressed as a function against the grate length and can be compared with the results transferred from the fixed bed. The calculated mass conversion is also used for validation of the KLEAA Code.

4.4.2.2. Material and energy balance

On the basis of the conducted mass balance the material (C, H, O, N, S) and energy balances are performed. They serve as a further plausibility check of the performed measurements. The equations are listed below:

$$\dot{m}_{C,input} = \dot{m}_{Fuel} \cdot x_{C,Fuel}$$ Equation 4.39

$$\dot{m}_{C,output} = \dot{m}_{FG} \cdot \frac{12}{44} \cdot x_{CO2,FG} + \dot{m}_{ash} \cdot x_{C,ash}$$ Equation 4.40

$$\dot{m}_{H,input} = \dot{m}_{Fuel} \cdot x_{H,Fuel} + \dot{m}_{Fuel} \cdot \frac{2}{18} \cdot \left(x_{H2O,Fuel} + x_{H2O,air}\right)$$ Equation 4.41

$$\dot{m}_{H,output} = \dot{m}_{FG} \cdot \frac{2}{18} \cdot x_{H2O,FG}$$ Equation 4.42

$$\dot{m}_{O,input} = \\ = \dot{m}_{Fuel} \cdot \left(x_{O,Fuel} + \frac{16}{18} \cdot x_{H2O,Fuel}\right) + \dot{m}_{total\ air} \cdot \left(x_{O2,air} + \frac{16}{18} \cdot x_{H2O,air}\right)$$ Equation 4.43

$$\dot{m}_{O,output} = \dot{m}_{FG} \cdot \left(x_{O2,FG} + \frac{32}{44} \cdot x_{CO2,FG}\right)$$ Equation 4.44

$$\dot{m}_{N,input} = \dot{m}_{total\ air} \cdot x_{N2,air}$$ Equation 4.45

$$\dot{m}_{N,output} = \dot{m}_{FG} \cdot x_{N2,FG}$$ Equation 4.46

Solving these equations gives the following results presented in table 4.10:

Table 4.10 – Material balance for wood chips, SBS®1 and BIOBS combustion in TAMARA pilot plant

	Wood chips			SBS®1			BIOBS		
Element	Input [kg/h]	Output [kg/h]	Deviation [%]	Input [kg/h]	Output [kg/h]	Deviation [%]	Input [kg/h]	Output [kg/h]	Deviation [%]
C	50.5	46.9	7.2	42.3	38.9	8.0	38.5	37.0	3.9
H	9.4	8.7	7.5	9.7	8.2	15.5	11.4	9.3	18.3
O	335.7	339.5	1.1	317.3	323.2	1.9	323.7	305.3	5.7
N	914	915	0.1	907	906	0.1	796	818	2.8

Deviations for all main elements for wood chips lie below 7.5%. This proves a very good accuracy of the performed measurements. The situation is not as good in case of SBS®1, especially for hydrogen, where the deviation between input and output equals 15.5% i.e., there is less hydrogen in the output. This might have been caused by the difference in the measured and actual water content in the SBS®1. The same remark applies also to BIOBS where the deviation in case of hydrogen is even higher and equals 18.3%. The campaign was carried out during exceptionally hot weather conditions, what might have led to an unintended fuel drying in the fuel conveyor. As a result, the actual water content in the combusted fuels was lower than of the analysed fuel samples. It has to be also kept in mind that the surface area of SBS®1 and BIOBS particles is much higher than of the wood chips (see Chapter 4.5), which facilitates a faster drying process.

Energy balance was calculated using measured mass flows of incoming and outgoing materials, their densities and temperatures (enthalpies). Obtained heat losses are in the range of typical pilot scale plants and small industrial facilities. The results are presented in Annex D.

Performed mass, material and energy balance have proven that the conducted measurements are satisfactory accurate and constitute an appropriate basis for the validation of the KLEAA Code. Very high amount of the air leaked into the facility in the grate area impairs, however, the quality of the validation. Combustion of the wood chips and SBS®1 occurs very rapidly and is completed roughly in the middle of the second primary air zone. There are only two gas sampling probes installed in this region of the grate meaning that it is not possible to point out where exactly the individual combustion stages take place.

5. Experimental results

5.1. Chemical and physical properties of the investigated fuels

Three different fuels were investigated – wood chips, SBS®1 and BIOBS. Wood chips have been chosen as the reference fuel for all test runs. The decision to choose this fuel was supported by its local availability, very good homogeneity and a guarantee of a very similar composition in different, delivered charges. Applied wood chips belong to the wood class A1 according to German waste classification (69). It is described as chemically untreated wood which underwent only mechanical processing and drying. In this case, wood chips consist almost exclusively of tree stumps chipped without bark to a particle size in the range of 10 to 40mm with an insignificant amount of fines below 10mm. This corresponds well with the wood chips of the class G30 as specified in the Austrian standard ÖNORM M 7133 and with the designation P16A as specified by the new European standard DIN EN 14961 (70). Proximate and elementary analyses are presented in Table 5.1. Combustion behaviour of this fuel in a fixed bed reactor, as well as in a moving grate firing is also well researched and a large database of experimental results is available at ITC.

SBS®1 (German: SubstitutBrennStoff) is a solid recovered fuel produced by REMONDIS Rhineland GmbH. The fuel is being produced since 1998 from high calorific fractions of municipal solid waste and bulky waste. Exact recipe of the fuel is the company's know-how and has not been made public. Analyses presented below are the result of a research at KIT performed on a small group of samples delivered for tests in the fixed bed reactor KLEAA and TAMARA test station. Results are shown below. Chlorine content for SBS®1 and below for BIOBS is based on an analysis performed by REMONDIS during the measurements campaign at the test facility TAMARA.

BIOBS (German BIOBrennStoff) is a not marketed experimental fuel also produced by REMONDIS. It is a solid recovered fuel produced of high calorific fractions of municipal solid waste, bulky waste but also of low-quality biomasses such as sieving overflows from the compost production. This ensures a high biogenic fraction in BIOBS reaching 84%, hence the name. Recipe of the fuel has been modified after the firing demonstration in TAMARA in order to reduce the content of fine particles which were causing high fly ash concentrations during the demonstration of the combustion (pre-test). Therefore the proximate and elementary composition of BIOBS presented below does not represent the fuel which was produced after the tests during the project RECOMBIO. It has to be remarked that analysed charge has a distinctive, low ash content for BIOBS. Usually, it can reach the level of this of SBS®1. Water content may also vary. The lowest registered value during the measurements at KIT was 30 wt. % and the highest ca. 37 wt. %. Presented is the average value.

The solid density, as well as the specific volumetric surface area of the fuel particles have been measured with the methods described in chapter 4.

Table 5.1 – Chemical and physical properties of the investigated fuels, *water ash free

Property	Unit	Fuel		
		Wood chips	SBS®1	BIOBS
Lower calorific value	MJ/kg wet	14.37	13.58	11.04
	Class acc. to (5)	n/a	4	4
Carbon	wt. % waf*	41.99	40.30	25.48
Biogenic carbon	wt. % of total carbon	100	69.8	86.2
Hydrogen	wt. % waf	5.26	5.15	3.25
Oxygen	wt. % waf	34.77	22.71	26.98
Nitrogen	wt. % waf	0.14	1.67	1.04
Sulphur	wt. % waf	0.03	0.18	0.13
Chlorine	wt. % waf	0.00	0.47	0.27
	Class acc. to (5)	n/a	2	2
Mercury	mg/MJ	0.000	0.009	0.008
	Class acc. to (5)	n/a	1	1
Water	wt. %	15.30	20.60	35.00
Ash	wt. %	2.52	9.39	8.13
Volatiles	wt. %	60.14	57.24	43.91
Fixed carbon	wt. %	22.05	15.15	12.97
Bulk density	kg/m^3	160	170/400	240
Solid density	kg/m^3	550	660	Not measured
Specific surface area	m^2/m^3	2173	10800 at $\rho_{bulk} = 170\ \left[\frac{kg}{m^3}\right]$ 3150 at $\rho_{bulk} = 400\ \left[\frac{kg}{m^3}\right]$	Not measured

According to Baker (67) measuring the specific surface area by the pressure drop in the bulk gives the best results when the bulk porosity is around 0.4. SBS®1 did not meet this condition and the measurement was performed twice; once with the fuel bulk as poured into the measuring instrument and once with the slightly compressed material with the porosity 0.4. Both measurements returned two radically different results and the model will be validated for both cases.

5.1.1. Sorting analysis and thermogravimetric analysis of the SBS®1

The KLEAA Code has been written with the simulation of combustion of technical fuels in mind. The first version of the model was able to simulate the combustion of spherical particles. In the previous chapter, it was explained that setting an appropriate (measured) surface area of the particles corresponding with the surface area of the wood chips allows simulating the combustion of this fuel. A solid recovered fuel consists however of substances different than wood and a "model SRF" needs to be defined. In order to find out what combustible substances are contained in the SBS®1, a sorting analysis of this fuel was carried out. It was found out that the major part of the fuel is composed of wood, paper, textiles and a number of plastics, from which the largest part is the polyethylene PE (bottle caps, yoghurt cups, etc.):

Table 5.2 – SBS®1 composition according to the sorting analysis

SBS®1 composition according to the sorting analysis [wt. %]				
Wood/paper	Sponge (Polyurethane)	Polyethylene	Textiles (natural, e.g., cotton)	Inerts (stones, sand, glass)
80.2	2.0	6.4	9.6	1.8

NIR detector installed above the conveyor belt during the measurement campaign at TAMARA plant revealed a more accurate composition of the SBS®1:

Table 5.3 – SBS®1 composition according to the near infrared detection

SBS®1 composition according to the near infrared detection [wt. %]								
Polystyrene EPS	Polyurethane	Packages	Paper, wood	PET	PE	Various plastics	PVC	Textiles
0.3	1.1	3.3	64.6	2.2	9.0	10.2	0.9	8.4

In total 9 different materials were detected. The pyrolysis of each of these substances must be considered in a mathematical model of combustion to obtain the best simulation results. Although it is theoretically possible, it would be difficult to implement all of these reactions into the KLEAA Code at once, therefore a simplification is needed. It has been suggested to group paper, wood, textiles, and packages in one category "biomass" and EPS, PU, PET, PE, PVC and other plastics in a second category "plastics". With such assumption, the "model SBS®1" is composed of roughly 75% biomass (wood) and 25% plastics. In order to investigate the pyrolysis of this content of "plastics" a thermogravimetric analysis of four pulverised SBS®1 samples has been carried out. The atmosphere was nitrogen, and the heating rate was set to 10K/min. The results are shown below:

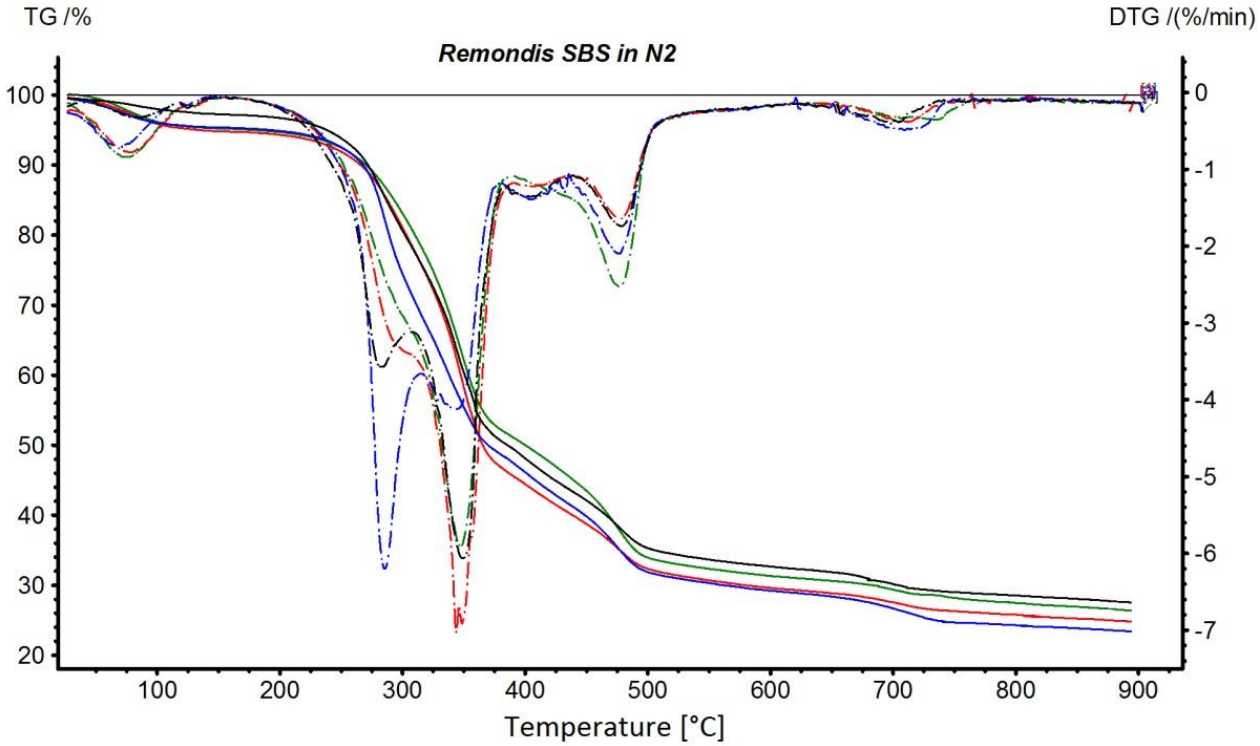

Figure 5.1 – Thermogravimetric analysis of the SBS®1 (TG – continuous line, DTG – dashed line)

The analysis revealed two temperature ranges around 280°C and 350°C where the material is devolatilised. This ranges can be identified as decomposition of cellulose and hemicellulose respectively. This is typical for biomass. Another significant peak around 480°C can be identified as decomposition of polyethylene.

Based on this information it has been suggested to describe SBS®1 in the KLEAA Code as a mixture of wood (75 wt. % dry) and of polyethylene (25 wt. % dry) and the additional sub-model for PE pyrolysis has been introduced to the model. An extensive description of the modified KLEAA Code is presented in the next chapter 6.

5.2. Combustion behaviour of the fuels in the KLEAA reactor

Characterisation of the fuels, wood chips, SBS®1 and BIOBS at KIT was focused on the combustion behaviour of various mixtures of these fuels. The main question was how the reactivity of the mixture depends on the share of the biomass modelled in this case by wood chips. In order to answer this question, a number of combustion tests with different fuel blends was carried out and the characteristic numbers were compared. Investigated fuel blends were as follows:

- SBS®1 mixed with wood chips in proportions 20%, 40%, 60%, 80% and 100% of SBS®1,
- BIOBS mixed with wood chips in proportions 20%, 40%, 60%, 80% and 100% of BIOBS.

Additionally, pure wood chips were combusted in KLEAA as a reference. Due to a very limited supply of SBS®1 and BIOBS, each mentioned mixture was fired only once. Experience with beech wood spheres and wood chips shows however that experiments at KLEAA are characterised by a very high reproducibility with regard to characteristic numbers (IR, MCR). Research by Bleckwehl (25) performed on the beech wood spheres (water content 30 %, diameter 10mm) have shown that the standard deviation for the characteristic numbers in the group of five test runs does not exceed 3%. Similar standard deviations are to be expected for very homogeneous fuels such as standardised wood chips used in the experiments for this study. SBS®1 and BIOBS are more complex fuels composed not only of waste derived biomass but also of various plastics and inert ingredients but they are subjected to constant, strict quality control by REMONDIS during the production process. Long term analyses of SBS®1 during the measurement campaign at TAMARA have shown, that the standard deviations of the water content and lower calorific values are 1.26% and 7% respectively. These values for BIOBS are 1.43% and 6.55% respectively. This proves that both fuels have an excellent homogeneity with regard to the composition and allows concluding that the reproducibility of the experiments performed on these fuels in KLEAA reactor will be also very high and comparable to this of the experiments on wood chips.

All tests were completed using the same settings of the KLEAA reactor:

- Combustion chamber wall temperature: 900 °C
- Fuel bed height: 24 cm
- Mass flow of primary air: 310 kg/h·m²
- Temperature of primary air: 25 °C

As mentioned above, all anticipated BIOBS and SBS®1 combinations with wood chips were investigated. The characteristic numbers were calculated. Charts and the summary are presented below.

5.2.1. Reaction front velocity

Observation of the reaction front velocity characteristics allows noticing a simple rule. The flame propagates faster when there is more wood in the fuel mixture. It can also be seen that the blends based on SBS®1 combust much faster than BIOBS blends. The main parameters influencing the reaction front velocity are the moisture of the blend and its bulk density. The conclusion is that adjusting the biomass (wood chips with a given water content) share in SBS®1 and BIOBS fuel blends is an easy way, to set an appropriate reaction front velocity.

Table 5.4 – Reaction front velocities for combustion of SBS®1 and BIOBS mixtures with wood chips

BIOBS with wood chips	**0 wt. % BIOBS (wood chips)**	**20 wt. % BIOBS**	**40 wt. % BIOBS**	**60 wt. % BIOBS**	**80 wt. % BIOBS**	**100 wt. % BIOBS**
Water content [wt. %]	15	19	24	28	32	35
Volatiles content [wt. %]	57	57	53	50	47	43
Bulk density [kg/m^3]	160	183	194	205	225	240
u_{RF} [mm/min]	19.8	14.7	12.3	10.2	6.9	5.5
SBS®1 with wood chips	**0 wt. % SBS®1 (wood chips)**	**20 wt. % SBS®1**	**40 wt. % SBS®1**	**60 wt. % SBS®1**	**80 wt. % SBS®1**	**100 wt. % SBS®1**
Water content [wt. %]	15	16	17	18	20	21
Volatiles content [wt. %]	57	60	59	58	58	57
Bulk density [kg/m^3]	160	163	163	164	165	170
u_{RF} [mm/min]	19.8	22.0	21.8	20.9	17.8	14.6

The reaction front velocity can be also presented in a more convenient way:

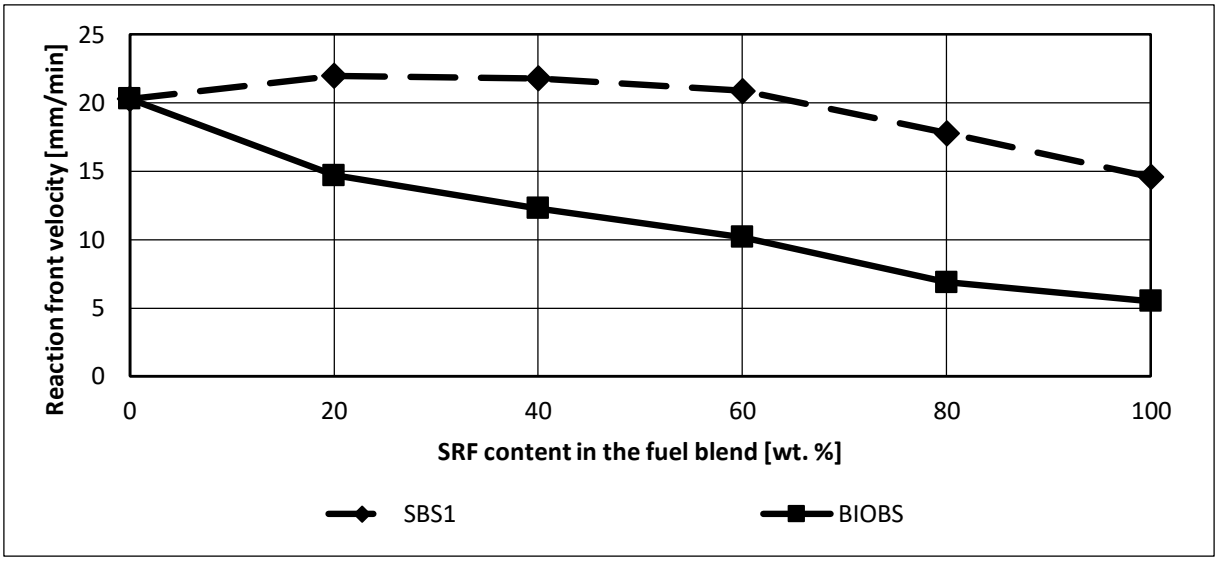

Figure 5.2 – Reaction front velocity for the combustion of SBS®1 and BIOBS blends in the KLEAA reactor

It can be noticed that the reaction front velocity increases in case of the BIOBS blends roughly linear with the decreasing amount of the BIOBS in the blend. The most important factors are in this case the water content in the blend and the bulk density. Both values decrease with the decreasing share of the BIOBS in the blend resulting with the uniform increase of the reaction front velocity. The blends based on the SBS®1 present a similar, but less obvious behaviour. The reaction front velocity for the mixtures with 20%, 40% and 60% of SBS®1 is very similar than for the wood chips since the bulk density and water content are comparable for all of them. First when the SBS®1 content reaches 80% and 100% the reaction front propagates slower than in case of wood chips which was expected considering higher water content in the SBS®1 (20 wt. % compared to 15 wt. % in the wood chips).

5.2.2. Mass conversion rate (MCR) and the ignition rate (IR):

Since the bulk densities of the wood chips and SBS®1 used in the experiments are similar, the ignition rate is mostly dependent on the reaction front velocity (see Equation 4.12). As for the mass conversion rate (Equation 4.13), two main combustion stages with two different MCRs can be distinguished for some fuel blends (Figure 5.3). The first stage (MCR I) is the main, quasi-stationary combustion phase where the feedstock is gasified and the volatiles together with a part of the produced char are combusted. In the next stage (MCR II) the char burnout takes place. As presented in figure 5.3. these stages are clearly visible during the combustion of the wood chips (thinnest line). As the content of the solid recovered fuel increases the difference between the conversion rate (inclination of the line) in both stages of the combustion becomes less apparent which is explained below.

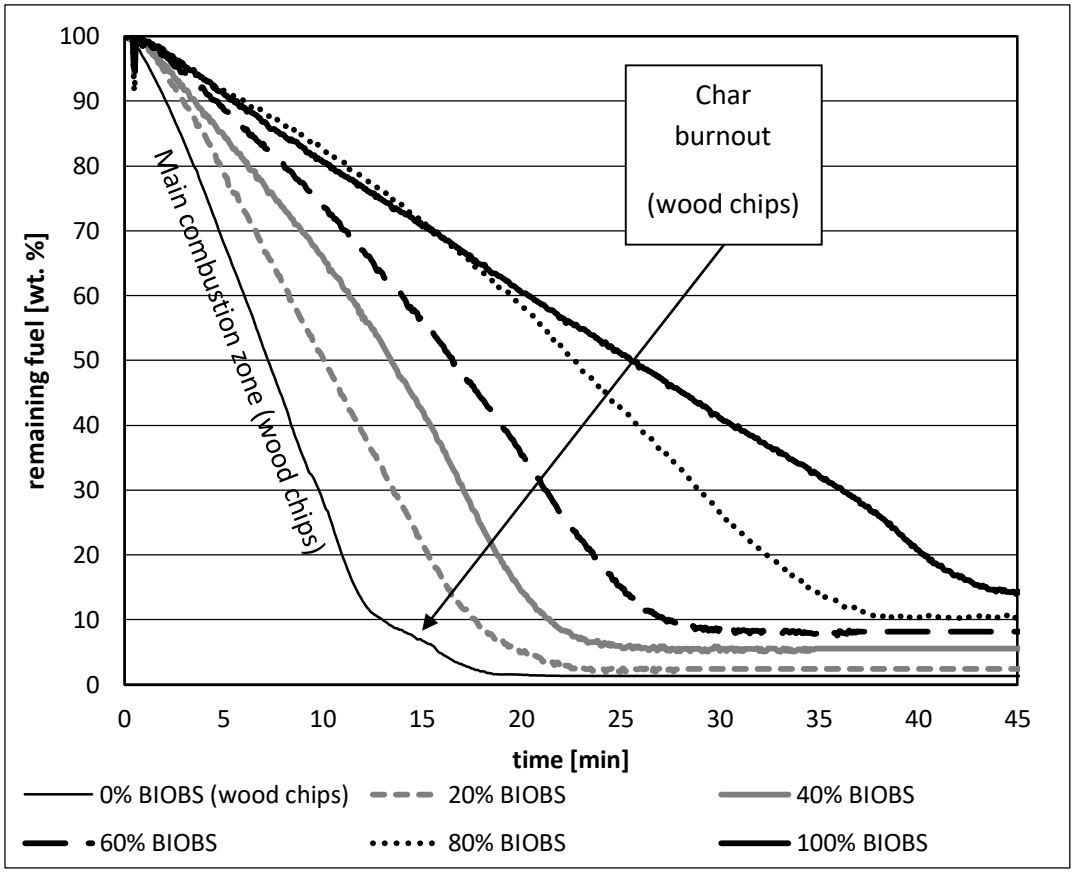

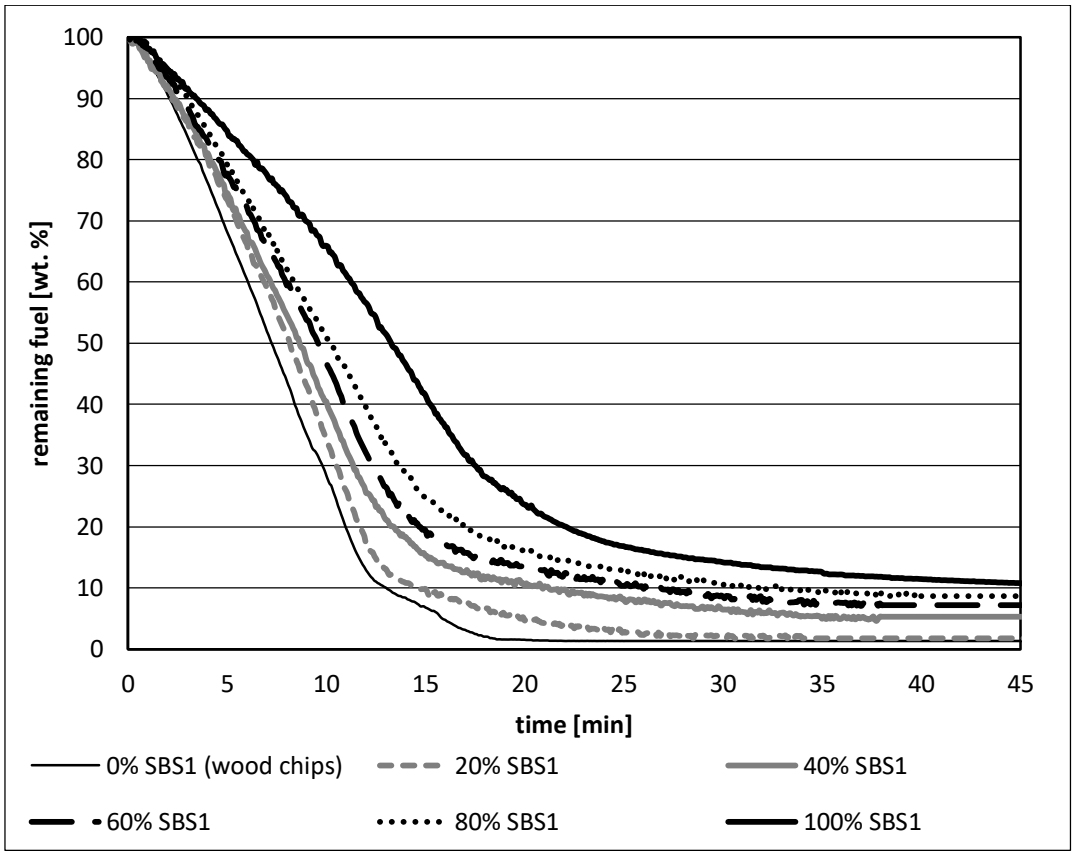

Figure 5.3 – Fuel conversion during the combustion of BIOBS and SBS®1 blends with wood chips in the KLEAA reactor

The mass conversion in the first phase of the combustion occurs faster in comparison to the char burnout in case of the wood chips which is reflected in the difference between the MCR I and II for this fuel (Figure 5.4). Relatively dry wood chips (15 wt. % of water) ignite faster (higher IR) than the rest of the fuel blends which means a faster mass conversion. It can be also observed that the char is combusted with a similar rate in case of all fuel blends. The initial water content has obviously no effect in this stage of combustion as the remaining char is dry. Very similar char burnout rates mean therefore that the char produced during the main combustion zone has roughly the same reactivity (surface area, emissivity, composition) in case of all fuels. The difference between the MCR I and II i.e., in both combustion stages for the pure BIOBS is much smaller because the high water content prevents fast combustion in the main combustion zone which occurs slightly faster than the char burnout (Figure 5.4). In this case the homogenous (volatiles) and heterogeneous (char) combustion can overlap and a pure heterogenic char burnout stage is hard to distinguish (Figure 5.3) i.e., the line representing the mass conversion is not explicitly bent as it is for pure wood chips when the char burnout starts (roughly 12 minutes after the ignition). Furthermore, the MCR I and IR in case of the BIOBS have similar values for the whole range of BIOBS share in the fuel blend. This means that the actual combusting layer of the fuel between feedstock surface and drying front surface is thin in comparison to this one for SBS®1.

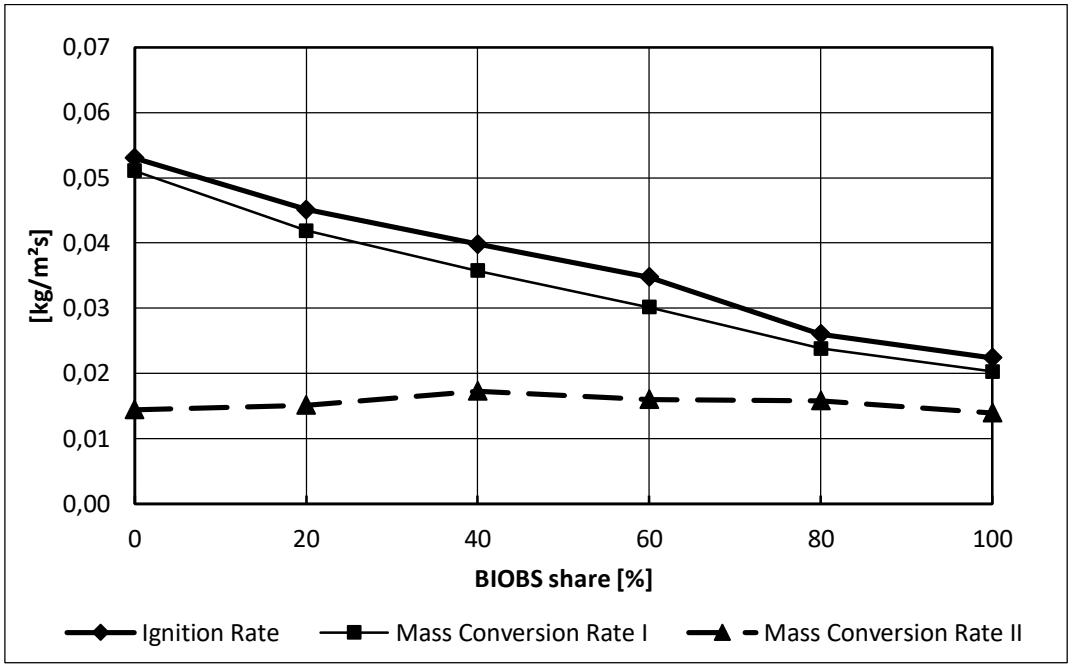

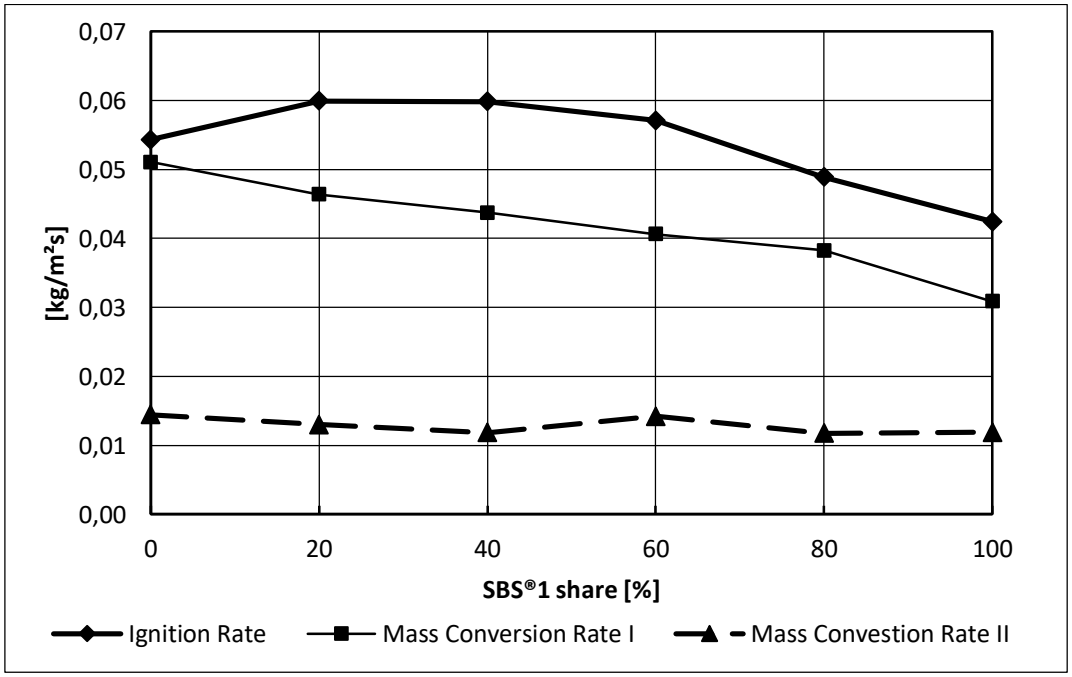

Figure 5.4 – MCR and IR for BIOBS and SBS®1 blends with wood chips

Adding more wood chips to both SRFs accelerates the combustion process and increases the difference between the MCR I and the MCR II. Keeping in mind these changes the BIOBS can be considered as a “homogenizing” supplement (instead of wet biomass) for the combustion process in power plants with grate firings relying mostly on biomass or SRF as fuel.

An almost linear increase of the MCR I and IR with the decrease of the BIOBS shares in the fuel mixtures can be noticed. Based on this observation it has been decided to choose only the results for the wood chips, 100% of SBS®1 and 100% of BIOBS for the purpose of the KLEAA Code validation. The production of the BIOBS was however cancelled after finishing the RECOMBIO project and the validation of the KLEAA Code was focused only on the wood chips and the SBS®1.

5.2.3. Temperatures

Below the temperatures registered during the combustion of all three fuels are presented. From the 13 thermocouples installed in the fuel vessel of the KLEAA reactor (Figure 4.7), five representative temperatures were chosen. T2 is mounted on top of the vessel and corresponds with the fuel bed surface at the beginning of the experiment. This thermocouple registers the moment of ignition and the initial temperature during the main combustion zone. As the fuel is converted the surface of the fuel bed progresses downwards and the T2 measures only the temperature of the gas above the fuel bed. The same situation occurs for the following thermocouples until one of them registers a temperature increase significantly higher than the previous ones. This moment is one of the indicators of the beginning of the char burnout phase. Such behaviour is observed during the combustion of biomass and solid recovered fuels rich in biomass. The typical example is the combustion of wood chips performed in the framework of this study:

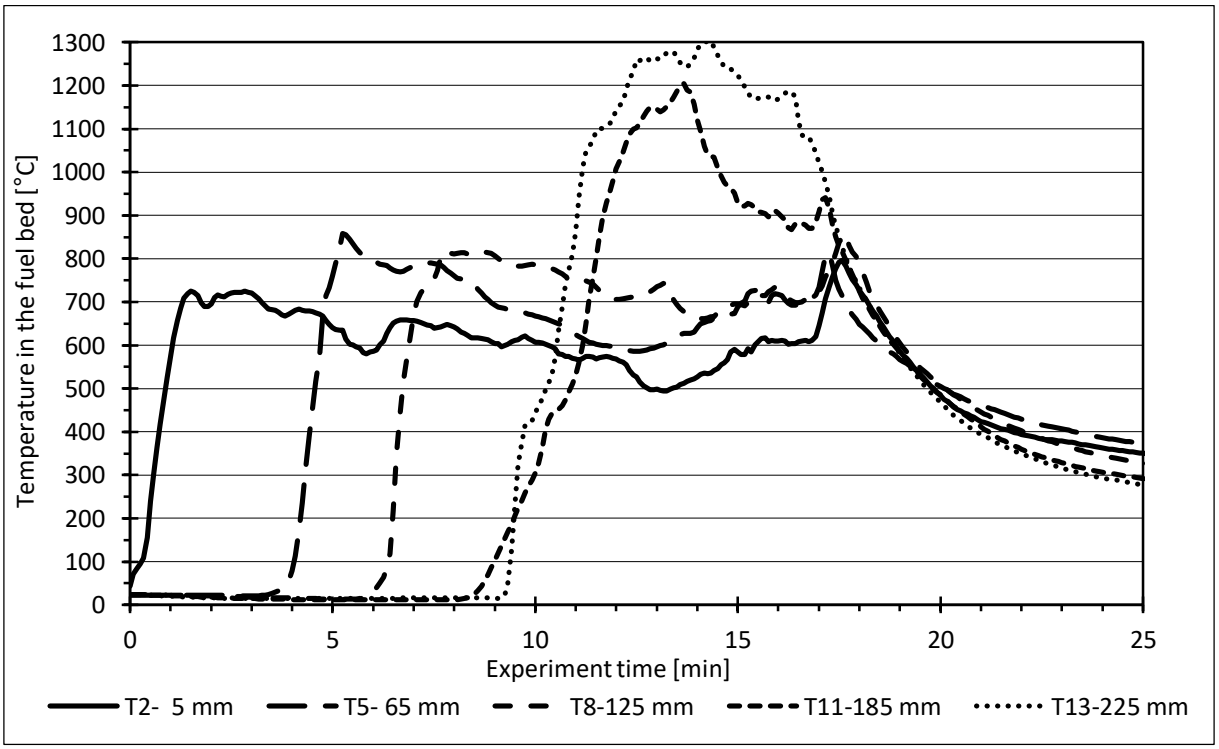

Figure 5.5 – Temperature in the fuel bed during wood chips combustion in the KLEAA reactor

The ignition occurs within the first minute after the beginning of the test and the temperature rises to about 700°C throughout the main combustion zone. The thermocouple installed at 185mm is the first to register the char burnout (MCR II) for which the maximal temperature is 1300°C.

The main combustion phase of the BIOBS (see figure below) is characterised by similar temperatures as above and is about two times longer than for the wood chips as the water content and the density of the BIOBS are higher. The char burnout (starting from T8) occurs at lower temperatures reaching about 1100°C. Considering that the mass conversion rate during the char burnout (MCR II) is comparable for wood chips and for the BIOBS, the lower temperatures in this combustion stage in case of BIOBS may indicate a lower calorific value of the char for this fuel.

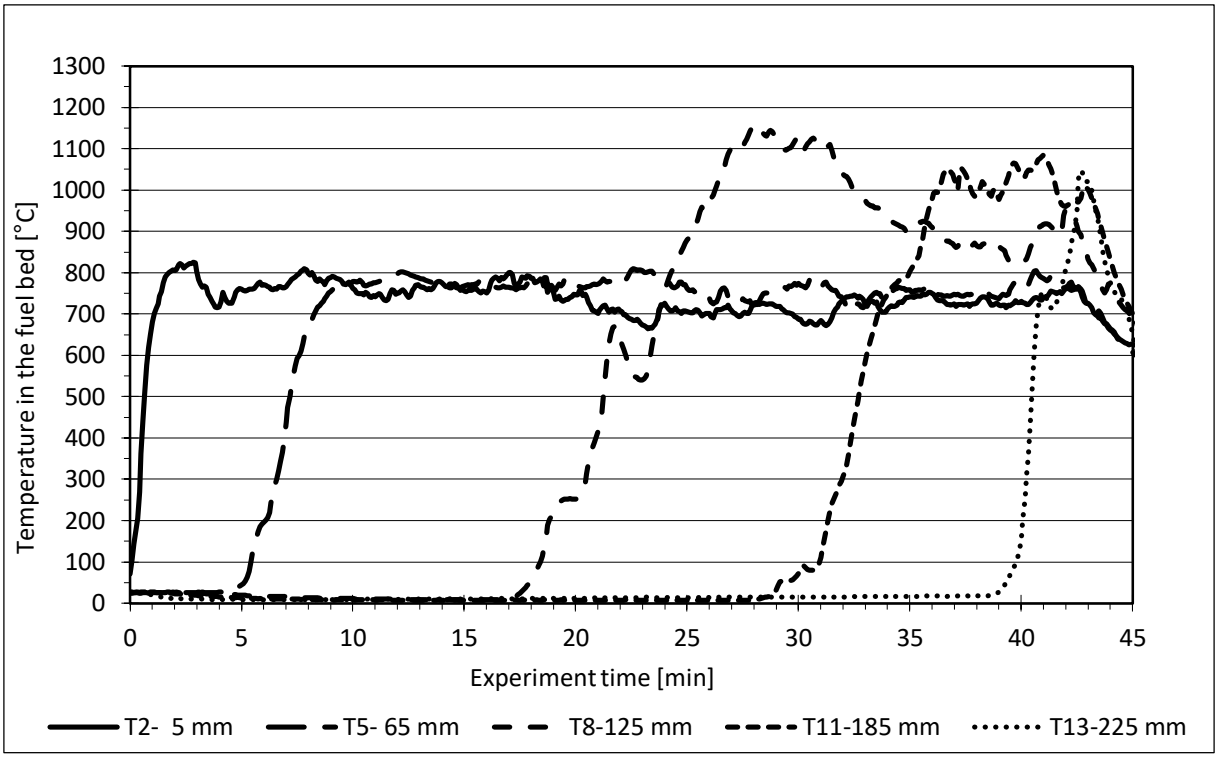

Figure 5.6 – Temperature in the fuel bed during BIOBS combustion in the KLEAA reactor

The temperatures during the combustion of SBS®1 present somewhat different behaviour:

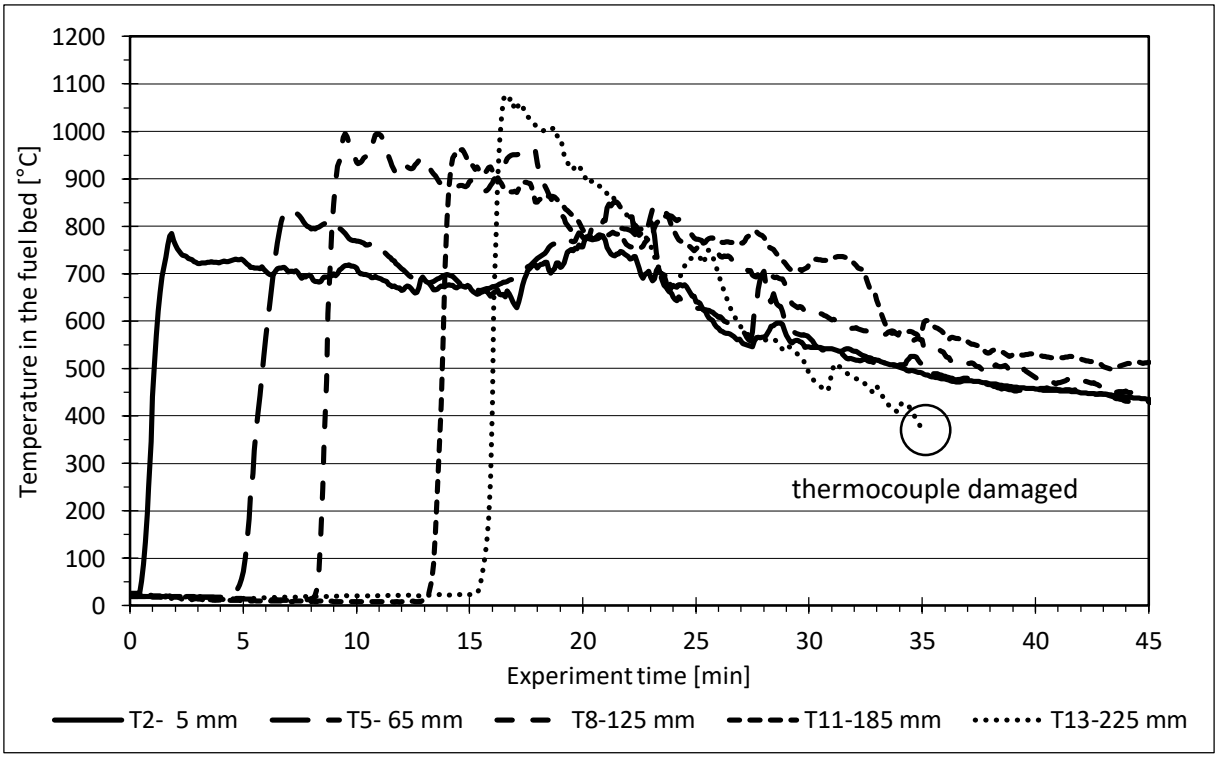

Figure 5.7 – Temperature in the fuel bed during SBS®1 combustion in the KLEAA reactor

Although the main combustion phase takes place under the same temperatures as for the previous fuels it is significantly shorter. The char ignites already after 15 minutes from the start of the test run

what is indicated by the temperature on the bottom of the fuel vessel (T13 at 225mm) which is about 200°C higher than during the main combustion stage. This combustion stage ends after about 25 minutes after the beginning of the test. The video taken above the fuel bed reveals, however, several "hot spots" throughout the entire course of the char burnout and after its end. The visible flame seen in these areas (Figure below) is a sign that the volatiles are still released from the fuel (possibly from hard plastics) which is also supported by the gas concentrations measured above the grate discussed in chapter 7. A possible reason for such behaviour will also be discussed in chapter 7.

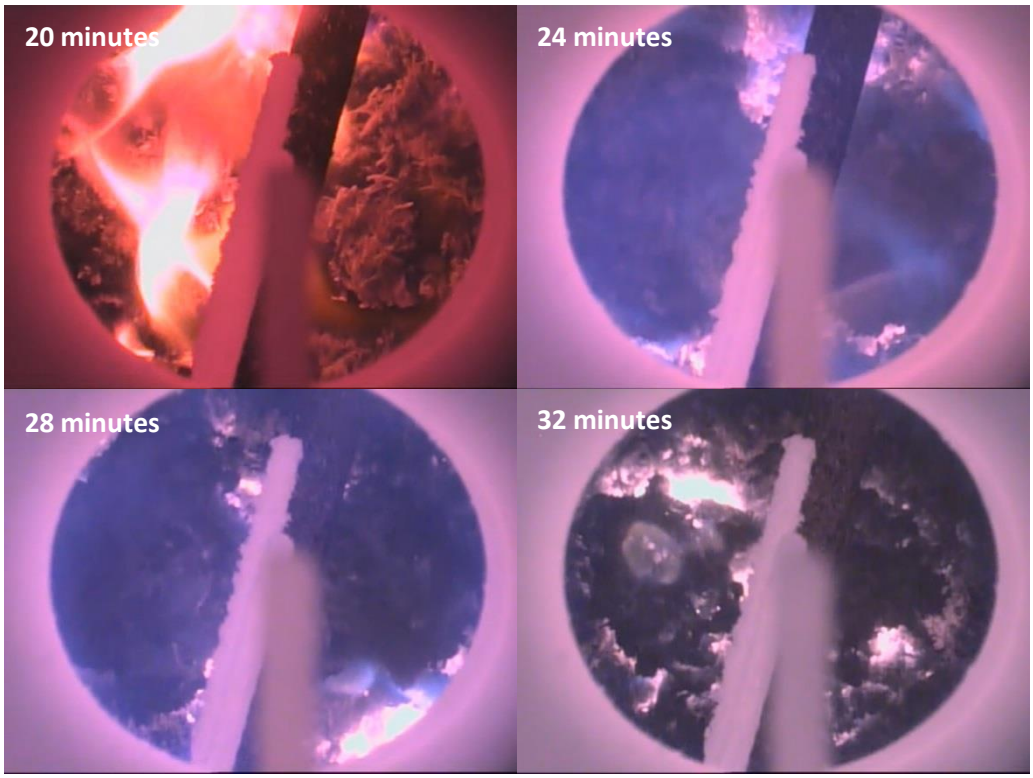

Figure 5.8 – Camera view above the fuel bed during SBS®1 combustion (flames visible in white rectangles)

5.2.4. Specific heat release

This important factor allows determining the thermal load of the grate bars (see Equation 4.14). The results are shown below:

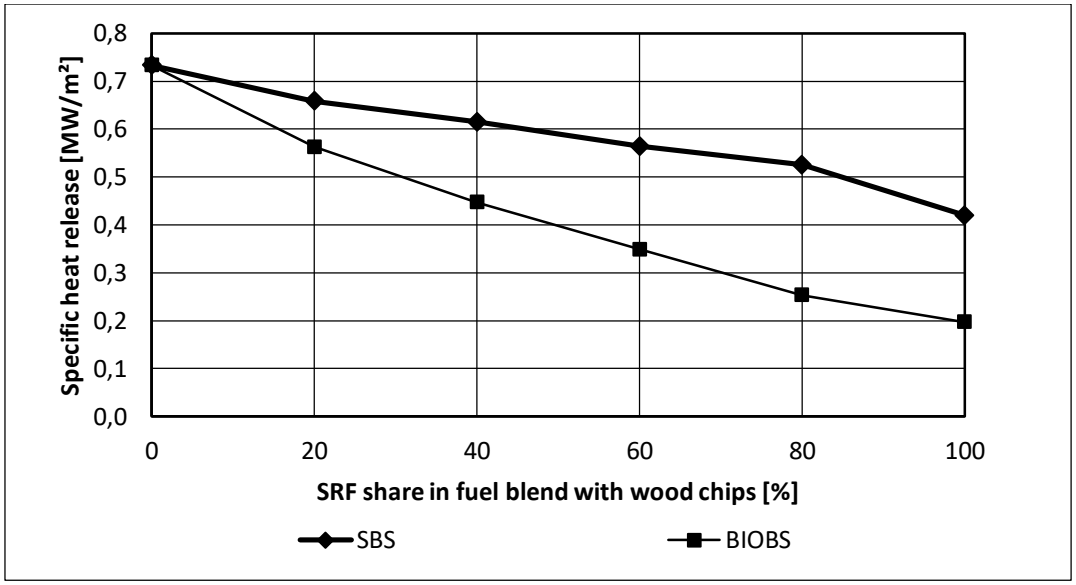

Figure 5.9 – Specific heat release of BIOBS and SBS® blends with wood chips

Large scale grate firings operate normally under the thermal load of the grate bars in a range of 0.7-1.0 MW/m^2. The calculated specific release for all the investigated fuels and their mixtures lies below this range meaning that the grate is not utilised to its full potential and it is possible to mix these fuels with fuels having higher calorific values if higher power output is needed. The calculated specific heat release together with the calorific values of the investigated fuels lying below 14MJ/kg (see chapter 4.2.1) means that no water cooling of the grate bars is necessary. It was however decided that the wood chips will be fired in TAMARA with the addition of a fine gravel in order to form a layer protecting the grate bars.

5.2.5. Local air ratio

All the KLEAA experiments with the mixtures of SBS®1 and BIOBS with wood chips have been conducted under the same conditions and settings. This also applies to the volumetric flow of the primary air which was set to 10Nm^3/h. The diagram below shows the local air ratio during the combustion of the mixtures of wood chips with SBS®1 calculated with Equation 4.15. It can be noticed that changing the proportion between the wood chips and SBS®1 results in a different average air ratio during the main combustion zone but no clear tendency can be recognised.

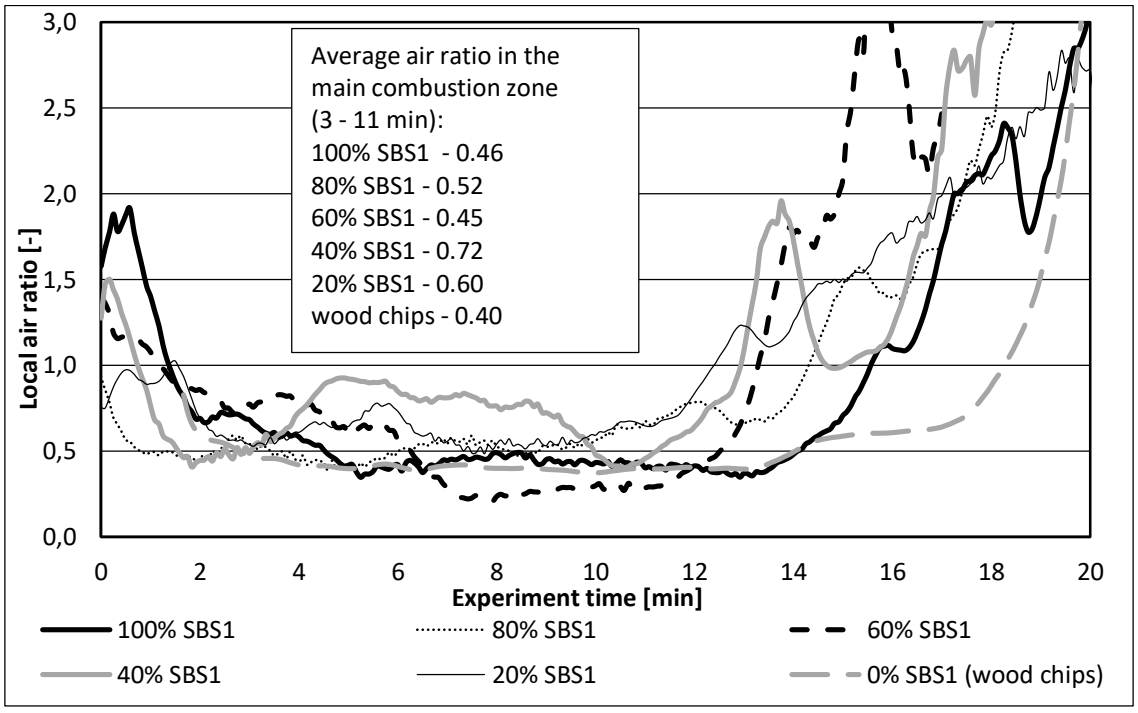

Figure 5.10 – Air ratios during the combustion of mixtures of SBS®1 and wood chips in the KLEAA reactor

This leads to a conclusion that the local air ratio does not change linearly (increase or decrease) with the weight share of the SBS®1 in the fuel blend. According to Equation 4.15, the air ratio is dependent on the O_2, CO, C_{org}, and H_2 concentration in the raw gas. The rate at which these gas species are released from the fuel bed is a function of a number of parameters. The most obvious ones are the fuel composition, residence time and the heating rate, which affects the distribution of the amount of gaseous, oily and watery pyrolysis products. The overall volatiles composition measured above the fuel bed is, however, a result of not only the heating rate of the fuel bed, but also of the gas temperature and the chemical interactions between the gas species, which are hard to predict accurately. The gas temperature is also a result of the way the fuel container is insulated. It is therefore not only fuel specific.

A slightly different behaviour can be observed during the combustion of the fuel blend based on the BIOBS (Figure 5.11 – Air ratios during the combustion of mixtures of BIOBS and wood chips). Here the

average air ratios increase with the increasing BIOBS share in the fuel mixture with the exception of 80% of BIOBS. The reason for such behaviour is the increasing water content of the fuel mixture with the increasing share of BIOBS. This results in a lower mass conversion rate for higher BIOBS shares and consequently higher air ratio as the amount of supplied primary air remains constant for each combustion test. The mixture with 80% of BIOBS brakes this trend, which could be explained by a measurement inaccuracy.

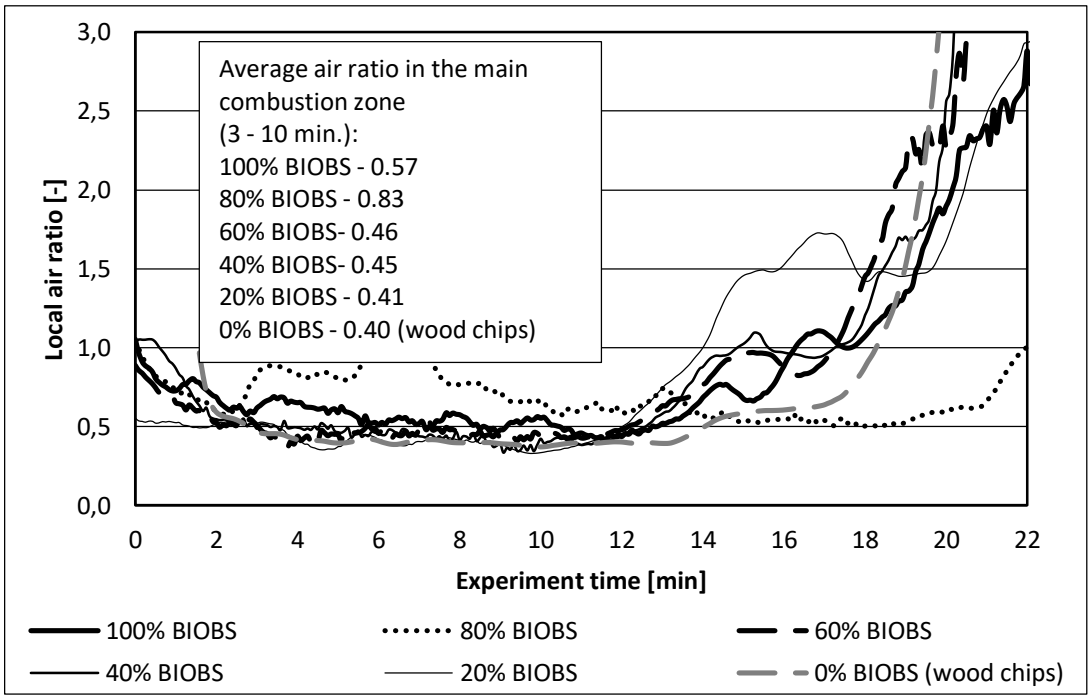

Figure 5.11 – Air ratios during the combustion of mixtures of BIOBS and wood chips

5.2.6. Conclusions

Experiments performed at fixed bed reactor KLEAA show, that:

- The difference between the stationary combustion and the char burn out in terms of the mass conversion rate decreases with increasing BIOBS share in the fuel. This means practically that the main combustion zone and the char burnout overlap stronger for higher BIOBS fractions. Small difference between the ignition rate and the mass conversion rate proves that the fuel bed combusts within a thin layer on its surface and grate bars should not have direct contact with the flames. Almost linear characteristic of the mass loss over time for pure BIOBS theoretically means that it is possible to equally distribute the thermal load of the grate assuming constant primary air distribution over its length,
- Mass conversion and the specific heat release of SBS® are very similar to the mixture of 45% BIOBS and 55% wood chips, which can be attributed to the similar bulk density and water content in both fuels,

- BIOBS can be considered as an alternative for wood chips for its homogenous combustion guaranteeing low thermal stress of the grate. Although it has to be kept in mind that the specific thermal output of BIOBS is lower because of its high moisture content and it may not meet the required power demand.

It is worth remarking that the production process of the BIOBS has been subjected to several improvements after test runs in KLEAA. The most significant improvement was an instalment of windshifters at the production site for the separation of fine particles from the fuel material. Based on the findings of Bleckwehl (25) it is anticipated that a different particle size distribution in the BIOBS, i.e., different specific surface area of the particles might change the combustion behaviour of this fuel in the main combustion zone. The tests in the TAMARA facility were performed with the optimised BIOBS. For this reason, the combustion behaviour transferred from the KLEAA reactor into the TAMARA facility might vary slightly from the one measured at TAMARA and the test runs with BIOBS are not used for model validation.

5.3. Combustion behaviour on the moving grate TAMARA

In this chapter, the results of the experiments with wood chips, SBS®1 and BIOBS at the TAMARA pilot plant are presented. It is qualitatively evaluated if the differences between the combustion behaviour for all three fuels observed before in the KLEAA reactor are also visible during the combustion in the TAMARA. Compared will be the mass conversion, air ratios, and temperatures.

5.3.1. Mass conversion

Conversion of the fuel along the grate has been calculated using the method described in chapter 4.3.7. It has been explained that for the evaluation of the experiments the gas concentrations along the grate are needed. They were measured with the gas sampling probes pictured in chapter 4.4.1. The measurement with each probe (from 1 to 5) at each location above the grate (see Figure 5.12) was no shorter than 10 minutes to make sure that the gas concentrations are not changing and the boiler operation is stable.

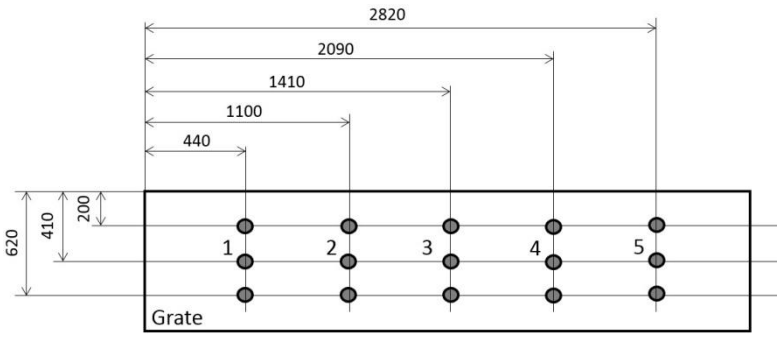

Figure 5.12 – Positions of the gas concentrations measurements

Measured values at each point (200, 410, 620 mm) were then averaged. The results for each fuel are shown in the table in Annex B. This data allowed the calculation of the fuel conversion on the grate. The result is shown below:

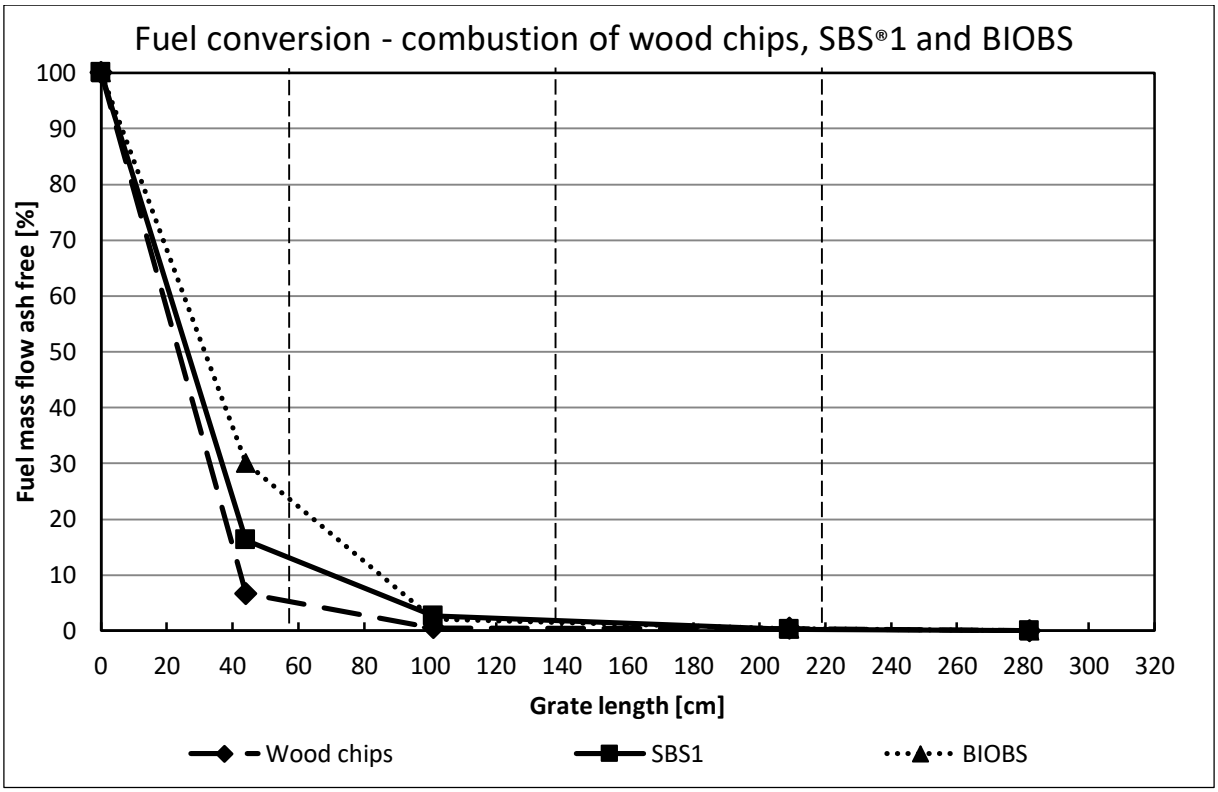

Figure 5.13 – Fuel conversion along the grate

Because of the different ash content in all three fuels (see Table 5.1) and different fuel mass flows (see Table 4.7) it has been decided to present the results ash free and in a normalised form (in % of the initial fuel mass flow without ash). The diagram reveals that all three fuels are combusted along the first meter of the grate. This is caused by a significant amount of the air leaked into the system most probably from the unrepairable cracks in the walls directly below the grate. Regardless of this difficulty the difference between the rate of fuel conversion of the wood chips, SBS®1 and BIOBS is clearly visible. At the first measurement point (44cm on the grate) 93% of the wood chips are completely converted. SBS®1 combusts a bit slower and at the same point, 84% of this fuel is combusted. BIOBS which has the highest water content combusts the slowest meaning that only 70% of the fuel is combusted at the first measurement point.

It has been noticed during the combustion tests at the KLEAA reactor that the mass conversion during the char burnout occurs slower than during the main combustion zone. The same tendency is visible in the experiments at the TAMARA plant although it cannot be stated that the main combustion zone is over at the first measurement point (44cm on the grate). It has to be kept in mind that there are no gas sampling probes between points 1 and 2 (between 44 and 101 cm of the

grate) and there are no means to determine where exactly the main combustion zone ends and the char burnout starts.

5.3.2. Air ratio

Maintaining under-stoichiometric conditions at the grate of the TAMARA facility was impossible due to the already mentioned air leakage. This caused the air ratios to exceed 1 in the first primary air zone (see Table 5.5) for each of the three fuels combusted on the moving grate.

Table 5.5 – Local air ratios during combustion tests at the TAMARA plant

Primary air zone	Air ratio [-]		
	Wood chips	SBS®1	BIOBS
1	1.1	1.0	1.7
2	>3	>3	1.9

In the second primary air zone, the combustion is almost completed in the case of wood chips and SBS®1 as indicated by the high air ratios (high oxygen content) and still occurs in case of the BIOBS. In the zones 3 and 4 almost only the presence of air was detected (see Appendix B), meaning that there is no combustion taking place in this region of the grate.

5.3.3. Temperatures in the fuel bed

The temperatures in the fuel bed on the grate in the TAMARA plant were measured with thermocouples type K, installed in ceramic stub pipes at the end of the gas sampling probes. The temperature measurements were performed at the same time as the gas samples were taken and the gas was flowing through the stub pipes, so that the sampling probes were effectively also suction pyrometers. The reason for that was to measure the actual gas temperature and minimise the influence of the heat radiating from the furnace walls and the glowing fuel bed. The results are presented below in Figure 5.14. It can be observed that they are lower than in the KLEAA reactor. The reason for this behaviour is the fact that the walls of the combustion chamber in the KLEAA reactor are electrically heated up to 900°C which influences the readings at the thermocouples on top of the fuel vessel (T2-T14). Furthermore, the heat losses through the walls of the TAMARA facility and higher air ratio contributes to the lower combustion temperatures.

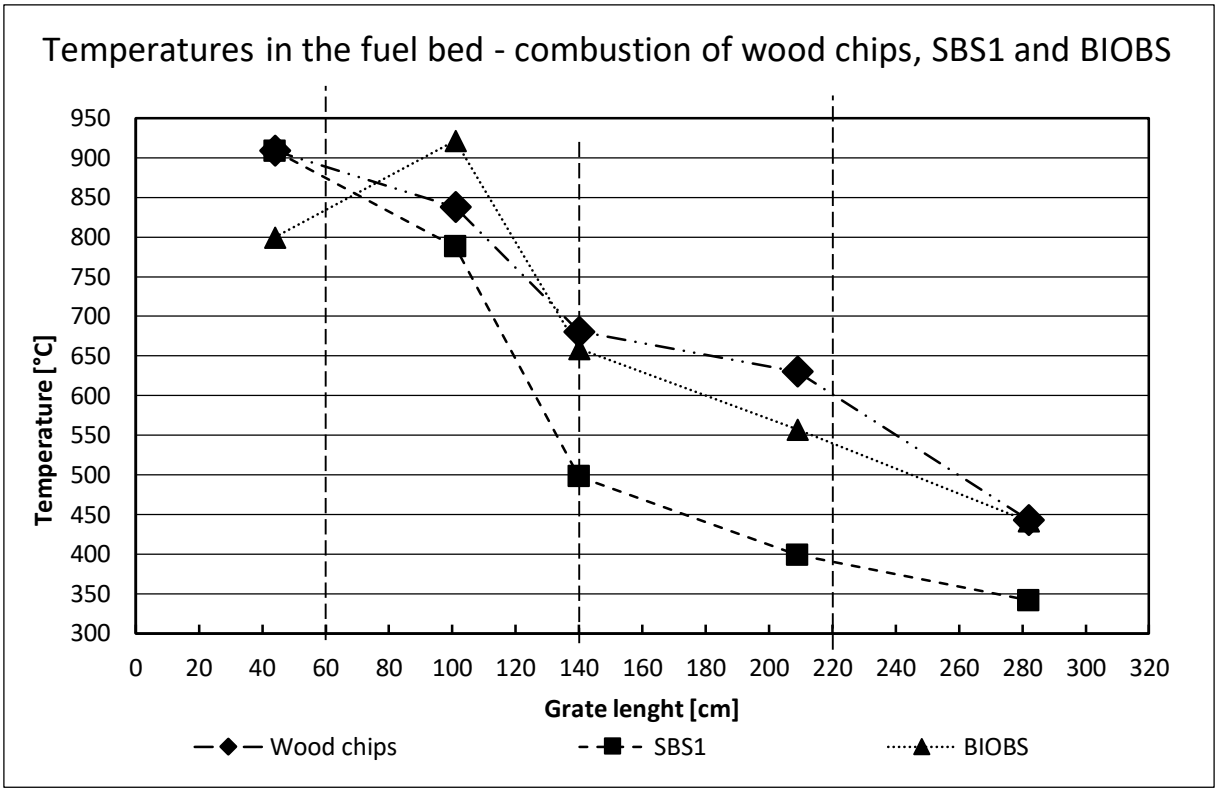

Figure 5.14 – Temperatures in the fuel bed in the TAMARA plant

The highest temperatures occurring during the combustion on a grate are normally (at an air ratio lower than 1) identified with the char burnout. The TAMARA plant operated however under over-stoichiometric conditions as presented in Table 5.5. This means that the volatiles released from the fuel bed and the char are combusted at the same time. This process occurs in case of wood chips in the first primary air zone and is indicated by the highest measured temperature of ca. 910°C. Although the temperature in the fuel bed during the SBS®1 combustion is comparable (also ca. 910°C) in the same zone it is visibly lower in the second, third and fourth primary air zone. This might indicate that the main combustion zone, as well as the char burnout for the SBS®1, actually takes place between 0 and 44 cm on the grate, slightly faster than for the wood chips. There are no thermocouples installed in this region of the grate to definitely support this conclusion. This also means that the measured temperatures might not be the highest that actually occurred during the combustion test. The actual highest temperatures could have occurred slightly in front of or behind the sampling point. The trends presented with the dotted and dashed lines in Figure 5.14 are only tentative.

The temperature in the fuel bed during the BIOBS combustion presents a different behaviour than during the combustion of wood chips and SBS®1. Here the highest temperature (920°C) is measured in the second primary air zone indicating that the burnout occurs between 50 and 100 cm on the grate. This corresponds very well with other measurements as there is still carbon monoxide present

(1.3 vol. %) in the second PA-Zone and circa 22% of the unburned fuel enters this region of the grate (see Figure 5.13).

The temperature above the grate in the third and fourth zone is the lowest in case of the wood chips and reaches 400°C and 340°C respectively. The most probable reason for this behaviour is the lowest ash content of wood chips of all the combusted fuels. A high specific air flow in the third grate zone (Table 5.6) cools down the remaining ash and grate bars faster than during the combustion of SBS®1 where the temperatures are 550°C and 440°C in the third and fourth grate zone respectively. Although the specific air flow during the test with BIOBS is the lowest (Table 5.6) and the ash content similar to the one of the SBS®1 which should mean a less intensive cooling, the temperature in the last two grate zones is comparable for these two fuels. This might be attributed to the fact that the NCV of the BIOBS is lower than of the SBS®1.

5.4. Transfer of the results from the fixed bed KLEAA on the TAMARA grate firing

It has been explained in chapter 4.4. that the specific flows of primary air in KLEAA and in TAMARA differ from each other due to a very high amount of the air leaked into TAMARA in some grate regions. It is therefore difficult to transfer the results from step two to step three but it has been performed and is discussed below. The transfer procedure was described in chapter 4.3.7. Analysis of the results obtained in both experimental setups allows drawing a conclusion that only three of four conditions are met:

- Comparable temperatures (see chapter 5.2.3. and 5.3.3),
- Low ash content (see chapter 4.2.1),
- Limited mixing on the moving grate (see chapter 4.2.1).

The last condition i.e., the same primary air flows is not met due to the initially unknown leaked air amount in the TAMARA plant. The total primary air flows in the KLEAA reactor and in each primary air zone of the TAMARA grate firing calculated after the measurements in the TAMARA plant are summarised in the table below:

Table 5.6 – Specific primary air flows in the KLEAA and TAMARA research stations

	Average specific primary air flow including leaked air flow [$Nm^3/h \cdot m^2$]											
	Wood chips				BIOBS				SBS®1			
KLEAA	240											
Primary air zone	1	2	3	4	1	2	3	4	1	2	3	4
TAMARA	805	356	465	171	275	206	269	86	596	207	467	176

Bearing in mind that the combustion in the TAMARA plant takes place mostly in the first primary air zone it is sufficient to consider only the primary air flow in this grate area while transferring the results from the KLEAA reactor. The primary air flows are comparable only for the BIOBS what allowed the transfer of the results without any additional experiments. In case of the wood chips, the flow in the first primary air zone is 805 [$Nm^3/h \cdot m^2$] which is 3.35 higher than the flow set in the KLEAA reactor which makes the transfer impossible. For this reason, it was decided to carry out the combustion tests in the KLEAA reactor again but with the primary air flow matching the one calculated in the first primary air zone in the TAMARA plant. The resulted mass conversion was then transferred on the moving grate using the residence time calculated in chapter 4.3.7. The comparison of this mass conversion transferred from the fixed bed to the actual mass conversion measured on the moving grate during the wood chips combustion is presented below:

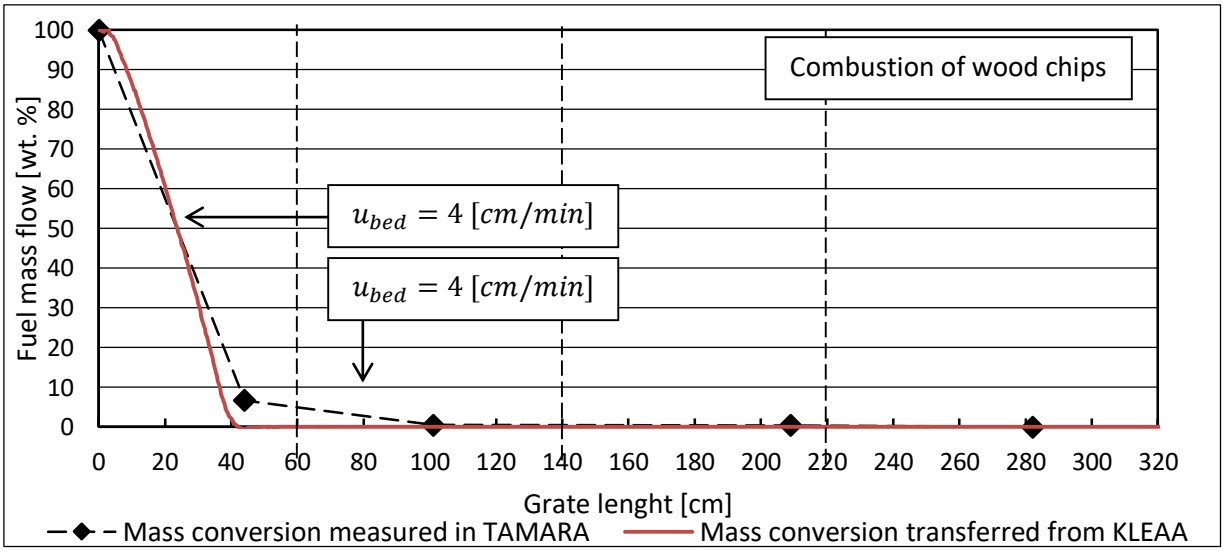

Figure 5.15 – Measured and transferred mass conversion during the combustion of wood chips

It can be observed that the transferred mass conversion corresponds very well with the one measured on the moving grate. Good results were also obtained while transferring the results from KLEAA to TAMARA for the BIOBS (Figure 5.16).

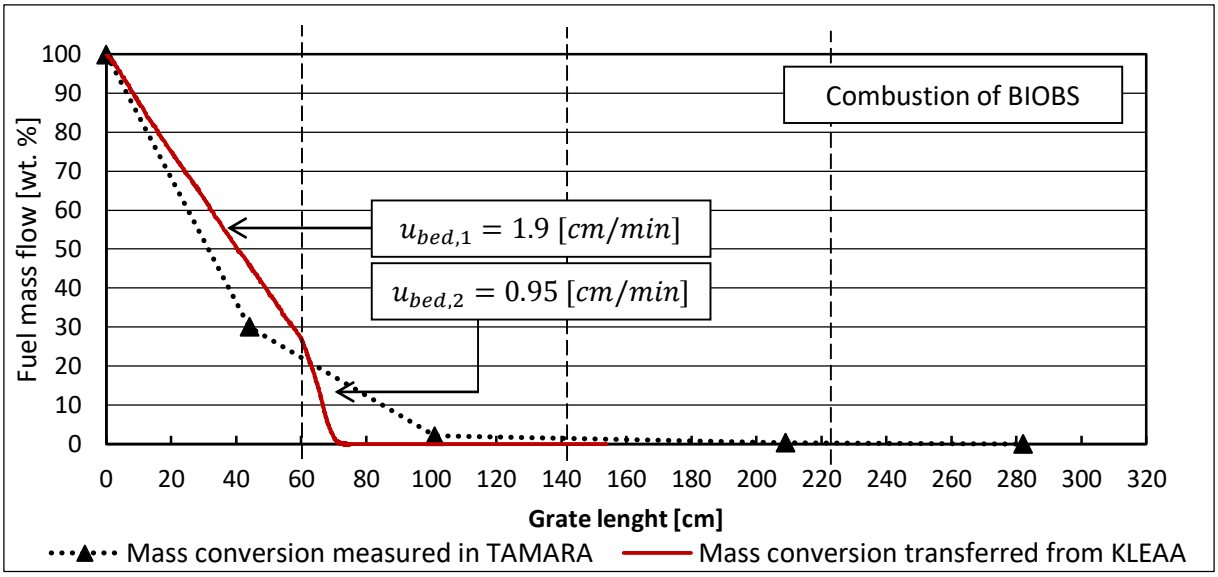

Figure 5.16 – Measured and transferred mass conversion during the combustion of BIOBS

The difference between the transferred mass conversion rate (red, continuous line) and the one measured in TAMARA (dashed line) is most likely associated with the mixing of the fuel on the moving grate. This process does not occur in the fixed bed, therefore, the transferred fuel conversion is slower than the measured in TAMARA.

6. KLEAA Code

This chapter gives a detailed presentation of the model referred to in this study. In the beginning, the model assumptions along with the changes in comparison to the previous KLEAA Code developed in (44) will be discussed. Further on the energy conservation equations together with the effective heat transfer coefficient will be explained. The following sections of the chapter will present the approach to drying of the fuel bed, pyrolysis process and heterogeneous solid combustion.

6.1. Model features

As mentioned in Chapter 2 Mätzing (44) developed the KLEAA Code according to the approach of "cascade of ideally stirred batch reactors." Two key features are:

- The model is one-dimensional,
- Heat transfer with the surroundings is not considered (process is adiabatic).

The fuel bulk is described as a packing of monodisperse spherical particles which is discretised into layers described mathematically as ideally stirred reactors. The height of each layer is defined by the average size of fuel particles and is by default set to 10 mm. The pressure in every layer is constant and equals 1 bar. In many simple fixed bed models (see chapter 2.4) drying, pyrolysis (degassing) and char burnout within the boundary of a single volume element (ideally stirred reactor) occur with a constant reaction rate in certain pre-defined temperature windows. This is not the case in the KLEAA Code, where the rate of the reactions is dependent on the temperature. For the sake of simplicity, all gaseous hydrocarbons released during the pyrolysis are however summarised as methane. The diffusion of the reaction products from the solid into gas phase and reactants from the gas into the solid is neglected. Instead, it is assumed that the products formed on the surface of solid particles and reactants from the gas are immediately present at the phase boundary and ready to react. The char burnout is modelled with the modified shrinking reacted core model. All gases are described as ideal gases. The composition of the fuel, its density, particle size, emissivity of the solid as well as the heat transfer coefficient between solid particles are calculated in each time step.

Several updates have been introduced since the first version of the KLEAA Code described in (44):

- Possibility to set the appropriate surface area of the particles independent of particle size,
- Solid Recovered Fuels are described as a mixture of biomass (hard or soft wood) and polyethylene,
- Pyrolysis model is based on five reactions for the thermal decomposition of the solid (biomass) and one additional reaction of the polyethylene decomposition,
- The pyrolysis of the polyethylene releases ethylene,

- The amount of the supplied primary air can be varied with time. This allows modelling of the air grading in different grate zones.

Furthermore, a more user-friendly, graphical output of the results delivered in real time during the simulation has been incorporated. A more stable solver has been applied (Livermore solver for ordinary differential equations).

Transferring the results from a fixed to a moving grate is based on the method described in chapter 4.4 and is integrated into the KLEAA Code. The fuel bed velocity is uniform throughout the course of the simulation.

Summarising, the updated KLEAA Code is able to simulate the combustion of fuels with particle shapes different from spherical. It also provides a mathematical description of the pyrolysis of a fuel composed of biomass (seen as wood) and plastics (which are considered to be polyethylene). Furthermore, it is possible to automatically transfer the results calculated for a fixed bed onto a grate firing with several primary air zones.

6.2. Mass balance

The mass balance in the KLEAA Code is formulated for each of the control volumes of the cascade of ideally stirred reactors. During the combustion the mass of the solid in a control volume decreases in result of several processes; drying, pyrolysis (degassing of volatiles) and char burnout:

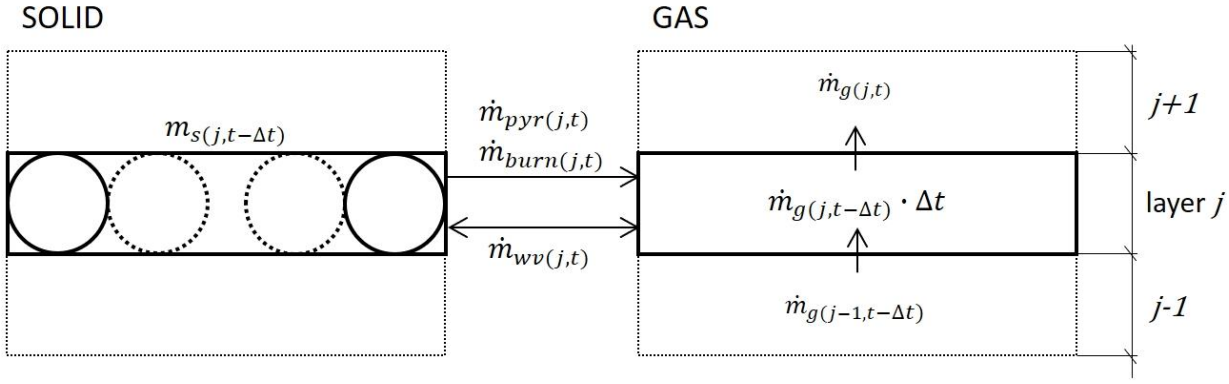

Figure 6.1 – mass balance in a single layer of the cascade of ideally stirred reactors in the moment *t*

These mass flows released from the solid are coming into the gas phase which is reflected in the mass balance for the gas phase.

This can be written mathematically as:

$$m_{s(j,t)} = m_{s(j,t-\Delta t)} - \left(\dot{m}_{pyr(j,t)} + \dot{m}_{burn(j,t)} \pm \dot{m}_{wv(j,t)}\right) \cdot \Delta t \qquad \text{Equation 6.1}$$

$$\dot{m}_{g(j,t)} = \dot{m}_{PA} + \sum_{j=1}^{j} \left(\dot{m}_{pyr(j,t)} + \dot{m}_{burn(j,t)} \pm \dot{m}_{wv(j,t)} \right)$$ Equation 6.2

Where:

$m_{s(j,t)}$ – mass of the solid remaining in the layer *j* after time *t*,

$m_{s(j,t-\Delta t)}$ – mass of the solid remaining in the layer *j* after time *t-Δt*,

$\dot{m}_{wv}$ – mass flow of the water evaporating from the solid or condensing back into the solid,

$\dot{m}_{pyr}$ – mass flow of the volatiles flowing out of the solid as a result of the pyrolysis process,

$\dot{m}_{burn}$ – mass flow out of the solid resulting from the char burnout.

The mass of the fuel particle in the beginning $m_{s(j,0)}$ is calculated from the known volume of the spherical particle and the measured solid density ρ_s:

$$m_{s(j,0)} = \rho_s \cdot V_{s,0}$$ Equation 6.3

The volume $V_{s,0}$ equals the volume of a sphere with the diameter of 10mm as stated in the model assumptions.

6.2.1. Drying

Drying occurs by evaporation, which is analogous to the heat and material transfer by convection (71). Therefore in order to calculate the mass flow of water evaporated from the solid into the gas the mass transfer coefficient β_{wv}, logarithmic partial pressure difference for water vapour between the particle surface and gas $\left(p_{gas} - p_{wv,ps}\right)$ and the surface area of the solid A_s are needed:

$$\dot{V}_{wv} = \frac{\beta_{wv} \cdot A_s \cdot \left(p_{wv,0} - p_{wv}\right)}{\rho_{wv} \cdot T_g \cdot R_{wv}}$$ Equation 6.4

Where:

A_s – effective surface area of the solid

$p_{wv,0}$ – saturation pressure of the water vapour at 100°C

p_{wv} – partial pressure of the water vapour in the gas at T_g

ρ_{wv} – density of the water vapour considered as an ideal gas, dependent on the temperature of gas T_g

T_g – gas temperature

$R_{wv} = R/M_D$

M_D – molar mass of water

$$\beta_{wv} = \frac{\alpha_{sg}}{\sqrt{\rho_{gas} \cdot c_{p,g} \cdot \frac{\lambda_g}{D} \cdot \frac{(p_{gas} - p_{wv,ps})}{p_{wv,gas}}}} \left[{}^{m}/_{s}\right]$$ Equation 6.5

Where:

α_{sg} – heat transfer coefficient between solid and gas

ρ_{gas} – density of the gas

$c_{p,g}$ – specific heat capacity of the gas

λ_g – thermal conductivity of the gas

D - gas diffusion coefficient defined by Kröll (71) as:

$$D = 22.6 \cdot 10^{-6} \cdot \frac{1}{p_{gas}} \cdot \left(\frac{T_g}{273}\right)^{1.81} \left[{}^{m^2}/_{s}\right]$$ Equation 6.6

$(p_{gas} - p_{wv,ps})$ - logarithmic partial pressure difference calculated from the following equation:

$$(p_{gas} - p_{wv,ps}) = \frac{p_{wv,0} - p_{wv}}{\ln\left(\frac{p_{gas} - p_{wv}}{p_{gas} - p_{wv,0}}\right)} \left[Pa\right]$$ Equation 6.7

Saturation pressure at T_g is given by:

$$p_{wv,0} = p_{wv,s}(T_0 = T_s) = 661 \cdot \exp(-1.91275 \cdot 10^{-4} + 7.258 \cdot 10^{-2} \cdot T_s - 2.939 \cdot 10^{-4} \cdot T_s^2 +$$

$$+9.841 \cdot 10^{-7} \cdot T_s^3 - 1.92 \cdot 10^{-9} \cdot T_s^4) \left[Pa\right]$$

Equation 6.8

Mass flow of the water vapour from the solid into the gas can be calculated from the volumetric flow:

$$\dot{m}_{wv} = \dot{V}_{wv} \cdot \rho_{wv}$$ Equation 6.9

One of the important features of the KLEAA Code is that the water evaporated in the lower parts of the moist fuel packing (where the primary air is supplied) can condense in the upper parts if the solid is cooled down by the flowing primary air and reaches a temperature below the condensation temperature of water.

6.2.2. Pyrolysis model

The first version of the model (44) used a one-step pyrolysis model for biomass known from (46) and (47). According to the chemical analysis the water and ash free beech wood consists of 50.1 wt. % of

carbon, 6.0 wt. % of hydrogen, 43.8 wt. % of oxygen and of 0.1 wt. % of trace elements (S, N, …) and can be described as $C_6H_9O_4$. Thermochemical decomposition of the original substance produces char (C_{fix}) and volatiles ($CO_2, CO, H_2O, CH_4, H_2$) and can be written in form of the following reaction:

$$C_6H_9O_4 \rightarrow 0.7CO_2 + 1.1CO + 1.5H_2O + CH_4 + H_2 + 3.2C_{fix} \quad (47)$$ Equation 6.10

This reaction is a first-order reaction and the reaction rate coefficient equals:

$$k = 4.4 \cdot 10^9 \cdot \exp\left(-\frac{141000}{RT}\right)\left[\frac{1}{s}\right] \text{ as recommended in (47)}$$ Equation 6.11

In course of the model development also a three-step pyrolysis model was tested which describes the fuel as wood consisting of cellulose, hemicellulose, and lignin. Thermochemical decomposition of all three species occurs parallel and is described by three chemical reactions. Each reaction is a first order reaction and has a separate reaction rate coefficient and an activation energy (44).

Validation of the KLEAA Code for combustion of beech wood spheres has shown good correlation with the experimental results from the KLEAA fixed bed reactor (44). Comparison of the results produced by the pyrolysis model alone proved however that it does not correspond well with the thermogravimetry results of a beech wood sample i.e., cellulose decomposes too fast. In order to address this problem, Mätzing developed a five-step pyrolysis model which splits the decomposition of cellulose into two steps – decomposition of cellulose into gas (as other authors (47)) and into tar. Tar is then decomposed into gas in another step:

Table 6.1 – Reactions of the five-step pyrolysis model (44)

Component	Reaction	Pre-exponential factor k_0 [1/s]	Activation Energy E_A [kJ/mol]
Cellulose	$C_6H_{10}O_5 \rightarrow Gas + 2.5C_{fix}$	$2 \cdot 10^8$	132
Cellulose	$C_6H_{10}O_5 \rightarrow 0.75Tar + 0.625C_{fix}$	$3 \cdot 10^{13}$	195
Tar (levoglucosan)	$C_6H_{10}O_5 \rightarrow Gas$	$2 \cdot 10^7$	122
Hemicellulose	$C_5H_8O_4 \rightarrow Gas + 2C_{fix}$	$1 \cdot 10^7$	105
Lignin	$C_{10}H_{10}O_4 \rightarrow Gas + 4.3C_{fix}$	$1{,}5 \cdot 10^{14}$	192
Polyethylene	$(C_2H_4)_{980} \rightarrow 980C_2H_4$	$2 \cdot 10^{16}$	$265 \cdot 10^3$

Pre-exponential factors and the activation energies for the second step of the cellulose and tar decomposition were adjusted to best-fit the modelling results to the thermogravimetry of a beech

wood sample. The diagram below shows a comparison between the experiment and the model calculation:

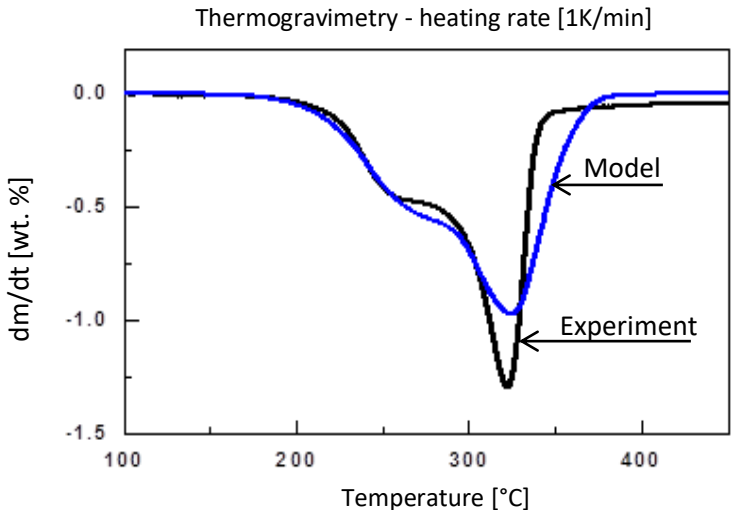

Figure 6.2 – Comparison of the TGA of beech wood and the modelling (3)

In the current version of KLEAA Code there is an additional equation for polyethylene pyrolysis:

$$(C_2H_4)_{980} \rightarrow 980C_2H_4 \qquad \text{Equation 6.12}$$

With the pre-exponential factor $k_0 = 2 \cdot 10^{16}$ [1/sec] and the activation energy $E_A = 2.65 \cdot 10^5$[kJ/mol] in accordance to data by Knümann (72). Level of polymerisation is set to 980 which corresponds to the logarithmic mean value calculated for the molecular masses of low and high density polyethylene.

The mass flow $\dot{m}_{i(j,t)}$ resulting from the pyrolysis of each component *i* (cellulose, hemicellulose, lignin, tars and polyethylene) of the fuel is given for each control volume *j* by:

$$\dot{m}_{i(j,t)} = -k_{i,pyr} \cdot m_{i(j,t-\Delta t)} \qquad \text{Equation 6.13}$$

$$k_{i,pyr(j,t)} = k_0 \cdot \exp\left(-\frac{E_A}{R \cdot T_{s(j,t)}}\right) \qquad \text{Equation 6.14}$$

k_0 and E_A are found in Table 6.1. The total mass flow $\dot{m}_{pyr}$ in Equation 6.1 is defined as:

$$\dot{m}_{pyr(j,t)} = \sum_i \dot{m}_{i(j,t)} \qquad \text{Equation 6.15}$$

Reaction rate coefficients k_0 and activation energies E_A are presented in Table 6.1.

Gasses released in course of the pyrolysis undergo in the gas phase several homogeneous reactions:

Table 6.2 – Homogeneous reactions in the gas phase (44)

Reaction	Pre-exponential factor k_0 [1/s]	Reaction rate r_j	Enthalpy of reaction $\Delta_R H$ [kJ/mol] at T=273K and p=1bar
$CO + 0.5O_2 \rightarrow CO_2$	$1.3 \cdot 10^{14}$	$k \cdot [CO] \cdot [O_2]^{0.5} \cdot [H_2O]^{0.5}$	-283.0
$CH_4 + 2O_2 \rightarrow CO_2 + 2H_2O$ Under abundance of oxygen $\lambda \geq 1$	$1.585 \cdot 10^{13}$	$k \cdot [CH_4]^{0.7} \cdot [O_2]^{0.8}$	-890.8
$CH_4 + 0.5O_2 \rightarrow CO + 2H_2$ Under deficiency of oxygen $\lambda < 1$	$4.4 \cdot 10^{8}$	$k \cdot [CH_4] \cdot [O_2]^{0.5}$	74.0
$H_2 + 0.5O_2 \rightarrow H_2O$	$2.5 \cdot 10^{16}$	$k \cdot [H_2]^{0.5} \cdot [O_2]$	-285.9
$CO + H_2O \rightarrow CO_2 + H_2$	$2.75 \cdot 10^{9}$	$k \cdot [CO] \cdot [H_2O]$	-41.2
$CO_2 + H_2 \rightarrow CO + H_2O$	$\frac{2.75 \cdot 10^{9}}{K_p}$	$k \cdot [CO_2] \cdot [H_2]$ $\ln(K_p) = -3.143 + \frac{3659}{T_g}$	41.2

6.2.3. Particle model and the heterogeneous char burnout

Fuel particles are heated up, dried and then pyrolyzed (degassed). The remaining core consisting of the fixed carbon and ash is heated up and oxidised. These heterogeneous processes and reactions lead to the further mass flow from the solid into the gas phase. This is reflected in the mass balance explained in 6.2. In order to define the mass flow related to the char burn out it is necessary to choose an appropriate particle model which will render the mass conversion during the mentioned process. An extensive description of such models can be found in (45). Evidence from a wide variety of situations indicates that the shrinking-core model (SCM) approximates real particles more closely than the progressive conversion model (PCM) in most cases. Observations with burning coal, wood, briquettes, and tightly wrapped newspapers also favour the shrinking-core model (45). In this model, the reaction occurs at the surface of the particle leaving behind a completely converted material and inert solid i.e., ash. Thus, an unreacted core of material which shrinks in size during the reaction exists at any time. The raw density of this core is assumed to be constant (45) over the course of the reaction. It is also assumed that the outer surface of the particle where the reaction takes place is constant during the whole process.

In light of these features, Mätzing (44) has chosen to model the char burnout with a shrinking core-model but the model was modified in such way that the density of the shrinking char particles changes over time according to the actual composition of the fuel. Furthermore, the surface area of the particles is calculated in every time-step of the simulation as the particle shrinks. Mass flow related to the carbon combustion takes the following form (73):

$$\dot{m}_{i(j,t)} = -k_{het,i} \cdot A_{s,t} \cdot M_{cfix} \cdot \frac{P_{CO(t,j)} - P_{CO,eq}}{R \cdot T_{s(t,j)}} \qquad \text{Equation 6.16}$$

Where:

$k_{het,i}$ - reaction rate constant for the heterogeneous reaction i (listed below),

$A_{s,t}$ – surface area of the solid at the moment t, the initial surface area of the particle $A_{s,0}$ is calculated with the Equation 6.29,

M_{cfix} – molecular mass of the char (carbon),

R – gas constant,

T_s – temperature of the solid at the time increment t,

$P_{CO(t,j)}$- pressure of the CO,

$P_{CO,eq}$ – equilibrium pressure of the CO.

Modelled reactions during the last phase of the heterogeneous fuel conversion i.e., of the char burnout are listed below:

$$C + H_2O \rightarrow CO + H_2 \quad k_{het1} = 1.6 \cdot 10^7 \cdot \exp\left(-2.2 \cdot \frac{10^5}{R} \cdot T_S\right)[mol/s] \qquad \text{Equation 6.17}$$

$$C + CO_2 \rightarrow 2CO \quad k_{het2} = 3.5 \cdot 10^6 \cdot \exp\left(-2.2 \cdot \frac{10^5}{R} \cdot T_S\right)[mol/s] \qquad \text{Equation 6.18}$$

$$C + 0.5O_2 \rightarrow CO \quad k_{het3} = 7 \cdot 10^5 \cdot \exp\left(-1.6 \cdot \frac{10^5}{R} \cdot T_S\right) \ [mol/s] \qquad \text{Equation 6.19}$$

$$C + O_2 \rightarrow CO_2 \quad k_{het4} = 9 \cdot 10^4 \cdot \exp\left(-2.25 \cdot \frac{10^5}{R} \cdot T_S\right)[mol/s] \qquad \text{Equation 6.20}$$

The total mass flow related to the char burnout equals:

$$\dot{m}_{burn(j,t)} = \sum_i \dot{m}_{i(j,t)} \qquad \text{Equation 6.21}$$

6.3. Energy balance

The fuel bed is described in the KLEAA Code as a close packing of spheres surrounded by the gas phase. Conservation equations are formulated for both phases.

The heat transfer occurs between the wall of the furnace above the fuel bed and the first, top layer of the fuel (control volume) $\dot{Q}_{ws}$, furnace wall and the gas released into the furnace $\dot{Q}_{wf}$, solid fuel

layer and the gas $\dot{Q}_{fs}$, solid fuel and the gas within the fuel bed $\dot{Q}_{sg}$ and also between two consecutive solid layers $\dot{Q}_{ll}$. Heat fluxes $\dot{Q}_{ws}$ and $\dot{Q}_{ll}$ are governed by an effective, radiative heat transfer coefficient. Part of the heat received by the solid is consumed to dry the fuel $\dot{Q}_{dry}$. Heat released from the chemical reactions is designated as $\dot{H}_{re}$. There are no temperature or gas concentration gradients within the control volumes and the system is reduced to a one-dimensional cascade of ideally stirred batch reactors connected with each other via conservation equations. In this chapter the energy conservation reactions are presented. The effective heat transfer coefficient is presented in Annex D.

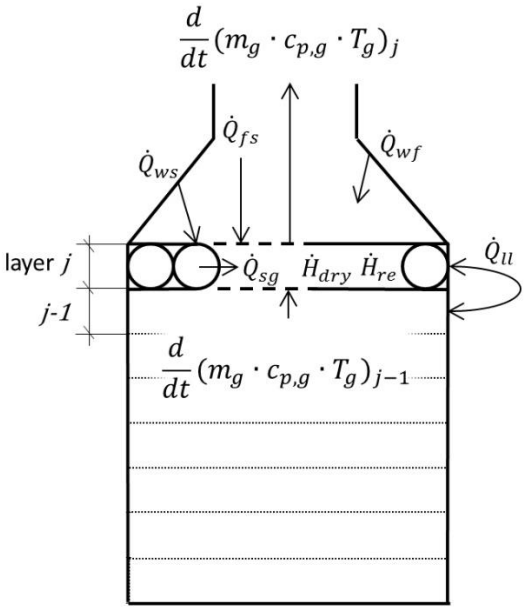

Figure 6.3 – Heat fluxes coming from and into a single fuel layer

Below the explanation of the heat fluxes mentioned above and the energy conservation equations are presented:

Heat fluxes:

$\dot{Q}_{ws} = \varepsilon_{ws} \cdot \sigma \cdot A_s \cdot \left({T_w}^4 - {T_s}^4\right)\ [W]$ – between the solid and the furnace wall Equation 6.22

Where:

ε_{ws} – emissivity between the solid and the furnace wall, explained in Annex E,

σ – Stefan-Boltzmann constant, $\sigma = 5.67 \cdot 10^{-8}\ \left[\frac{W}{m^2 K^4}\right]$

A_s – effective surface area between the solid and the gas (solid and furnace wall),

T_s – temperature of the solid,

T_w – temperature of the furnace wall.

$\dot{Q}_{fs} = \sigma \cdot A_s \cdot \left(\varepsilon_{fs} \cdot {T_{fg}}^4 - \alpha_{fs} \cdot {T_s}^4\right) [W]$ – between solid and the flue gas Equation 6.23

Where:

ε_{fs} – emissivity between the solid and gas in the furnace, explained in Annex E,

α_{fs} – absorption coefficient between the solid and furnace gas, explained in Annex E.

$\dot{Q}_{wf} = \sigma \cdot A_{fw} \cdot \left(\varepsilon_{fw} \cdot {T_{fg}}^4 - \alpha_{fw} \cdot {\mathrm{T}_w}^4\right) [W]$ – between the wall and the flue gas Equation 6.24

Where:

A_{fw} – effective surface area between the furnace wall and gas,

ε_{fw} – emissivity between the furnace wall and gas, explained in the Annex E,

α_{fw} – absorption coefficient between the furnace wall and gas, explained in the Annex E,

T_{fg} – gas temperature in the furnace,

T_w – temperature of the furnace wall.

$\dot{Q}_{sg} = \alpha_{sg} \cdot A_s \cdot (T_s - T_g) [W]$ – between the solid and gas Equation 6.25

Where:

α_{sg} – overall heat transfer coefficient between the solid and gas, explained in Annex E.

$\dot{Q}_{ll} = \alpha_{solid} \cdot A_s \cdot (T_{s,j} - T_{s,j\pm1}) [W]$ Equation 6.26

Where:

α_{solid} – overall heat transfer coefficient between consecutive solid layers, explained in Annex E,

$T_{s,j}$ – temperature of the solid in the layer *j,*

$T_{s,j\pm1}$ – temperature of the solid in the layer $j\pm1$ (neighbouring layer)

The heat exchange between the layers can occur in either direction in dependence on the temperature difference between the layers. If the temperature of the top layer *j* is higher than of the bottom one *j-1* the heat flux is directed downwards. The situation is opposite when the bottom layer is hotter than the top layer.

$$\frac{dH_{dry}}{dt} = \mp \dot{m}_{wv} \cdot h_{evap} = \mp \dot{m}_{wv} \cdot c_{p,wv} \cdot (T_s - T_0)\ [W]$$ Equation 6.27

Where:

$\dot{m}_{wv}$ – mass flow of the water evaporated from the solid or condensed back into solid,

h_{evap} – enthalpy of evaporation ($h_{evap} = 2260\ [kJ/kg]$),

$c_{p,wv}$ – specific heat capacity of water vapour at 100°C ($c_{p,wv} = 2.08\ [kJ/kg]$),

T_0 – reference temperature ($T_0 = 297.15\ [K]$).

$$\frac{dH_{re}}{dt} = \sum_k \nu_{ik} \cdot r_k \cdot \Delta_R H_k\ [W]$$ Equation 6.28

Where:

ν_{ik} – stoichiometric factor of species i in the reaction k,

r_k – reaction rate of the reaction k,

$\Delta_R H_k$ – enthalpy of reaction k.

It is assumed in the model that the enthalpy released from the heterogeneous reactions is split evenly and one half of it is assigned to the solid and the other half to the gas. Enthalpy released from the homogeneous reactions is assigned in the gas phase and can be transported into the solid through the convection and radiation.

The surface area A_s is calculated using the specific surface area of the fuel particles S_v measured with the method presented in chapter 4.2.2.2.:

$$A_s = V_s \cdot S_v\ [1/m]$$ Equation 6.29

where the V_s is the volume of one stirred reactor i.e., of a cylinder with the diameter of 24 cm and height of 1 cm (equals the diameter of one fuel particle, see model assumptions).

Solid:

$$\frac{dH_{s(j,t)}}{dt} = \varepsilon_{ws} \cdot \sigma \cdot A_s \cdot \left({T_s}^4 - {T_w}^4\right) + \sigma \cdot A_s \cdot \left(\varepsilon_{fs} \cdot {T_{fg}}^4 - \alpha_{fs} \cdot {T_s}^4\right) -$$

$$-\alpha_{sg} \cdot A_s \cdot (T_s - T_g) + \alpha_{solid} \cdot A_s \cdot (T_{s,j} - T_{s,j\pm1}) - \frac{dH_{dry}}{dt} - \frac{dH_{re,s}}{dt} - \frac{dm}{dt} \cdot c_{p,s} \cdot T_s$$

Equation 6.30

Gas:

$$\frac{dH_{g(j,t)}}{dt} = -\sigma \cdot A_s \cdot \left(\varepsilon_{fs} \cdot {T_{fg}}^4 - \alpha_{fs} \cdot {T_s}^4\right) - \sigma \cdot A_{wf} \cdot \left(\varepsilon_{fw} \cdot {T_{fg}}^4 - \alpha_{wf} \cdot {T_w}^4\right) +$$

$$+\alpha_{sg} \cdot A_s \cdot (T_s - T_g) + \frac{dH_{dry}}{dt} - \frac{dH_{re,g}}{dt} + \frac{dm}{dt} \cdot c_{p,s} \cdot T_s + \frac{dm_{g,j-1}}{dt} \cdot c_{p,g,j-1} \cdot T_{g,j-1} - \frac{dm_{g,j}}{dt} \cdot c_{p,g,j} \cdot T_{g,j}$$

Equation 6.31

Emissivity coefficients between the solid, gas and the furnace wall, as well as the heat transfer coefficients are presented in Annex E.

7. Validation of the model

In the following chapter, the experimental results discussed in chapter 5 will be compared to the simulations performed with the latest version of the KLEAA Code. In order to validate the model the calculated and experimentally obtained mass conversion behaviours and the gas concentrations above the fuel bed will be compared. Because the temperatures in the combustion chamber and the primary air distribution vary from each other in the KLEAA reactor and in the TAMARA facility the validation procedure will be split between both facilities. The KLEAA Code will be validated only for two for the wood chips and for SBS®1. First, the combustion of wood chips in the KLEAA reactor will be simulated and the result will be compared with the experimental data. Then the combustion of the same fuel in the TAMARA pilot plant will be simulated and compared. Further on, the same procedure will be applied for the SBS®1.

Summary of all four steps is shown below:

1. Validation of KLEAA Code for combustion of wood chips in a fixed bed,
2. Validation of KLEAA Code for combustion of wood chips in a grate firing,
3. Validation of KLEAA Code for combustion of SBS1 in a fixed bed,
4. Validation of KLEAA Code for combustion of SBS1 in a grate firing.

Composition and the production process of the BIOBS were improved after the combustion tests at TAMARA in 2011 because the original, rich in fines fuel, led to high fly ash emissions from the fuel bed during the combustion (74). Furthermore, production of the BIOBS was discontinued after these modifications and after the combustion demonstration in the large scale power plant Wachtberg. There were no plans to introduce the use of the BIOBS in the industry nor to resume its production. For this reason, the model validation will be focused on the combustion of the wood chips and the SBS®1 which find their wide use in CHP plants.

7.1. Simulation of the wood chips combustion in the fixed bed

Several key settings of the simulation of wood chips combustion with the KLEAA Code will be summarised in a table below. The core part of this chapter consists of a comparison of the mass conversion behaviour, characteristic numbers of the three-step characterisation concept – IT, IR and MCR and of gas concentrations (O_2, CO, CO_2, CH_4, H_2O) above the fuel bed released during the experiment and generated by the model.

Table 7.1 – Settings of the simulation of wood chips combustion in the fixed bed

Property	Symbol	Unit	Settings for Wood chips	
Bulk density	ρ_{bulk}	kg/m^3	170	
Solid density	ρ_s	kg/m^3	580	
Fuel amount	m_{fuel}	kg	1.64	
Dry wood mass fraction	C_{wood}	kg_{wood}/kg_{fuel}	0.85	
Water mass fraction	C_{water}	kg_{water}/kg_{fuel}	0.15	
Ash mass fraction	C_{ash}	kg_{ash}/kg_{fuel}	0.02	
Sp. surface area	S_V	m^2/m^3	665	2000
Primary air flow	$\dot{m}_{PA}$	$kg/m^2 \cdot h$	310	
Primary air temp.	ϑ_{PA}	$°C$	15	
Furnace temp.	ϑ_{fw}	$°C$	900	

The lower specific surface area i.e., 665m²/m³ (Table 7.1) corresponds to the specific surface area of spherical particles with the mean diameter of 9mm. This mean particle size was determined for the wood chips by the sieving analysis as described in 4.2.2. The specific surface area measured by the pressure drop equals roughly 2000m²/m³ and it is expected that the model will render the most accurate results for this value.

7.1.1. Mass conversion

Figure 7.1 presents simulation results for the rate of the mass conversion calculated for different specific surface areas of the fuel particles compared to the experimental results (dashed thick line). Studying this diagram allows drawing several conclusions. First of all, it can be clearly recognised that the rate of the fuel conversion in the main combustion zone simulated for $S_v = 2000\ [m^2/m^3]$ corresponds very well to the measured one. This is an important observation as it shows that the updated model together with the input of the specific surface area estimated by the method

developed in course of this study brings correct results. Furthermore, the char burnout starts in both cases roughly at the same moment i.e., 12 minutes after the beginning of the combustion test. A slightly slower measured fuel conversion in comparison to the one simulated for $S_v = 2000\ [m^2/m^3]$ can be also observed in course of the main combustion phase and can indicate that a more precise measuring procedure for the specific surface area is needed.

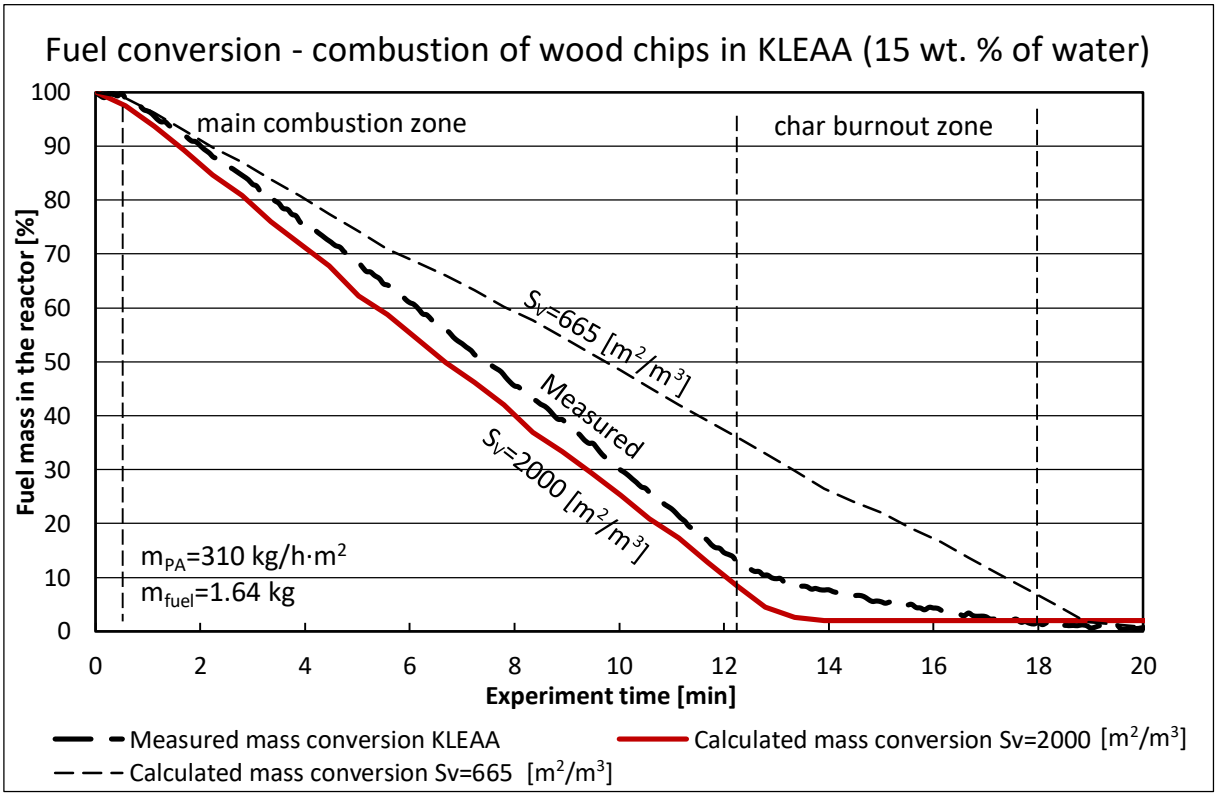

Figure 7.1 – Simulated and measured fuel conversion rate in KLEAA

Another finding is that the simulated char burnout is much shorter than the measured one. This issue and its possible reasons will be discussed later on in chapter 7.1.2. Combustion of the wood chips for which the specific surface area was set to $S_v = 665\ [m^2/m^3]$ takes a longer time until the complete conversion which occurs 19 minutes after the start of the experiment. The char burnout phase is again very short.

Summarising, the measured specific surface area $S_v = 2000\ [m^2/m^3]$ has proven to be plausible for wood chips. It has to be kept in mind that it was measured with a new method and has to be considered as a rough estimation. For this setting the model was able to correctly predict the mass conversion rate for wood chips with a relative deviation of 4.35% from the mean measured MCR I. The reaction front velocity and the ignition rate was simulated within a reasonable relative deviation of 8.97% and 8.47% respectively. This deviations are likely caused by the difference between the actual and the estimated specific surface area of fuel particles. Furthermore, the characteristic

numbers are also expected to deviate in range of ±3% from measurement to measurement as stated by Bleckwehl (25).

Table 7.2 – Comparison of the calculated and measured IRs, RFVs, and MCRs for combustion of wood chips with 15 wt. % water content

Characteristic Number	Symbol	Unit	Wood chips 15 wt. % water		Deviation [%]
			Measured	Simulated	
Reaction front velocity	u_{RF}	mm/min	20.3	22.3	8.97
Ignition rate	IR	$kg/m^2 \cdot s$	0.054	0.059	8.47
Mass conversion rate I	$MCR1$	$kg/m^2 \cdot s$	0.048	0.046	4.35

The mass conversion rate during the char burnout zone (MCR II) was however not simulated correctly. Similar inconsistency in case of the char burnout phase was observed also during the model validation for the wood spheres (44) with similar water content as the wood chips investigated in this study. Simulation performed in (44) for dry wood spheres (2 wt. % of water) returned however correct results in the char burnout zone. In order to validate the KLEAA Code for wood chips also a simulation of the combustion of dry wood chips has been performed with the specific surface area set to $S_v = 2000\ [m^2/m^3]$ and the water content to 2 wt. %.

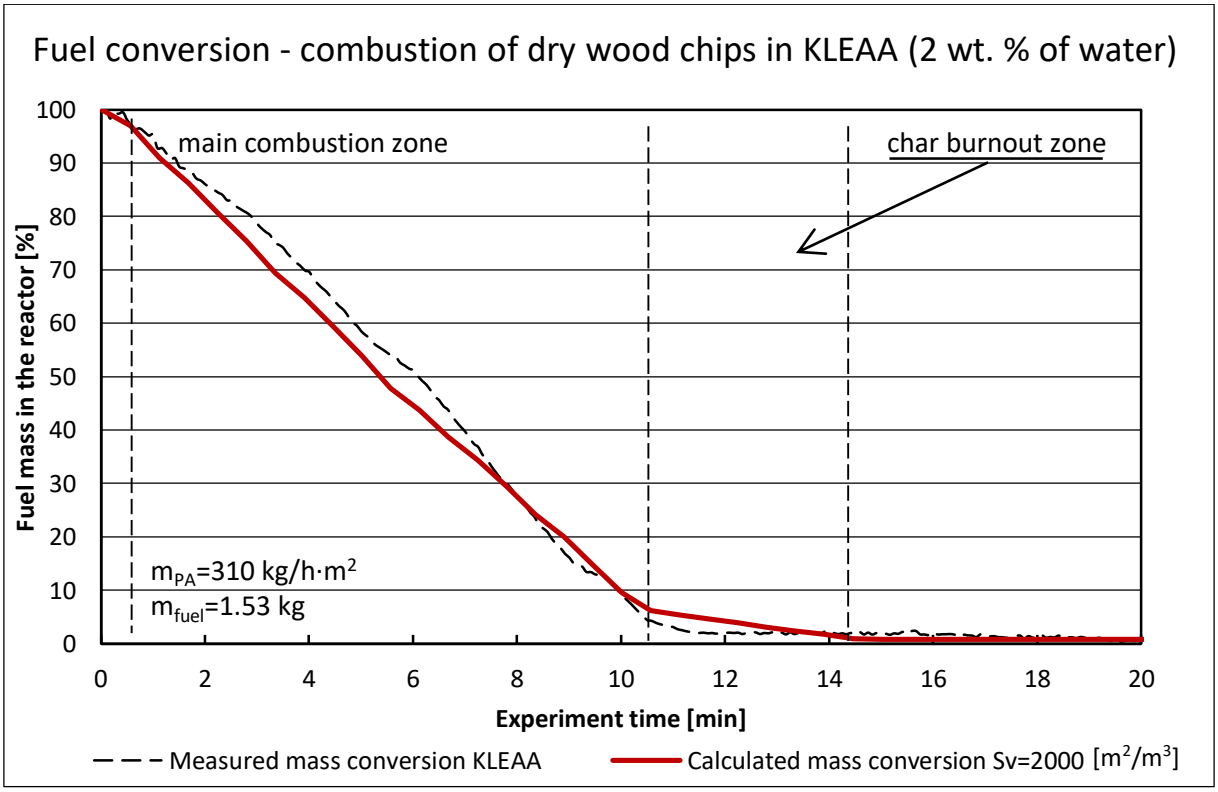

Figure 7.2 – Fuel conversion during the combustion of dry wood chips in the KLEAA reactor

In this case, there is a clear char burnout zone visible in the simulation results. Mass conversion rates in the main combustion zone (MCR I) and during the char burnout were simulated correctly:

Table 7.3 – Comparison of the calculated and measured MCRs for combustion of wood chips with 2 wt. % water content

Characteristic Number	Symbol	Unit	Wood chips 2 wt. % water		Deviation [%]
			Measured	simulated	
Mass conversion rate I	$MCR1$	$kg/m^2 \cdot s$	0.058	0.063	7.94
Mass conversion rate II	$MCR2$	$kg/m^2 \cdot s$	0.010	0.010	0.00

7.1.2. Gas concentrations above the fuel bed

Analysis of the fuel mass conversion rates has shown that applying the specific surface area of 2000m²/m³ for wood chips provides the best simulation results what corresponds very well with the estimated specific surface area. Further on, the simulated gas concentrations will be compared to the measured mean gas concentrations above the fuel bed. The measured gas concentrations can deviate up to 3% (relative) from the mean value (25).

Oxygen concentration during the experiment is shown in Figure 7.3. The simulation corresponds very well with the experimental data, especially during the main combustion zone. Simulated O_2 concentration, as well as other gas concentrations, were characterised by a numerical noise making the interpretation of the results difficult. The noise was caused by the numerical process and is not associated with any physical or chemical process. It was therefore decided to smooth (exponential smoothing) the results in order to present them in a more convenient way. The raw data sequence in the following formula is represented by x_t beginning at time $t = 0$, and the output of the exponential smoothing algorithm is written as s_t, which may be regarded as a best estimate of what the next value of x will be. When the sequence of observations begins at time $t = 0$, the simplest form of exponential smoothing is given by the formulas:

$$s_0 = x_0 \qquad \text{Equation 7.1}$$

$$s_t = \alpha x_t + (1 - \alpha) s_{t-1}, t > 0 \qquad \text{Equation 7.2}$$

The most optimal presentation of the results was obtained with the smoothing factor $\alpha = 0.3$. Unsmoothed, raw data is presented in Annex F.

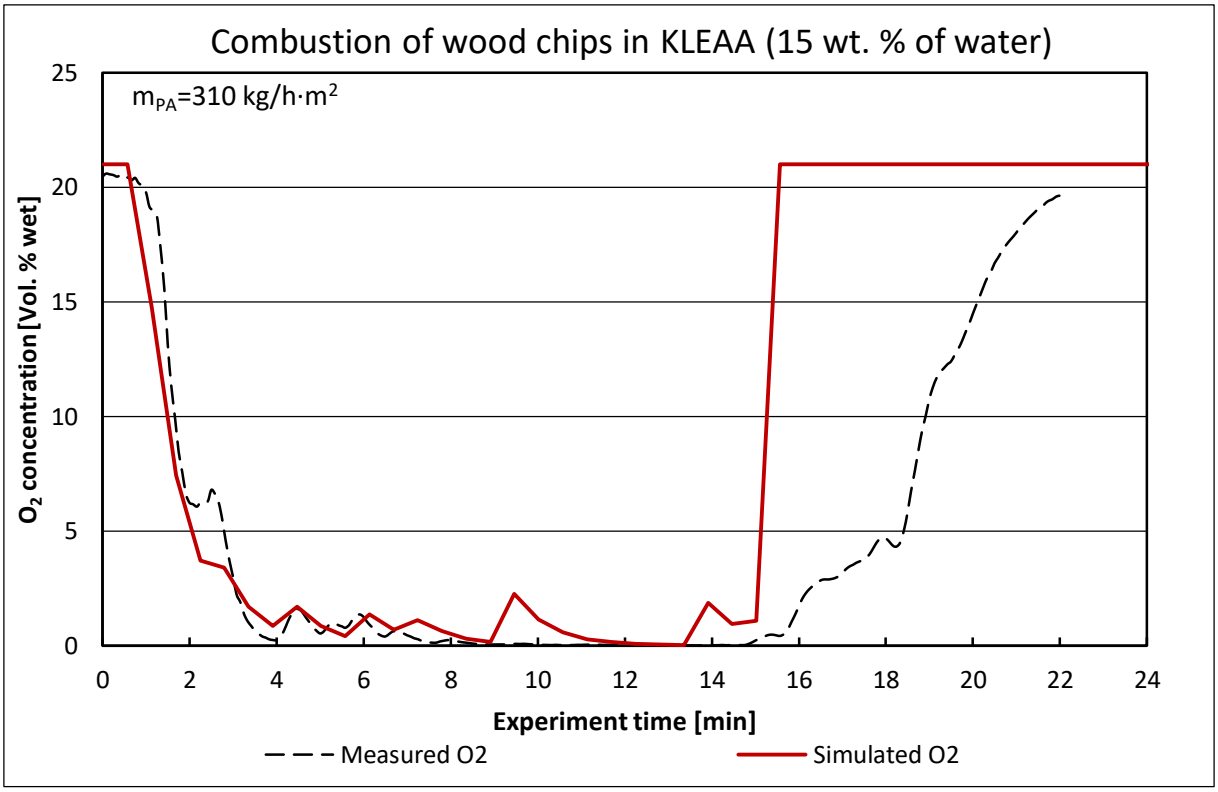

Figure 7.3 – Oxygen concentration above the fuel bed during wood chips combustion in the KLEAA reactor

It can be clearly recognised in Figure 7.3 that the simulated O_2 concentration raises rapidly after 15 minutes which means that the combustion process is finished at that point. This corresponds well with the simulated mass conversion behaviour presented in figure 7.1. Measured O_2 concentration suggests however that the process still continues till minute 22 and it can be identified as char burnout. This observation is supported by studying the CO_2 and CO concentrations above the fuel bed presented in Figure 7.4 and Figure 7.5.

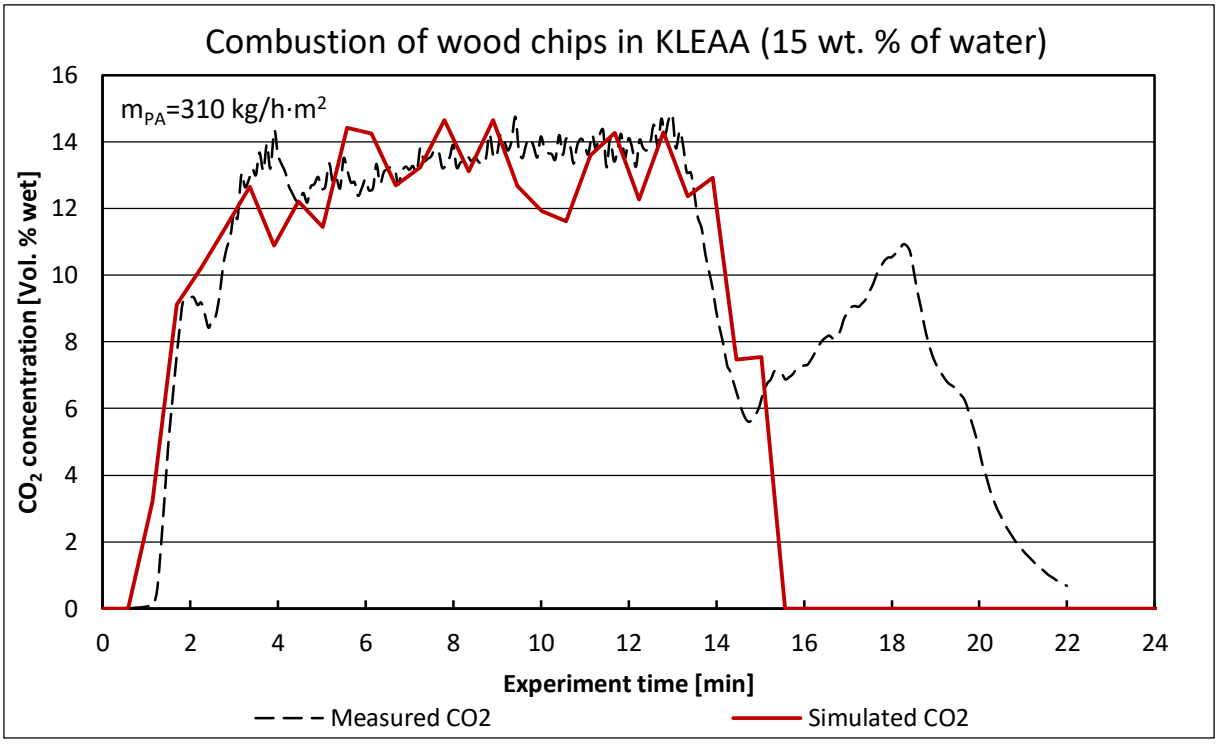

Figure 7.4 – Carbon dioxide concentration above the fuel bed during wood chips combustion in the KLEAA reactor

Figure 7.4 presents the CO_2 concentrations and proves that the KLEAA Code has simulated emission of this gas during the main combustion zone accurately. Char burnout zone is however missing. Possible explanations will be discussed later on in this chapter.

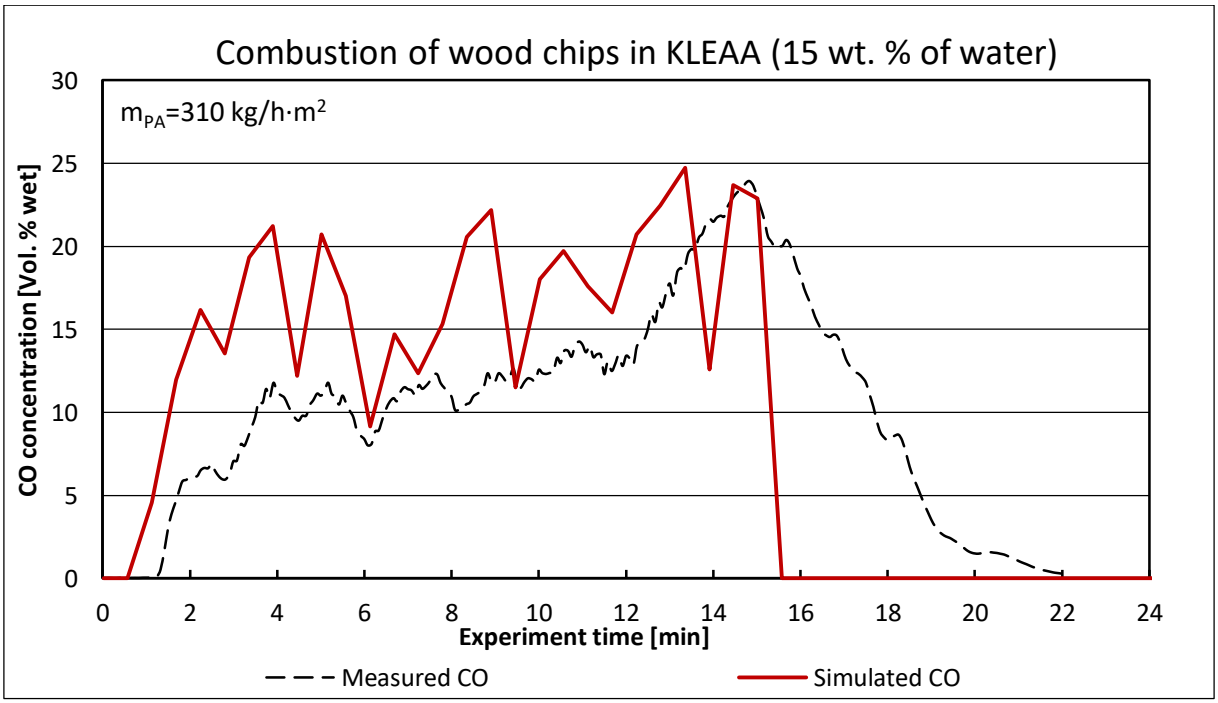

Figure 7.5 – Carbon monoxide concentration above the fuel bed during wood chips combustion in the KLEAA reactor

Figure 7.5 shows the CO emission from the fuel bed. The measured carbon monoxide concentration rapidly raises after the ignition to about 6 Vol. % and then raises slowly over the course of the main combustion zone to almost 13 vol. % after 12 minutes. Then the char burnout starts which results with a CO peak with its maximum at 23.5 vol. % at minute 15. Simulated CO emission presents a somewhat different behaviour. The gas concentration after the ignition rises to nearly 17 vol. % on average at minute 3 and goes up slightly during the process up to 22 vol. % after 14 minutes. After that, the combustion is finished. No recognisable CO peak identifiable as char burnout is visible.

Studying the simulated hydrogen emission from the fuel bed reveals though that it does not correspond to the measured one and oscillates between 10 and 14 vol. % which is over three times more than measured. The measured H_2 concentration rises slowly from the start of the combustion from 0 vol. % to a maximum value of 8 vol. % at minute 13.

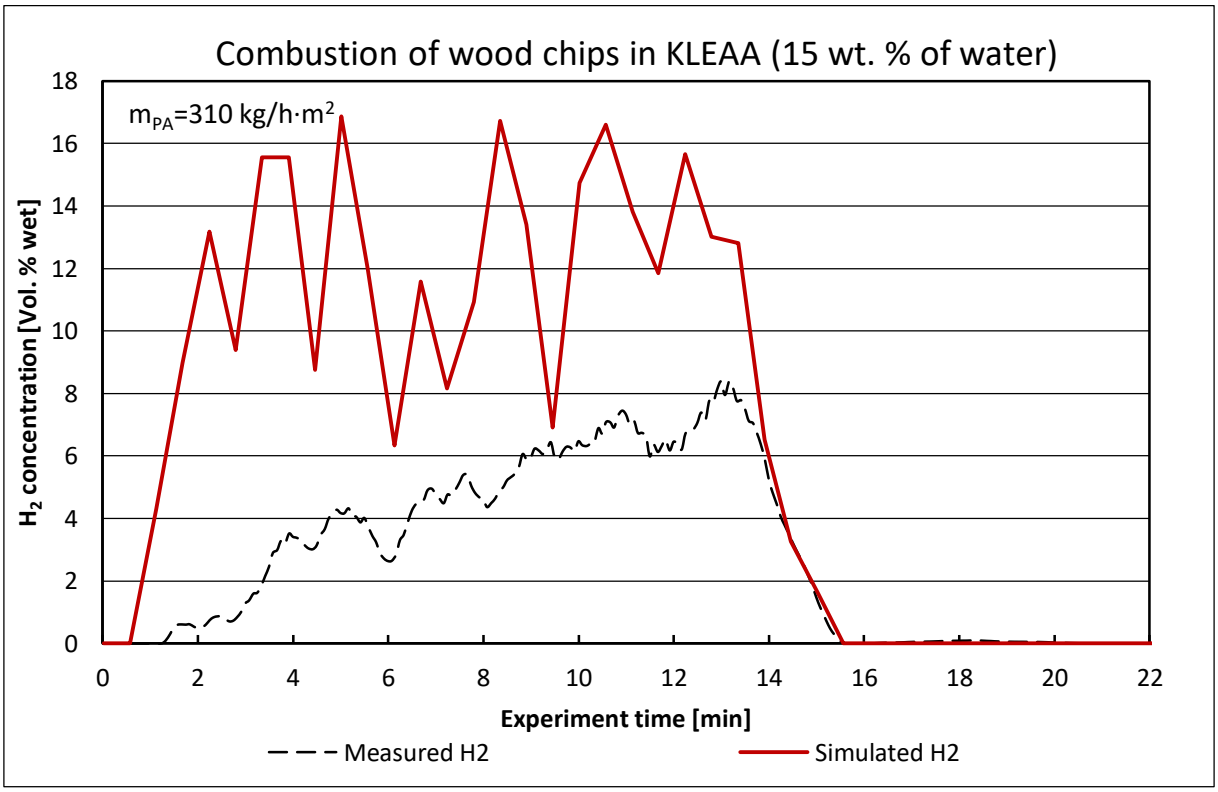

Figure 7.6 – Hydrogen concentration above the fuel bed during wood chips combustion in the KLEAA reactor

It can be observed that the simulated CO and H_2 concentrations are both too high. This behaviour could be caused by the inaccuracy in the kinetics of the following reactions:

$$C + H_2O \rightarrow CO + H_2$$ Equation 7.3

$$CH_4 + 0.5O_2 \rightarrow CO + 2H_2$$ (air ratio below 1) Equation 7.4

Reaction kinetics in the KLEAA Code were validated in (25) for wood spheres and they deliver correct results for two boundary cases – dried beech wood spheres (water content 2 wt.%) and very wet beech wood spheres (water content 45 wt. %). The water content of 45 wt. % has been chosen as the second boundary on the basis of the findings of Bleckwehl who found out that the ignition rate (IR) and mass conversion rate in the main combustion zone (MCR I) are almost equal for this water content. This means practically that the ignited amount of fuel is almost immediately combusted. At the same time, there is a large abundance of water reacting during the main combustion phase with the fixed carbon produced during degassing (see reactions of pyrolysis in chapter 5.5). This results in an extremely short char burnout zone which is often not recognisable (e.g., mass conversion of BIOBS, see chapter 5).

If the reaction (Equation 7.3) was taking place too fast, the CO and H_2 concentrations would be too high, fixed carbon would be consumed too fast and H_2O emission to the furnace would be too low. This is the case observed in the current version of the model. In case of the H_2O emissions (Figure 7.8), the consistency of the simulated and measured results is however very good within the first 10 minutes of the combustion. Both values lie between 14 and 18 vol. % in the main combustion zone. That does not mean that this explanation is wrong. The amount of water evaporating from the fuel during the main combustion is simply much higher than the water consumed in course of the reaction 7.3. Another explanation for the inconsistencies in the CO and H_2 concentrations is a too high temperature of the fuel bed calculated by the KLEAA Code (Figure 7.9) and therefore a too high reaction rate in case of the gasification of carbon with water (Equation 7.3).

The gasification of methane (Equation 7.4) also can contribute to the increase of the simulated H_2 and CO concentrations. The simulated CH_4 concentration is lower than the measured one which might indicate that the methane is decomposed too fast in course of the reaction 7.4 as shown in Figure 7.7:

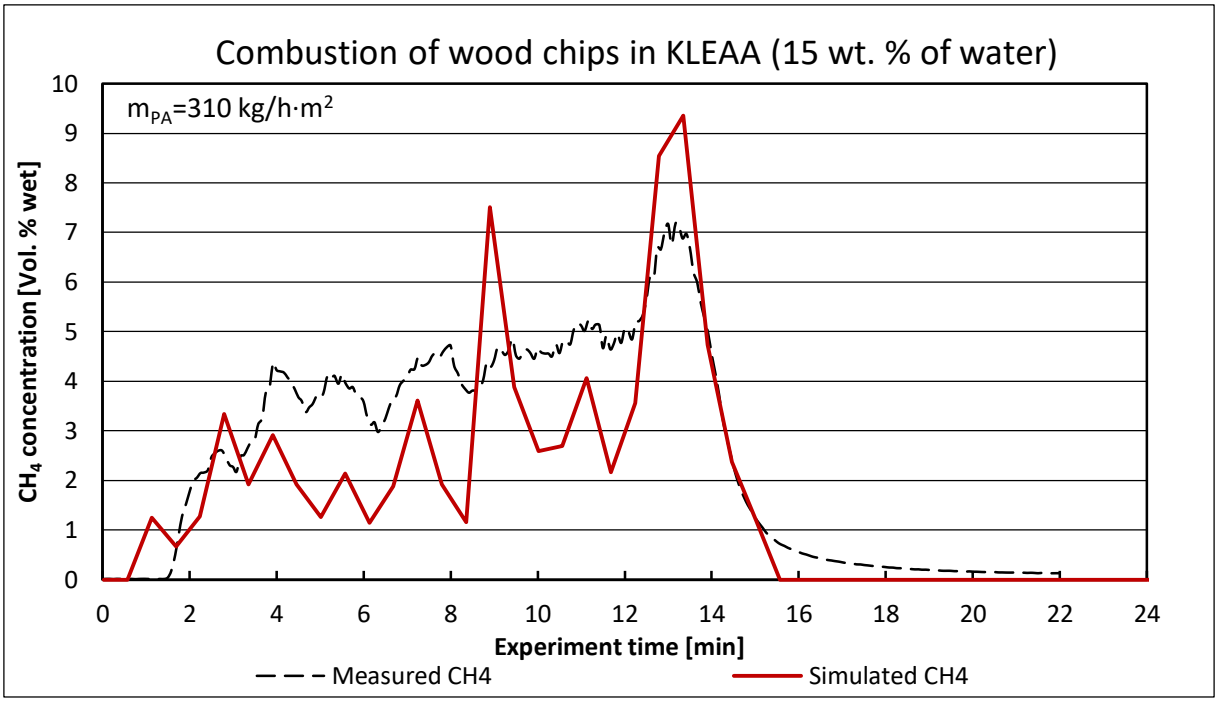

Figure 7.7 – Methane concentration above the fuel bed during wood chips combustion in the KLEAA reactor

At the beginning of the experiment, the methane concentration rises fast after the ignition to 2.5 vol. % and then as the ignition front proceeds downwards it gradually increases up to 5 vol. % in the minute 12. At the end a 7 vol. % high CH_4 peak can be recognised. Simulated methane concentration presents the same increasing trend in course of the main combustion zone but is roughly 1.5 vol. % below the measured one.

The last discussed gas concentration is the water vapour. Accurate results of the simulation for the H_2O concentration regardless the issue with the heterogeneous reaction of the fixed carbon and water vapour can be a result of a relatively small share of the water which can be consumed in course of this reaction in comparison to the total amount of water released through drying.

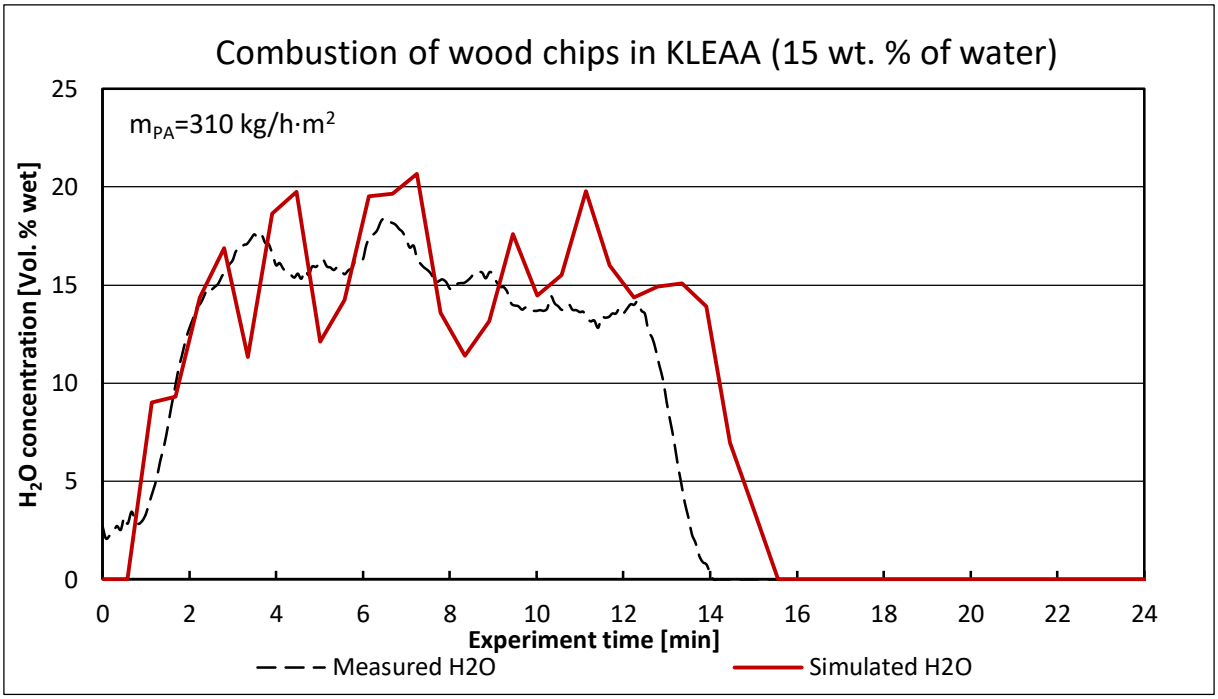

Figure 7.8 – Water concentration above the fuel bed during wood chips combustion in the KLEAA reactor

The reaction kinetics were mentioned as one of the reasons for the lack of a clearly recognisable char burnout zone in the simulation results and too high calculated concentrations of the hydrogen and carbon monoxide. The second reason might be the fact that the solid mass transfer is not considered in the KLEAA Code. The char particles forming in the fuel bed fall down and accumulate in the lower parts of the fuel vessel in reality. This means that there is more reacting material on the bottom of the fuel vessel during the char burnout in reality than in the modelled fuel bed. Another reason for the inaccuracy of the simulation in the char burnout is the bed temperature which is discussed in the next section.

7.1.3. Temperatures in the fuel bed

Temperature above and in the fuel bed plays an important role in the entire combustion process. It is together with the surface area a key factor defining the rate of the heat transfer and therefore the rate of the drying, pyrolysis, ignition and the char burnout. The rate of these processes has obviously a great influence on the temperature itself. Finding the right balance between the kinetics of the reactions and the temperature is, therefore, one of the most important steps of the model development.

The measured and simulated temperatures during the wood chips combustion in the KLEAA reactor are presented below. The experiment has shown that the temperature in the main combustion zone is maintained between 700°C and 800°C and it increases in the char burnout zone to roughly 1200°C. It is expected that the simulated temperatures will be higher due to the assumption that the process

is adiabatic. The simulation result confirms this expectation; the calculated temperature in the main combustion zone reaches 900°C and roughly 1650°C in the short peak during the char burnout:

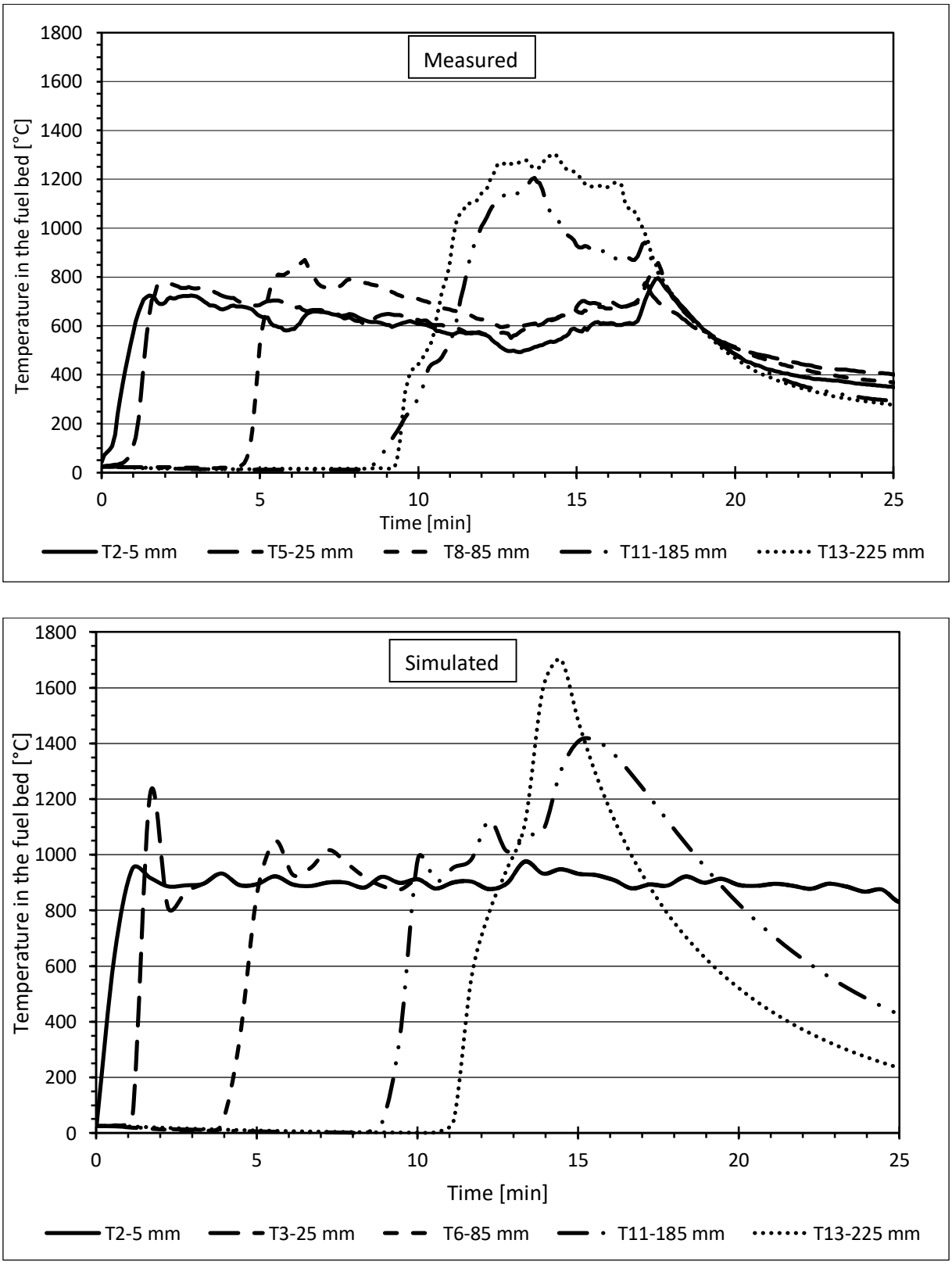

Figure 7.9 – Measured (above) and simulated (below) temperatures in the fuel bed during the combustion of wood chips in the KLEAA reactor

As shown in Figure 7.9 the simulated temperatures are ca. 200K higher than the measured ones. The difference is even higher during the char burnout and reaches 450K. More interesting is however the fact that the model predicted the char burnout zone in terms of the temperature regardless of the inconsistencies in the CO, H_2 and methane concentration (see chapter 7.1.2.)

It can be also noticed that the simulated solid temperature at the thermocouple T2 reaches about 900^{o}C (Figure 7.9) and maintains this level over the course of the simulation (25 min). This is caused by the fact that the fuel particles in the KLEAA Code have fixed locations corresponding to each layer. They do not fall down to the bottom of the fuel vessel as the fuel is being converted but stay in their original locations in form of the ash particles at the end of the combustion (no solid mass transport between the layers). These particles in the first layer (T2) absorb the heat radiated from the furnace wall (900^{o}C) but the heat transfer from this layer to the next is strongly dependent on the surface of the particles (Equation 6.26) which in this case corresponds with the surface of the ash particles and is strongly limited. The bottom layers are therefore not affected by this radiation and are cooled down by the primary air coming from the bottom and flowing freely through the fuel/ash layers. The lack of the solid transport in the KLEAA Code is therefore a major limitation of the model responsible for the shortcomings of temperature prediction.

The discussed differences between the measured and simulated temperatures as well as between the gas concentrations allow concluding the following. Fitting the kinetics of the water gas shift reaction and of the methane decomposition might not be a sufficient effort to improve the simulation results. It might be necessary to introduce the heat losses term in the energy balance. For the purpose of investigating these heat losses, an additional temperature measurement on the outer surface of the fuel vessel (cylinder) of the KLEAA reactor was performed (Figure 7.10) for wood chips.

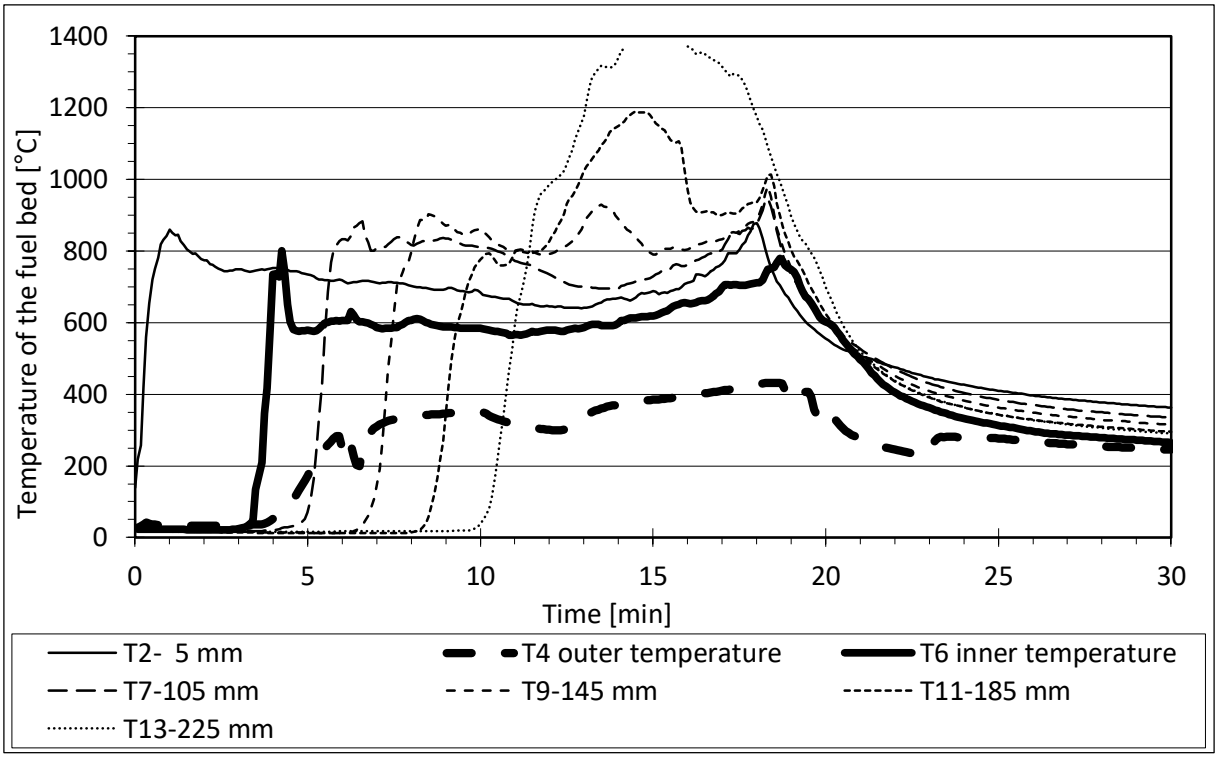

Figure 7.10 – Temperature on the outer surface of the fuel vessel (dashed line)

The temperature of the outer surface of the fuel cylinder rises for about 1 to 2 minutes and then stays at roughly the same level of 350°C for the rest of the experiment. It can be therefore assumed that the heat loss through the insulation around the fuel cylinder is stationary. After further assumption that the cylinder is not insulated and the air temperature around it equals 20°C a maximal possible heat loss through radiation and free convection can be calculated according to (66).

Assumptions:

$\vartheta_{air} = 20℃$

$\vartheta_{wall} = 350℃$

$\vartheta_{average} = 185℃$

Air parameters for the average air temperature of 185°C (66):

$\lambda_{air} = 0.036 \frac{W}{mK}$ – thermal conductivity

$\nu_{air} = 31 \cdot 10^{-6} \frac{m^2}{s}$ – kinematic viscosity

$Pr = 0.6981$ – Prandtl number

$\beta_{air} = \frac{1}{T_{air}} = 0.00341 \frac{1}{K}$ – thermal expansion coefficient

With these parameters and the height of the fuel cylinder h of 25 cm the Grashof, Rayleigh and Nusselt numbers, as well as the heat transfer coefficient are calculated (66):

$$Gr = \frac{g \cdot h^3 \cdot \beta_{air} \cdot (\vartheta_{wall} - \vartheta_{air})}{{\nu_{air}}^2} = 1.795 \cdot 10^8$$ Equation 7.5

$$Ra = Gr \cdot Pr = 1.253 \cdot 10^8$$ Equation 7.6

$$Nu = \{0.825 + 0.387 \cdot [Ra \cdot f_1(Pr)]^{1/6}\}^2 = 90$$ Equation 7.7

$$f_1(Pr) = 0.345$$

$$\alpha = \frac{Nu \cdot \lambda}{h} = 12.962 \frac{W}{m^2 K}$$ Equation 7.8

Heat loss through convection equals:

$$\dot{Q}_{conv} = A \cdot \alpha \cdot (\vartheta_{wall} - \vartheta_{air}) = 0.76\ kW$$ Equation 7.9

Where A is the surface area of the fuel container. Heat loss through radiation is calculated from the equation below (66):

$$\dot{Q}_{rad} = A \cdot \sigma \cdot \varepsilon \cdot \left(T_{wall}^4 - T_{air}^4\right) = 1.41\ kW$$ Equation 7.10

Where:

$\sigma = 5.67 \cdot 10^{-8} \frac{W}{m^2 K^4}$ – Stefan-Bolzmann constant

$\varepsilon = 1$ – emissivity of the fuel vessel

In total the maximal heat losses through the wall of the fuel vessel equal:

$$\dot{Q}_{loss} = 2.17\ kW$$

In the next step the heat released from the fuel bed has to be calculated:

$$\dot{Q}_{bed} = \dot{Q}_{gas} + \dot{Q}_{loss}$$ Equation 7.11

Latent enthalpy of the gas released from the fuel bed $\dot{Q}_{gas}$ can be calculated when the amount of the released gas, its temperature and composition are known. All these values are measured during the combustion tests at KLEAA. The average enthalpy of the gas released during the combustion of wood chips from the ignition till the end of the char burnout equals:

$$\dot{Q}_{gas} = 3.78\ kW$$

The relative heat loss can be defined as:

$$n = \frac{\dot{Q}_{loss}}{\dot{Q}_{gas} + \dot{Q}_{loss}} \cdot 100\% \qquad \text{Equation 7.12}$$

and equals:

$$n = 36.5\%$$

Relative heat loss of 36.5% is a significant amount and should be considered an extreme (the highest possible) and a rather tentative value. It is, however, worth and recommended investigating the influence of this heat loss on the results delivered by the KLEAA Code. This could be achieved by performing several simulations for wood chips with equations 6.30 and 6.31 multiplied by a fixed factor Ψ corresponding to the heat loss (sink) when:

$$\frac{dH_{s(j,t)}}{dt} > 0$$

And

$$\frac{dH_{g(j,t)}}{dt} > 0$$

In this way, an indication of what happens in the fuel bed under lower temperatures could be given. It was therefore decided to conduct two simulations with the heat sink Ψ of 15% and 30%. The achieved temperatures in the fuel bed are presented in the figures below:

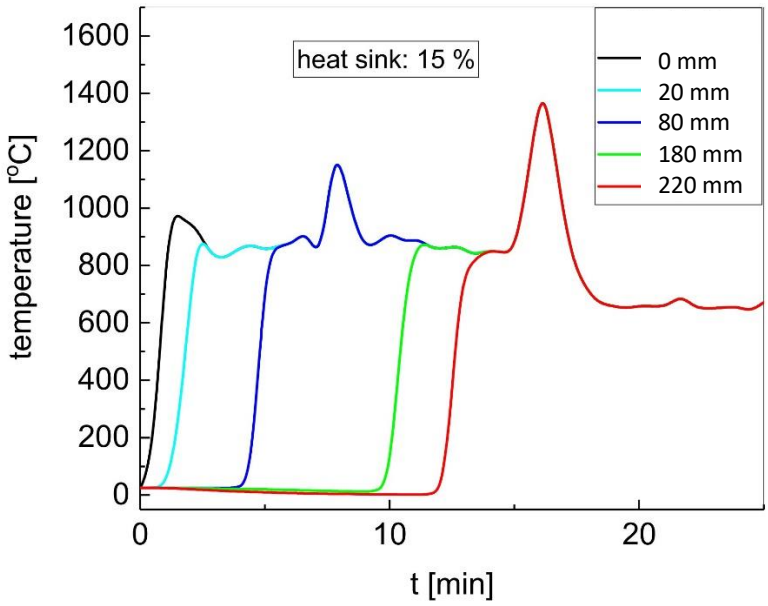

Figure 7.11 – Simulated temperatures in the fuel bed with a heat sink of 15%

The fuel bed temperature with a heat sink of 15% is slightly reduced in comparison to the temperature simulated without it (see Figure 7.9) but not close enough to the measured one. The

bottom temperature (red line, 220 mm) rises after about 12 minutes (the bottom part of the fuel bed ignites) which is later than without the heat sink and much later than in case of the measured bottom temperature (T13 in Figure 7.9). The peak temperature of 1400°C is also still about 100K too high and the peak is too short in comparison to the measured one indicating that the char burnout does not occur slower, which was the main goal of applying the heat sink.

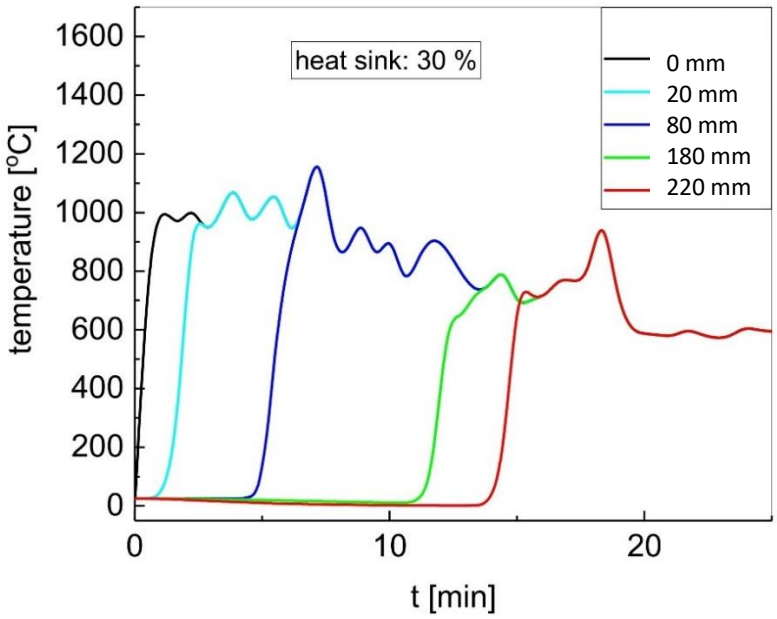

Figure 7.12 – Simulated temperatures in the fuel bed with a heat sink of 30%

Increasing the heat sink even further to 30% results in the bed temperature closer to the measured one, especially in the middle of the fuel bed, where the heat coming from the furnace above the fuel bed is negligible. The ignition front reaches the bottom of the fuel vessel (red line) however after 14 minutes, much later than in reality (after ca. 9 minutes, see Figure 7.9). Furthermore, the bottom temperature i.e., during the char burnout is much too low.

The simulations performed with heat sinks of 15% and 30% show that the bed temperature can be decreased but the ignition front moves much lower than in reality. This proves that incorporating the heat loss into the KLEAA Code is not sufficient to improve the simulation results during the char burnout phase. It might be however a necessary step in the process of the KLEAA Code development provided, that the heat loss is modelled in real time (in every time step of the simulation) and not considered to be constant as in the aforementioned tentative calculations.

7.2.Simulation of the SBS®1 combustion in the fixed bed

Combustion of solid recovered fuels takes the difficulty of modelling one step further in comparison to the modelling of the combustion of pure biomass. It was decided to model the additional component in these fuels i.e. plastics as polyethylene. The amount of this component in the SBS®1 has been set to 20 wt.% based on the sorting analysis and detection of plastics in the fuel with the NIR-measurement. The assumption that all the plastics can be summarised as PE as well as the reaction kinetics of the thermal decomposition of polyethylene can be inaccurate. Furthermore, the method used for the estimation of the specific surface area of the fuel particles was proven to be less accurate when the porosity of the bulk material is higher than 0.4 (see chapter 4.2.2.2). It has been therefore decided to investigate how much influence two measured specific surface areas of the fuel particles have on the simulated mass conversion of the SBS®1. The parameters of the simulation are presented below:

Property	Symbol	Unit	Settings for SBS®1	
Bulk density	ρ_{bulk}	kg/m^3	160	
Solid density	ρ_s	kg/m^3	660	
Fuel amount	m_{fuel}	kg	1.43	
Dry wood mass fraction	C_{wood}	kg_{wood}/kg_{fuel}	0.52	
Water mass fraction	C_{water}	kg_{water}/kg_{fuel}	0.20	
PE mass fraction	C_{PE}	kg_{PE}/kg_{fuel}	0.20	
Ash mass fraction	C_{ash}	kg_{ash}/kg_{fuel}	0.08	
Specific surface area	S_V	m^2/m^3	10000	3000
Primary air flow	$\dot{m}_{PA}$	$kg/m^2 \cdot h$	310	
Primary air temp.	ϑ_{PA}	$°C$	15	
Furnace temp.	ϑ_{fw}	$°C$	900	

Table 7.4 – settings of the simulation of SBS®1 combustion in the fixed bed

The results of the simulations of the SBS®1 combustion in the fixed bed are presented and evaluated in the next section.

7.2.1. Mass conversion

The simulation of the combustion of SBS®1 was initially performed with the specific surface area of the particles set to 10000 m^2/m^3 which was close to the measured one 10800 m^2/m^3 (for the high bulk porosity). The first look at the mass conversion characteristics presented below reveals that the simulated one does not resemble the measured one at all.

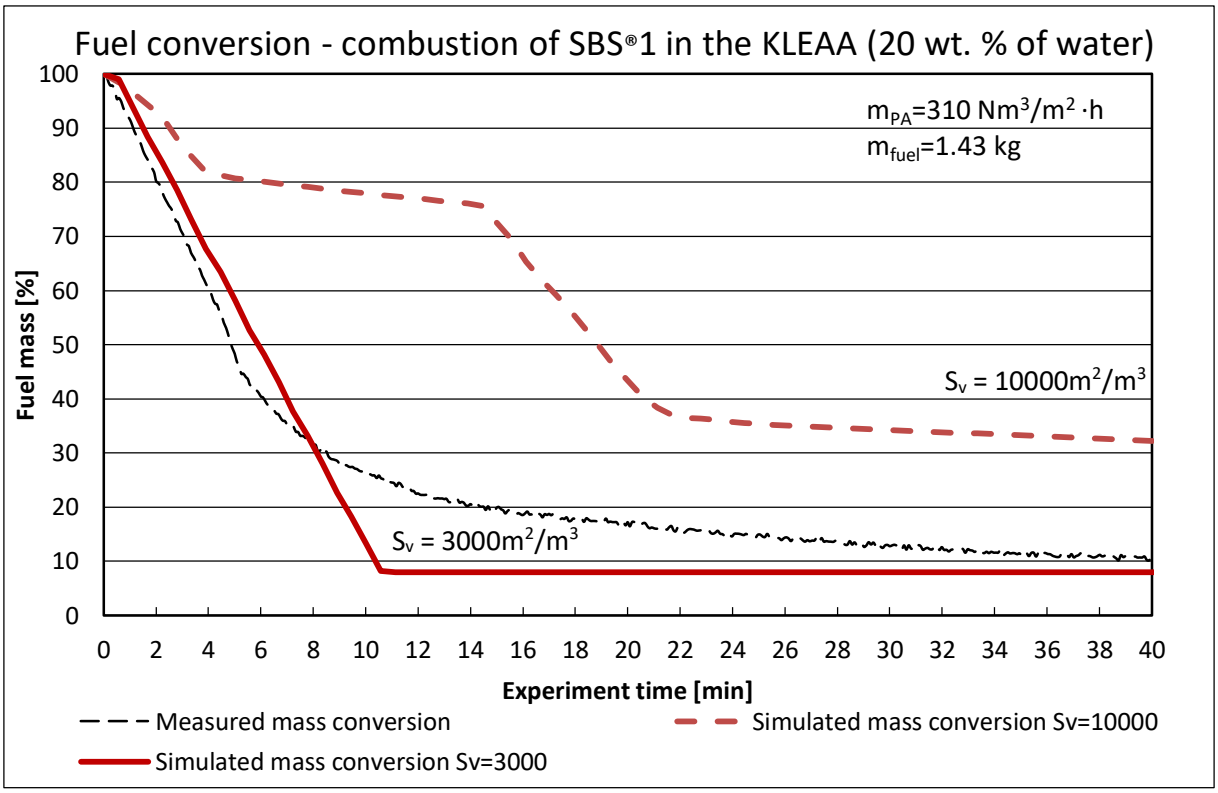

Figure 7.13 – Measured and simulated mass conversion during SBS®1 combustion in the KLEAA reactor

The simulated mass loss of the fuel at the specific surface area of 10000m^2/m^3 is similar to the results obtained from a thermogravimetric analysis of a fuel. Closer examination of the simulation results allows presuming that the fuel is dried in the first 4 minutes and it loses about 20% of its initial weight. This corresponds very well with the proximate analysis of the fuel. Further on an intensive mass loss starts at 14.5 minutes, lasts for about 4 minutes and could be identified as pyrolysis.

Studying the simulated temperatures in the fuel bed has shown that the lower part of the fuel packing has a temperature of the incoming primary air and only a thin, top layer is heated up by the radiation coming from the furnace walls. This temperature does not exceed 750°C.

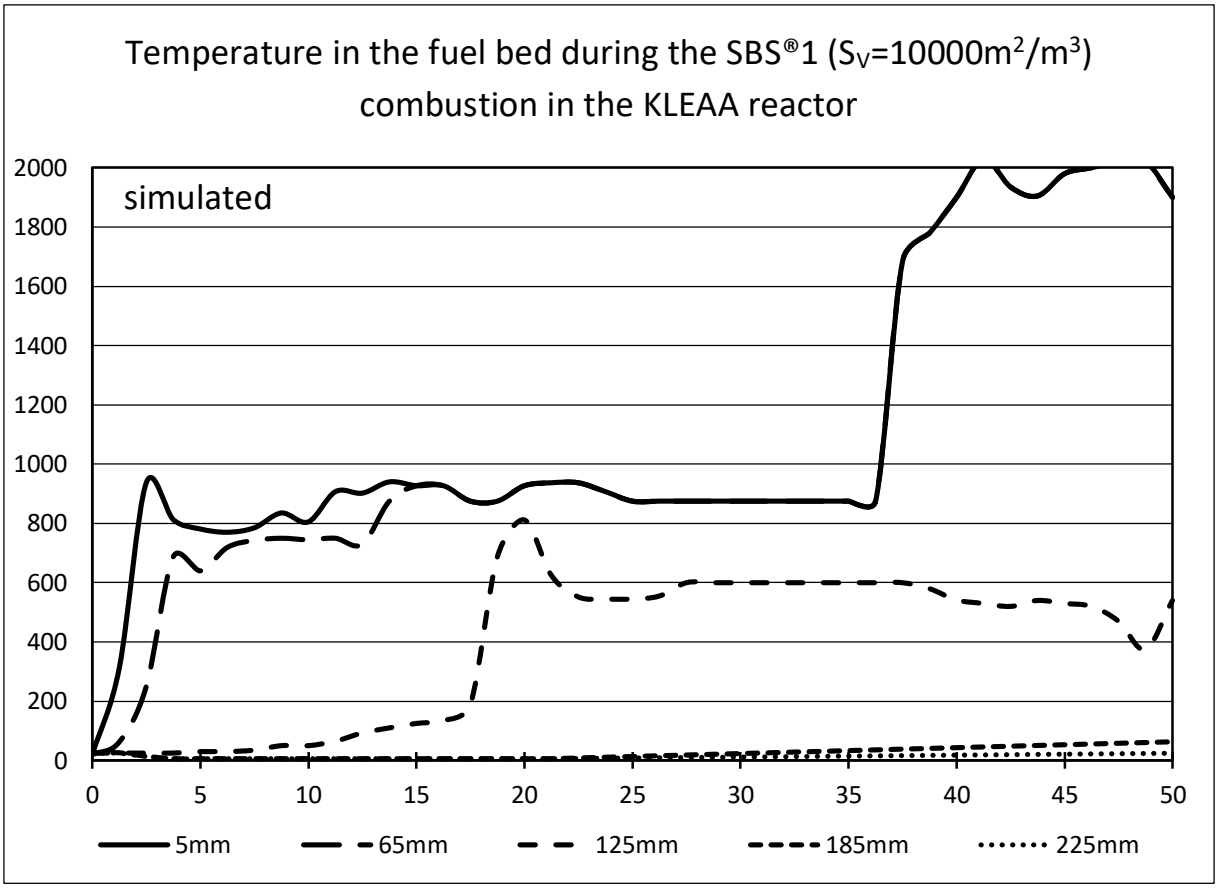

Figure 7.14 – Temperature in and above the fuel bed during the SBS®1 (S_V=10000m²/m³) combustion in the KLEAA reactor

It can be concluded that the convective cooling of the fuel bed by the primary air supplied from below greatly exceeds the heat flux radiating from the furnace resulting in very low temperatures of the fuel bed and in the lack of the combustion. This observation has led to the conclusion that such high S_v is not plausible. The reason for that is a high inaccuracy of the measurement of the surface area when the porosity of the fuel bulk is higher than 0.4. In case of the SBS®1, the porosity was 0.66 and it has been decided to repeat the surface measurement but with a slightly compressed SBS®1. The resulted porosity was 0.4 and the measured surface area of the fuel particles was around 3000m²/m³ (see chapter 4.2.2.2). When this specific surface area was set in the model the combustion took place and the simulation has delivered a mass conversion rate in the main combustion zone closer to the measured one (Figure 7.11).

Similar to the simulation of the wood chips combustion in the KLEAA reactor the model was unable to predict the char burnout zone correctly. The char burnout during SBS®1 combustion presents a very different behaviour than during the combustion of wood chips (see chapter 5.2). The char burnout zone is not easily distinguishable as it was in case of the wood chips. It starts roughly 18 minutes after the ignition and changes its intensity after that till the end of the test. Later on the

remaining 10 wt. % of the combustible material glows slowly on the bottom of the fuel vessel. This long period lasts for about 20 minutes. Such combustion behaviour can be a result of hardly combusting components in the fuel, possibly fire retardants. A lot of materials being the part of bulky waste, which is a main component of the SBS®1 fuel, such as furniture, upholstery or other textiles contain fire retardants. Another reason can be an effect observed during combustion tests of other fuels rich in plastics. During these experiments at the KLEAA reactor, the plastics on the top of the fuel bed melt at the beginning of the combustion. Part of them is pyrolyzed but the rest flows downwards the fuel bulk, cools down and solidifies on the fuel particles. In effect, the specific surface area of these particles might be reduced and the fuel in the bottom of the batch reactor can contain an increased amount of plastics in comparison to the original fuel. There is no possibility to simulate this effect in the KLEAA Code.

7.2.2. Gas concentrations above the fuel bed

The simulation performed with the measured specific surface area set to 3000m^2/m^3 delivered a mass conversion rate closer to the measured one. It has been therefore decided to validate the model further using this setting.

The oxygen concentration above the fuel bed is presented in

Figure 7.15. Measured and simulated O_2 concentrations drop rapidly from roughly 20 vol. % to 0 vol. % indicating the ignition of the fuel within the first minute of the experiment. The measured O_2 concentration equals 0 vol. % in the main combustion zone. After roughly 5 minutes the volatiles are depleted and the oxygen concentration rises slightly to about 2 vol. %. After this moment the O_2 concentration drops again to 0 vol. % what is the most probable at the beginning of the char burnout. This phase lasts for 2 minutes. The last stage of the combustion starts after 8 minutes of the experiment and lasts for about 35 minutes. During this period about 10% of the initial fuel mass i.e., half of the char is converted (see the proximate analysis in chapter 5.1.) and the oxygen concentration rises slowly and almost linear from 10 vol. % to 20 vol. %. A possible reason for that i.e., melted plastics in the bottom of the fuel vessel was already mentioned in 7.2.1. The simulated oxygen concentration equals 0 vol. % until 12 minutes after the ignition and corresponds to the measured one only between the start of the combustion and 8 minutes after the ignition.

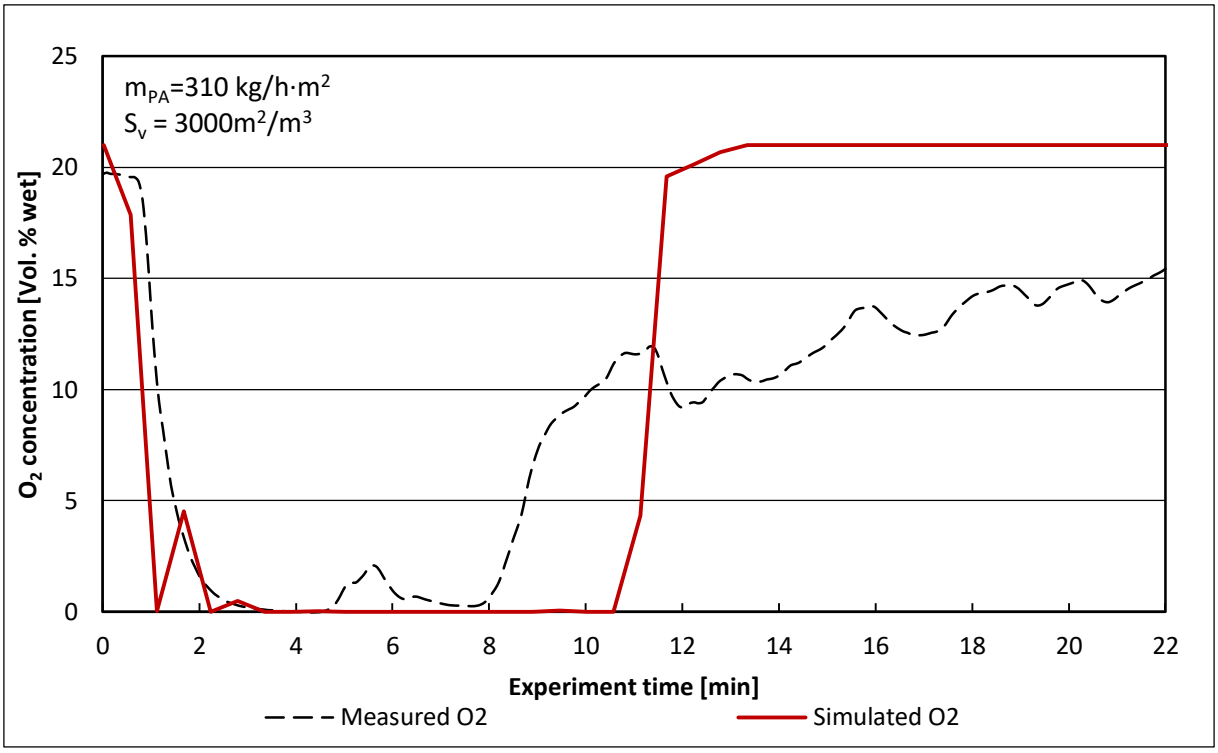

Figure 7.15 – Measured and simulated oxygen concentration above the fuel bed during SBS®1 combustion in the KLEAA reactor

The simulated carbon dioxide concentration above the fuel bed is presented below in Figure 7.16.

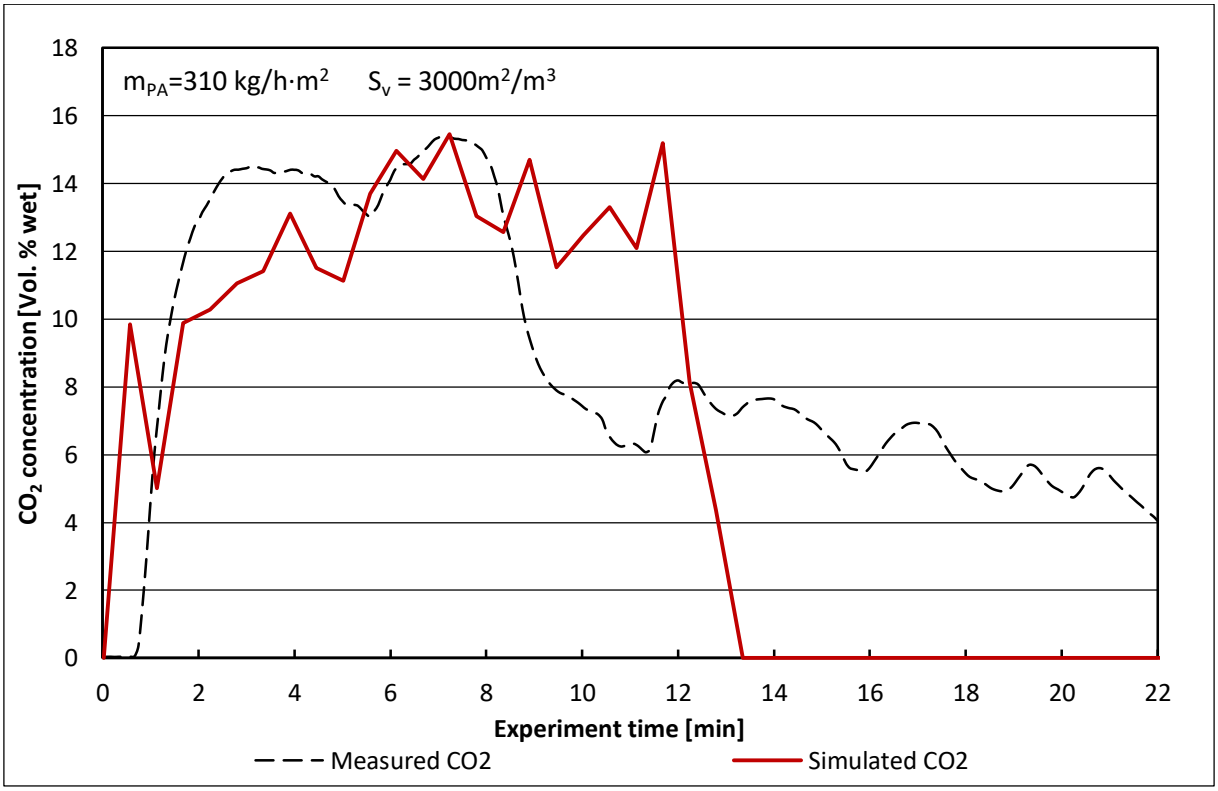

Figure 7.16 – Measured and simulated carbon dioxide concentration above the fuel bed during SBS®1 combustion in the KLEAA reactor

The simulated carbon dioxide above the fuel bed corresponds with the measured one only to a limited extent. Starting from the ignition the CO_2 concentration in the main combustion zone was simulated correctly and equals on average 13 vol. % whereas the measured gas concentration is slightly higher and equals 14 vol. %. The model predicts the end of combustion after roughly 12 minutes from the ignition. In reality, the fuel bed still releases CO_2 after 12 minutes but at a much lower rate as in the main combustion zone. This behaviour is specific to the SBS®1 and was proven to be reproducible in 3 consecutive experiments in the KLEAA reactor. As discussed in section 7.2. such combustion behaviour can be a result of the fire retardants possibly contained in the fuel or melting plastics which enclose fuel particles in the lower (colder) parts of the bed and burn even after the clear main combustion phase.

A similar trend can be observed in case of the simulated CO concentration above the fuel bed (Figure 7.17). The carbon monoxide concentration is almost identical to the one predicted for the combustion of wood chips and equals on average about 17 vol. % over the course of combustion. In reality, the concentration of CO released from the SBS®1 fuel bed in the main combustion zone is ca. 10 vol. % (minute 2 to 5) and 7 vol. % during the char burnout (minute 6 to 8). During the already mentioned, long phase of char glowing almost no carbon monoxide is released.

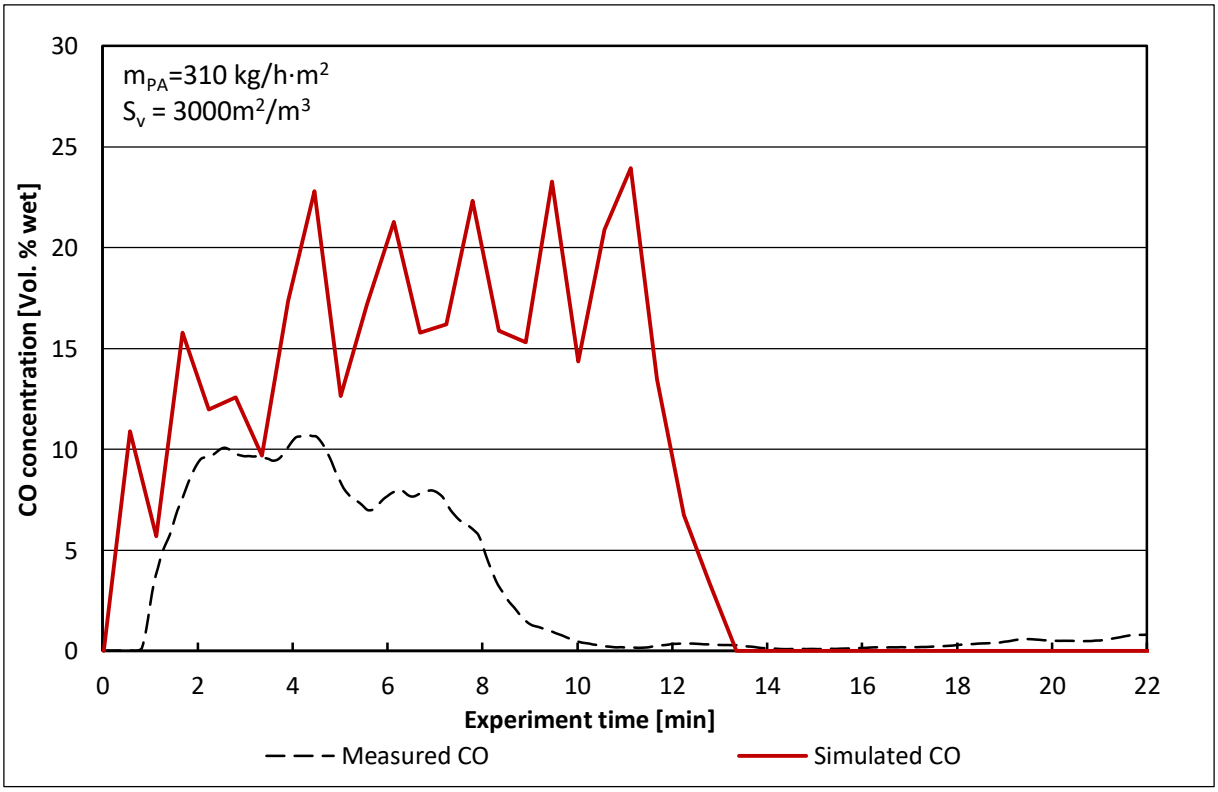

Figure 7.17 – Measured and simulated carbon monoxide concentration above the fuel bed during SBS®1 combustion in the KLEAA reactor

Hydrogen was released during the SBS®1 combustion only in the first 4 minutes of the experiment (Figure 7.18). The concentration did not exceed 1 vol. % with the exception of a slight peak after 4 minutes at the end of the main combustion zone. The model predicted, however, an extensive release of H_2 from the fuel bed. The simulated gas concentration varies strongly between 3 and 27 vol. % from the ignition and until the 11th minute. This behaviour does not correspond with the measured hydrogen concentration.

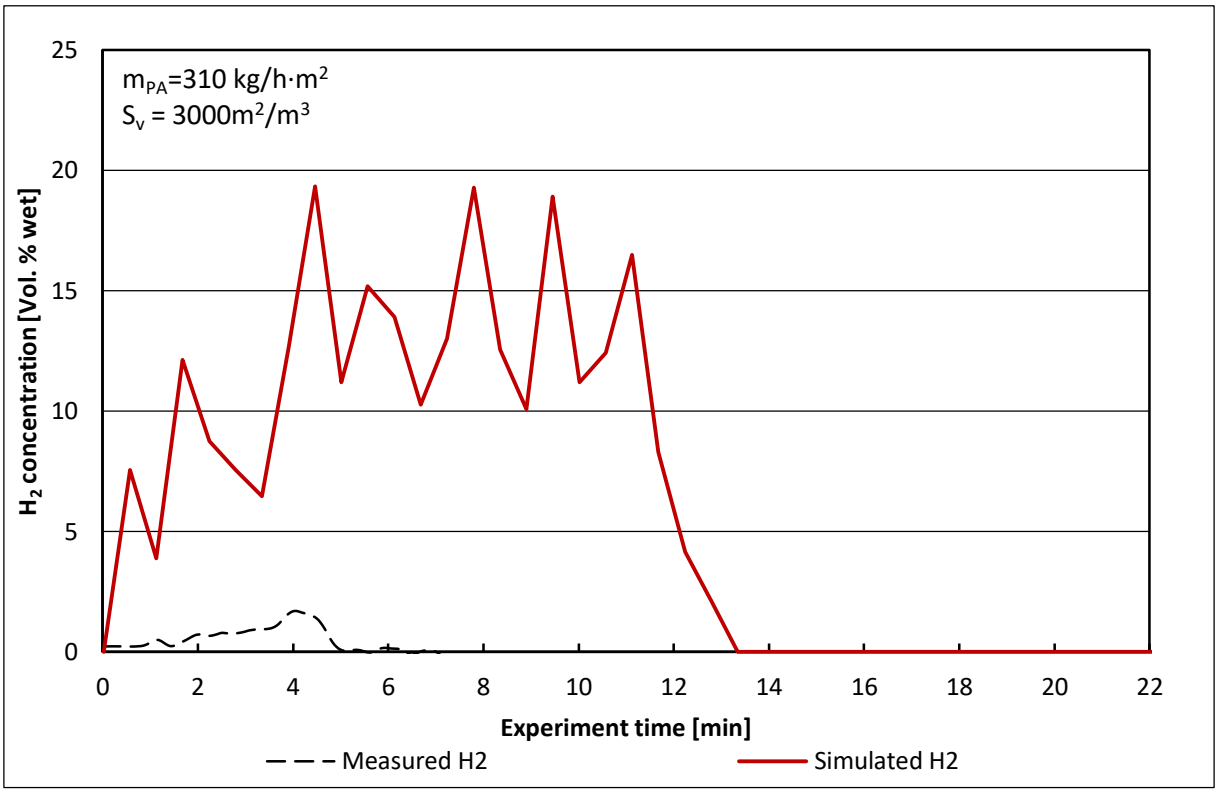

Figure 7.18 – Measured and simulated hydrogen concentration above the fuel bed during SBS®1 combustion in the KLEAA reactor

In contrary to the almost perfectly simulated emission of water vapour from the fuel bed during the wood chips combustion, the predicted H_2O concentration in case of the SBS®1 combustion is much less accurate (Figure 7.19) On the other hand, the measured H_2O emission is quite peculiar in comparison to typical ones observed during biomass combustion. Here the water vapour is released over the course of the whole experiment time, even during the stage initially identified as the char burnout. The simulated H_2O concentration rises rapidly at the beginning of the combustion, reaches a value of about 22 vol. % on average and drops to 0 vol. % after 12 minutes. The actual water vapour concentration reaches its maximum of 14 vol. % after 5 minutes which is ca. 64% of the simulated value i.e., the model predicted too high water concentration above the fuel bed.

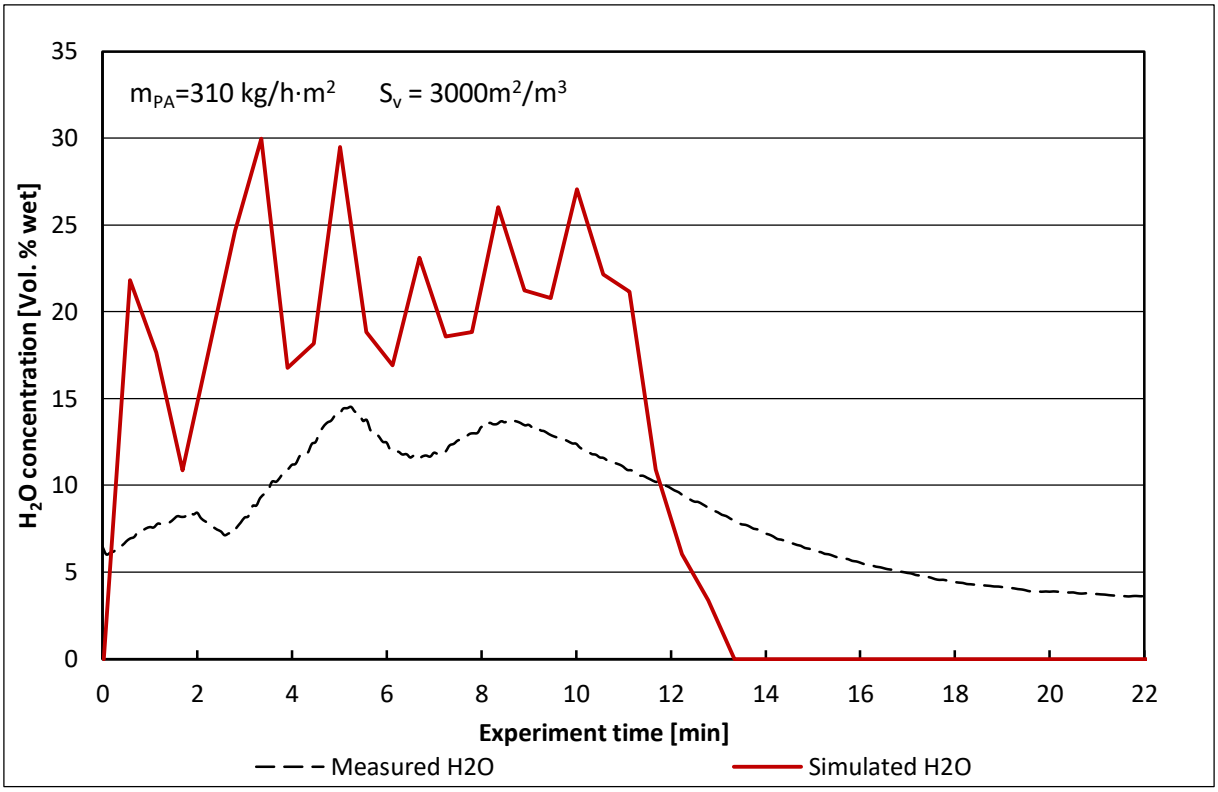

Figure 7.19 – Measured and simulated water vapour concentration above the fuel bed during SBS®1 combustion in the KLEAA reactor

The KLEAA code generates a similar result for the methane release from the fuel during the SBS®1 combustion as during the wood chips combustion. The simulated concentration of CH_4 (Figure 7.20) rises after the ignition to about 4 vol. % and then increases linear reaching its maximum value of ca. 8 vol. % after 11 minutes.

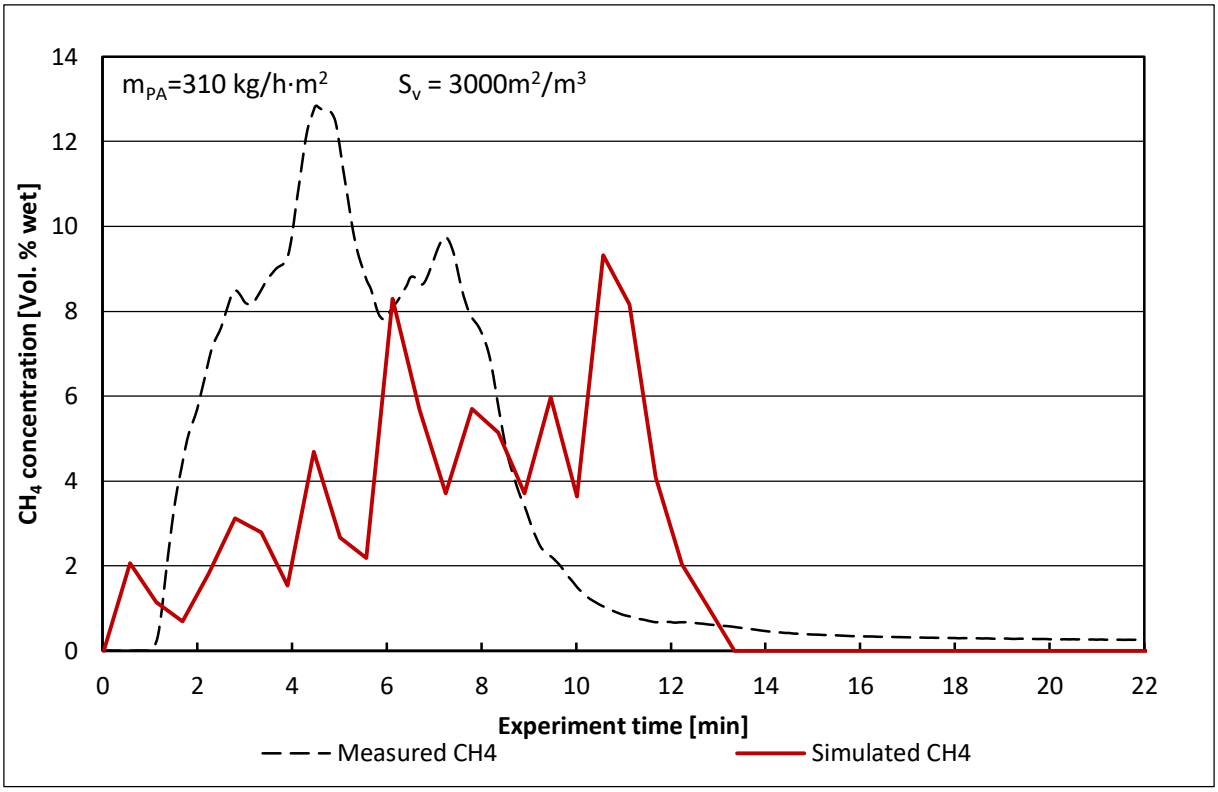

Figure 7.20 – Measured and simulated methane concentration above the fuel bed during SBS®1 combustion in the KLEAA reactor

The measured CH_4 concentration presents, however, a different behaviour. It rises in the main combustion zone to about 13 vol. % at 4.5 minutes and drops forming another peak of 9.5 vol. % after 7 minutes. This second peak occurs in the stage of combustion which was at first identified as char burnout.

The combustion behaviour of SBS®1 differs from the combustion of pure biomass significantly and it cannot be easily distinguished where the main combustion ends and the char burnout starts. The methane concentration above the fuel bed with its peak around 8 minutes after the ignition excludes the possibility of occurrence of a pure char burn out at that time. It can be concluded that the main combustion zone and the char burnout overlap each other. Similar behaviour was observed in case of a very wet biomass and BIOBS which is also very humid. The reason why the main combustion zone and the char burnout take place at the same time during combustion of these fuels is the humidity which permits a rapid ignition rate which is only marginally higher than the mass conversion rate and the fuel burns only in a thin layer of the fuel bed. This combined with the abundance of oxygen from the primary air allows simultaneous release of volatiles, their immediate combustion, and the char burnout. SBS®1 is on the other hand relatively dry and the lack of the clear char burnout zone cannot be explained by the humidity of the fuel. A possible reason can be the already mentioned melting of the plastics which enclose fuel particles, solidify and hinder the release of the volatiles from the

insides of these particles. Another explanation can be the complexity of the fuel composition. It contains not only woody biomass and polyethylene as it was suggested for the model description, but also different kinds of biomasses (of vegetable and animal origin) and plastics. Furthermore, these components are contained in particles very different from each other in shape and size. The pyrolysis of larger particles of hard, smooth plastics will take a longer time than the pyrolysis of more porous biomass particles. In the effect, these large plastic pieces will fall down to the bottom of the fuel vessel where they will combust together with the remaining char. This theory can be supported by a low but noticeable concentration of methane observed above the fuel bed during the whole combustion process. Furthermore, several hotspots during the char burnout were registered by the camera. Flames coming out of these hotspots indicate that the volatiles are still released from the fuel bed even during this last stage of combustion (see Figure 5.8 in chapter 5.2.3).

The issues discussed above render a mathematical description of the thermal decomposition of solid recovered fuels in terms of the rate of pyrolysis and the composition of its products a very challenging if not impossible task. Although the KLEAA Code was proven to simulate the combustion of wood chips rather precisely it was unable to accurately simulate the combustion of SBS®1 due to a simplified approach to the physical, chemical and mathematical description of this fuel. The method of measuring the specific surface area of the fuel particles developed in the framework of this study is suitable only for a rough estimation. It is also important to realise that each component of the fuel can have a different average particle size. In order to measure their specific surface area, it is necessary to sort each of these components out and measure them separately. Then, every single one should be described in the model in terms of the surface area and the reaction kinetics. It is possible to set in the KLEAA Code only one average specific surface area for all particles. It might be therefore difficult to accurately simulate the combustion of solid recovered fuels with the current version of the KLEAA Code.

7.2.3. Temperatures in the fuel bed

The measured temperatures in the fuel bed oscillate between 600^{o}C and 650^{o}C in the main combustion zone (Figure 7.21). The char burnout starts after about 5 minutes which results with the temperature of 1000^{o}C measured at the thermocouples T11 and T13. The KLEAA Code simulated the temperatures in the main combustion zone reaching 900^{o}C which is roughly 300^{o}C too high, analogously to the case of the wood chips. The char burnout predicted by the model starts after about 9 minutes after the ignition which is 4 minutes too late in comparison to the experiment. A possible cause was discussed in chapter 7.2.2.

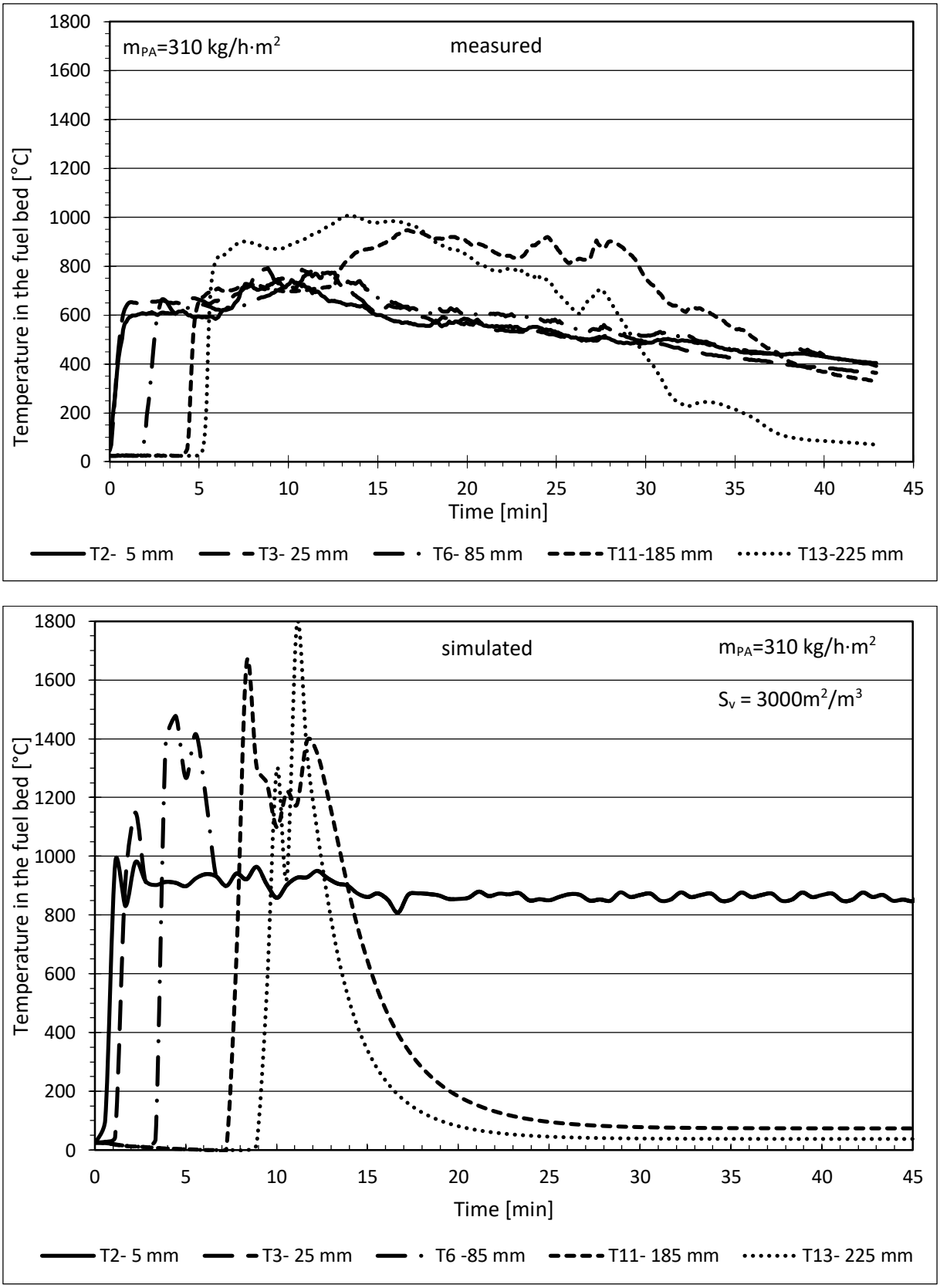

Figure 7.21 – Measured (above) and simulated (below) temperatures in the fuel bed during the combustion of SBS®1 chips in the KLEAA reactor

Simulated temperatures at the thermocouples T2, T3 and T6 register 900^{o}C over the course of the whole combustion process (Figure 7.21). A possible explanation was discussed in the chapter 7.1.3; the temperatures simulated by the KLEAA Code are temperatures of the solid particles which do not fall down as in reality, but stay at their original position and are heated up by the most upper layer whose temperature was set to 900^{o}C.

7.3. Simulation of the wood chips combustion on the moving grate

In the following chapter, the KLEAA Code will be validated for the combustion of wood chips in the pilot plant TAMARA. Only the simulation of the combustion of wood chips with the specific surface area of 2000m²/m³ will be performed as this value was proven in 7.1. to provide the best results for the KLEAA reactor. Two parameters have to be investigated with special attention while validating the model for combustion in TAMARA. Firstly the primary air flows in all primary air zones and secondly the fuel bed velocity on the grate, as they are the key parameters while transferring the results from the fixed to the moving bed. The simulation settings are presented below:

Table 7.5 – Simulation settings for combustion of wood chips in TAMARA

*wood as a mixture of cellulose, hemicellulose, and lignin (see model description in chapter 6)

Property	Symbol	Unit	Settings for Wood chips
Bulk density	ρ_{bulk}	kg/m^3	170
Solid density	ρ_s	kg/m^3	550
Fuel mass flow	$\dot{m}_{fuel}$	kg/h	120
Dry and ash free wood mass fraction*	C_{wood}	kg_{wood}/kg_{fuel}	0.69
Water mass fraction	C_{water}	kg_{water}/kg_{fuel}	0.15
Ash mass fraction	C_{ash}	kg_{ash}/kg_{fuel}	0.16
Specific surface area	S_V	m^2/m^3	2000
Total flows of air (primary+leaked) in the grate zones 1-4	$\dot{m}_{PA1}$	kg/h	645
	$\dot{m}_{PA2}$	kg/h	294
	$\dot{m}_{PA3}$	kg/h	384
	$\dot{m}_{PA4}$	kg/h	141
Primary air temperature	ϑ_{PA}	$°C$	15
Furnace temperature	ϑ_{fw}	$°C$	1100
Theoretical residence times in grate zones 1-4	$t_{res,theor1}$	min	6
	$t_{res,theor2}$	min	6
	$t_{res,theor3}$	min	12
	$t_{res,theor4}$	min	12

The residence times presented in the table above are the theoretical values set in the process control system. Research conducted by Peters and Hunsinger (59) has shown that fine wood chips are

pushed forward by the grate bars slower than the coarse fraction and the residence time for the fine particles can be much higher than the theoretical ones set in the process control system. This phenomenon was discussed in chapter 4.3.7 (see Table 4.6). Taking into consideration these findings the actual residence times $t_{res,i}$ and velocities $u_{fb,i}$ of the fuel bed on the grate in each primary air zone i (80cm) were calculated:

$$t_{res,i} = t_{res,theor,i} \cdot \frac{t_{res}}{t_{res,theor}} \qquad \text{Equation 7.13}$$

$$u_{fb,i} = \frac{l_{zone,i}}{t_{res,i}} \qquad \text{Equation 7.14}$$

This resulted in the following velocities of the fuel bed:

Table 7.6 – Calculated fuel bed velocities in each primary air zone

Primary air zone	$t_{res,i}(d_p)\ [min]$	$u_{fb,i}\ \left[\frac{cm}{min}\right]$
1	20	4
2	20	4
3	41	2
4	41	2

The simulation results are discussed in the following chapter.

7.3.1. Mass conversion

The diagram below shows the simulation results compared to the experimental results:

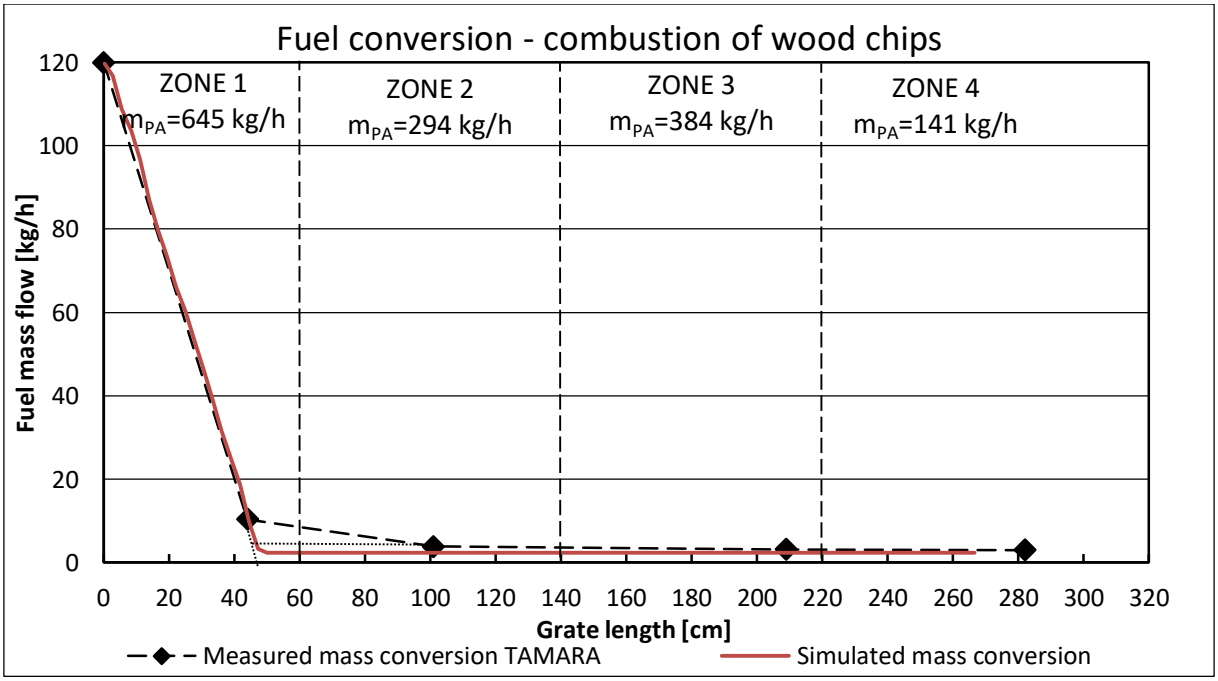

Figure 7.22 – Fuel conversion during wood chips combustion in the TAMARA plant compared to the simulation results

It has been proven that the simulation of wood chips combustion in the TAMARA facility generates very good results when the fuel bed velocity is set to 4 and 2 cm/min as presented in Table 7.6.

7.3.2. Gas concentrations above the grate

Simulated and measured local oxygen concentration above the grate is presented below. The dashed line between the gas sampling points (black diamonds) is only tentative.

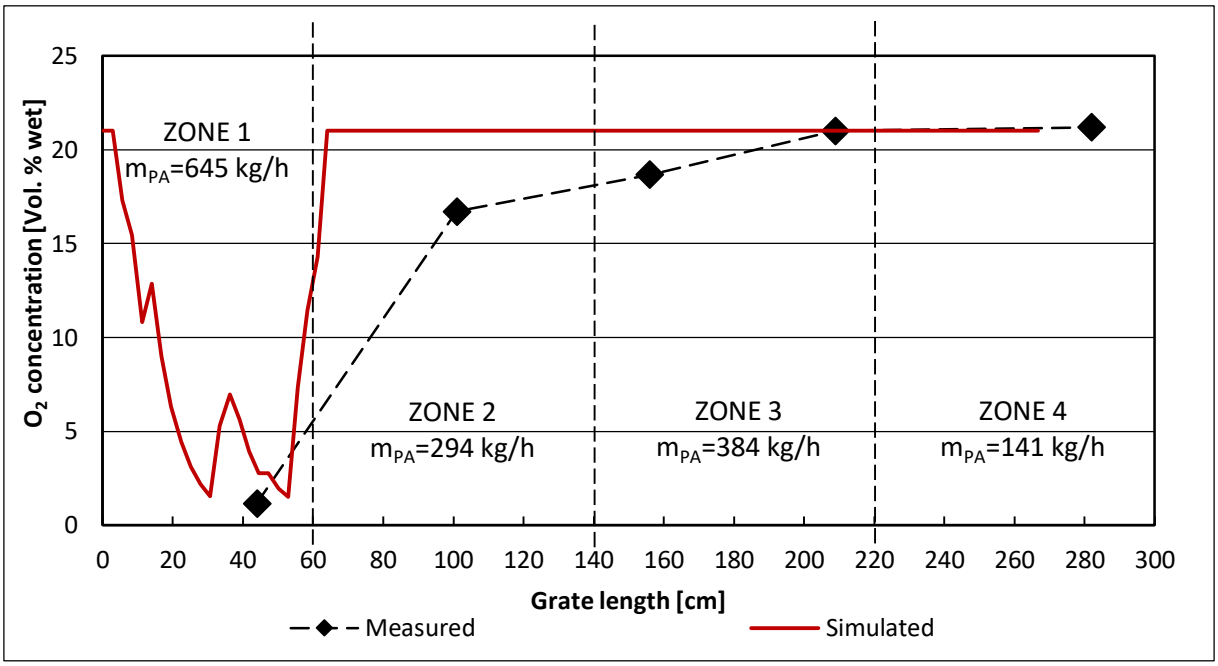

Figure 7.23 – Oxygen concentration above the grate during wood chips combustion in the TAMARA plant

It can be concluded from the measurement that the combustion takes place in the first primary air zone. The volumetric (wet) oxygen concentration in the first sampling point (44 cm on the grate) is 1% and it is anticipated that the main combustion zone occurs between 15 cm and 45 cm of the grate, where there was no sampling point. The simulated value corresponds quite well with the measured one and equals on average 3.5% between 20 cm and 40 cm. The simulation result in this situation can give some indication on the process in the grate area where no gas concentrations have been measured. The simulated oxygen concentration rises rapidly after 50 cm and reaches 21 vol. % meaning the end of the combustion process. The measured value rises slower, what can indicate that the actual combustion within the bed takes place to some extent up to 1 meter on the grate, where the volumetric oxygen concentration is 16.7%. It has to be kept in mind that the gas sampling was performed about 30 cm above the fuel bed, where the measured oxygen concentration can be higher than the concentration directly on the surface of the fuel bed due to the gas mixing in the furnace. The reason for such behaviour may be the flow of the oxygen-rich gas from the third and fourth grate zone backwards to the second and the first grate zone increasing the measured oxygen concentration in the gas above the grate. A similar effect can be observed in case of the carbon

dioxide concentrations above the grate presented in Figure 7.24. The results of the measurements and of the simulation are very consistent with each other at the first sampling point. CO_2 concentrations at sampling points 2 (101cm) and 3 (156cm) lie between 2 and 3 vol. %, whereas the simulated values in these points equal 0 vol. % indicating lack of the combustion in this grate area.

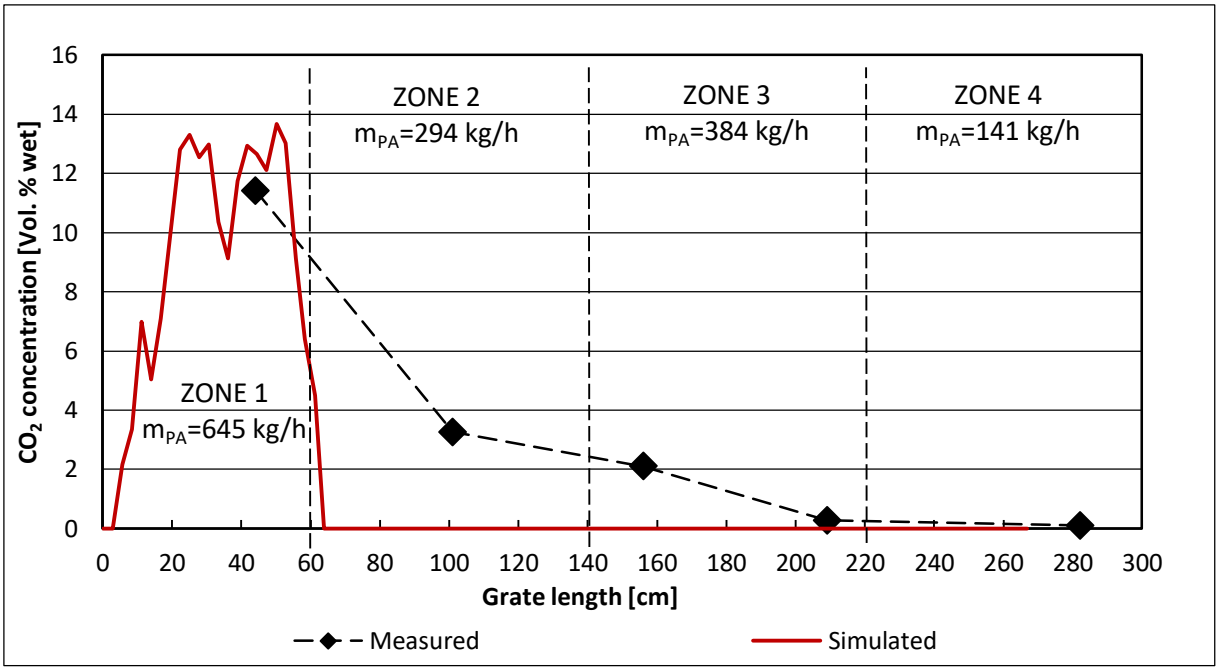

Figure 7.24 – Carbon dioxide concentration above the grate during wood chips combustion in the TAMARA plant

Good simulation results can be seen for the release of the carbon monoxide from the fuel bed. The CO concentration simulated by the KLEAA Code is on average 7 vol. % and equals the value measured at the sampling point 44 cm deep on the grate as presented in Figure 7.25. The experimental results are not available for the grate region between the fuel hopper and the first sampling point. It can be however expected that the simulated CO concentration is about 4% higher than the actual one in this grate area, similar as it was for the simulation of the wood chips combustion in the KLEAA reactor (Figure 7.5). Possible reasons for such result have been already discussed in chapter 7.1.2.

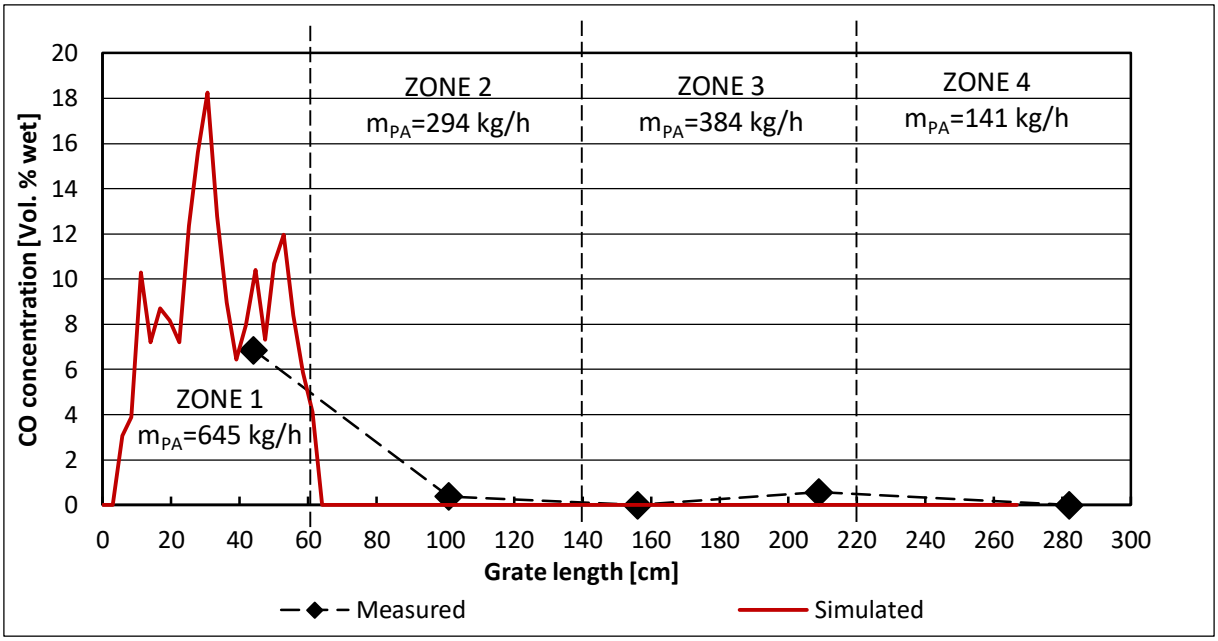

Figure 7.25 – Carbon monoxide concentration above the grate during wood chips combustion in the TAMARA plant

The figure 7.26 below presents the comparison of the simulated and measured hydrogen concentration above the grate. Similar to the simulation results for the KLEAA reactor, the hydrogen concentration is over the double the measured one at the first gas sampling point at 44 cm and equals about 5 volumetric %. The simulated hydrogen concentration in the rest of the grate length is consistent with the measurements and equals 0 volumetric %.

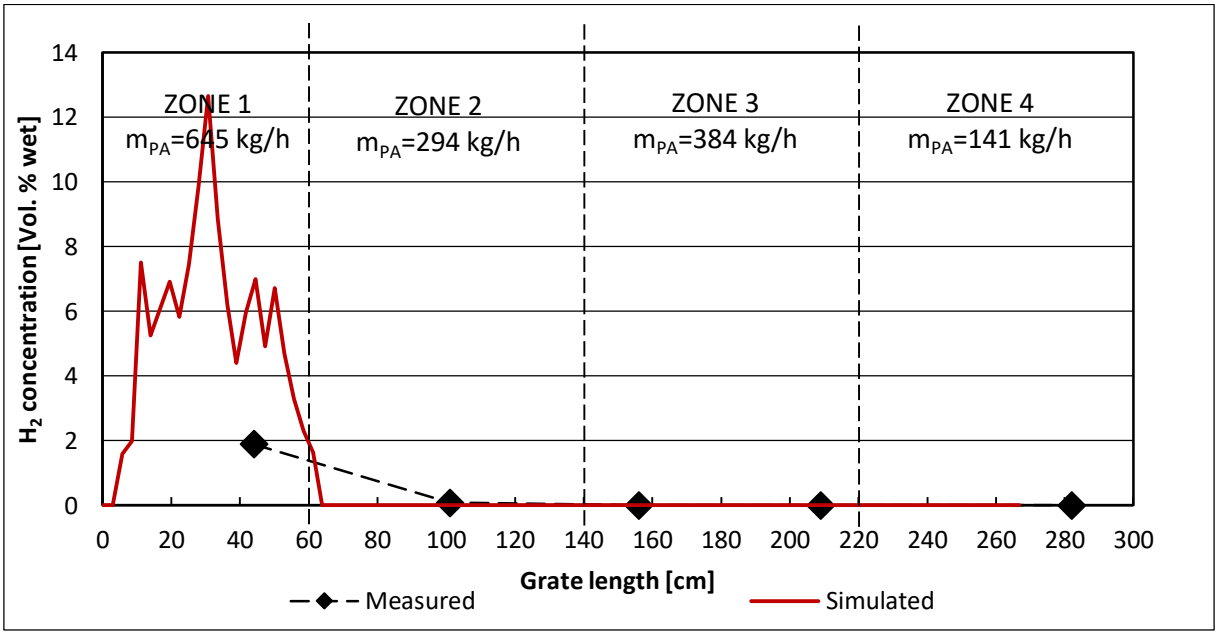

Figure 7.26 – Hydrogen concentration above the grate during wood chips combustion in the TAMARA plant

The simulated water concentration presented below is characterised by a significant noise, although it corresponds very well with the water concentration measured at the sampling point 1.

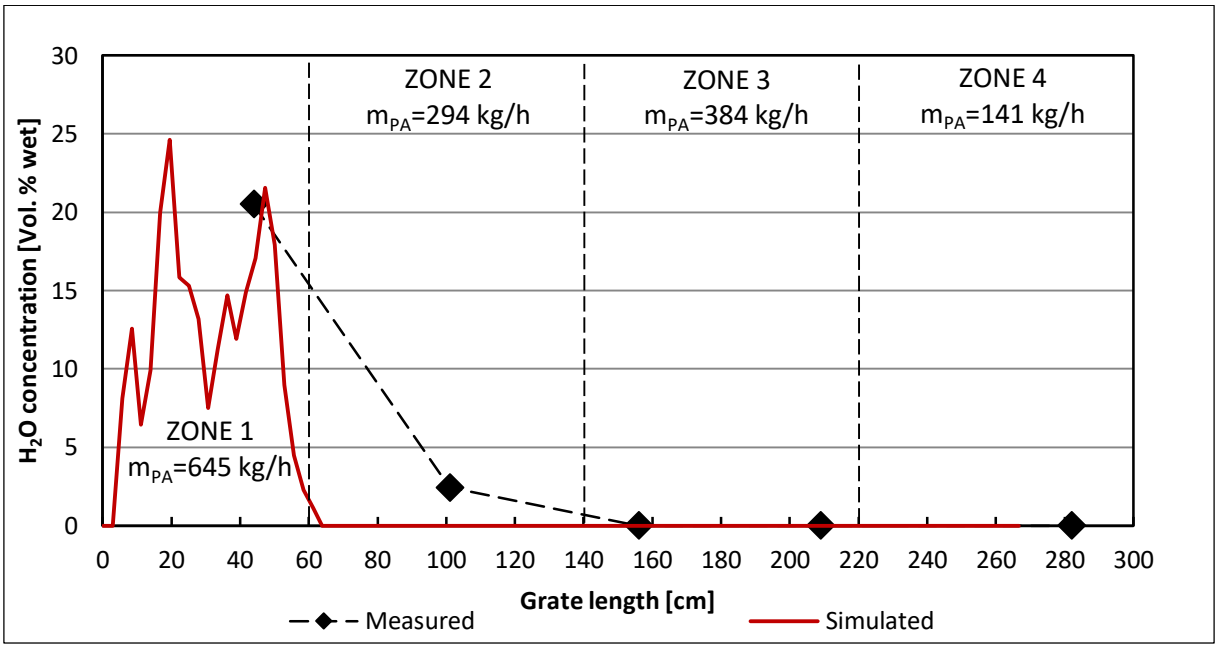

Figure 7.27 – Water concentration above the grate during wood chips combustion in the TAMARA plant

The concentration of methane (Figure 7.28) can be compared only at the first sampling point, similar as it was done for the previous gas concentrations:

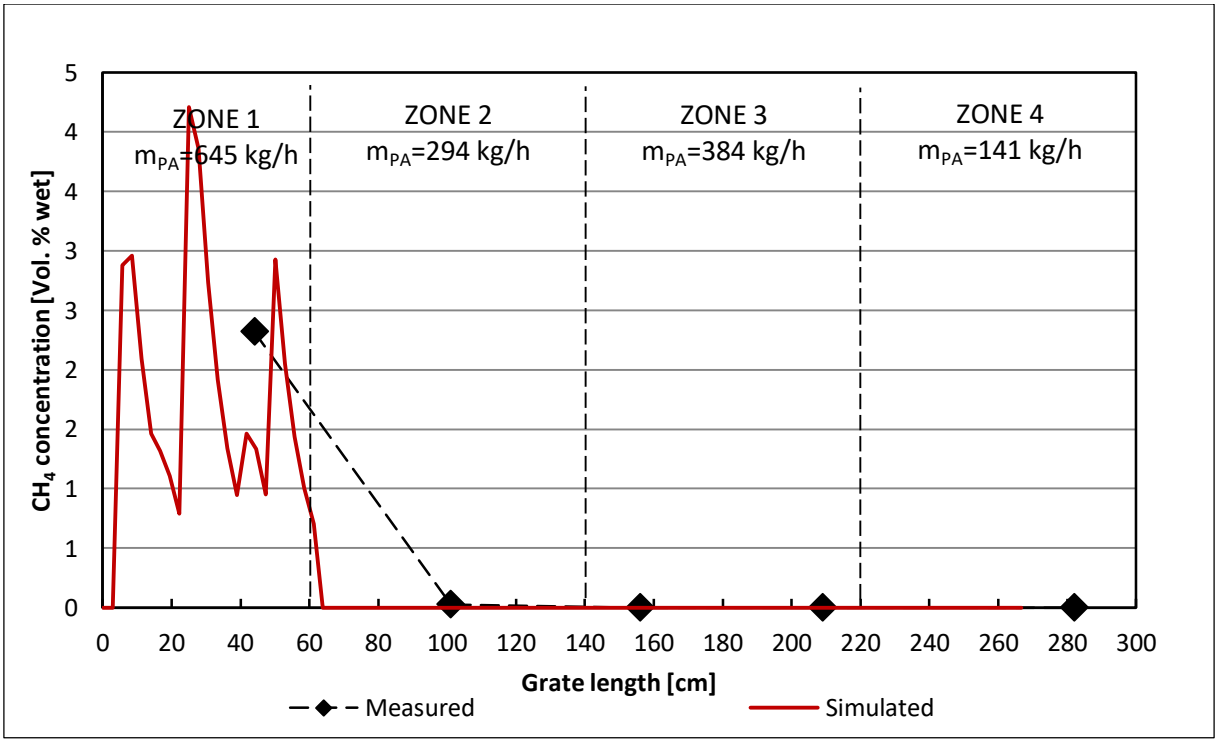

Figure 7.28 – Methane concentration above the grate during wood chips combustion in the TAMARA plant

Studying the diagram above and all the previous diagrams presenting the gas concentrations above the fuel bed leads to a conclusion that the measurements performed at the TAMARA pilot facility are suited for the model validation only to a limited degree. The first sampling point lies in case of the wood chips in the grate area where the combustion is almost completed. The KLEAA Code reproduces, however, all gas concentrations between the fuel hopper and this point as a continuous signal. These gas concentrations should be measured every several centimetres for a better model validation. Alternatively, the leaked air flows should be avoided to assure longer burnout extending to the whole grate length and reaching the ash discharge. Both options were impossible to realise in the TAMARA facility. Therefore the comparison of the gas concentrations in only one point (44cm) provides a limited validation of the model. Regardless of this inconvenience, the mass conversion rate was simulated reasonably well.

7.3.3. Temperature in fuel bed on the grate

Temperature of the fuel bed (solid) was measured with several thermocouples attached to the grate bars and pointing up about 70mm into the fuel bed. Temperature measured in this manner has its maximum of 900^{o}C in the first grate zone. This does not correspond with the simulated temperature in this grate area (see Figure 7.29) which equals 1400^{o}C in this point (60cm). This difference can be once again attributed to the heat losses through the furnace walls, a phenomenon not modelled in the KLEAA Code (see also 7.1.3).

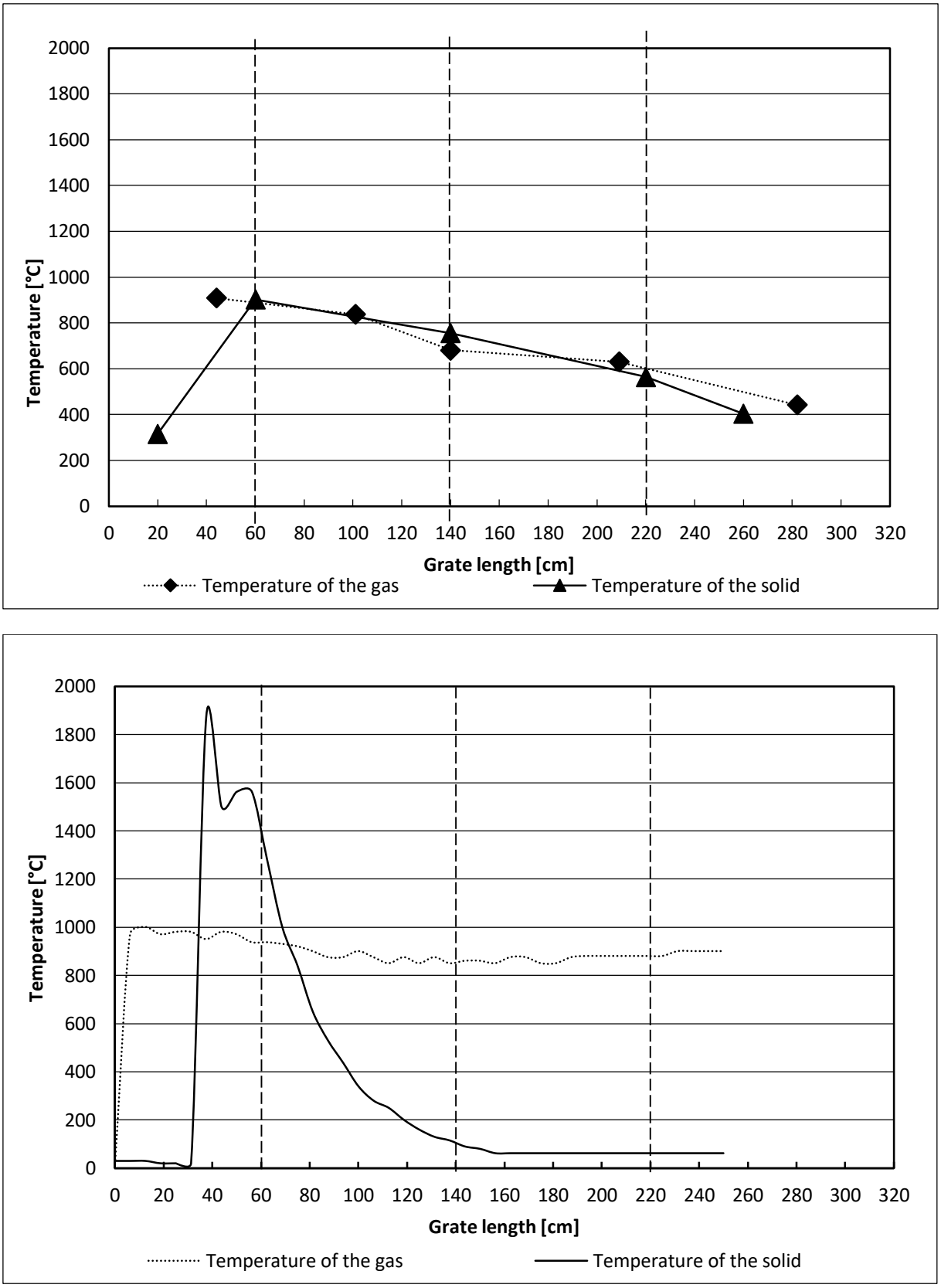

Figure 7.29 – Measured (above) and simulated (below) temperature in the grate during the wood chips combustion in the TAMARA facility

In reality, the temperature gradually decreases along the grate and reaches ca. 400°C at the end. This is caused by the fact that the combustion process occurs only in the first primary air zone and the

remaining ash in the next zones is cooled down by the flowing primary air and heated up by the hot furnace walls. This results in roughly the same temperature of the gas and the solid (thin ash layer) in the third and fourth grate zone.

The simulated temperatures present a different behaviour. The furnace wall in the KLEAA Code is kept at the constant temperature of 900^{o}C. In the model, there is no possibility to gradually set a certain profile of the wall temperature along the grate. Furthermore the temperature at the exit of the fuel vessel which should in reality correspond with the gas temperature is affected by the ash particles which according to the model do not fall down onto the grate but stay in their corresponding layer in the cascade and are heated up by the furnace wall to the temperature close to the one set in the simulation (900°C). The heat transfer from this layer to the next one is strongly dependent on the surface of the particles (Equation 6.26) which in this case corresponds with the surface of the ash particles and is strongly limited. The bottom layers are therefore not affected by the radiation from the furnace wall and are cooled down by the primary air coming from the bottom and flowing freely through the fuel/ash layers. This results in the gas temperature above the fuel surface of almost 900^{o}C in the second, third and fourth grate zone. At the same time, the bottom of the ash bed is cooled by the air to the temperature of 25^{o}C (Figure 7.29).

7.4. Simulation of the SBS®1 combustion on the moving grate

In the following chapter, the simulation results for the SBS®1 combustion will be compared to the measurement results. The specific surface area of 3000m²/m³ was proven to provide the best results for the KLEAA reactor in terms of the mass conversion in the main combustion phase and this value will be used for the simulation. Simulation settings are presented below:

Table 7.7 – Simulation settings for combustion of SBS®1 in TAMARA

Property	Symbol	Unit	Settings for SBS®1
Bulk density	ρ_{bulk}	kg/m^3	160
Solid density	ρ_s	kg/m^3	720
Fuel mass flow	$\dot{m}_{fuel}$	kg/h	105
Wood mass fraction	C_{wood}	kg_{wood}/kg_{fuel}	0.52
Water mass fraction	C_{water}	kg_{water}/kg_{fuel}	0.20
PE mass fraction	C_{PE}	kg_{PE}/kg_{fuel}	0.20
Ash mass fraction	C_{ash}	kg_{ash}/kg_{fuel}	0.08
Specific surface area	S_V	m^2/m^3	3000
Total flows of air (primary and leaked) in the grate zones 1-4	$\dot{m}_{PA1}$	kg/h	492
	$\dot{m}_{PA2}$	kg/h	171
	$\dot{m}_{PA3}$	kg/h	386
	$\dot{m}_{PA4}$	kg/h	145
Primary air temperature	ϑ_{PA}	$°C$	15
Furnace temperature	ϑ_{fw}	$°C$	1000
Theoretical residence times in grate zones 1-4	$t_{res,theor1}$	min	6
	$t_{res,theor2}$	min	6
	$t_{res,theor3}$	min	12
	$t_{res,theor4}$	min	12

The effective fuel bed velocity was determined in accordance with the findings of Peters and Hunsinger (59) similar as for the wood chips (Equation 7.14). The mean fuel bed velocity equals 3 cm/min for the mean fuel particle size of 6.7mm (Table 4.6).

7.4.1. Mass conversion and the oxygen concentration above the grate

The simulation performed with the fuel bed velocity calculated in the previous section generates the following result:

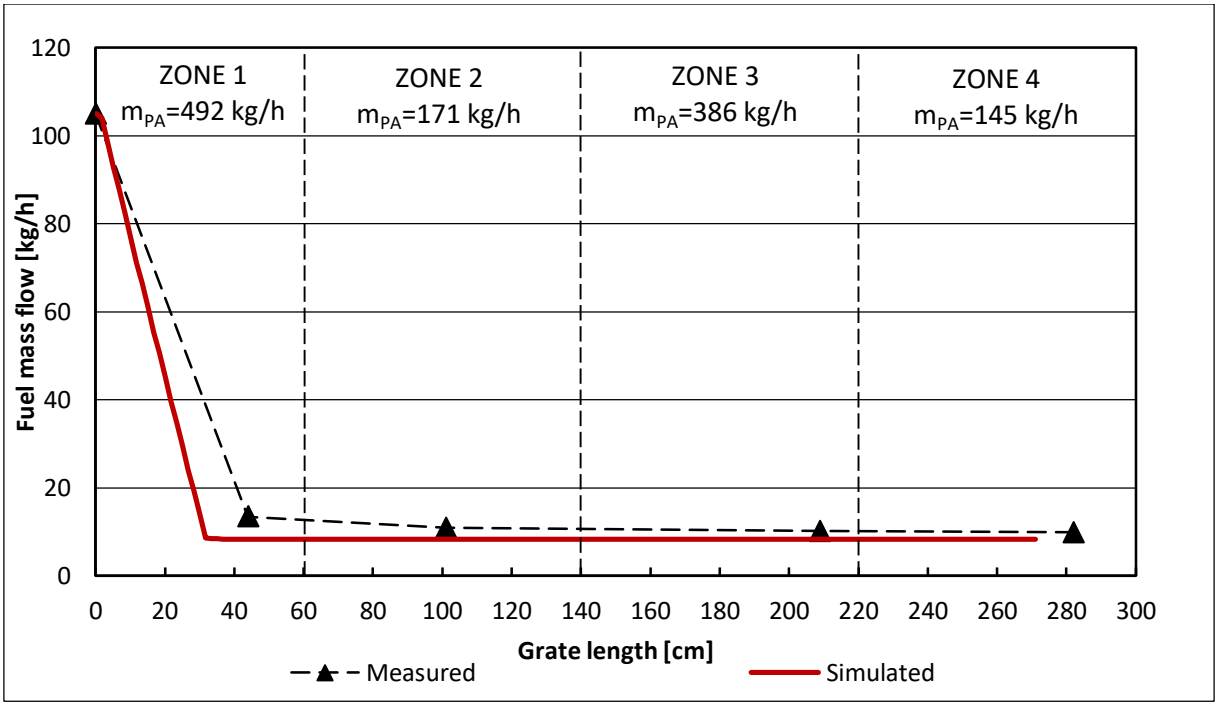

Figure 7.30 – Measured and simulated mass conversion during SBS®1 combustion in the TAMARA facility

The simulated fuel conversion is completed roughly 15 cm before the measured one. It is a good result considering the inaccuracy of the estimation of the specific surface area. This means that the simulated gas concentrations are located within the first 30 cm of the grate in front of the first gas sampling point as shown in the example below (Figure 7.31) and the KLEAA Code can be validated for the combustion of the SBS®1 to a very limited extent i.e., only the mass conversions can be compared.

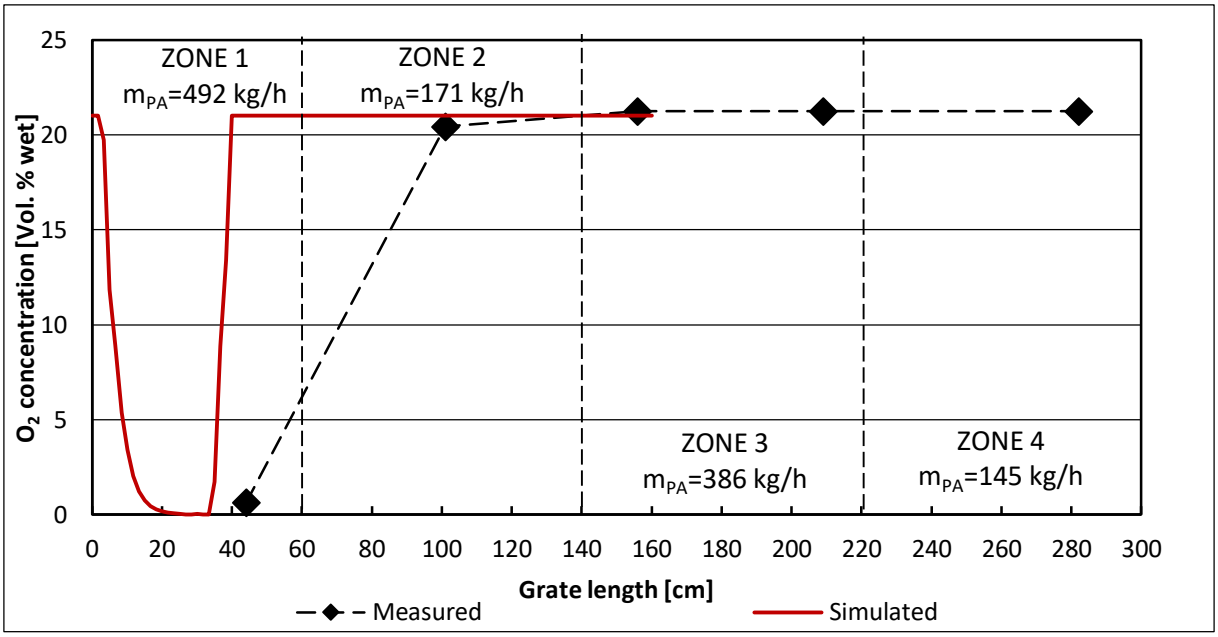

Figure 7.31 – Oxygen concentration above the grate during SBS®1 combustion in the TAMARA facility

8. Summary

The first goal of this study was to investigate and describe the combustion behaviour of one biomass i.e., of the wood chips and of two solid recovered fuels (left side of Figure 8.1 below) experimentally. This work was carried out as a part of the of the work within the EU project RECOMBIO. The primary motivation was to improve the production process of one fuel, i.e., of the BIOBS, for which a well-described combustion was necessary. The fuels were therefore described chemically and physically (chapter 4.2.2 and chapter 5.1), combusted and characterised in the KLEAA reactor equipped with a fixed grate (chapter 5.2) and in the TAMARA pilot scale forward acting grate (chapter 5.3). The second goal, the numerical investigation was realised with a mathematical model KLEAA Code (chapter 6). In order to make a simulation of the combustion of the experimentally investigated technical fuels possible the model was improved (chapter 6.1. and 6.5) and a new measuring method was developed (chapter 4.2.2.1 and 4.2.2.2) for the estimation of the solid density of the fuel and of the specific surface area of their particles.

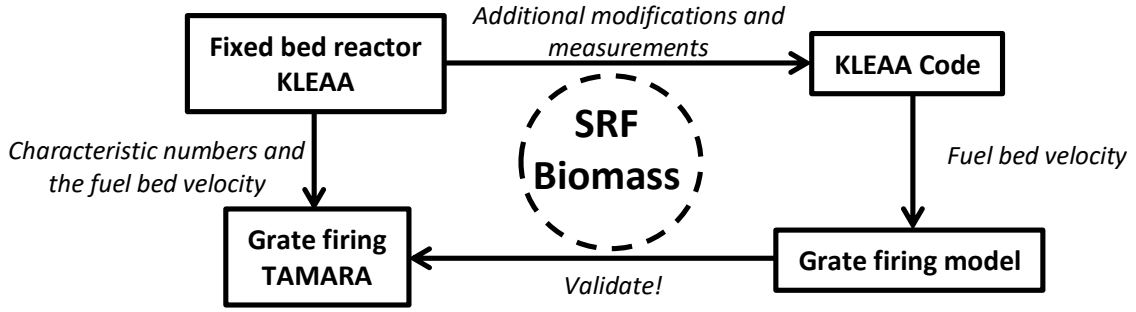

Figure 8.1 – Schematic representation of the tasks carried out in this study

The experimental objective was achieved using the three-step characterisation method developed at the Institute of Technical Chemistry at KIT. The first step, the chemical description of the fuel i.e., the elementary and proximate analysis together with the determination of the lower calorific value was reinforced with the sieving analysis and sorting analysis. Furthermore, an estimation of the solid density of the fuel and of the specific surface area of their particles was performed using a new method suggested and tested in this thesis.

The sieving analysis was relevant for the estimation of the effective fuel bed velocity which is a function of the particle size. The fuel bed velocity is a key factor while transferring the results from the fixed grate onto the moving grate. This transfer is largely dependent on the method used to determine the mean residence times on the grate (chapter 4.3.7). It was assumed that the fuels consist of monodisperse particles and all of them are being pushed by the grate bars towards the ash discharge with the same velocity – the effective fuel bed velocity. This assumption was made in

accordance with the KLEAA Code in which all fuel particles are assumed to have the same size i.e., the mean diameter found in course of the sieving analysis.

It was possible to estimate the amount of plastics in the SBS®1 with the sorting analysis and to suggest its description in the KLEAA Code with respect to the pyrolysis model. For the matter of simplicity, it was assumed in the KLEAA Code that a solid recovered fuel is a mixture of a woody biomass and plastics summarised in the model for pyrolysis as polyethylene, as this material was found to be a dominant plastic in the SBS®1.

The density of the fuel particles and their surface area were necessary to simulate the combustion of the wood chips and the SBS®1 with the KLEAA Code and were measured with a new method proposed in the framework of this study.

The solid density of the fuel particles was measured with a pycnometer built especially for this purpose and using a special powder (Lycopodium spores) instead of the commonly used water or glycerine.

Once the solid densities of the fuels were found they were used to calculate the porosity of a fuel bulk, a value needed for the second method suggested and tested in this study and applied to measure the specific surface area of the fuel particles. Here the pressure drop in the fuel bulk was measured and the surface area was calculated using the equation suggested by Eisfeld and Schnitzlein (67). The results obtained in this study show that the values measured for the particles with a known geometry (spheres, cubes, cuboids) tend to be higher than the actual ones. The best results were obtained for the spheres as they lack sharp edges and tend to build relatively regular bulks in comparison to the cubes and plates. That being said it is recommended to investigate in the future the influence of the specific surface area of a bulk on the pressure drop further for particles with different shapes and sizes, and to experiment with the influence of the flow velocity on the produced results. Ultimately a sufficient database should be created to pinpoint what factors have a negative influence on the quality of the results in order to minimise it.

Estimation of these two parameters was necessary to simulate the combustion of the investigated fuels and to validate the newest version of the KLEAA Code.

The second step in the characterisation concept i.e., combustion in the fixed bed was carried out for all three fuels i.e., for the wood chips, the BIOBS and for the SBS1. In course of the step three, during the measurements at the pilot facility TAMARA it turned out that direct transfer of the results from the step two to step three will be possible only for the BIOBS. The specific primary air flow, a key parameter for the transfer of the results which needs to be the same for the KLEAA reactor and the

TAMARA varied in case of the wood chips and the SBS®1 due to the high amount of the air leaking into the TAMARA facility in the grate area. Transferring the results demanded, therefore, additional combustion tests in the KLEAA reactor for both fuels and with an adjusted primary air flow. This was realised only for the wood chips, as there was no more SBS®1 available. Nevertheless, the transferred mass conversion for the wood chips and the BIOBS has shown that the effective fuel bed velocity on the moving grate of TAMARA was estimated with a good accuracy and that it can be also used in the KLEAA Code for transferring.

The KLEAA Code was improved allowing the fuel density, surface area of the particles and the content of polyethylene in the fuel to be set in the simulations. Furthermore, the model is now able to simulate the combustion on a moving grate. This was achieved by adding an air staging separately for every grate zone and the possibility to input the effective fuel bed velocity in the simulations.

At this point all parameters for the KLEAA Code which had to be measured were known, the model was improved and the results necessary to validate it for the simulations of technical fuels were obtained. The validation of the model for fixed and moving beds was the second goal of this study. The simulations were however performed only for the wood chips and the SBS®1 as the production of BIOBS was discontinued after the test runs in the TAMARA facility and before the method of measuring the raw solid density and the specific surface area were developed.

The simulated combustion behaviour was compared to the measurements with a good result for the wood chips fired in the KLEAA reactor (chapter 7.1). The model was able to predict the mass conversion in the main combustion zone correctly but the char burnout phase was too short. The concentrations of O_2, CO_2 and H_2O were simulated with a good accuracy. The simulated carbon monoxide and hydrogen concentrations above the fuel bed were however too high and the concentration of methane was too low in comparison to the measured ones. There are two reactions in the model which might be responsible for this result if they occur too fast (e.g., when the calculated fuel bed temperature is too high) i.e., the gasification of the fixed carbon with water vapour and the gasification of methane with oxygen. Modifying the energy conservation equations in the model and including the heat losses through the thermal insulation of the fuel vessel, which according to the estimation in chapter 7.1.3 can reach about 36%, could improve the results. Two additional simulations of the combustion of wood chips in the fixed bed with heat sinks of 15% and 30% were therefore performed. The effect of the heat loss on the bed temperature was in the first case minimal but the ignition velocity was reduced, which was unwanted but expected. The heat sink of 30% could reduce the temperature close to the measured one, but the ignition front velocity was further reduced. This proves that incorporating the heat loss into the KLEAA Code is not sufficient to improve the simulation results during the char burnout phase. A possible reason for the inaccuracy of

the simulation during the char burnout might be also the fact that the solid mass transfer is not considered in the KLEAA Code. The char particles forming in the fuel bed fall down in reality and accumulate in the lower parts of the fuel vessel. This means that there is more reacting material on the bottom of the fuel vessel during the char burnout in reality than in the modelled fuel bed.

The tendencies observed in the simulation results for the combustion of wood chips on the fixed grate repeat themselves in the combustion behaviour on the moving grate TAMARA. The mass conversion was simulated with a good accuracy, so were also the CO_2, O_2 and H_2O concentration above the grate. The temperatures in the grate were however much lower than the simulated ones due to the heat losses in the furnace. The fact that these losses are not considered in the model and the simulated temperatures are higher might be also the reason for the inconsistencies in the concentrations of methane and carbon monoxide, similar as it was in case of the simulation for the KLEAA reactor.

Simulation of the combustion of solid recovered fuels is due to their chemical and physical complexity a very difficult task. It was attempted in this study to mathematically describe such fuels using as an example the SBS®1, a fuel produced by REMONDIS Rheinland GmbH and characterised by a high quality i.e., a very homogeneous (for a solid recovered fuel) composition and a low chlorine content. It was suggested to define this fuel as a mixture of biomass (wood) and polyethylene and incorporate an additional reaction, thermal decomposition of this plastic into the model of pyrolysis in the KLEAA Code. The specific surface of the fuel particles was measured with the same method as for the wood chips. The combustion behaviour of the SBS®1 defined in this simplified way was not simulated correctly. The measured mass conversion, temperatures and gas concentrations did not allow to identify a visible char burnout zone. The reason can be an effect observed during combustion tests with other fuels rich in plastics. During these experiments in the KLEAA reactor the plastics on the top of the fuel bed melt at the beginning of the combustion. Part of them is pyrolyzed but the rest flows downwards the fuel bulk, cools down and solidifies on the fuel particles. In effect, the specific surface area of these particles might be reduced and the fuel in the bottom of the batch reactor can contain an increased amount of plastics in comparison to the original fuel. This phenomenon might impede the char burn out and is impossible to model in the current KLEAA Code.

All things considered, the improved KLEAA code and the methods developed to measure the specific surface area and the solid density of the investigated fuels delivered good results for the combustion of biomass on the fixed and on the moving grate. The model and the methods can be however developed further, which can positively influence the quality of the simulation results. Further improvements of the model were discussed during the model validation:

- Including the heat loss in the energy conservation equations in the model (see chapter 7.1.3.),
- Fine tuning of the kinetics of the gasification of carbon and the decomposition of methane (see chapter 7.1.2.),
- Possibly introducing more steps (reactions) in the pyrolysis model in order to model the thermal decomposition of the biomass and plastics more accurate,
- Further development of the method of measuring the specific surface area of fuel particles (see chapter 4.2.2.) to improve the accuracy,
- Possibly incorporating the transport equations for the solid phase allowing the fuel particles to fall down and to improve the simulation results in the char burnout.

It is recommended to undertake several other steps in order to assure a better model validation and to provide more accurate simulation results for the combustion on the moving grate:

- More accurate estimation of the fuel bed velocity (see chapter 4.3.7.) by performing measurements on the actual fuels that will be simulated,
- Providing a better resolution of the gas concentrations measurements above the moving grate i.e., applying more gas sampling points per grate length.

Measurements carried out in a large scale forward acting grate would most likely provide the best results for these two steps.

These improvements give the KLEAA Code the chance to become a valuable and accurate tool for the investigation of the combustion of a variety of biogenic fuels, for which the solid density and the specific surface area of the particles can be measured with the new methods. Results obtained with the KLEAA Code in the future can be for example used as boundary conditions for CFD simulations of biomass boilers and can reinforce a design process of such units.

References

1. *Bekanntmachung zur Förderung von Untersuchungen zu übergreifenden Fragestellungen im Rahmen der Gesamtstrategie zum weiteren Ausbau der Erneuerbaren Energien. 2012.* Berlin: Bundesministerium für Umwelt, Naturschutz und Reaktorsicherheit.

2. Glorius T. 2009. RECOMBIO Recovered Fuels combined with Biomass - Collaborative Project proposal.

3. Mätzing H., Gehrmann H.-J., Kolb T., and Seifert H. 2010. Experimental and Theoretical Investigation of Biomass Conversion in a Fixed Bed, San Francisco: International Conference on Thermal Treatment Technologies.

4. Directive 91/689/EEC. 1991. *Council Directive on hazardous waste,* Luxembourg: Office for Official Publications of the European Communities.

5. EN 15359:2011. 2011. *Solid recovered fuels - Specifications and classes,* Brussel: European Committee for Standardisation.

6. EN 13531:2004. 2004. *Packaging – Requirements for packaging recoverable in the form of energy recovery, including specification of minimum inferior calorific value,* Brussel: European Committee for Standardisation.

7. Directive 2000/76/EC. 2000. *Directive of the European Parliament and of the Council on the incineration of waste,* Brussel.

8. Pacyna J. 1987. Atmospheric Emissions of As, Cd, Pb and Hg from High Temperature Processes in Power Generation and Industry, Lilleslrom, Norway: John Wiley & Sons Ltd.

9. Pacyna E., Pacyna J., Steenhuisen F., and Wilson S. 2006. Global anthropogenic mercury emission inventory for 2000, s.l.: ELSEVIER, Vol. Atmospheric Environment 40.

10. Scholz R., Beckmann M., and Schulenburg F. 2001. *Abfallbehandlung in Thermischen Verfahren,* Leipzig: Teubner Verlag.

11. Achternbosch M., Bräutigam K.-R., and Vehlow J. 2002. 13. DVV-Kolloquium Thermische Verfahren der Abfallbehandlung-Entwicklungen, Optimierung, Bewertung. *Transferfaktoren.* Weimar.

12. Archer E., Baddeley A., Klein A., Schwager J., and Whiting K. 2005. Mechanical-Biological-Treatment: A Guide for Decision Makers, Processes, Policies and Markets, s.l.: Juniper Consultancy Services Ltd.

13. Gehrmann H.-J., Maier J., Kipshagen F.-J., Nowak P., Pfrang-Stotz G., Paur H.-R., Seifert H., and Glorius T. 2012. Kraftwerkstechnik. *Mitverbrennung von Solid Recovered Fuels mit hohem biogenen Anteil in Kraftwerken,* Dresden: Verlag Karl Thome-Kozmiensky, vol. 4.

14. Nicholls P. 1934. USBM Report 378. *Underfeed Combustion, Effect of Preheat and Distribution of Ash in Fuel Beds,* Washington: Bureau of Mines.

15. Weintraub M., Orning A., and Schwartz C. 1967. USBM Report 6908. *Experimental Studies of Incineration in a Cylindrical Combustion Chamber,* Washington: Bureau of Mines.

16. Rogers J. E. l., Sarofim A. F., and Howard J. B. 1972. National Incineration Conference. *Effect of Underfire Air Rate on a Burning Simulated Refuse Bed,* New York.

17. Gort R. 1995. *On the Propagation of a Reaction Front in a Packed Bed: Thermal Conversion of Municipal Solid Waste and Biomass,* Twente: University of Twente.

18. Fatehi M., Kaviany M. 1994. Combustion and Flame 99. *Adiabatic Reverse Combustion in a Packed Bed*.

19. Shin D., Choi S. 2000. Combustion and Flame 121. *The combustion of simulated waste particles in a fixed bed,* s.l.: ELSEVIER.

20. Rönnbäck M., Axell M., Gustavsson L., Thunman H., and Lecher B. 2000. Progress in Thermochemical Biomass Conversion. *Combustion Processes in a Biomass Fuel Bed-Experimental Results,* s.l.: Wiley-Blackwell.

21. Yang Y. B., Sharifi V., and Swithenbank J. 2004. Fuel 83. *Effect of air flow rate and fuel moisture on the burning behaviours of biomass and simulated municipal solid wastes in packed beds,* Sheffield (UK): ELSEVIER.

22. Yang Y., Ryu C., Khor A., Sharifi V., and Swithenbank J. 2005. Fuel 84. *Fuel size effect on pinewood combustion in a packed bed,* Sheffield: ELSEVIER.

23. van Kessel L. B. M., Arendsen A. R. J., de Boer-Meulman P. D. M., and Brem G. 2004. Fuel 83. *The effect of air preheating on the combustion of solid fuels on a grate,.* s.l. :ELSEVIER.

24. Schumacher F., Meichelböck H., Merz A., and Vogg H. 1994. GVC-Symposium Abfallwirtschaft Herausforderung und Chance. *Entwicklung und Inbetriebnahme eines Laborofens zum Studium der Verbrennung von Reststoffen auf Rostsystemen,* Würzburg.

25. Bleckwehl S. 2010. Dissertation. *Charakterisierung der verbrennungstechischen Eigenschaften fester Brennstoffe im Festbett,* Stuttgart: Universität Stuttgart.

26. Gehrmann H.-J., Kolb T., Seifert H., Mark F. E., Frankenhaeuser M., Aafko S., Wittstock K., and Kolb J. 2010. Environmental Engineering Science. *Synergies Between Biomass and Solid Recovered Fuel in Energy Conversion*.

27. Thome-Kozmiensky K. J. 1985. *Verbrennung von Abfällen,* Berlin: EF-VERLAG für Energie- und Umwelttechnik GmbH.

28. *RECYCLING Almanach. 2009.* s.l.: Reed Business Information.

29. Schroer C., Konys J. 2002. *Rauchgasseitige Hochtemperatur-Korrosion in Müllverbrennungsanlagen,* Karlsruhe: Forschungszentrum Karlsruhe GmbH.

30. Löwenstein R. 1934. Wärme. *Verbrennungsverlauf von Steinkohle an einer Wanderrostfeuerung,* vol. 57.

31. Schulte F., Tanner E. 1933. Zeitschrift VDI. *Stand un Entwicklung der Feuerungstechnik*.

32. Werkmeister H. 1932. Dissertation. *Versuche über den Verbrennungsverlauf bei Steinkohlen mittlerer Kerngrößen,* Hannover: Technische Hochschule Hannover, 1932.

33. Beckmann M. 1995. *Mathematische Modellierung und Versuche zur Prozessführung bei der Verbrennung und Vergasung in Rostsystemen.* Clausthal-Zellerfeld: CUTEC-Institut GmbH.

34. Beckmann M., Scholz R. 2000. 5th European Conference on Industrial Furnaces and Boilers. *Residence Time Behaviour of Solid Material in Grate Systems,* Porto.

35. Thunmann H., Leckner B. 2000. Fuel Vol. 80. *Ignition and Propagation of a Reaction Front in a Cross-Current Bed Combustion of Wet Fuels*.

36. Żelkowski J. 2004. *Kohlecharakterisierung und Kohleverbrennung-Kohle als Brennstoff, Physik und Theorie der Kohleverbrennung, Technik,* Essen: VGB PowerTech Service GmbH.

37. Zabetta E., Hotta A., Moulton B., and Hiltunen M. 2009. ELECTRIC POWER 2009. *Biomass and Waste Co-combustion - European Experience,* Rosemont, Illinois.

38. Gehrmann H.-J., Kolb T., Seifert H., Waibel P., Matthes J., and Keller H. 2011. European Biomass Conference and Exhibition - Procedeengs. *Co-Combustion of Low Rank Fuels in Power Plants,* Berlin.

39. Gerhardt A., Maier J., and Glorius T. 2008. *The RECOFUEL-Project - Demonstration of Co-firing of Solid Recovered Fuels in European Lignite Fired Power Plants,* Venice.

40. Gehrmann H.-J., Seifert H., Beckmann M., and Glorius T. 2012. Chemie Ingenieur Technik. *Ersatzbrennstoffe in der Kraftwerkstechnik,* Weinheim: WILEY-VCH Verlag GmbH & Co. KGaA.

41. Schumacher F. 2006. Dissertation. *Untersuchung des Reaktionsfortschritts bei der Festbettverbrennung auf Rostsystemen,* Karlsruhe: Universität Fridericiana Karlsruhe.

42. Raupenstrauch H. 1991. Dissertation. *Ein Beitrag zur Computersimulation reagierender Schüttschichten,* Graz: Technische Universität Graz.

43. Lohf A. 1999. Dissertation. *Modellierung der Chemisch-physikalischem Vorgänge im Müllbett von Rostfeuerungsanlagen.* Darmstadt: Technische Universität Darmstadt.

44. Mätzing H. 2010. *Internal Report: Experimental and Theoretical Investigation of Biomass Conversion in a Fixed Bed*.

45. Levenspiel O. 1999. *Chemical Reaction Engineering,* New York City: John Wiley & Sons.

46. Ranzi E., Cuoci A., Faravelli T., Frassoldati A., Migliavacca G., Pierucci S., and Sommariva S. 2008. Energy & Fuels. *Chemical Kinetics of Biomass Pyrolysis,* Milano, Italy: American Chemical Society.

47. Di Blasi C. 2007. Progress in Energy and Combustion Science 34. *Modelling Chemical and Physical Processes of Wood and Biomass Pyrolysis,* Naples, Italy: ELSEVIER.

48. Gruber T. 1993. Abfallwirtschaftsjournal Nr. 10. *Modell zur Verbrennung auf dem Rost,* Berlin: Thome-Kozmiensky Verlag.

49. Gruber T. 1993. Dissertation. *Vorgänge bei der Verbrennung von Hausmüll auf dem Rost,* Berlin: Technische Universität Berlin.

50. Warnecke R., Reinsdorf T., and Koralewska R. 2002. Fachtagung Thermische Abfalbehandlung. *Modell für die Beschreibung instationären Vorgänge auf Rosten für Abfallverbrennung* Berlin.

51. Yang Y. B., Goh Y. R., Zakaria R., Nasserzadeh V., and Swithenbank J. 2002. Waste Management 22. *Mathematical modelling of MSW incineration on a travelling bed,* Sheffield: PERGAMON.

52. Yang Y. B., Ryu C., Goodfellow J., V. Nasserzadeh Sharifi V., and Swithenbank J. 2004. Process Safety and Environmental Protection 82. *Modelling Waste Combustion in Grate Furnaces,* Sheffield: Institution of Chemical Engineers.

53. Peters B. 1995. 3rd European Conference on Industrial Furnaces and Boilers. *A detailed Model for Devolatilisation ond Combustion of Waste Material in Packed Beds.* Portugal.

54. Krüll F. 2001. Dissertation. *Verfahren zur numerischen Simulation von Müllrostfeuerungen,* Bochum: Ruhr-Universität.

55. Krüll F., Kremer H., and Wirtz S. 1998. VDI Bericht 1390. *Feuerraumsimulation einer Müllverbrennungsanlage bei gleichzeitiger Simulation der Verbrennung auf dem Rost,*Düsseldorf.

56. Jaworski T., Wandrasz J. W. 2000. VDI Berichte 1540. *Mathematische Modellierung des Verbrennungsprozesses in der Abfallschicht auf dem Wanderros des Kessels*.

57. Pättikangas T. J. H., Saastamoinen J. J., Suitinen J., and Kjäldman K. 2000. 5th European Conference on Industrial Furnaces and Boilers. *Numerical Simulations of Grate Firing of Coal,* Porto.

58. Peters B., Krebs L., and Frey M. 1995. VDI Bericht 1193. *Numerische Simulation einer Müllverbrennungsanlage,* Düsseldorf: VDI-Verlag Düsseldorf.

59. Peters B., Dziugys A., Hunsinger H., and Krebs L. 2005. Chemical Engineering Science 60. *An Approach to Qualify the Intensity of Mixing on a Forward Acting Grate*.

60. Brosch B., Wirtz S., and Scherer V. 2011. *A particle based model for combustion of municipal waste in grate firing systems*.

61. Couch G. R. 1988. IEA Coal Research Report IEACR 13. *Lignite Resources and Characteristics* London.

62. Skorupska N. M. 1993. IEA Research Report IEACR 52. *Coal Specifications - Impact on Power Station Performance,* London.

63. Krevelen D. W., Schuyer J. 1957. Coal Science. *Aspects of Coal Constitution.,* s.l.: Elsevier Verlag.

64. VGB-Richtlinie VGB-210. *Charakterisierung von Kraftwerkskohlen* Essen: VGB PowerTech e.V., 2003.

65. Webb P. A. 2001. Volume and Density Determinations for Particle Technologists, s.l.: Micromeritics Instrument Corp.

66. Gnielinski V. 2006. VDI-Wärmeatlas s.l.: Springer-Verlag Berlin Heidelberg New York.

67. Baker M. J. 2011. CFD simulation of flow through packed beds using the finite volume technique s.l.: University of Exeter.

68. Džiugys A. 2006. Granular Matter 8. *Evaluation of the residence time of a moving fuel bed on a forward acting grate* s.l.: Springer-Verlag.

69. Verordnung über das Europäische Abfallverzeichnis. 2001.

70. ISO 17225-1:2014. 2014. Solid biofuels - Fuel specifications and classes.

71. Kröll K., Krischer O. 1950. Die Vorgänge in Trocknungs- und Erwärmungstrommeln, Berlin: Springer-Verlag.

72. Knümann R., Bockhorn H. 1994. Combustion Science and Technology 101.

73. Specht E. 1992. Kinetik der Abbaureaktion, s.l.: Technische Universität Clausthal.

74. Nowak P., Gehrmann H. J., Maier J., Pfrang-Stotz G., Paur H.-R., Seifert H., and Glorius T. 2012. International Journal of Chemical and Environmental Engineering Systems. *Co-firing of solid recovered fuels with Biomass in Grate Firings*.

75. Carslaw H. S, and Jaeger J. C. 2000. Conduction of Heat in Solids, Oxford: Clarendon Press.

76. Kohlgrüber K. 1986. Gaswärme international 35. *Formeln zur Berechnung des Emissionsgrades von CO2- und H2O-Gasstrahlung bei Industrieöfen, Brennkammern und Wärmetauschern*.

77. Hottel H. C., Sarofim A. F. 1967. *Radiative transfer,* New York: McGraw-Hill.

78. Schlünder E. U. 1984. Chemical Engineering and Processing Volume 11, Issue 1. *Heat transfer to packed and stirred beds from the surface of immersed bodies,* s.l.: ELSEVIER.

79. Stephan P. 2006. VDI Wärmeatlas. *Wärmeübertragung Partikel-Fluid in durchströmten Haufwerken,* s.l.: Springer Verlag Berlin Heidelberg New York.

80. Vehlow J., Rittmeyer C., Vogg H., Mark F., and Hayen H. 1994. GVC-Symposium Abfallwirschaft Herausforderung und Chance. *Einfluss von Kunstoffen auf fie Qualität der Resmüllverbrennung,* Würzburg.

81. Lee S.-H., Themelis N. J., and Castaldi M. J. 2006. *High temperature in waste to energy boilers*.

82. Nielsena H. P., Frandsena F. J., Dam-Johansena K., Baxterb L. L. 1999. *The implications of chlorine-associated corrosion on the operation of biomass-fired boilers.* Bd. Progress in Energy and combustion science.

83. Krause H. H., Vaughan D. A., and Boyd W.K. 1975. *Corrosion and deposits from combustion of solid waste Part III- Effects of sulfur on boiler tube metals.*.

84. Lakshnikutty B., Narayanan K. V. 2006. *Stoichiometry and Process Calculations.* , s.l.: PHI Learning Pvt. Ltd..

85. Holger M. 1980. Chemie Ingenieur Technik Volume 52, Issue 3. *Wärme- und Stoffübertragung in der Wirbelschicht*.

86. Achternbosch M., Bräutigam K.-R., and Vehlow J. 2002. Thermische Verfahren der Abfallbehandlung - Entwicklungen, Optimierung, Bewertung. *Transferfaktoren,* Weimar.

87. Kurz D. 2014. *Numerische Simulation industrieller Rostfeuerungen nach der Euler-Euler Methode.* Stuttgart.

88. CEN/TS 15440:2006. 2007. *Solid recovered fuels. Method for the determination of biomass content*. Brussel: European Committee for Standardisation.

Annex A – Parameters measured in the TAMARA pilot facility

Combustion of wood chips

MCR-Notation	Dimension	Denotation	Value
W 58 701	kg/h	Feed wood	120
W 58 703	kg/h	Feed SRF	0
W 58 706	kg/h	Feed gravel	20
F 52 746	m^3/h	Primary air zone 1	49
F 52 747	m^3/h	Primary air zone 2	100
F 52 748	m^3/h	Primary air zone 3	200
F 52 766	m^3/h	Primary air zone 4	49
T 52 102	°C	Primary air temperature	32
F 52 743	m^3/h	Secondary air	159
P 51 329	mbar	Furnace pressure	-0.25
T 51 107	°C	Gas temperature grate before the finned wall of the boiler	1 112
T 51 151	°C	Gas temperature grate before the start of finned wall of the boiler	1 065
T 51 108	°C	Gas temperature grate before the start of finned wall of the boiler	981
	°C	Gas temperature before boiler	496
T 53 113	°C	Gas temperature after boiler	251
T 53 114	°C	Gas temperature before quench 2	235
T 53 132	°C	Gas temperature after quench 2	204
T 54 133	°C	Gas temperature before fabric filter	195
T 55 201	°C	Gas temperature after scrubber before scrubber 1	172
T 55 203	°C	Gas temperature after scrubber 1 before scrubber 2	53
T 55 204	°C	Gas temperature after scrubber 2	51
F 57 771	Nm^3/h	Exhaust gas volume flow rate before stack	1 189
T 57 205	°C	Gas temperature before stack	76

MCR-Notation	Dimension	Denotation		Value
Q 71 011	mg/m³	HCl	Raw gas before fabric filter, not normalised	12.62
Q 71 012	mg/Nm³	SO_2		4.18
Q 71 013	mg/Nm³	NO		124.85
Q 71 014	mg/Nm³	NO_x		122.91
Q 71 015	mg/Nm³	CO		2.05
Q 71 016	Vol.-% dry	CO_2		9.48
Q 71 017	Vol.-% wet	H_2O		9.61
Q 71 018	Vol.-% dry	O_2		11.01
Q 71 019	mg/Nm³	C_{org}		2.77
Q 55 501	Vol.-% wet	O_2	Raw gas after fabric filter	11.46
Q 71 110	mg/Nm³	Dust	Clean gas before stack, not normalised	4.65
Q 71 112	mg/Nm³	SO_2		1.64
Q 71 113	mg/Nm³	NO_x		128.01
Q 71 115	mg/Nm³	CO		2.06
Q 71 121	Vol.-% wet	H_2O		17.47
Q 71 118	Vol.-% dry	O_2		12.97
Q 71 119	mg/Nm³	C_{org}		-0.09
Q 71 122	mg/Nm³	N_2O		3.20

Combustion of SBS®1

MCR-Notation	Dimension	Denotation	Value
W 58 701	kg/h	Feed wood	0
W 58 703	kg/h	Feed SRF	105
W 58 706	kg/h	Feed gravel	1
F 52 746	m^3/h	Primary air zone 1	44
F 52 747	m^3/h	Primary air zone 2	90
F 52 748	m^3/h	Primary air zone 3	209
F 52 766	m^3/h	Primary air zone 4	54
T 52 102	°C	PA- Preheating	35
F 52 743	m^3/h	Secondary air 1	120
P 51 329	mbar	Oven pressure	-0.25
T 51 107	°C	Gas temperature grate before the finned wall of the boiler	1 063
T 51 151	°C	Gas temperature grate before the start of finned wall of the boiler	1 013
T 51 108	°C	Gas temperature grate before the start of finned wall of the boiler	900
	°C	Gas temperature before boiler	563
T 53 113	°C	Gas temperature after boiler	274
T 53 114	°C	Gas temperature before quench 2	267
T 53 132	°C	Gas temperature after quench 2	211
T 54 133	°C	Gas temperature before fabric filter	202
T 55 201	°C	Gas temperature after scrubber before scrubber 1	175
T 55 203	°C	Gas temperature after scrubber 1 before scrubber 2	54
T 55 204	°C	Gas temperature after scrubber 2	52
F 57 771	Nm^3/h	Exhaust gas volume flow rate before chimney	1 097
T 57 205	°C	Gas temperature before stack	80

MCR-Notation	Dimension	Denotation		Value
Q 71 011	mg/m³	HCl	Raw gas before fabric filter, not normalised	869.76
Q 71 012	mg/Nm³	SO_2		72.18
Q 71 013	mg/Nm³	NO		276.06
Q 71 014	mg/Nm³	NO_x		265.02
Q 71 015	mg/Nm³	CO		2.07
Q 71 016	Vol.-% dry	CO_2		8.00
Q 71 017	Vol.-% wet	H_2O		9.17
Q 71 018	Vol.-% dry	O_2		11.93
Q 71 019	mg/Nm³	C_{org}		3.23
Q 55 501	Vol.-% wet	O_2	Raw gas after fabric filter	11.78
Q 71 110	mg/Nm³	Dust	Clean gas before stack, not normalised	4.24
Q 71 112	mg/Nm³	SO_2		1.97
Q 71 113	mg/Nm³	NO_x		114.57
Q 71 115	mg/Nm³	CO		1.85
Q 71 121	Vol.-% wet	H_2O		18.37
Q 71 118	Vol.-% dry	O_2		13.38
Q 71 119	mg/Nm³	C_{org}		0.43
Q 71 122	mg/Nm³	N_2O		3.44

P 53 308	bar	Steam pressure	4.85
F 53 744	kg/h	Amount of steam	347
T 53 140	°C	Water temperature before boiler entry	53
M 52 721	%	Relative air moisture induction air	26.93
P 55 336 (above the monitors)	mbar	Absolute air pressure	1 005
T 52 104	°C	Temperature induction air	34

Combustion of BIOBS

MCR-Notation	Dimension	Denotation	Value
W 58 701	kg/h	Feed wood	0
W 58 703	kg/h	Feed SRF	150
W 58 706	kg/h	Feed gravel	1
F 52 746	m^3/h	Primary air zone 1	37
F 52 747	m^3/h	Primary air zone 2	71
F 52 748	m^3/h	Primary air zone 3	139
F 52 766	m^3/h	Primary air zone 4	34
T 52 102	°C	PA- Preheating	36
F 52 743	m^3/h	Secondary air 1	100
P 51 329	mbar	Oven pressure	-0.24
T 51 107	°C	Gas temperature grate before the finned wall of the boiler	1 013
T 51 151	°C	Gas temperature grate before the start of finned wall of the boiler	951
T 51 108	°C	Gas temperature grate before the start of finned wall of the boiler	849
	°C	Gas temperature before boiler	490
T 53 113	°C	Gas temperature after boiler	255
T 53 114	°C	Gas temperature before quench 2	237
T 53 132	°C	Gas temperature after quench 2	210
T 54 133	°C	Gas temperature before fabric filter	201
T 55 201	°C	Gas temperature after scrubber before scrubber 1	176
T 55 203	°C	Gas temperature after scrubber 1 before scrubber 2	57
T 55 204	°C	Gas temperature after scrubber 2	55
F 57 771	Nm^3/h	Exhaust gas volume flow rate before chimney	1 030
T 57 205	°C	Gas temperature before stack	81

MCR-Notation	Dimension	Denotation	Value	Value
Q 71 011	mg/m³	HCl	Raw gas before fabric filter, not normalised	429.01
Q 71 012	mg/Nm³	SO_2		29.10
Q 71 013	mg/Nm³	NO		224.12
Q 71 014	mg/Nm³	NO_x		214.20
Q 71 015	mg/Nm³	CO		3.01
Q 71 016	Vol.-% dry	CO_2		8.44
Q 71 017	Vol.-% wet	H_2O		11.32
Q 71 018	Vol.-% dry	O_2		11.36
Q 71 019	mg/Nm³	C_{org}		2.92
Q 55 501	Vol.-% wet	O_2	Raw gas after fabric filter	10.65
Q 71 110	mg/Nm³	Dust	Clean gas before stack, not normalised	4.48
Q 71 112	mg/Nm³	SO_2		3.17
Q 71 113	mg/Nm³	NO_x		117.13
Q 71 115	mg/Nm³	CO		2.38
Q 71 121	Vol.-% wet	H_2O		20.58
Q 71 118	Vol.-% dry	O_2		13.04
Q 71 119	mg/Nm³	C_{org}		-0.12
Q 71 122	mg/Nm³	N_2O		2.15

P 53 308	bar	Steam pressure	4.81
F 53 744	kg/h	Amount of steam	322
T 53 140	°C	Water temperature before boiler entry	69
M 52 721	%	Relative air moisture induction air	17.11
P 55 336 (above the monitors)	mbar	Absolut air pressure	1 013
T 52 104	°C	Temperature induction air	34

Annex B – Gas concentrations measured over the fuel bed in the TAMARA pilot facility

Wood chips							
Sampling Probe	PA Zone	Gas concentrations [wet vol. %]					
		O_2	CO_2	CO	H_2	CH_4	H_2O
1	1	1.16	11.42	6.85	1.90	2.32	20.50
2	2	16.70	3.26	0.38	0.08	0.03	2.43
3	3	18.70	2.10	0.50	0.0	0.00	0.00
4	3	21.00	0.27	0.00	0.00	0.00	0.00
5	4	21.20	0.1	0.00	0.00	0.00	0.00
SBS®1							
Sampling Probe	PA Zone	Gas concentrations [wet vol. %]					
		O_2	CO_2	CO	H_2	CH_4	H_2O
1	1	0.62	10.12	0.0056	2.46	2.82	25.26
2	2	20.44	0.35	0.0056	0.11	0.02	2.32
3	3	21.25	0.30	0.00	0.00	0.00	0.00
4	3	21.25	0.11	0.00	0.00	0.00	0.00
5	4	21.25	0.11	0.00	0.00	0.00	0.00
BIOBS							
Sampling Probe	PA Zone	Gas concentrations [wet vol. %]					
		O_2	CO_2	CO	H_2	CH_4	H_2O
1	1	8.53	10.19	1.32	0.49	0.23	32.00
2	2	9.78	10.09	1.26	0.44	0.20	14.23
3	3	19.90	1.20	0.00	0.00	0.00	0.00
4	3	19.95	1.20	0.00	0.00	0.00	0.00
5	4	21.22	0.08	0.00	0.00	0.00	0.00

Annex C – Gas weight fractions measured over the fuel bed in the TAMARA pilot facility

Wood chips							
Sampling Probe	PA Zone	Gas concentrations [wet wt. %]					
		O_2	CO_2	CO	H_2	CH_4	H_2O
1	1	1.28	17.41	6.64	0.13	1.78	12.79
2	2	18.51	4.97	0.36	0.006	0.02	1.51
4	3	23.28	0.41	0.00	0.00	0.00	0.00
5	4	23.49	0.15	0.00	0.00	0.00	0.00
SBS®1							
Sampling Probe	PA Zone	Gas concentrations [wet wt. %]					
		O_2	CO_2	CO	H_2	CH_4	H_2O
1	1	0.69	15.53	0.0054	0.17	1.58	16.06
2	2	22.8	0.54	0.00	0.008	0.01	1.46
4	3	23.71	0.17	0.00	0.00	0.00	0.00
5	4	23.72	0.17	0.00	0.00	0.00	0.00
BIOBS							
Sampling Probe	PA Zone	Gas concentrations [wet wt. %]					
		O_2	CO_2	CO	H_2	CH_4	H_2O
1	1	9.63	15.83	1.30	0.03	0.13	20.35
2	2	11.05	15.67	1.24	0.03	0.11	9.05
4	3	22.54	1.86	0.00	0.00	0.00	0.00
5	4	23.98	0.13	0.00	0.00	0.00	0.00

Annex D – Energy balance for the TAMARA facility

D.1. Combustion of wood chips

Input	Mass flow [kg/h]]	c_p [kJ/kgK]	ϑ [°C]	NCV [kJ/kg]	H [kW]
Fuel	120	2	20	12340	430
Primary air	458	1	32		5
Secondary air	178	1	32		1.8
Air quench	14	1	20		0.1
Leaked air	773	1	20		2.5
Water quench	6	4.18	20		0.1
Boiler water	409	4.40	70		35
Sum					474
Output		c_p [kJ/kgK]	ϑ [°C]		H [kW]
Flue gas after the boiler	1531	1	326		76
Steam	409	1.07	195		328
Sum					405
Heat losses		14%			

D.2. Combustion of the SBS®1

Input	Mass flow [kg/h]]	c_p [kJ/kgK]	ϑ [°C]	NCV [kJ/kg]	H [kW]
Fuel	105	2	20	15895	464
Primary air	450	1	35		5
Secondary air	136	1	35		1.5
Air quench	12	1	20		0.1
Leaked air	708	1	20		2.8
Water quench	6	4.18	20		0.1
Boiler water	347	4.40	53		22
Sum					499
Output		c_p [kJ/kgK]	ϑ [°C]		H [kW]
Flue gas after the boiler	1394	1	259		76
Steam	347	1.07	202		278
Sum					355
Heat losses		29%			

D.3. Combustion of the BIOBS

Input	Mass flow [kg/h]]	c_p [kJ/kgK]	ϑ [°C]	NCV [kJ/kg]	H [kW]
Fuel	150	2	20	7700	324
Primary air	323	1	36		3.6
Secondary air	115	1	36		1.3
Air quench	13	1	20		0.1
Leaked air	685	1	20		2.9
Water quench	0	4.18	20		0.0
Boiler water	322	4.40	69		27
Sum					359
Output		c_p [kJ/kgK]	ϑ [°C]		H [kW]
Flue gas after the boiler	1307	1	304		1.1
Steam	322	1.07	200		70
Sum					329
Heat losses		8%			

Annex E – Emissivity coefficients and heat transfer coefficients in the KLEAA Code

E.1. Emissivity coefficient between the solid and the gas in the furnace

Calculated from the equation below:

$$\varepsilon_{ws} = \frac{1}{\frac{1}{\varepsilon_w} + \frac{1}{\varepsilon_s} - 1} \qquad \text{Equation 0.1}$$

Where ε_w stands for the emissivity of the furnace wall and equals 0.9 (75) and ε_s is calculated on the basis of the actual fuel composition:

$$\varepsilon_s = x_{ash} \cdot \varepsilon_{ash} + x_{wood} \cdot \varepsilon_{wood} + x_{PE} \cdot \varepsilon_{PE} + x_C \cdot \varepsilon_C \qquad \text{Equation 0.2}$$

$x_{ash}, x_{wood}, x_{PE}, x_C$ stand for the content of the ash, wood (biomass), polyethylene (simplified description of plastics) and char in the fuel respectively. Emissivity coefficient of the ash ε_{ash} is assumed to be constant throughout the combustion process and equals 0.7. ε_{wood} on the other hand is temperature dependent and is calculated from:

$$\varepsilon_{wood} = 0.882 - 5.117 \cdot 10^{-5} \cdot \vartheta_s - 7.888 \cdot 10^{-8} \cdot {T_s}^2 \qquad \text{Equation 0.3}$$

The emissivity of the polyethylene ε_{PE} is assumed to be equal ε_{wood}. The coefficient ε_C needed for the Equation 6.22 is also temperature dependent and equals:

$$\varepsilon_C = 0.6 + 7.4 \cdot 10^{-5} \cdot T_s \qquad \text{Equation 0.4}$$

In Equation 6.23 there are two coefficients which need to be explained; emissivity ε_{fs} and absorptivity α_{fs} between the solid and the gas in the furnace. According to Kohlgrüber (76) The emissivity of the flue gas in the furnace equals:

$$\varepsilon_{fs} = f_{H2O} \cdot \varepsilon_{H2O} + f_{CO2} \cdot \varepsilon_{CO2} - \Delta\varepsilon \qquad \text{Equation 0.5}$$

Where:

$$\varepsilon_i = \sum_{k=0}^{3} \sum_{l=0}^{3} a_{4k+l+1} \cdot x^l \cdot y^k \qquad \text{Equation 0.6}$$

$$i = H_2O, CO_2$$

$x = \ln(\vartheta_g)$ Equation 0.7

$y = \ln(p_i \cdot s)$ Equation 0.8

s – mean free path

Coefficient a_{4k+l+1} for water vapour and carbon dioxide is summarised below:

a_{4k+l+1} for water vapour				
	l = 0	l = 1	l = 2	l = 3
k = 0	26.412E+00	-1.3598E+01	2.2795E+00	-1.2832E-01
k = 1	-1.3918E+00	7.5115E-01	-1.2239E-01	7.1782E-03
k = 2	1.4293E+00	-6.6175E-01	1.0101E-01	-5.2440E-03
k = 3	-1.4829E-02	1.8248E-02	-4.5251E-03	3.1868E-04
a_{4k+l+1} for CO2				
	l = 0	l = 1	l = 2	l = 3
k = 0	128.73E+00	-6.0730E+01	9.3744 E+00	-4.7979E-01
k = 1	4.454E+00	-2.1948E+00	3.5752E-01	-1.8382E-02
k = 2	2.6485 E+00	-1.3808E+00	2.3320E-01	-1.2779E-02
k = 3	5.1218E-01	-2.4582E-01	3.9059E-02	-2.0384E-03

Table 0.1 – Coefficient a_{4k+l+1} for water vapour and CO_2 (76)

The correction factors f_{H2O} and f_{CO2} equal (76):

$$f_i = 1 + \sum_{k=0}^{3} \sum_{l=0}^{2} a_{2k+l} \cdot x^l \cdot y^k$$ Equation 0.9

$i = H_2O, CO_2$

$x_{H2O} = 0.5 \cdot (p_i + p_{tot} - 1)$ Equation 0.10

$x_{CO2} = lnp_i$ Equation 0.11

$y = \ln(p_i \cdot s)$ Equation 0.12

Coefficient a_{4k+l+1} for water vapour and carbon dioxide is summarised below:

a_{2k+l} for water vapour		
	l = 1	l = 2
k = 0	8.1028E-01	-4.1483E-01
k = 1	-2.0002E-01	6.3244E-02
k = 2	1.4513E-02	1.1723E-02
k = 3	4.5380E-03	8.0798E-04
a_{2k+l} for CO_2		
	l = 1	l = 2
k = 0	3.1590E-01	3.2064E-02
k = 1	-1.3491E+00	-3.4701E-01
k = 2	3.6131E+00	1.1825E+00
k = 3	-2.9953E+00	-1.0747E+00

Table 0.2 – Coefficient a_{2k+l} for water vapour and CO_2 (76)

The correction factor Δε equals (76):

$$\Delta\varepsilon = \sqrt{x \cdot (1-x)} \cdot (\sum_{k=0}^{2}\sum_{l=0}^{2} a_{3k+l+1} \cdot x^l \cdot y^k) \quad \text{Equation 0.13}$$

$$i = H_2O, CO_2$$

$$x = \frac{p_{H2O}}{p_{H2O} + p_{CO2}} \quad \text{Equation 0.14}$$

$$y = \ln^2[(p_{H2O} + p_{CO2}) \cdot s] \quad \text{Equation 0.15}$$

Coefficient a_{3k+l+1} for the correction factor Δε is summarised below:

	l = 0	l = 1	l = 2
k = 0	-1.8418E+00	-1.7034E+00	1.7269E+00
k = 1	-1.6073E+00	5.9237E+00	-5.8522E+00
k = 2	1.0157E-01	-5.8297E-01	5.6835E-01

Table 0.3 – Coefficient a_{3k+l+1} for the correction factor Δε (76)

When $p_{H2O} + p_{CO2} < 1000Pa$ the Δε is set to 0.

The emissivity and absorptivity coefficients between the furnace wall and the gas in the furnace equal:

$$\varepsilon_{fw} = \frac{1}{\frac{1}{\varepsilon_f} + \frac{1}{\varepsilon_{w\infty}} - \frac{1}{\varepsilon_{f\infty}}} \quad \text{Equation 0.16}$$

$$\alpha_{fw} = \varepsilon_{wf} \cdot \left(\frac{T_f}{T_w}\right)^{0.5} \quad \text{Equation 0.17}$$

Analogously the emissivity and absorptivity coefficients between solid and gas in the furnace can be determined (77):

$$\varepsilon_{fs} = \frac{1}{\frac{1}{\varepsilon_f} + \frac{1}{\varepsilon_{s\infty}} - \frac{1}{\varepsilon_{f\infty}}} \quad \text{Equation 0.18}$$

$$\alpha_{fs} = \varepsilon_{fs} \cdot \left(\frac{T_f}{\vartheta_s}\right)^{0.5} \quad \text{Equation 0.19}$$

E.2. Total heat transfer coefficient for solid

Heat flux $\dot{Q}_{ll}$ takes place between consecutive layers of solid. For each layer, the overall total heat transfer coefficient α_{solid} is formulated:

For the heat transfer into a fuel layer thermal resistance $1/\alpha_{solid}$ is defined as series connection of thermal resistance between layers $1/\alpha_{ll}$ and of thermal resistance of a fuel bed itself $1/\alpha_{bed}$:

$$1/\alpha_{solid} = 1/\alpha_{ll} + 1/\alpha_{bed} \quad \text{Equation 0.20}$$

Heat transfer coefficient α_{ll} is a sum of a radiative heat transfer coefficient α_{rad} and of conductive heat transfer coefficient formulated for heat flow between neighbouring fuel particles (spheres) α_{pp}:

$$\alpha_{ll} = \varphi \cdot \alpha_{pp} + \alpha_{rad}$$ Equation 0.21

φ is called the surface coverage and equals 0.8 for a packing of monodisperse spherical particles. According to Schlünder (78) the heat transfer coefficient α_{pp} is defined as follows:

$$\alpha_{pp} = \frac{4 \cdot \lambda_g}{d_p} \cdot \left[\left(1 + \frac{2(l+\delta)}{d_p} \right) \cdot \ln \left(1 + \frac{d_p}{2(l+\delta)} \right) - 1 \right]$$ Equation 0.22

Where δ is the roughness of the particles and is set in the KLEAA Code to $5 \cdot 10^{-6}$. l stands for mean free path length of gas particles flowing through a packing of spheres:

$$l = 2 \cdot \frac{2-\gamma}{\gamma} \cdot \sqrt{\frac{2 \cdot \pi \cdot R \cdot T_g}{M_g}} \cdot \frac{\lambda_g}{p \cdot \left(2 \cdot c_{p,g} - \frac{R}{M_g} \right)}$$ Equation 0.23

The accommodation factor γ is defined as follows (78):

$$\frac{1}{\gamma} = 1 + 10^{\left[0.6 - \frac{1+1000/T_g}{c} \right]}$$ Equation 0.24

Factor "c", depends on the molar mass of gas flowing through the packing and is set to 2.8 (as for the air) (78). The radiative heat transfer coefficient α_{rad} is defined by Schlünder (78) as:

$$\alpha_{rad} = C_w \cdot 4 \cdot \frac{\left(T_{s(j-1,t)}^4 - T_{s(j,t)}^4 \right)}{\left(T_{s(j-1,t)} - T_{s(j,t)} \right)}$$ Equation 0.25

Where $T_{s(j-1,t)}$ is temperature of the layer on top and $T_{s(j,t)}$ is temperature of the neighbouring layer from below at the moment t. C_w is defined as:

$$C_w = \frac{\sigma}{\left(\frac{1}{\varepsilon_w} + \frac{1}{\varepsilon_s} - 1 \right)}$$ Equation 0.26

Coefficient ε_w standing for emissivity of the wall above fuel bed is applied only for the first fuel layer being heated up directly by radiation coming from the combustion chamber. Emissivity ε_w of the combustion chamber walls is assumed to be constant. Emissivity of the solid ε_s depends on the solid composition (see 6.3.2.)

Remaining heat transfer coefficient describing conductivity of solid in each layer j at time t is formulated below:

$$\alpha_{bed(j,t)} = \frac{2 \cdot \sqrt{(\lambda \cdot c_p \cdot \rho)_{s(j,t)}}}{\sqrt{\pi \cdot t}} \text{ (66)}$$ Equation 0.27

E.3. Convective heat transfer coefficient

Convective heat transfer coefficient between solid and gas α_{sg} is calculated according to Gnielinski (79):

$$\alpha_{sg} = \frac{Nu_{bulk} \cdot \lambda_g}{d_p}$$ Equation 0.28

Diameter d_p corresponds to the diameter of a spherical fuel particle:

$$d_p = \sqrt[3]{\frac{6}{\pi} \cdot \frac{m_{p(j,t)}}{\rho_{s(j,t)}}}$$ Equation 0.29

The heat transfer coefficient for a whole packing of spheres is higher than for a single particle, which is expressed by the factor describing the form of the particles (spheres) f_a used to calculate Nusselt number Nu:

$$Nu_{bulk} = f_a \cdot Nu_{sp}$$ Equation 0.30

Where Nu_{sp} is the Nusselt number for a single particle (sphere.) According to Gnielinski (79), for a monodisperse packing the f_a is as follows:

$$f_a = 1 + 1.5 \cdot (1 - \psi)$$ Equation 0.31

Nusselt number for a single sphere Nu_{sp} is formulated as:

$$Nu_{sp} = 2 + \sqrt{Nu_{lam}^2 + Nu_{tur}^2}$$ Equation 0.32

With following Nusselt numbers of laminar and turbulent flows Nu_{lam} and Nu_{tur}:

$$Nu_{lam} = 0.664 \cdot \sqrt{Re_\psi} \cdot \sqrt[3]{Pr}$$ Equation 0.33

$$Nu_{tur} = \frac{0.037 \cdot Re_\psi^{0.8} \cdot Pr}{1 + 2.443 \cdot Re_\psi^{-0,1} \cdot \left(Pr^{2/3} - 1\right)}$$ Equation 0.34

These equations are valid for Reynolds numbers between 10^{-1} and 10^4 as calculated for the particle diameter d_p:

$$Re_{\psi} = \frac{u_{empty} \cdot d_p}{\nu \cdot \psi}$$ Equation 0.35

Annex F – Simulated gas concentrations above the fuel bed (unsmoothed)

F.1. Combustion of wood chips in KLEAA

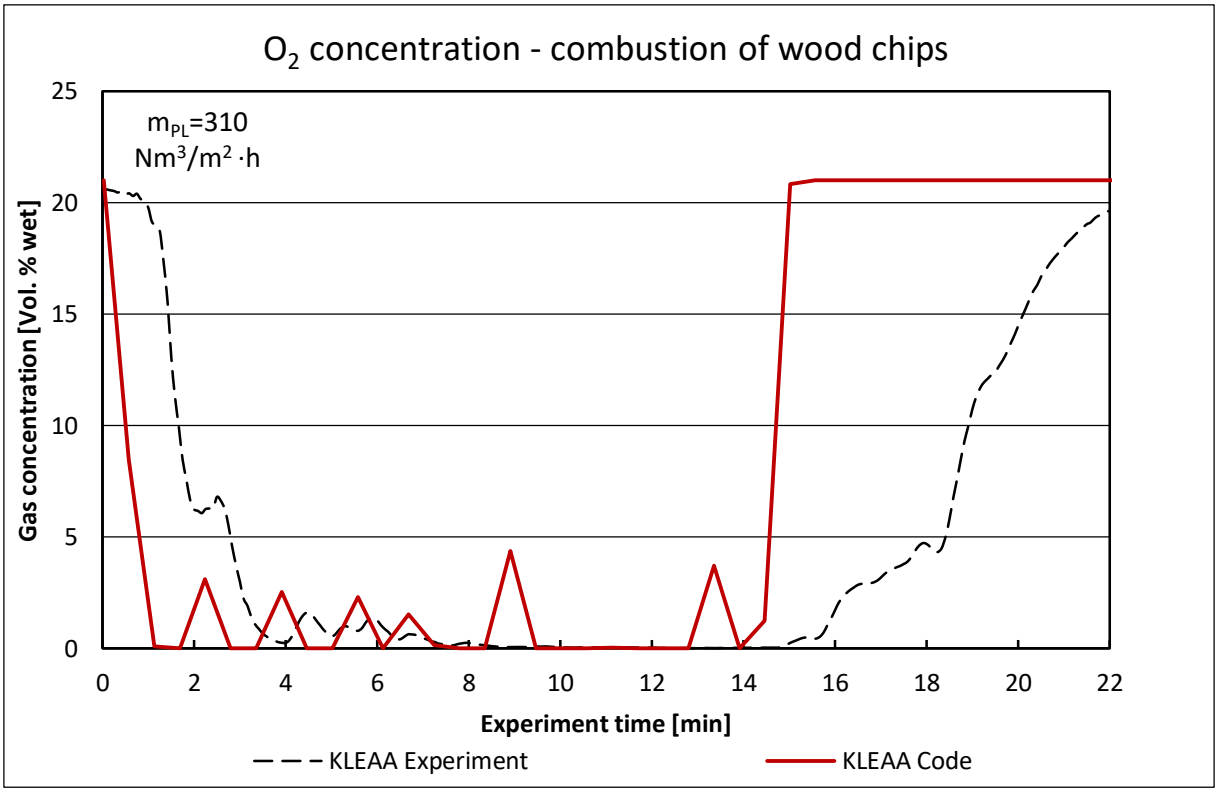

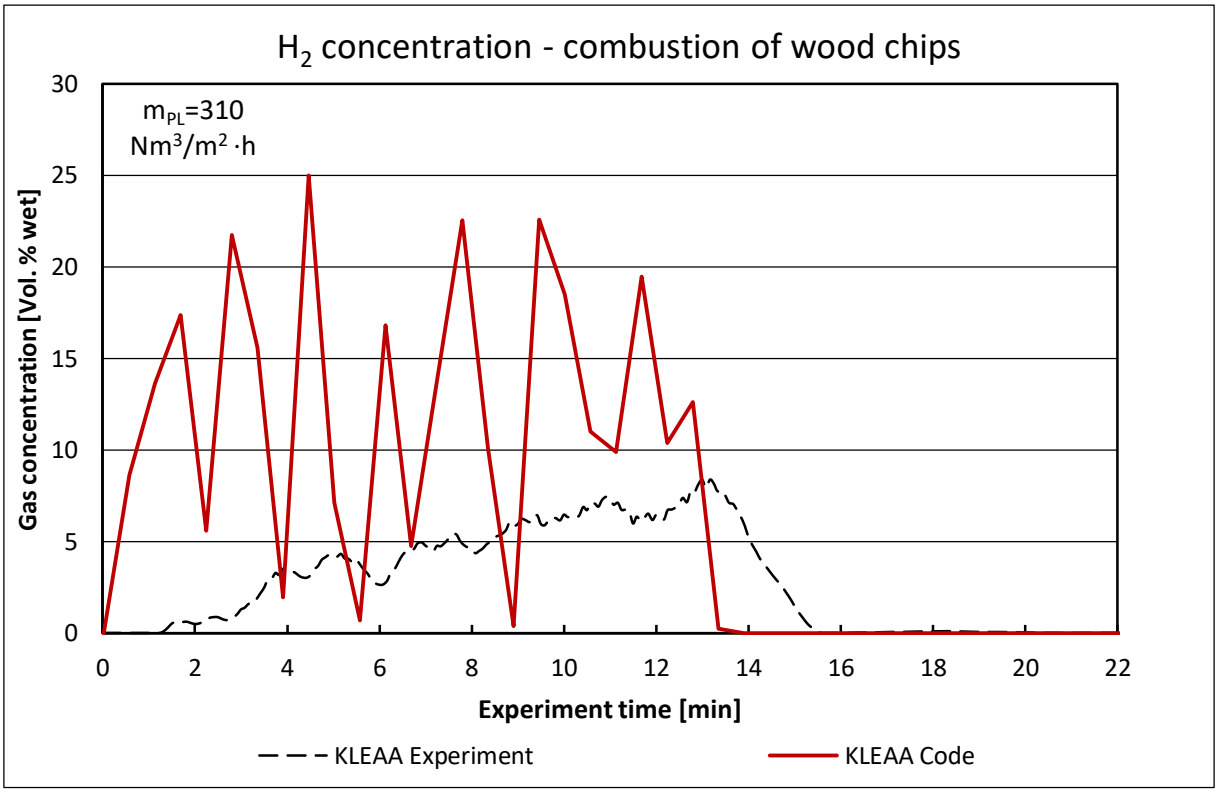

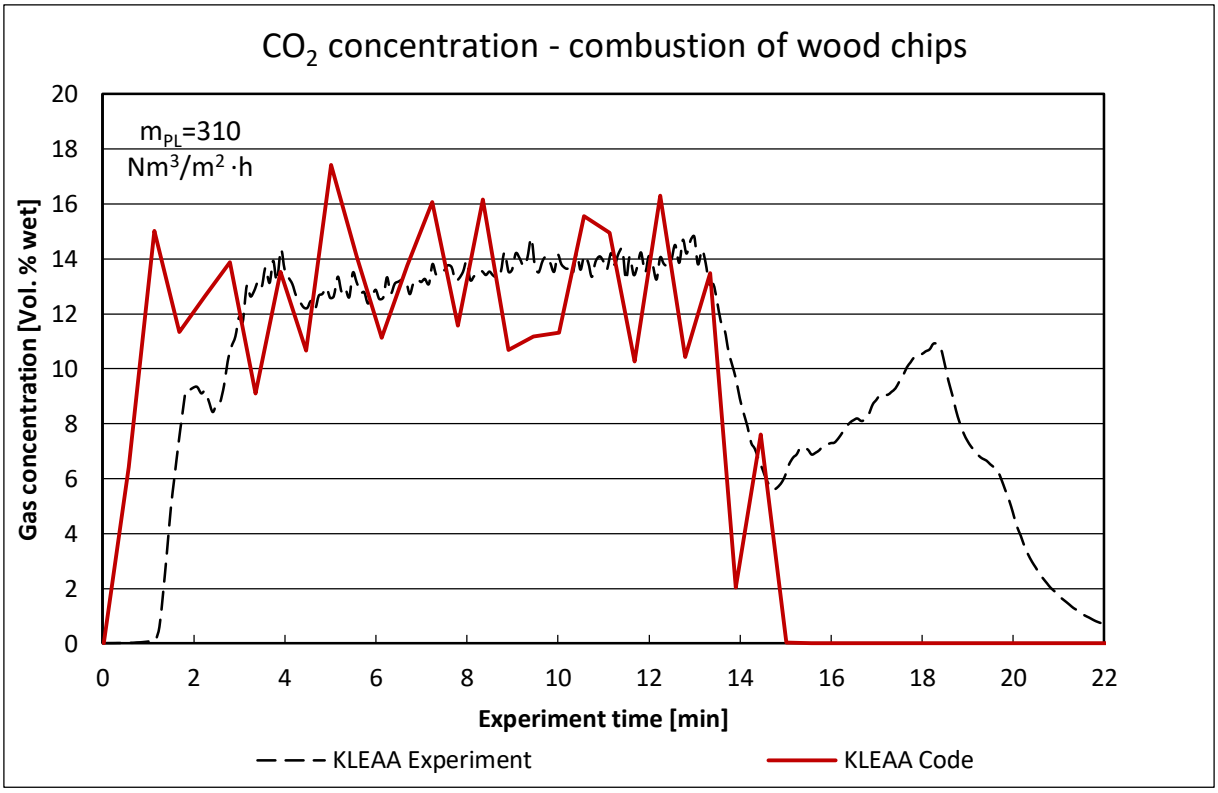
CO2 concentration - combustion of wood chips
mPL=310
Nm3/m2·h
Gas concentration [Vol. % wet]
Experiment time [min]
KLEAA Experiment
KLEAA Code

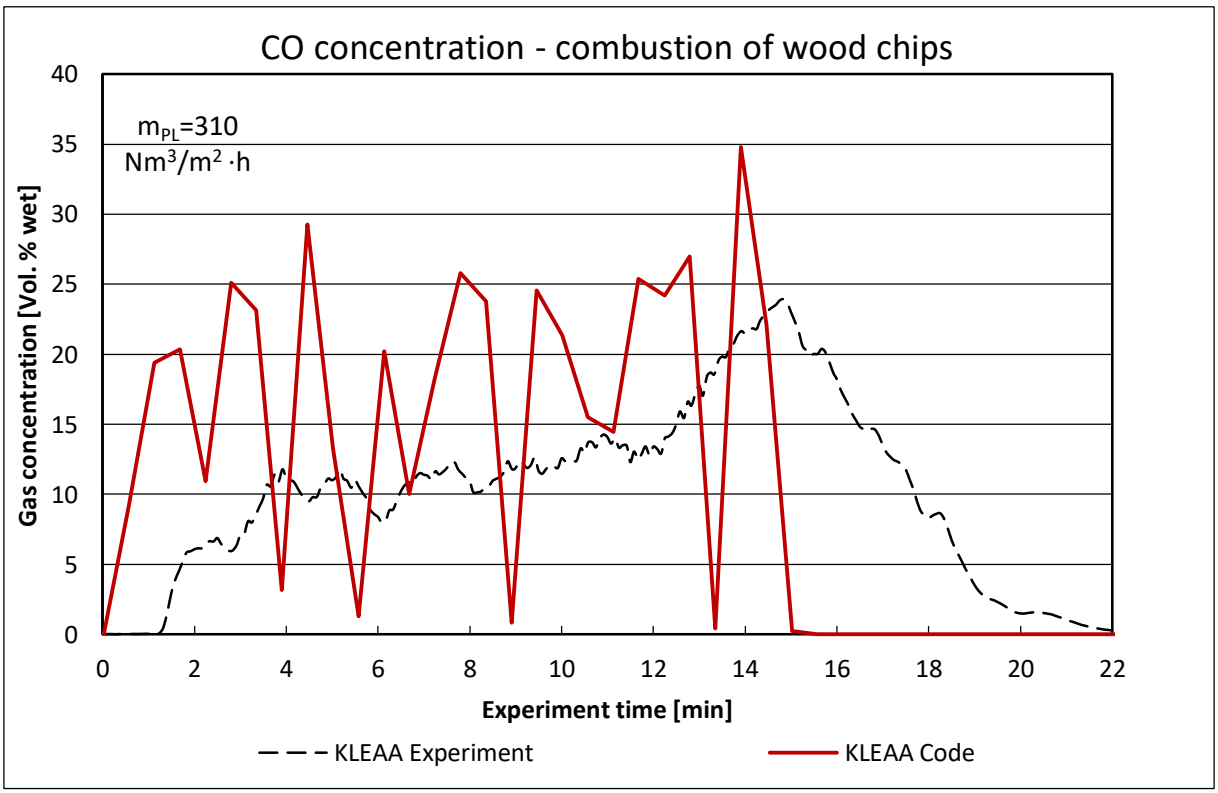
CO concentration - combustion of wood chips
mPL=310
Nm3/m2·h
Gas concentration [Vol. % wet]
Experiment time [min]
KLEAA Experiment
KLEAA Code

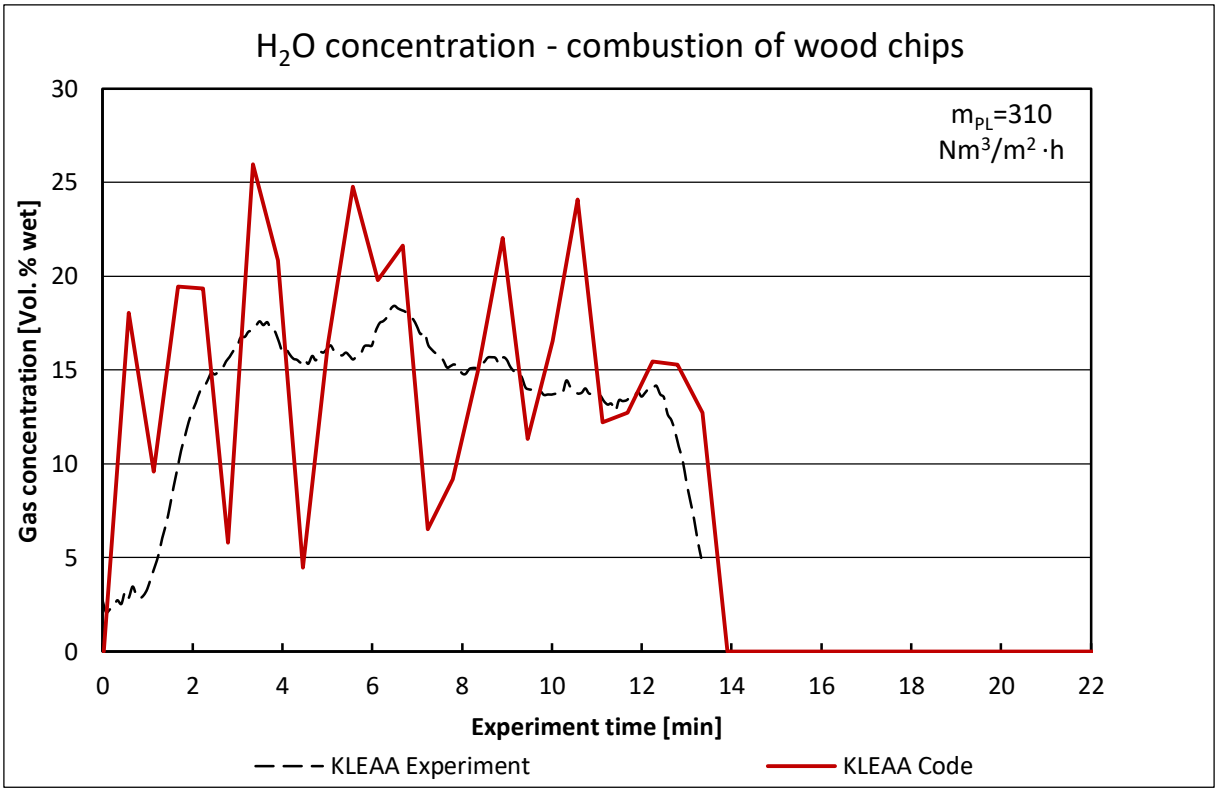
H2O concentration - combustion of wood chips
mPL=310
Nm3/m2 ·h
Gas concentration [Vol. % wet]
Experiment time [min]
KLEAA Experiment
KLEAA Code

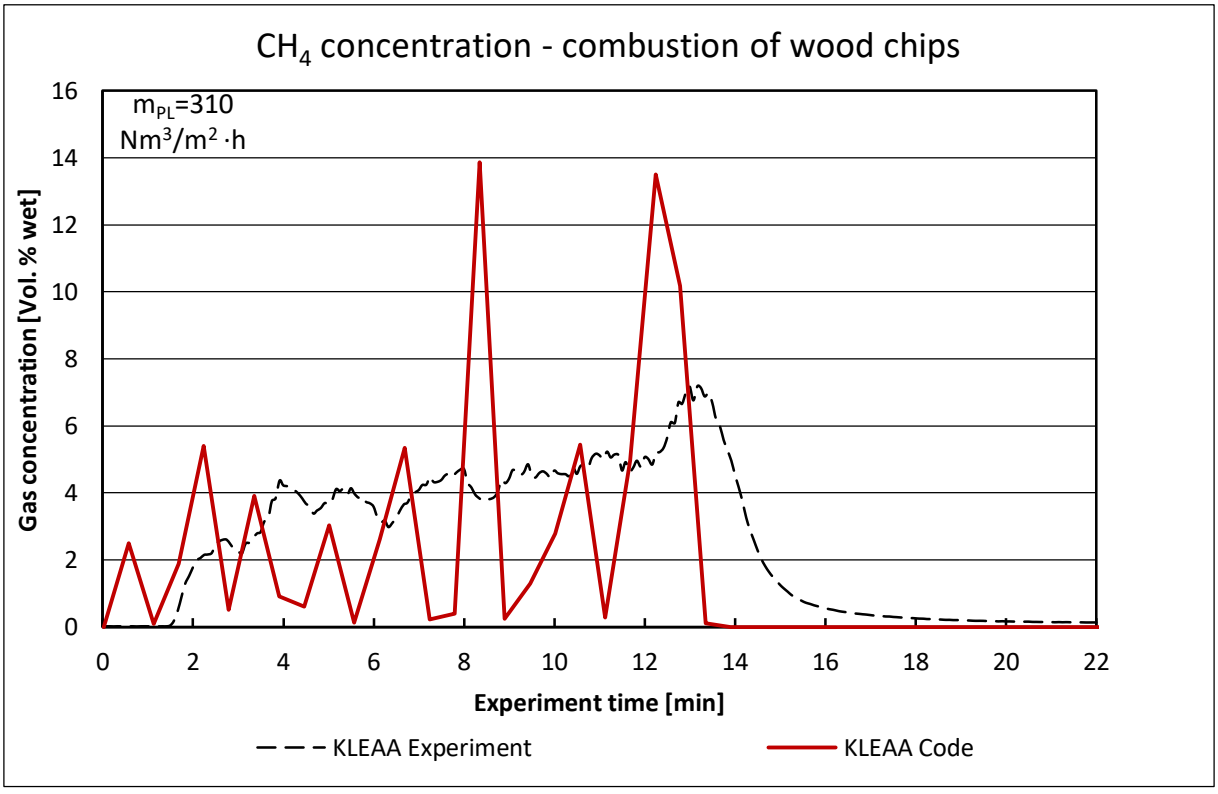
CH4 concentration - combustion of wood chips
mPL=310
Nm3/m2 ·h
Gas concentration [Vol. % wet]
Experiment time [min]
KLEAA Experiment
KLEAA Code

F.2. Combustion of SBS®1 in KLEAA

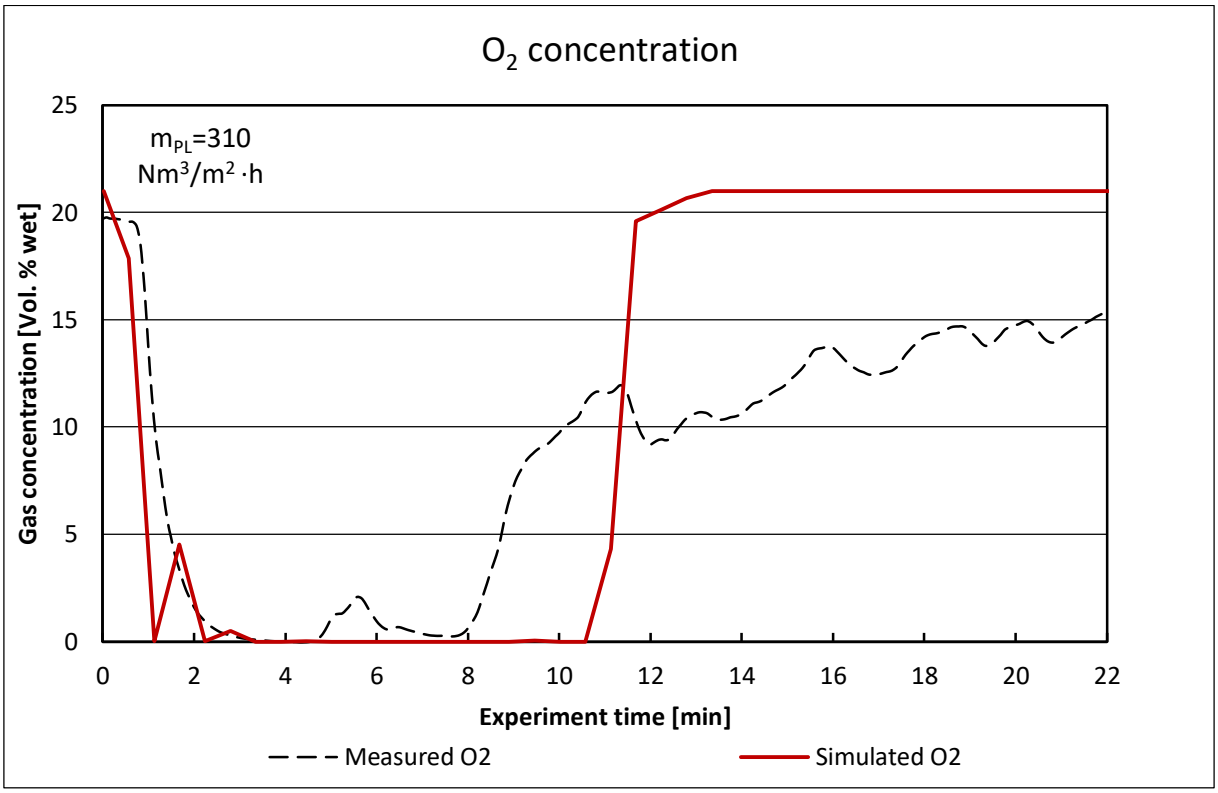

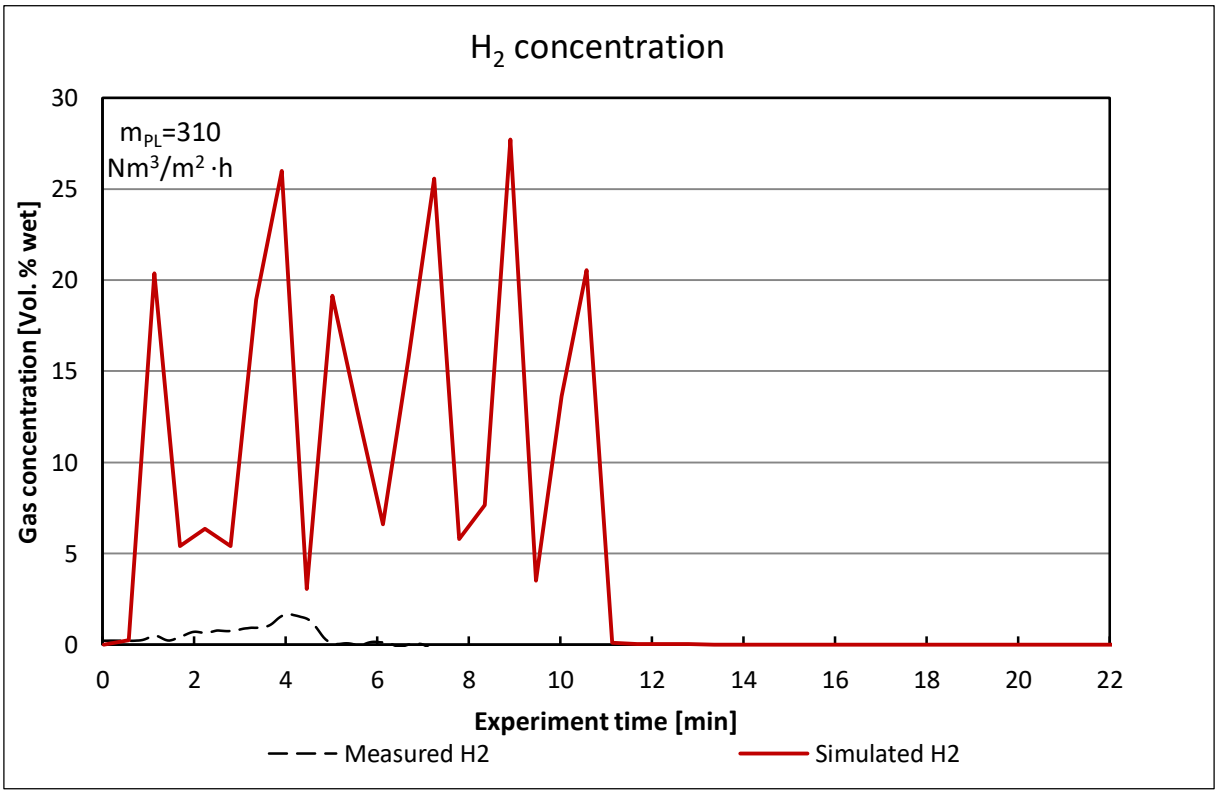

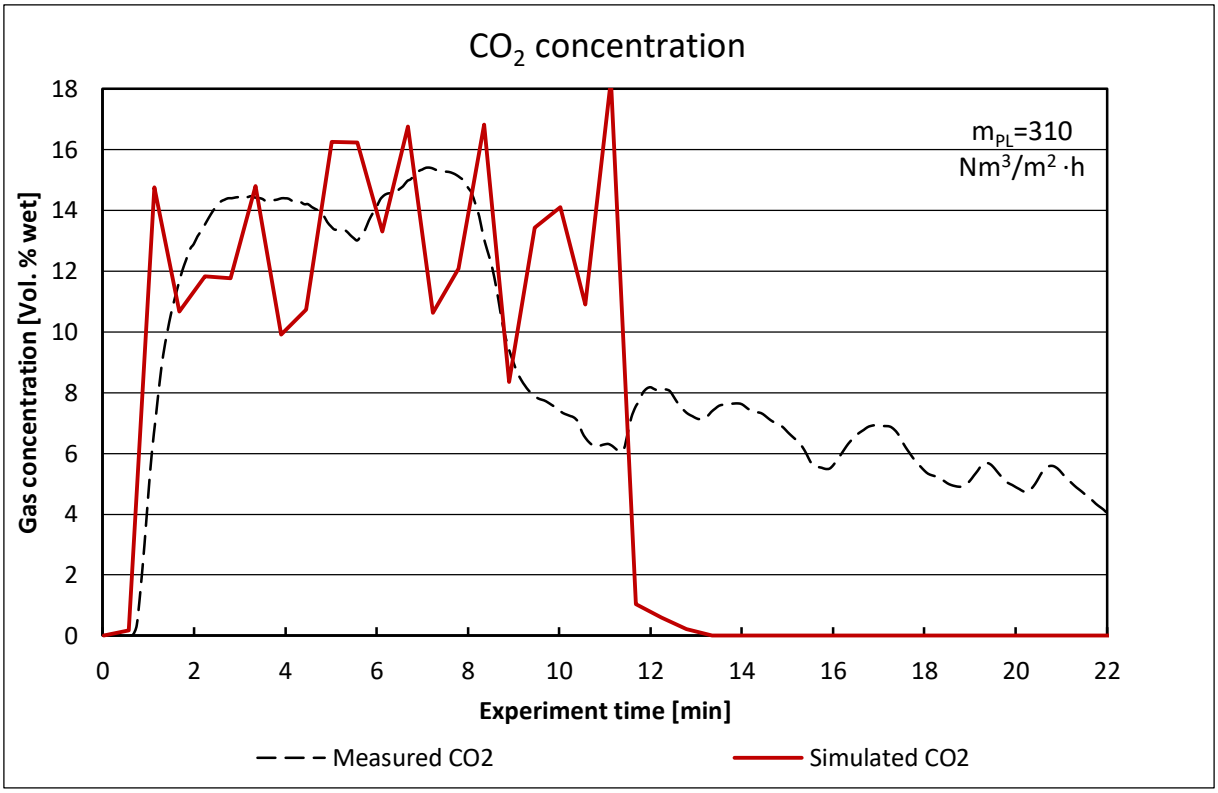
CO2 concentration
mPL=310
Nm3/m2 ·h
Gas concentration [Vol. % wet]
Experiment time [min]
Measured CO2
Simulated CO2

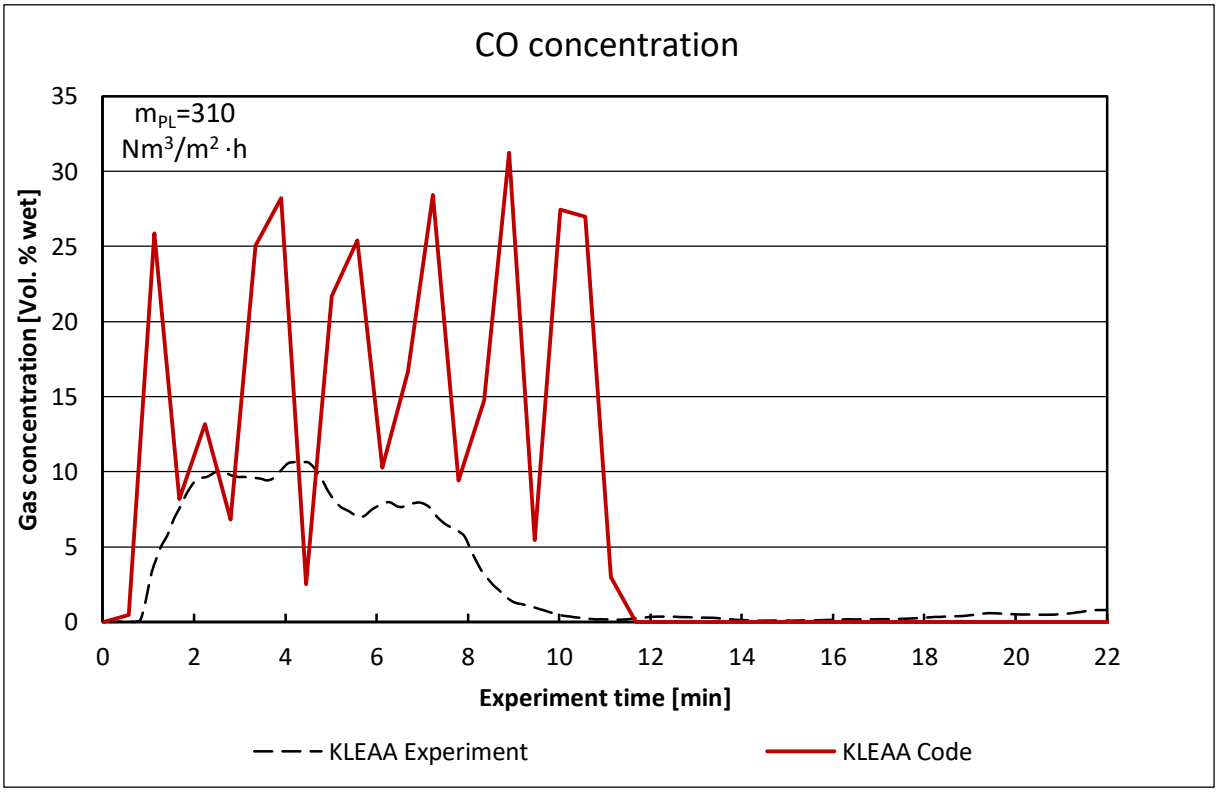
CO concentration
mPL=310
Nm3/m2 ·h
Gas concentration [Vol. % wet]
Experiment time [min]
KLEAA Experiment
KLEAA Code

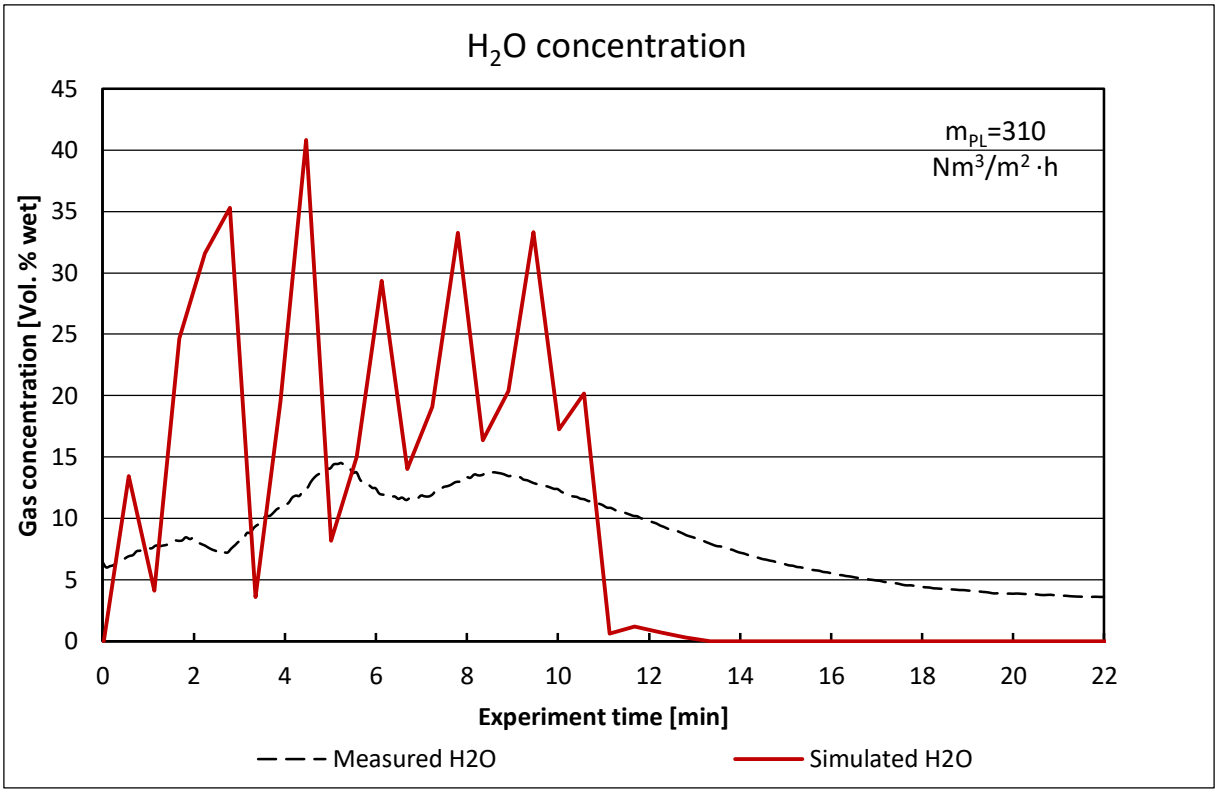
H2O concentration
mPL=310
Nm3/m2·h
Gas concentration [Vol. % wet]
Experiment time [min]
Measured H2O
Simulated H2O

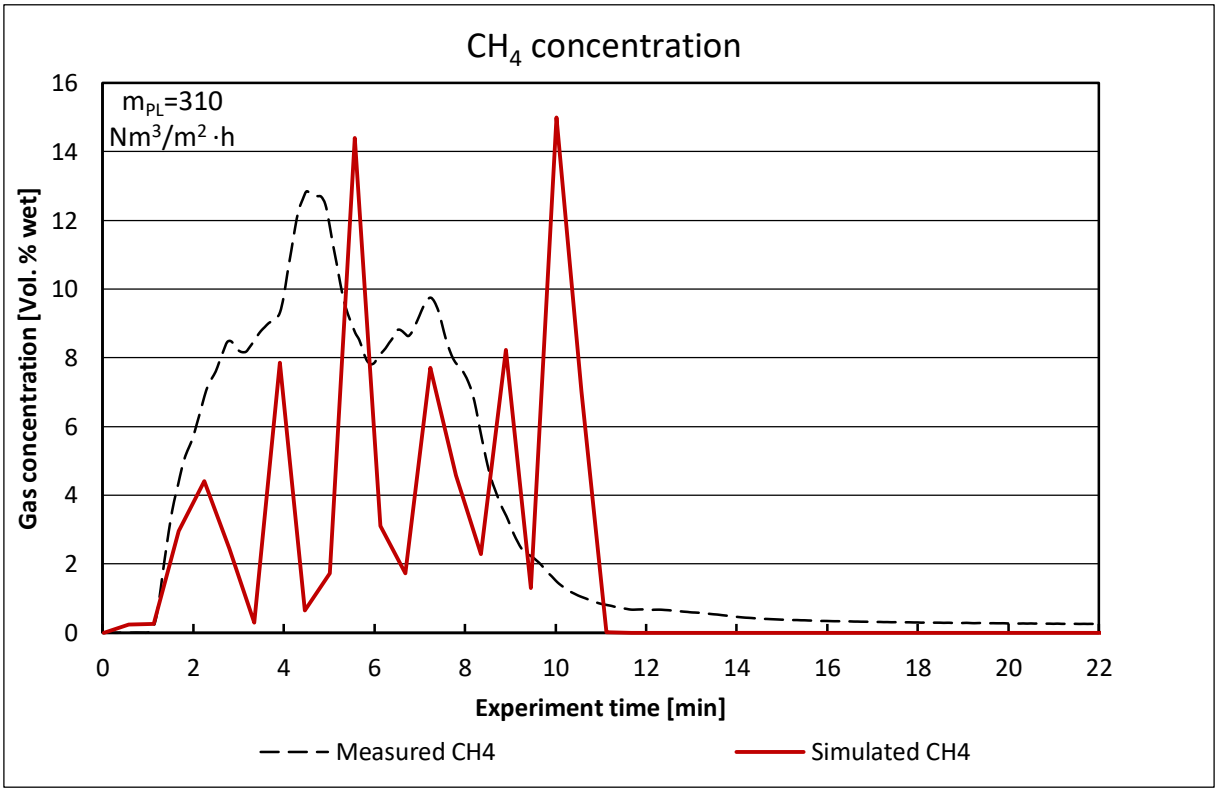
CH4 concentration
mPL=310
Nm3/m2·h
Gas concentration [Vol. % wet]
Experiment time [min]
Measured CH4
Simulated CH4

F.3. Combustion of wood chips in TAMARA

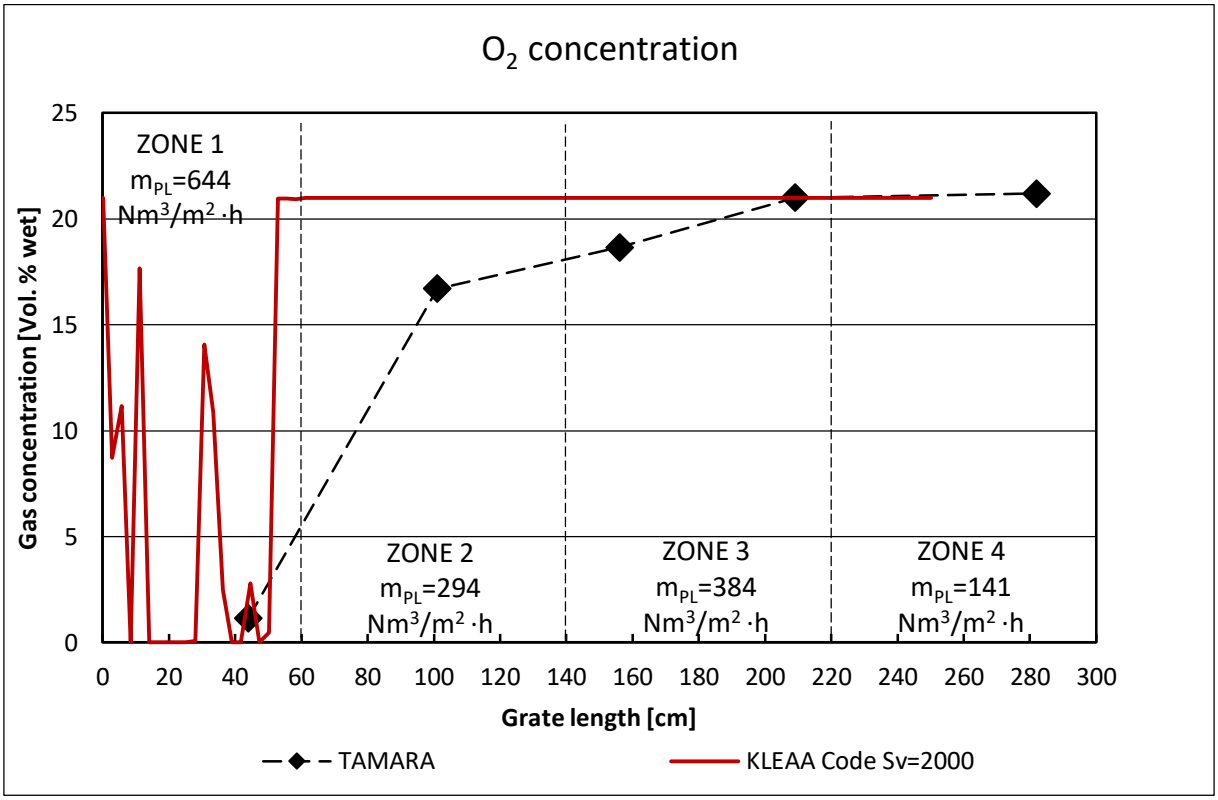

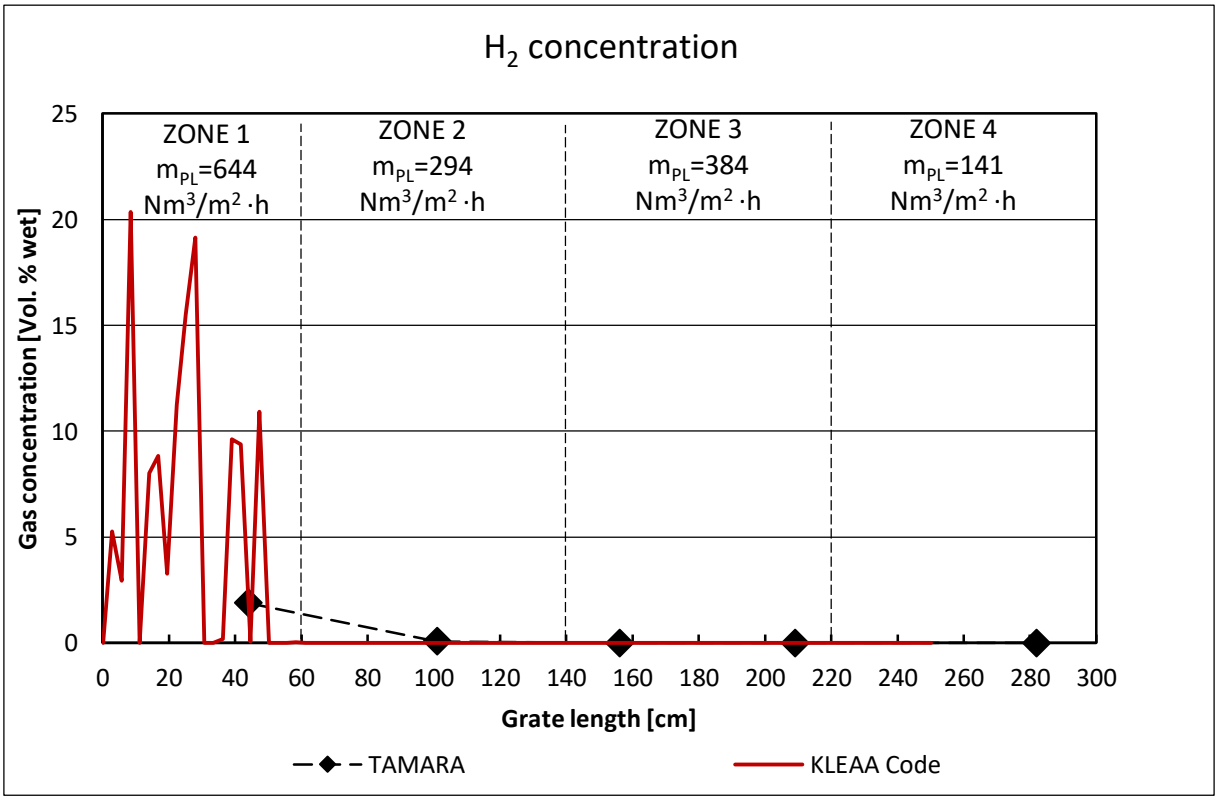

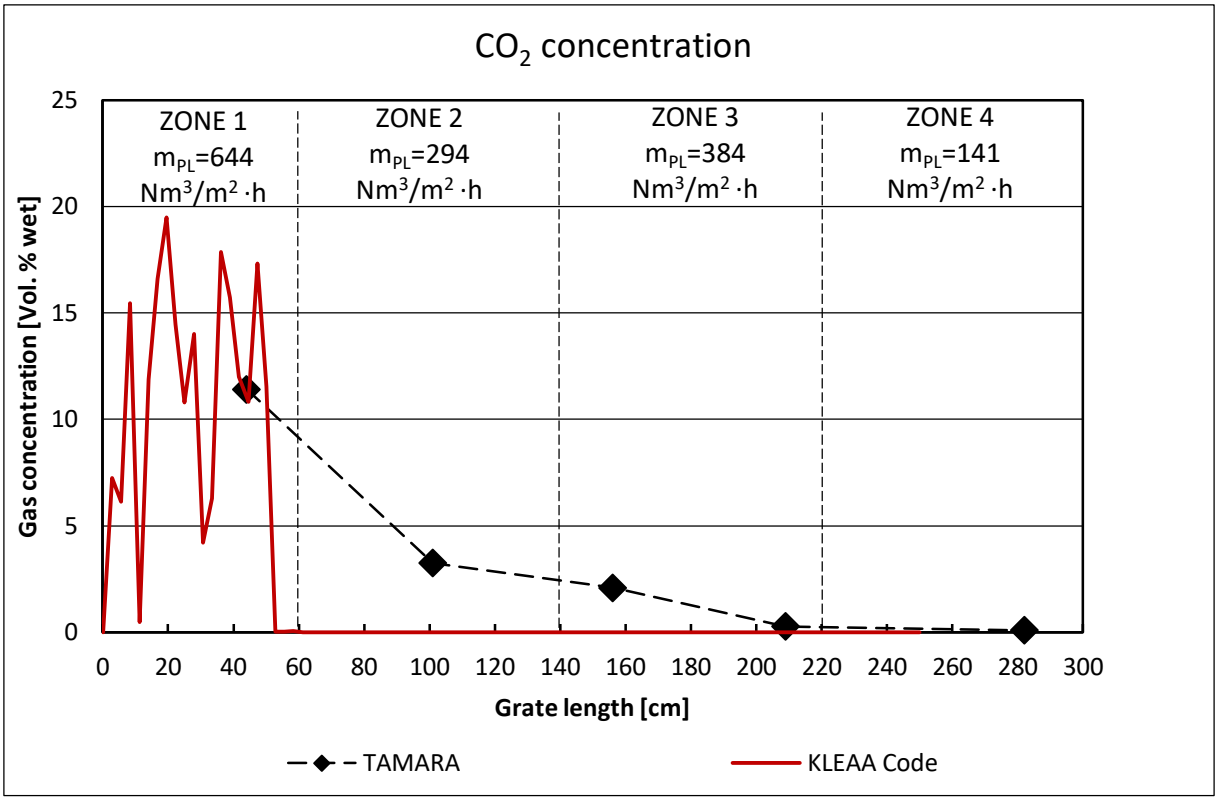
CO2 concentration
ZONE 1
mPL=644
Nm3/m2 ·h
ZONE 2
mPL=294
Nm3/m2 ·h
ZONE 3
mPL=384
Nm3/m2 ·h
ZONE 4
mPL=141
Nm3/m2 ·h
Gas concentration [Vol. % wet]
Grate length [cm]
TAMARA
KLEAA Code

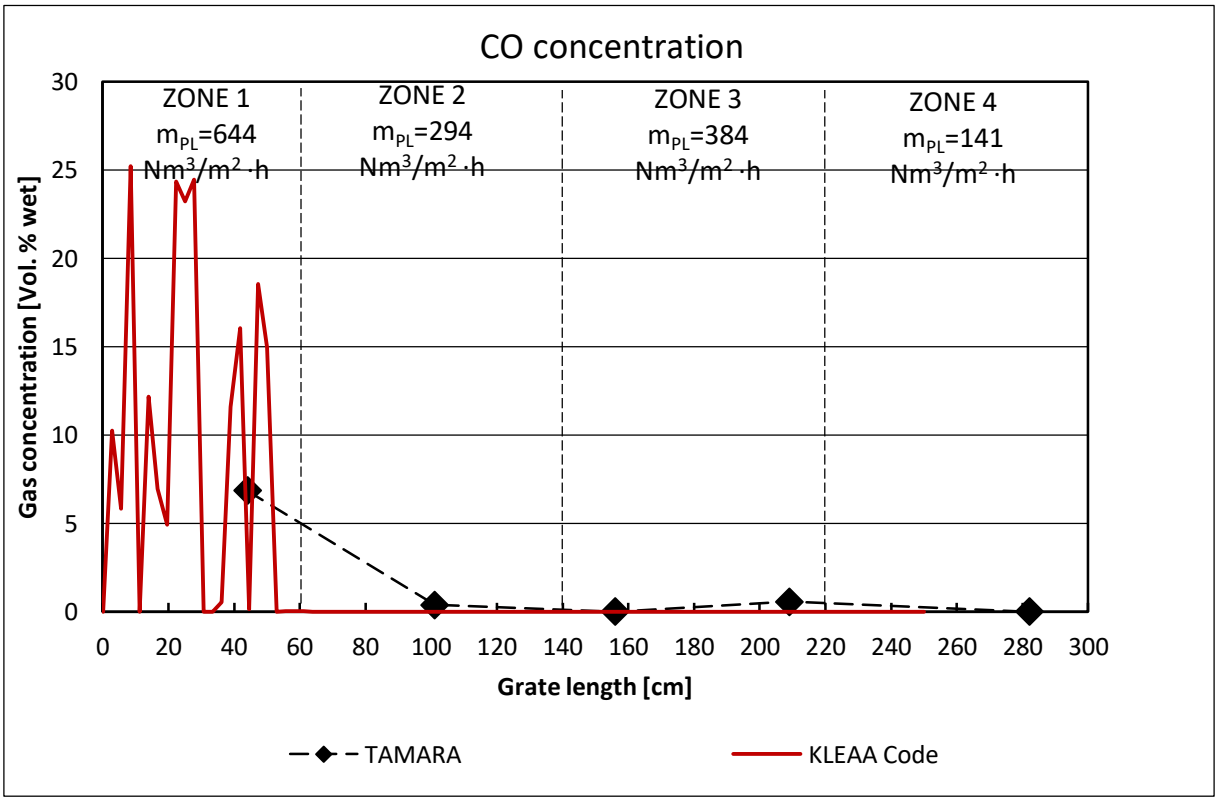
CO concentration
ZONE 1
mPL=644
Nm3/m2 ·h
ZONE 2
mPL=294
Nm3/m2 ·h
ZONE 3
mPL=384
Nm3/m2 ·h
ZONE 4
mPL=141
Nm3/m2 ·h
Gas concentration [Vol. % wet]
Grate length [cm]
TAMARA
KLEAA Code

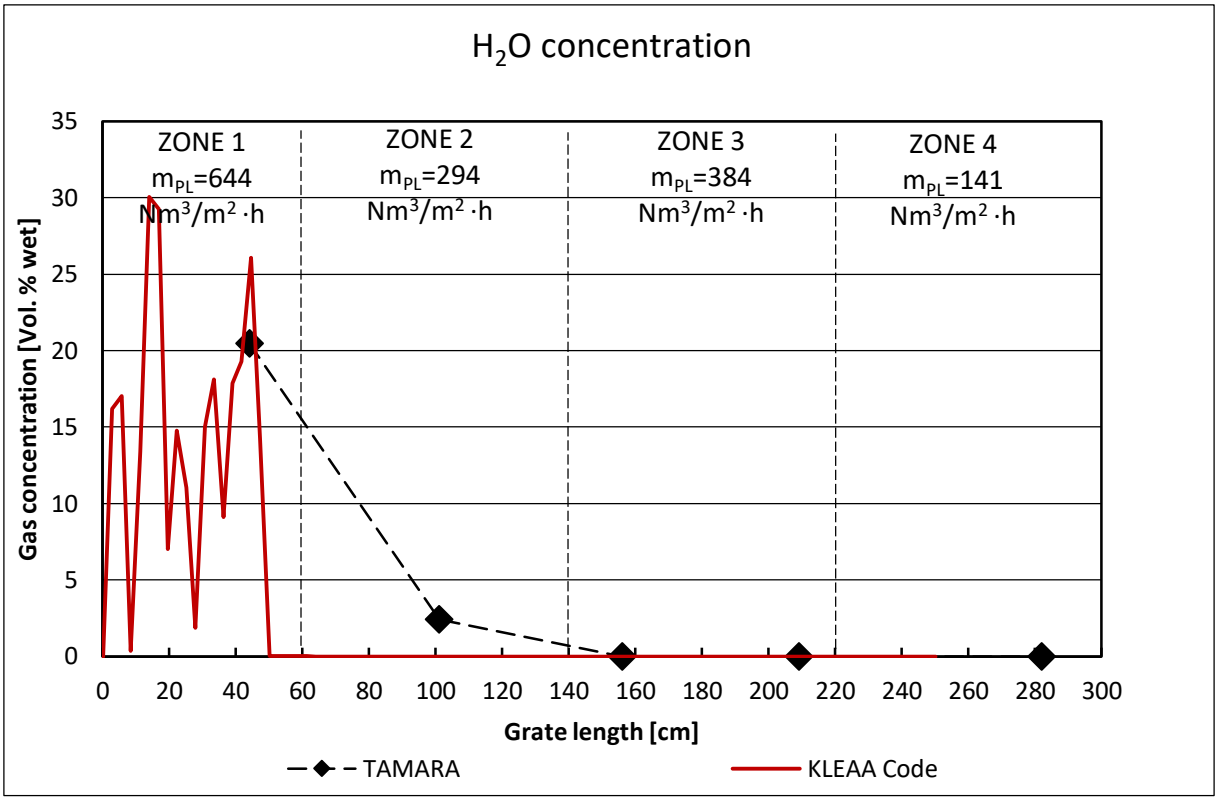
H2O concentration
ZONE 1
mPL=644
Nm3/m2·h
ZONE 2
mPL=294
Nm3/m2·h
ZONE 3
mPL=384
Nm3/m2·h
ZONE 4
mPL=141
Nm3/m2·h
Gas concentration [Vol. % wet]
Grate length [cm]
TAMARA
KLEAA Code

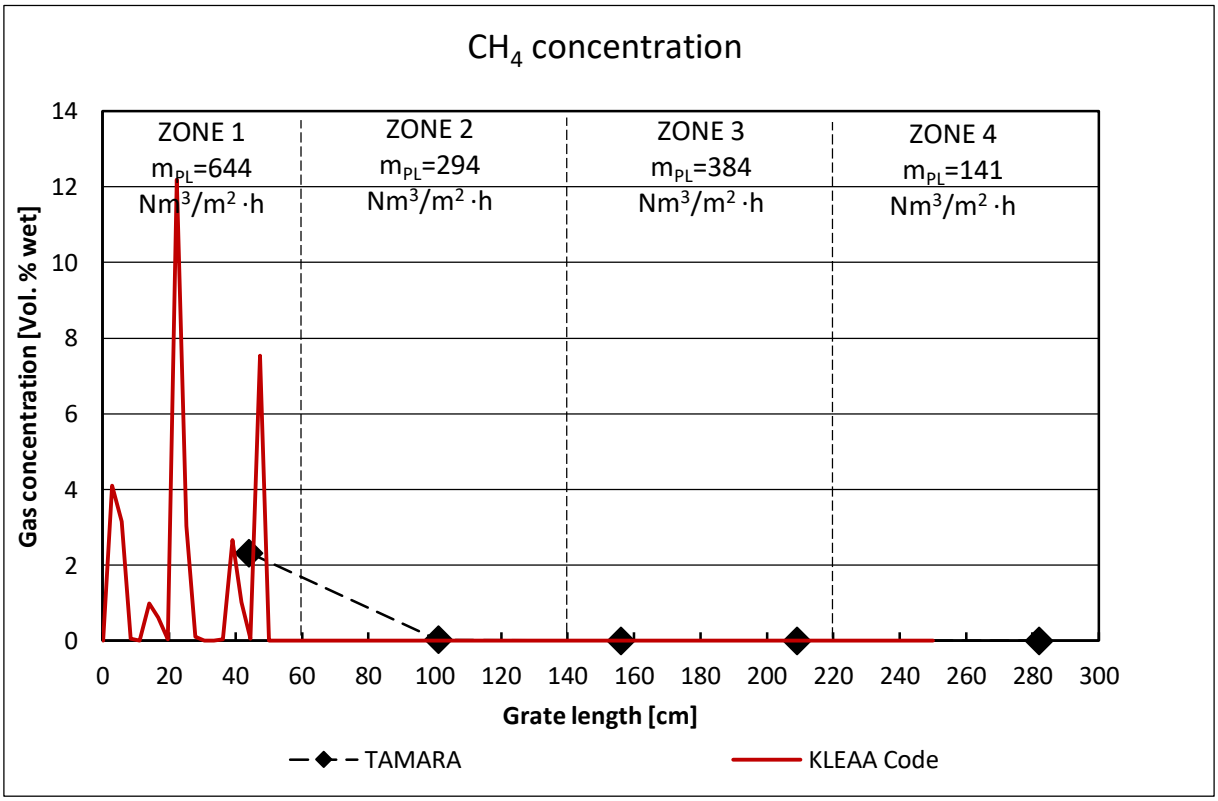
CH4 concentration
ZONE 1
mPL=644
Nm3/m2·h
ZONE 2
mPL=294
Nm3/m2·h
ZONE 3
mPL=384
Nm3/m2·h
ZONE 4
mPL=141
Nm3/m2·h
Gas concentration [Vol. % wet]
Grate length [cm]
TAMARA
KLEAA Code